Borehole BDS-5 near Derrière-Monterri, Courgenay, Switzerland

Synthesis report

Berichte der Landesgeologie
Rapports du Service géologique national
Rapporti del Servizio geologico nazionale
Reports of the Swiss Geological Survey

David Jaeggi and Paul Bossart
Editors

Mont Terri Project

Schweizerische Eidgenossenschaft
Confédération suisse
Confederazione Svizzera
Confederaziun svizra

Federal Department of Defence,
Civil Protection and Sport DDPS

Federal Office of Topography swisstopo

Borehole BDS-5 near Derrière-Monterri, Courgenay, Switzerland

Synthesis report

Berichte der Landesgeologie
Rapports du Service géologique national
Rapporti del Servizio geologico nazionale
Reports of the Swiss Geological Survey

David Jaeggi and Paul Bossart
Editors

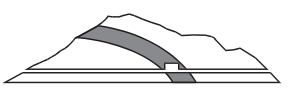

Mont Terri Project

Schweizerische Eidgenossenschaft
Confédération suisse
Confederazione Svizzera
Confederaziun svizra

Federal Department of Defence,
Civil Protection and Sport DDPS

Federal Office of Topography swisstopo

Editor
Swiss Geological Survey (SGS)

Recommended quotation
Jaeggi, D. & Bossart, P. (2016): Borehole BDS-5 near Derrière-Monterri, Courgenay, Switzerland. Synthesis report. – Ber. Landesgeol. *6.*

Cover photo

Impression
1500 copies

Order
swisstopo, CH-3084 Wabern, or e-mail to mapsales@swisstopo.ch

ISSN 1661-9285
ISBN 978-3-302-40091-4

Schweizerische Eidgenossenschaft
Confédération suisse
Confederazione Svizzera
Confederaziun svizra

Federal Department of Defence,
Civil Protection and Sport DDPS

Federal Office of Topography swisstopo

SCK•CEN
STUDIECENTRUM VOOR KERNENERGIE
CENTRE D'ETUDE DE L'ENERGIE NUCLÉAIRE

ANDRA
la maîtrise des déchets radioactifs

OBAYASHI

BGR

nagra.

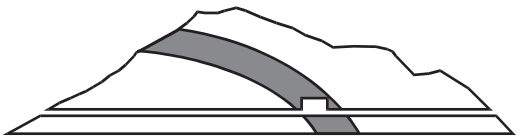

Mont Terri Project

Chevron

nwmo
NUCLEAR WASTE MANAGEMENT ORGANIZATION
SOCIÉTÉ DE GESTION DES DÉCHETS NUCLÉAIRES

CRIEPI

JAEA

U.S. DEPARTMENT OF ENERGY

IRSN
INSTITUT DE RADIOPROTECTION ET DE SÛRETÉ NUCLÉAIRE

enresa

GRS

Supported by:
Federal Ministry of Education and Research
on the basis of a decision by the german Bundestag

Organisations involved

Project Partners

ANDRA	Agence nationale pour la gestion des déchets radioactifs, France
BGR	Bundesanstalt für Geowissenschaften und Rohstoffe, Germany
Chevron	Chevron Energy Technology ETC, US
CRIEPI	Central Research Institute of Electric Power Industry, Japan
DOE	U.S. Department of Energy, Office of Nuclear Energy, US
ENRESA	Empresa Nacional de Residuos Radiactivos, S.A., Spain
ENSI	Swiss Federal Nuclear Safety Inspectorate, Switzerland
GRS	Gesellschaft für Anlagen- und Reaktorsicherheit mbH, Germany
IRSN	Institut de radioprotection et de sûreté nucléaire, France
JAEA	Japanese Atomic Energy Agency, Japan
Nagra	National Cooperative for the Disposal of Radioactive Waste, Switzerland
NWMO	Nuclear Waste Management Organisation, Canada
OBAYASHI	Obayashi Corporation, Japan
SCK•CEN	Studiecentrum voor Kernenergie, Centre d'étude de l'énergie nucléaire, Belgium
swisstopo	Federal Office of Topography, Switzerland

Direction of the Project and Project Management

swisstopo	Federal Office of Topography

Responsible for the Mont Terri motorway tunnel system

FEDRO	Federal Roads Office, Switzerland

Authorisations

RCJU	République et Canton du Jura Département de l'Environnement et de l'Equipement

Authors and Chapters

List of Authors

D. Jaeggi, P. Bossart, C. Nussbaum, A. Morard	swisstopo, Switzerland
H. Bläsi	University of Berne, Institute of Geological Sciences, Switzerland
B. Hostettler	Natural History Museum, Bern, Switzerland
J.-M. Matray	IRSN/PRP-DGE/SRTG/LETIS, France
D. Bailly	Independent, Le Rocher des Noues, France
G. Klee	MeSy-Solexperts, Bochum, Germany
C. Aubourg, R. Alzaruk	Université de Pau et des Pays de l'Adour, France

Preface of the editors

swisstopo is pleased to present this report on the BDS-5 borehole at derrière Monterri. This borehole was drilled in the framework of the DS (Determination of Stress) experiment, which was carried out between 2006 and 2013; the borehole itself was drilled in 2011. It crosses the Folded Jura in the hanging wall, then the tectonic detachment zone and finally enters into the Tabular Jura in the footwall. One major aim was the determination of in-situ stresses caused by hydraulic fracturing. From the 15 experiment partners, ANDRA, BGR, Chevron, IRSN, Nagra, NWMO, and swisstopo were involved and contributed to the project.

A large number of scientists, engineers and technicians have significantly contributed to the success of this borehole. One of them needs to be given special mention: it was Peter Blümling from Nagra who initiated and always supported the idea of estimating the in-situ stresses, not only within the Mont Terri rock laboratory, but also in its neighbourhood and in the northern limb of the Mont Terri anticline. Additionally, he was a great motivator for all scientists who were involved in the DS-experiment and was able to convince several Mont Terri project partners to finance the project.

The editors would also especially like to thank the following people: Marcos Buser and Pascal Mertenat from the cantonal Commission de Suivi, Jean Fernex and Sandrine Schmidt from the environmental department ENV (JU), who approved the project and provided swisstopo with the authorisation for the project. Tim Vietor from Nagra is thanked for leading the experiment as principal investigator, and Peter Connolly from Chevron and Tom Lam from NWMO are thanked for their expertise as experiment delegates. We would then like to thank the following scientists, engineers, and technicians who were involved in the drilling, logging, data evaluation, and interpretation: Jean-Philippe Rey and his drilling staff (Stump Foratec AG), Klaus Brauch and his team (Terratec), Bernd Zetzsche (Balance Point Control) and Achim Reisdorf (Universität Basel). Site support was provided by Peter Müller (now at company Dr. Heinrich Jäckli AG), Thierry Theurillat and Gilbert Joliat, both swisstopo. Benoît Valley (University of Neuchâtel) reviewed the stress chapter and gave us very useful comments. We thank Alain Morard (swisstopo) as well, who reviewed the stratigraphy chapter of this report. Nicola Kern and Linda Wymann, both swisstopo trainees, are thanked for drawing and improving the figures.

swisstopo
Director Mont Terri Project
Dr. Paul Bossart

Vorwort des Herausgebers

swisstopo freut sich, Ihnen hier den Bohrbericht BDS-5 präsentieren zu dürfen. Diese Bohrung wurde bei Derrière Monterri (Kanton Jura) im Jahre 2011 abgeteuft, im Rahmen des von 2006 bis 2013 laufenden DS-Experimentes (Bestimmung des Spannungsfeldes im Felslabor Mont Terri). Diese Bohrung durchquert den Faltenjura im Hangenden, durchörtert eine tektonischen Überschiebung und endet im liegenden Tafeljura. Ein wichtiges Ziel war die Bestimmung der in-situ-Spannungen mittels der Methode des «hydraulic fracturing». Von den 15 Mont-Terri-Experiment-Partnern waren die ANDRA, BGR, Chevron, IRSN, Nagra, NWMO und swisstopo am Projekt beteiligt.

Eine grössere Anzahl von Wissenschaftlern, Ingenieuren und Technikern haben wesentlich zum Erfolg dieser Bohrung beigetragen. Ein Name muss dabei besonders erwähnt werden: Peter Blümling von der Nagra, der das DS-Experiment initiert hat. Er hatte die Idee, das Spannungsfeld auch ausserhalb des Felslabors Mont Terri im Nordschenkel der Mont-Terri-Antiklinale zu ermitteln. Er war auch der Motivator für viele Wissenschaftler, die am DS-Experiment beteiligt waren und konnte verschiedene Mont-Terri-Projektpartner davon überzeugen, das Projekt zu finanzieren.

Die Redaktoren möchten weiter folgenden Personen danken: Marcos Buser und Pascal Mertenat von der kantonalen Überwachungskommission, Jean Fernex und Sandrine Schmidt vom kantonalen Umweltschutzamt (JU), welche das Projekt von swisstopo bewilligt haben. Tim Vietor von der Nagra, Peter Connolly von Chevron und Tom Lam von NWMO werden als Versuchsleiter und Experimentdelegierte verdankt. Folgende Wissenschaftler, Ingenieure und Techniker waren an Bohrung, Bohrkernaufnahme, Logging, Datenauswertung und Interpretation beteiligt: Jean-Philippe Rey und die Bohrcrew (Stump ForaTec AG), Klaus Brauch und sein Team (Terratec), Bernd Zetzsche (Balance Point Control) und Achim Reisdorf (Universität Basel). Technische Unterstützung vor Ort leisteten Peter Müller (jetzt bei Büro Dr. Heinrich Jäckli AG), Thierry Theurillat und Gilbert Joliat (beide swisstopo). Benoît Valley (Universität Neuenburg) überprüfte das Spannungs-Kapitel und gab uns dabei wertvolle Hinweise. Wir danken auch Alain Morard (swisstopo) für die Überprüfung des Kapitels Stratigraphie in diesem Bericht. Nicola Kern und Linda Wymann, welche bei swisstopo im Felslabor ein Praktikum absolvierten, danken wir für das Zeichnen und die Verbesserung der Figuren.

swisstopo
Direktor Mont-Terri-Projekt
Dr. Paul Bossart

Préface de l'éditeur

swisstopo a le plaisir de présenter ce rapport sur le puits de forage BDS-5 situé à «derrière Monterri», dans la partie frontale du Jura plissé. Ce puits a été réalisé en 2011 dans le cadre de l'expérience DS (Determination of Stress). Le forage recoupe le chevauchement principal du Jura, délimitant au-dessus le Jura plissé et au-dessous le Jura tabulaire. L'objectif majeur a été la détermination des contraintes in situ par fracturation hydraulique. Faisant partie des 15 partenaires d'expériences, ANDRA, BGR, Chevron, IRSN, Nagra, NWMO et swisstopo ont été impliqués et ont contribué au projet.

Un grand nombre de scientifiques, ingénieurs et techniciens ont participé de manière significative au succès de ce puits de forage. Mais un scientifique doit spécialement être mentionné: Peter Blümling, de la Nagra, qui a initié et toujours soutenu l'idée d'estimer les contraintes in situ, non seulement au sein du laboratoire souterrain Mont Terri mais aussi dans les environs et dans le flanc nord de l'anticlinal du Mont Terri. Il a su motiver tous les scientifiques qui étaient impliqués dans l'expérience DS et convaincre les différents partenaires du projet Mont Terri de financer le projet.

Les rédacteurs désirent remercier particulièrement les personnes suivantes: Marcos Buser et Pascal Mertenat de la Commission de Suivi du canton du Jura, Jean Fernex et Sandrine Schmidt de l'Office de l'environnement ENV (JU), qui ont approuvé le projet et donné l'autorisation à swisstopo. Tim Vietor de la Nagra est remercié pour avoir mené l'expérience en tant que responsable d'expérience, Peter Connolly de Chevron et Tom Lam de NWMO sont remerciés pour leur expertise en qualité de délégués d'expérience. Ensuite, nous tenons à remercier les scientifiques, ingénieurs et techniciens suivants, qui ont été impliqués dans le forage, les diagraphies, l'évaluation et l'interprétation des données: Jean-Philippe Rey et son équipe de forage (Stump Foratec AG), Klaus Brauch et son personnel (Terratec), Bernd Zetzsche (Balance Point Control) et Achim Reisdorf (Université de Bâle). Le soutien de site a été fourni par Peter Müller (à présent à l'entreprise Dr. Heinrich Jäckli AG), Thierry Theurillat et Gilbert Joliat, les deux de swisstopo. Benoît Valley (Université de Neuchâtel) a révisé le chapitre des contraintes et nous a procuré des commentaires très utiles. Nous remercions également Alain Morard (swisstopo) qui a passé en revue le chapitre de la stratigraphie de ce rapport. Nicola Kern et Linda Wymann, stagiaires de swisstopo, sont remerciés pour l'élaboration et l'amélioration des figures.

swisstopo
Directeur du Projet Mont Terri
Dr. Paul Bossart

Prefazione dell'editore

swisstopo ha il piacere di presentare il presente rapporto sul trivellazione BDS-5 situato «derrière Monterri», nella parte frontale del Giura piegato. Il trivellazione è stato realizzato nel 2011 nell'ambito dell'esperimento DS (Determination of Stress). Questo interseca lo sovrascorrimento principale del Giura, delimitante al di sopra il Giura piegato e al di sotto il Giura tabulare. L'obiettivo principale è stato la determinazione dello stato di sforzo in situ per fratturazione idraulica. Dei 15 partners di questo esperimento ANDRA, BGR, Chevron, IRSN, Nagra, NWMO e swisstopo sono stati coinvolti e hanno contribuito al progetto.

Un grande numero di scienziati, ingegneri e tecnici hanno partecipato in maniera significativa al successo del trivellazione, ma uno scienziato deve essere menzionato in modo speciale: Peter Blümling della Nagra, il quale ha iniziato e sempre sostenuto l'idea di stimare lo stato di sforzo in situ, non solamente all'interno del laboratorio di Mont Terri ma anche nelle sue vicinanze e nel fianco nord dell'anticlinale di Mont Terri. Egli ha saputo motivare tutti gli scienziati coinvolti nell'esperimento DS e convincere i differenti partners del progetto Mont Terri a finanziare il progetto.

I redattori desiderano particolarmente ringraziare le seguenti persone: Marcos Buser e Pascal Mertenat della Commission de Suivi del Canton Giura, Jean Fernex e Sandrine Schmidt dell'Ufficio dell'ambiente ENV (JU) che hanno approvato il progetto e dato l'autorizzazione a swisstopo. Tim Vietor della Nagra è ringraziato per aver condotto l'esperimento come responsabile, Peter Connolly di Chevron e Tom Lam di NWMO sono ringraziati per le perizie in qualità di delegati dell'esperimento. Inoltre teniamo a ringraziare i seguenti scienziati, ingegneri e tecnici che sono stati implicati nella trivellazione, nelle misure geofisiche in pozzo, nella valutazione e l'interpretazione dei dati: Jean-Philippe Rey e la sua squadra di trivellazione (Stump Foratec AG), Klaus Brauch e il suo personale (Terratec), Bernd Zetzsche (Balance Point Control) e Achim Reisdorf (Università di Basilea). Il supporto del sito è stato fornito da Peter Müller (attualmente della ditta Dr. Heinrich Jäckli AG), Thierry Theurillat e Gilbert Joliat, entrambi di swisstopo. Benoît Valley (Università di Neuchâtel) ha riletto il capitolo del stato di sforzo in situ e ci ha fornito utili commenti. Ringraziamo ugualmente Alain Morard (swisstopo) che ha riletto il capitolo sulla stratigrafia di questo rapporto. Nicola Kern e Linda Wymann, entrambi stagisti di swisstopo, sono ringraziati per lo sviluppo e le migliorie delle figure.

swisstopo
Direttore del Progetto Mont Terri
Dr. Paul Bossart

Glossary

ABI	Acoustic borehole imager
AMS	Anisotropy of magnetic susceptibility
API	American petroleum index
BDZ	Borehole disturbed zone
CPS	Counts per second
DIL	Dual induction log
DS	Determination of stress experiment, conducted in the framework of the Mont Terri Project
EDS	Energy dispersive spectrometry
EDZ	Excavation damaged zone
FWS	Full wave form sonic
GR	Natural gamma ray
HTPF	Hydraulic tests on pre-existing features
NRM	Natural remanent magnetization
OBI	Optical borehole imager
SGR	Spectral gamma ray
TC	Temperature conductivity
UCS	Uniaxial compressive strength

Extended Summary

D. Jaeggi, P. Bossart, C. Nussbaum

The BDS-5 borehole was drilled in 2011 in the framework of the DS (Determination of stress) experiment of the Mont Terri Consortium. The main aim of the experiment was to determine the stress state in the Mont Terri anticline by combining numerical modeling with new stress measurements. The BDS-5 borehole was the last borehole of the DS experiment and at the same time the first one to be located outside the rock laboratory. The wellhead is located at Derrière-Monterri, between Courgenay and St.Ursanne. Additionally to the main aim of determining magnitudes and orientations of the different components of the in-situ stress tensor, further aims were also formulated. One of these was to record and study the stratigraphy of the Opalinus Clay and its bounding formations outside of the rock laboratory and, especially, the properties of the Paleogene sediments. Furthermore, the evaluation of the variability and distribution of facies types and marker horizons within the Opalinus Clay is an important task with respect to the situation encountered at the rock laboratory level. Another significant question to be solved consisted of the analysis of the composition and geometry of the main detachment as well as the role and position of Paleogene sediments with respect to this thrust zone. Testing the drilling procedure across a large fault zone with a confined unit and with a high swelling potential in the hanging wall and a karstified and fractured limestone in the footwall is an important issue as well, especially in regard to the planned investigation boreholes at potential sites for nuclear waste repository. Investigation of hydraulic pore water pressures across the main detachment and their long-term evolution, as well as the analysis of pore water pressure time series, are crucial objectives for the assessment of properties of aquifers and aquicluds. Another aim was to study the origin of fault gouges observed on core material and to assess their magnetic properties.

Lithology and Stratigraphy

The Tabular Jura is present between depths of 216.5–102.4 m. The lowermost part of the borehole lies within the Vellerat Formation, which, from bottom to top, consists of beige and grey marls containing numerous calcareous lumachella beds with gastropods and oysters (Röschenz Member), beige and reddish limestone with abundant oncoids (Hauptmumienbank Member), and beige, slightly marly micritic limestone (Bure Member). Within the Vellerat Formation, the Hauptmumienbank was a conspicuous marker bed in the lower part of the borehole. Next, up to a depth of 146 m, more than 45 m of beige or chalky white micritic limestone with bivalves, serpulids, and echinoderms of the Courgenay Formation occur. Within this formation, a karstified section is present between 163 and 168 m depth, which is 66 m below the former rock surface. The transition to the overlying Reuchenette Formation at a depth of 146 m is marked by a conspicuous fault gouge. The top of the Tabular Jura is built of Kimmeridgian platform carbonates of the Reuchenette Formation. The rock consists of beige or white micritic limestone, which is partially pelsparitic and oolitic. During its evolution, this formation emerged several times intermittently, as proven by numerous tracks of sauropod and theropod tracks, which were found quite recently in the Ajoie basin NW of the drill site. At 102.4 m, the surface of the Reuchenette Formation is strongly karstified. Eocene fillings such as Bolus Clay and bean ore present. Since no larger open cavities were encountered, the former karst system is completely sealed off. The former corroded erosional surface is conformably overlain by a thin series of Paleogene sediments. From bottom to top they consist of greenish to grey silty marls, partly nodular with sandy limestone and siltstones (Septarien-Ton), beige nodular, laminated and crusty limestone with abundant freshwater gastropods (Delsberg-Süsswasserkalk), and a thin cover of greenish and grey silty marls of a non-specified unit, most likely of Paleogene age as well. The total thickness of the Paleogene sediments is 7.1 m. A 3.2 m thick tectonic mélange of Paleogene components marks the transition to the hanging wall.

Above the main detachment, the Folded Jura is present from 92.1 m up to the surface. The lowermost part of the Folded Jura is represented by strongly tectonized Opalinus Clay. Up to about 55 m, numerous faults and fault zones can be encountered. Up to 46.9 m, the Opalinus Clay consists of dark, locally sandy clays with changing amounts of bioclastic material. Further up, the clay seems to be slightly bituminous with many spurs and grooves. The rock contains numerous shells from the bivalve *Bositra buchi*. From 37.1 to 26.4 m, the clay contains numerous ammonites and bioclastic material. A conspicuous layer with numerous small pyrite crystals is present at 32.7 m, about 6 m below the next prominent transition. At that level, above a tectonic breccia, the carbonate-rich sandy facies of the Opalinus Clay is present. This facies consists of grey sandy clay with an intercalation of 5 cm-thick layers of bioclastic limestone and large bioclastic nodules. Continuing from there, at 22.0 to 14.2 m, the sandy facies consisting of grey sandy clays with a large amount of sand lenses, ripples, and nodules due to burrowing is present. The top of the Opalinus Clay is built of weathered argillaceous and mica-bearing clays with changing amounts of sand. The rock surface is located at 6.3 m and overlain by loose rock, consisting of displaced, unconsolidated silty to clayey gravels.

Geophysical logging detected most of the lithological marker beds and, furthermore, showed the nature of transi-

tional boundaries. The most prominent transitions are the intraformational boundaries from shaly to sandy to carbonate-rich and again shaly facies in the Opalinus Clay, the transition from the Folded Jura in the hanging wall to the Tabular Jura in the footwall encompassing the tectonic mélange and the Paleogene sediments, the karstified upper part of the Reuchenette Formation, and the Hauptmumienbank Member just above the marly Röschenz Member in the lowermost part of the borehole.

Tectonics

In the borehole BDS-5, the main detachment is developed in a 3.2 m thick zone from 92.1–95.3 m, which can be designated as a tectonic mélange. The colorful tectonic mélange suggests a Paleogene age of the strongly deformed rocks contained within it. It consists of small packages of internally non-disturbed, sometimes rotated multi-colored marls, floating in a confluent marly matrix. The tectonic mélange, which represents the main detachment, is located between the basis of the strongly deformed Opalinus Clay in the hanging wall and the Paleogene sediments which lie directly on the karstified surface of the limestone of the Reuchenette Formation in the footwall. A total thickness of 7.1 m was encountered for the Paleogene sediment on core material of the BDS-5 borehole. The top of the footwall consists of lacustrine freshwater sediments and marine Septarien-Ton. At that position, these sediments show only minor deformation. In the hanging wall, the Opalinus Clay is extremely deformed in the area between 92 and 88 m, where it has completely lost its original internal structure. Many fault zones and single faults are present between 88 and 56 m; the original structure of the rock is still preserved, however.

Hydrogeology

Pore water pressure monitoring and frequency analysis of time series revealed two hydraulically separated units: an upper confined unit in the Opalinus Clay and a lower aquifer in the limestone of Oxfordian and Kimmeridgian age.

The pore water pressure in the Opalinus Clay of the Folded Jura is still rising after 3 years of equilibration time, although at a very slow rate. The pressure rose from around 1.5 bar to 4.5 bar. After two distinct sudden pressure drops during the initial four months after installation, the pressure signal has become quite smooth over a longer period and evidently has not been affected by tidal effects until now, as a frequency analysis of the pressure signal time series revealed. It is clearly the signal of a confined, very low, permeable unit, at a location in which the pressure is still not in equilibrium. The lower pressure transducer in the Tabular Jura and below the main detachment, in the limestone of the Reuchenette Formation, is affected by atmospheric pressure and large-scale pressure variations. Variations of the pressure signal at that location can be correlated with meteoric data from a surface station located in the vicinity. The analysis of pressure variations over the last three years shows an annual fluctuation of 0.01 bar or 10 cm of head difference with a minimum in early April to early May. There is a large hydraulic head difference of about 7 bar between the Opalinus Clay in the hanging wall and the Late Jurassic limestone in the footwall.

Analysis of the two-year pressure series show that the selected harmonics of the tides are only expressed in carbonated layers surrounding the Opalinus Clay and thus in the aquifer of the Malm limestone of the Tabular Jura, below the main detachment. The diurnal harmonics, lunar diurnal, the principal lunar semi-diurnal, and the principal solar semi-diurnal were detected on this dataset. For the Malm aquifer the specific storage was estimated as $2.7 \pm 0.1 \times 10^{-6}\,m^{-1}$. The analysis of pressure time series in the upper part, the Opalinus Clay of the Folded Jura above the main detachment, indicated that the main gravitational harmonics are absent.

In-situ stresses

A total of 11 hydraulic fracturing tests and 10 impression packer tests were carried out in borehole BDS-5. Only the footwall data can be considered for analysis, since that was the only location at which axial fractures could be induced by hydraulic fracturing tests. In the footwall, re-opening and shut-in pressures systematically increase with depth. There, depth-functions for maximum horizontal stress- and minimum horizontal stress-magnitudes could be derived and yield for S_h 4.3 MPa and for S_H 8.3 MPa at 107 m depth or rock laboratory level. Vertical stress S_v is determined with a rock density of 2500 kg/m^3 and yields 2.7 MPa at rock lab level. Analysis of stress directions in borehole BDS-5 suggests an S_H trending towards N14°±19° for the depth interval between 108 and 192.5 m. Klee (2011) provided an interpretation for the tests in the hanging wall as well, suggesting a decoupling across the main detachment. A detailed review of the data by swisstopo, however, revealed that only pre-existing features could be opened by these tests. A reliable interpretation of the data is thus not feasible. The derived orientation of S_H in the footwall is consistent with the regional and large-scale stress tensor above the main basal detachment within the Triassic evaporites. A topographic control is postulated for the S_H in the hanging wall above.

With the currently available dataset of 33 in-situ stress measurements of the rock laboratory and its close vicinity, it could be shown that the results are very heterogeneous. An anisotropic stress field in combination with the anisotropic rock causes the interpretation of in-situ stress tests to become a challenging task. Despite this fact, the authors of this report evaluated three major controls on the in-situ stress state at Mont Terri, which are: excavation/construction control, depth control, and the control of lithology or rock competence. For every in-situ test, the stress field is a combination of these three controlling factors. The authors furthermore defined three cases applicable for most of the carried-out in-situ tests. An adapted stress tensor is proposed for every case. The first case concerns short boreholes on the rock laboratory level, situated in Opalinus Clay. For this case, the stress tensor of Martin & Lanyon (2003) and Bossart & Wermeille (2003) with a sub-vertical σ_1 dominated by the overburden is proposed. σ_2 and σ_3 are located in the horizontal plane, but are not well-defined in their orientation. The second one comprises long vertical boreholes in the rock laboratory and in the Opalinus Clay. Here, the stress tensor of Enachescu (2011) with σ_1 trending towards 033° horizontally and σ_2 sub-vertically oriented and controlled by

the overburden is proposed. The third case comprises boreholes in competent rock, such as limestone or dolomites, where the stress tensor of Shin (2006, 2009), with a σ_1 of 15 MPa and trending horizontally towards 320°, is proposed. σ_3 is sub-vertical and 4 MPa in magnitude.

In spite of a large number of in-situ stress measurements having been carried out, inconsistencies are still present and further tests in the vicinity of the Mont Terri rock laboratory, including data from surface boreholes, should be carried out in the future.

Magnetic data

Two samples of the BDS-5 borehole were analyzed thoroughly on their magnetic properties. The main questions which arose were whether recent seismic events which had formed gouges were observable on core material in the Opalinus Clay section or whether aseismic deformation was the main process of the observed structures. Furthermore, the existence of earthquake-induced features would imply that thrusting in the Jura Mountain range is still ongoing, which in turn would prove the existence of active faults.

Two samples from the lower part of the Opalinus Clay in the hanging wall and the Delsberg-Süsswasserkalk just below the main detachment in the footwall were analyzed. Chemical analysis of the black bodies within the freshwater limestone at a depth of 98.5 m revealed that they are mainly composed of organic matter. Consequently, these are undeformed accumulations of organic matter within a lacustrine environment and not "pseudotachylites", which would infer a seismic origin. No seismic event was detected on the rock material and the two conspicuous samples. Anisotropic magnetic susceptibility data indicate a stretching along the fold axis of the Mont Terri anticline, which is consistent with the maximum horizontal stress orientation in N–S direction. Palaeomagnetic data suggest that the gouges do not originate from recent activity and that remagnetization took place before 0.78 Ma or earlier. The palaeomagnetic record exhibits well-defined components in the gouge, indicating that a physical process – chemical or thermal, for instance – is responsible of the magnetic imprint after the gouge formation.

Interpretation and integration of results

For the Opalinus Clay, the stratigraphic succession encountered at the BDS-5 borehole is comparable to the situation in the Mont Terri rock lab, located 1.5–2 km to the SSE. The prominent facies changes from shaly to sandy to carbonate-rich sandy and back again to the shaly facies were similarly recognizable. Furthermore, the prominent marker horizons, such as the pyrite layer located about 6 m below the basis of the carbonate-rich sandy facies, seems to be present on a regional scale. A biostratigraphic analysis based on ammonites at borehole BDS-5 indicated that only the upper 40 m of the Opalinus Clay are of Aalenian age. At 40.8 m, the Torulosum subzone already marks the Toarcian. In the Mont Terri rock laboratory, the lower quarter – about 35 m of the Opalinus Clay succession – is of Toarcian age, as a biostratigraphic investigation has shown (Reisdorf et al. 2014). However, at borehole BDS-5 this part of the stratigraphic record is strongly affected by faults and fault zones, which successively increase towards the main detachment at 92.1 m depth. Thus, there will be a thickening of strata due to repetitions. The 3.2 m thick fault zone at BDS-5 is comparable to most of the prospection boreholes of the A16 motorway, where thicknesses between 0 and 3.7 m were encountered in five boreholes and 14 m in a sixth borehole. The thickness of the tectonized zone is most likely dependent on the occurrence or absence of competent rocks in the hanging wall or the footwall, respectively. However, the main detachment is always developed at the top of the Paleogene sediments and is developed in a tectonic mélange, consisting of Paleogene components rotated in a completely deformed fine-grained matrix, whereas Paleogene sediments below this mélange remain more or less undeformed. Furthermore, many conjugated thrusts delocalized the tectonic stress above the main detachment in the overturned northern limb of the Mont Terri anticline. This suggests that depending on where the basal detachment or the tectonic mélange is regarded on a geological section, the total displacement can be different. Conspicuous levels with shining surfaces and black layers turned out to be of organic origin and not the result of seismic events. Furthermore, a prominent fault gouge in the strongly deformed Opalinus Clay was analyzed in terms of magnetic properties, and yielded an age older than 0.78 Ma. This implies that these fault gouges did not originate from recent activity. Analyzed pyrites were not chemically altered, which suggests that no O_2-rich fluids are circulating in the sampled gouge. Based on these premises, it was also interesting to receive the results from the hydraulic fracturing campaign and compare the results of the hanging wall and footwall, respectively. Unfortunately, only the tests in the footwall, in the Late Jurassic limestone below the main detachment, yielded reliable data and were interpretable with standard methods. The evaluated stress directions in the footwall are consistent with the regional scale tectonic stress regime with a maximum horizontal stress axis striking close to N–S or slightly NNE–SSW. The stress state in the hanging wall is most likely to be dominated by topographical effects, but no reliable values for magnitudes and directions of horizontal stresses can be given.

The strike directions of S_H and S_h in the footwall are consistent with data from other studies carried out in the rock laboratory and its vicinity (e.g. Enachescu 2011, who postulated N33° for S_H in the Opalinus Clay in the 55 m deep borehole BDS-4). The analysis of hydraulic pore pressure time series revealed two entirely separated and hydraulically different units: the extremely low permeable confined unit in the hanging wall and the fractured limestone aquifer in the footwall below the basal detachment. In the Tabular Jura below the basal detachment, the pore pressure time series assumedly represents undisturbed conditions. The behavior of pressure variations suggests a well-developed fractured or even karstified aquifer which is in contact with catchment areas reacting to meteoric alimentation. Those catchment areas are most likely located towards the northern Ajoie plain, where the Malm limestone is exposed or only thinly covered by Paleogene sediments. However, in the hanging wall above the basal detachment – which is not considered to be representative of initial and undisturbed conditions by the time series – the atmospheric and thermal influence was

observed by the occurrence of a principal solar semi-diurnal signal.

Altogether, a plethora of investigations were carried out on the BDS-5 borehole, enabling us to better understand the processes which occur in such a complex geological environment. Furthermore, test sequences were trained and improved for future, similar projects. Numerous measurements carried out in this borehole comprise a pillar of knowledge for regional geology and should be extended with further regional studies or comparable projects in the future.

Table of Contents

List of Figures

List of Tables

1. Introduction

D. Jaeggi

1.1 Aim of borehole and location

Since 1996, a plethora of experiments and tests to evaluate the in-situ stress state of the Mont Terri anticline and the underground rock laboratory have been conducted in the Mont Terri rock laboratory. Among other experiments, the DS (Determination of stress) experiment was explicitly established in order to combine in-situ stress measurements with numerical modeling. After several experiments and boreholes in the Mont Terri underground rock laboratory more than 200 m below surface, it was decided to perform a further deep drill at the surface in order to gain a means to cross-check the results from former studies. Apart from evaluating the in-situ stress state, the requirements of the borehole were to i) reach the main thrust (interface between Folded and Tabular Jura) at a depth of about 100 m, ii) avoid water-bearing or highly permeable formations that could be in direct contact with springs, iii) be at a sufficient distance to the Mont Terri motorway tunnel, yet not too far away, in order to profit from the knowledge of the available prospecting boreholes, iv) stay more or less on a section with the rock lab, perpendicular to the fold axis of the Mont Terri anticline, v) stay outside protected groundwater zones or catchment areas and vi) retain easy access to the drill site by car/truck.

The chosen site near Derrière-Monterri (2578.544.4/1248.762.0/621.5) fulfilled the above-mentioned requirements for this borehole. The borehole is located between St.Ursanne and Courgenay, about 1.5 km NW of the Mont Terri rock laboratory and about 200 m west of the axis of the Mont Terri motorway tunnel (Fig. 1-1). From the geological investigation carried out for the motorway tunnel (Norbert & Schindler 1988, Schaeren & Norbert 1989), several boreholes up to 200 m deep were available along the tunnel trace. This considerably facilitated the prognosis of the complex geology. A direct interpolation, however, was not possible due to the strongly non-cylindrical shape of the Mont Terri anticline.

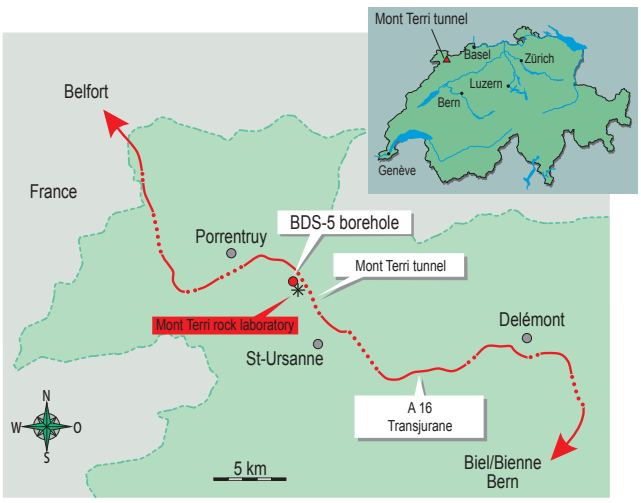

Fig. 1-1: Location of the area of investigation with the borehole BDS-5.

After submission of a pre-report (not published) on the planned works and the geological and hydrogeological situation at the drill site, the permission for the project was given by the ENV (environmental department of the Canton of Jura). The borehole BDS-5 and all investigations carried out were financed by the experiment partners of the DS (Determination of stress) experiment, Nagra, Chevron, NWMO and BGR. swisstopo took the lead on the on-site works and was responsible for permissions and geological documentation of the borehole. At the end of the testing phase, the partners of the LP (Long-term monitoring of pore pressures) experiment, ANDRA, IRSN, Nagra, swisstopo, Chevron, and NWMO, decided to install two standalone pressure transducers connected to a GSMII data logger in the borehole for long-term monitoring of pore pressures. After completion of the works, swisstopo summarized the on-site activities and the results from the geological documentation in a technical report TR2012-05 (Jaeggi et al. 2014). This technical report forms an important basis for this study.

1.2 Drilling procedure and completion

After the permitting period, the drilling works at BDS-5 were carried out from the end of May to the beginning of July 2011 by the contractor Stump Foratec AG, Bern. The works on site were coordinated by the Swiss Geological Survey, swisstopo. The drill rig, a Gelma II on a truck, was equipped for wireline and fluid-based drilling. The borehole was entirely cored. The borehole was drilled with an inhibitive drilling mud (polymer guar gum) in order to guarantee borehole stability in the argillaceous parts. The first 7.7 m were drilled with 168 mm and a single-core barrel. A temporary steel casing was installed. Then, the machine was changed to wireline drilling at a diameter of PQ (122.3 mm), yielding 84.8 mm cores. With this diameter, the borehole preceded to a depth of 113.5 m, about 10 m into the well-cemented hard limestone of the uppermost Tabular Jura. After logging by the company Terratec, Germany and hydraulic fracturing by MeSy, Germany a cemented steel casing 105 × 115 mm was installed. The drill rig was changed to 101 mm diameter wireline drilling, yielding 63.4 mm cores.

Fig. 1-2: 12 “shaped charge” explosives with the shot tube for borehole perforation on the right hand side and the fuses on the left hand side, just before assembly.

The borehole was continued up to a final depth of 216.5 m, about 114 m below the top of the Tabular Jura. Subsequently, geophysical logging and hydraulic fracturing campaigns were carried out. swisstopo permanently mapped and sampled the core material at several locations. Finally, the company Bereuter, BPC, Germany carried out a borehole perforation at a depth interval of 67.4–68.4 m. The perforation was carried out with 12 holes of 10–12 mm diameter, arranged in a spiral manner along a section of one meter (Fig. 1-2). Afterwards, two Keller PAA-36XW, 30 bar pressure transducers were installed at 67 and 125 m depth in the Opalinus Clay and the Reuchenette Formation, respectively. The sensors were connected to an autonomous GSM-II module, which was placed in a pre-shaft at the well head.

The completion of the borehole occured as indicated on the sketch (Fig. 1-3). The lower sensor was emplaced into a large interval between 200 and 118 m at a depth of 125 m, while the upper one was emplaced into a smaller interval be-

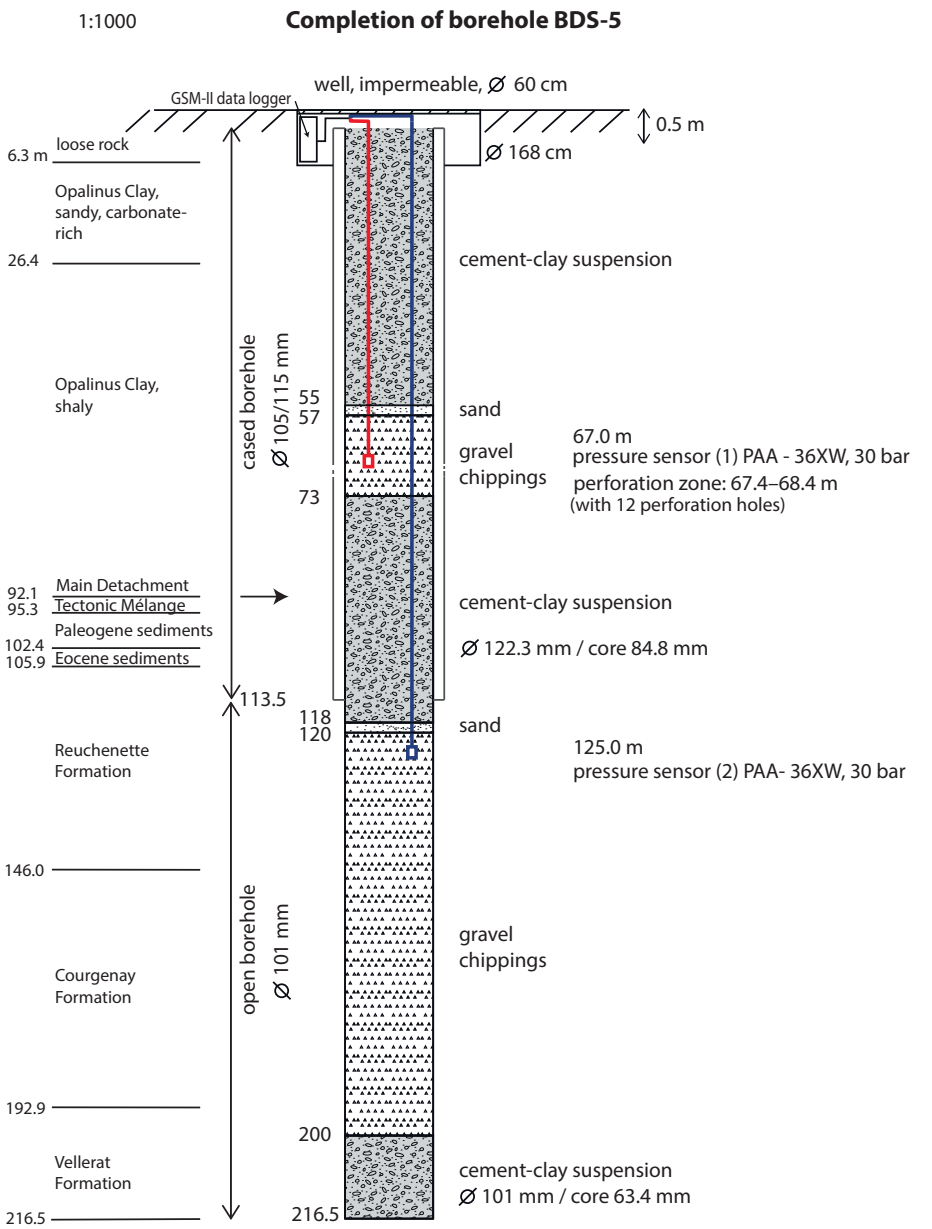

Fig. 1-3: Drilling diameters and completion of borehole BDS-5.

tween 73 and 55 m at a depth of 67 m. The rest of the borehole was filled up with a cement-clay suspension.

1.3 Test sequence and investigations carried out

During the drilling process, swisstopo carried out simultaneous core description together with the extraction of samples for thin section analysis in collaboration with external experts. The detailed procedure is described in chapter 3.1 of this report. Logging and hydraulic fracturing were both performed in the two open borehole sections 0–113.5 m and 113.5–216.5 m, respectively.

Logging was carried out by the contractor Terratec Geophysical Services, Heitersheim (Germany), once before (prefrack logs) and once after (postfrack logs) each of the two hydraulic fracturing tests, leading to a total of 4 necessary mobilizations (Klaudius et al. 2011). The objective of the geophysical logging was to generate oriented images of the borehole wall and to measure other physical parameters important for characterizing and determining the most important transitions along the stratigraphic column. All logs were carried out in the borehole filled up with inhibitive drilling mud (polymer guar gum). With the acoustic borehole imager (ABI), it was possible to create a continuous, high-resolution 360 degree image of the borehole wall. Especially due to the ability of analyzing the amplitude image, which represents changes in the acoustic signal of the rock, orientations of structural features such as faults, fractures and bedding planes could be determined on the log directly. With the full wave form sonic log (FWS), the full sonic wave-train at all three receivers as well as the velocity of the first arrival is re-

Table 1-1: *Test sequence for logging and hydraulic fracturing of borehole BDS-5.*

Date	Depth / range [m]	Description of activities
31.5.2011–14.6.2011	0.0–113.5	**Wireline drilling ø 122.3 mm**
15.6.2011	7.0–113.5	**Logging** 1. acoustic borehole imager (ABI) 2. dual induction (DIL) 3. temperature conductivity (TC) 4. full wave form sonic (FWFS) 5. caliper (3 arms, non-oriented)
16.6.2011–17.6.2011	7.0–113.5	**Hydraulic fracturing (mounted on steel rods)** Fracks at: 110.5 m, 108.0 m, 80.2 m, 70.3 m, 63.2 m, 24.1 m Hydraulic testing before and after hydraulic fracturing
17.6.2011	7.0–113.5	**Logging after hydraulic fracturing** 1. acoustic borehole imager (ABI) 2. spectral gamma log (SGR) 3. caliper (3 arms, non-oriented) 4. temperature conductivity (TC)
20.6.2011	0.0–113.5	Cementation of casing (ID 105 mm, AD 115 mm)
22.6.2011–28.6.2011	113.5–216.5	**Wireline drilling ø 101 mm**
29.6.2011	113.5–216.5	**Logging** 1. acoustic borehole imager (ABI) 2. caliper (4 arms, oriented) 3. 16"–64" laterolog (ELOG) 4. full wave form sonic (FWFS) 5. spectral gamma (SGR) 6. temperature conductivity (TC)
30.6.2011–1.7.2011	113.5–216.5	**Hydraulic fracturing** (wireline based) Fracks at: 128.5 m, 148.0 m, 156.0 m, 182.5 m, 192.5 m Hydraulic testing before and after hydraulic fracturing
1.7.2011	113.5–216.5	**Logging** after hydraulic fracturing 1. acoustic borehole imager (ABI) 2. caliper (4 arms, oriented) 3. temperature conductivity (TC)
4.7.2011	67.6–68.6	Borehole perforation by BPC/Bereuter 12 shots of 10–12 mm evenly distributed, penetration depth: 16"
5.7.2011	125.0	Installation of pressure transducer within gravel pack
6.7.2011	67.0	Installation of pressure transducer within gravel pack and cementation up to –2 m below ground.
13.7.2011	0.0	Completion of well head

corded simultaneously. With this data, elastic parameters of the surrounding rock mass can be estimated. The natural gamma ray measurement (GR) which is integrated in most logging tools was used for measuring the counts per second (CPS) of the natural total gamma radiation. The gamma counts have not been calibrated for American Petroleum Index (API). In addition to the standard GR probe, a spectral gamma probe was used, measuring the full energy spectrum and allowing determination of the K, U and Th concentrations. Splitting of the total signal into these fractions is especially of interest for the geological interpretation of transitions and boundaries between formations and members. Resistivity measurements were performed using both a dual induction (DIL) and a 16"– 64" laterolog (ELOG) probe. Both probes use two different electrode spacings in order to measure the near and far field resistivity within the formation. Temperature and conductivity measurements were taken with a TC-probe. The geometry of the borehole was measured with a 3-arm caliper during the first two logging campaigns and with a 4-arm caliper in the third and fourth one.

Hydraulic fracturing was carried out by the contractor MeSy, Bochum (Germany) in two phases (Klee 2012): firstly, the upper part of the borehole (hanging wall, including a frack below in top of the footwall) and secondly, the lower part (footwall below the main detachment). Hydraulic fracturing was performed for intervals of 70 cm length in between 2 packers of 1 m sealing-length each, resulting in a total tool length of 2.7 m. While for the first testing phase, the packer was mounted on steel rods, the second testing phase was performed with the wireline technique. After hydraulic fracturing of a section was completed, the impression packers were inserted for fracture detection. In addition to the impression packers, the identification of induced or stimulated fractures was supported by the comparison of pre- and post-frack acoustic borehole images from the ABI. The temporal course of the testing activities for logging and hydraulic fracturing is provided below in Table 1-1.

In the course of the hydraulic fracturing, simple in-situ hydraulic tests such as pressure pulse tests and step-rate injection tests were carried out for the estimation of hydraulic conductivity before and after hydraulic fracturing as well. Furthermore, laboratory tests were carried out on core material of the limestone in the footwall. Density, ultrasonic velocities and elasticity, and fracture toughness were measured and hydrofrack tests on mini-core samples performed. The data of the laboratory tests were then used in combination with the in-situ stress data as input parameters for simulations with the fracture mechanics code FRAC (Rummel & Hansen 1989) in order to correspond with the observed in-situ hydraulic fracturing pressure records.

In addition to the above-mentioned investigations, hydraulic pressure data was also collected over the last 3 years. The pressure time series were analyzed on their spectra (Matray & Bailly 2014) in order to monitor the properties of the aquifers and aquicluds such as stationary or non-stationary behavior and to estimate their hydraulic properties such as the specific storage coefficient by using simplified groundwater hydraulic models.

Two conspicuous samples from the BDS-5 borehole deemed to represent specimens of recent seismic activity have been furthermore thoroughly analyzed on their magnetic properties (Aubourg et al. 2012). The samples were analyzed with a scanning electron microscope (SEM) coupled with energy dispersive spectrometry (EDS) and standard reflected-light polarizing microscopes. Anisotropy of magnetic susceptibility (AMS) was measured by using an anisometer, and natural remanent magnetization was performed with a magnetometer.

2. Geological overview

D. Jaeggi, C. Nussbaum

2.1 Regional stratigraphy

The borehole is located in the region of St.Ursanne, between Porrentruy and Delémont, within the Jura mountain range constituted by the Jura fold-and-thrust belt. The basal detachment along which the detached Mesozoic strata of the Folded Jura was overthrusted onto the autochthonous Tabular Jura of the Ajoie region, starting in Mid-Miocene about 10.5 Ma before present (Kälin 1993, Bollinger et al. 1993, Becker 2000), crops out about 1 km north of the drilling site. The basal detachment is located within Middle – Late Triassic evaporites. This tectonic setting led to the present-day geological situation at Derrière-Monterri, where Middle Triassic to Middle Jurassic rocks of the Folded Jura lie on top of Late Jurassic rocks of the Tabular Jura.

The simplified synthetic stratigraphic column of the region is displayed below (Fig. 2-1). Above the basement with some late Paleozoic clastic sediment several hundred meters of Triassic limestone, dolomites, marls and evaporites follow, marking changing depositional environments from marine to continental. The dolomitic marls, dolomites and evaporites of the Keuper are the oldest rocks to crop out in the vicinity of the borehole. During the Early Jurassic, a fully marine environment with a successively increasing water depth developed again, leading to the formation of calcareous, marly, and argillaceous rocks denoted as the Staffelegg Formation (Reisdorf et al. 2011). Together with rocks of the Keuper, these rocks form the core of the Mont Terri anticline. They are visible at the surface and were mapped in the Mont Terri area by several authors (Laubscher 1963, Freivogel & Huggenberger 2003). The Staffelegg Formation, which reaches a thickness of up to 50 m, is followed by the 130 m thick Opalinus Clay, a monotonous succession of dark argillaceous rocks with some sandy or carbonate-rich facies variations (e.g. Schaeren & Norbert 1989, Bläsi et al. 1991, Wetzel & Allia 2003, Bossart & Thury 2008, Reisdorf et al. 2014). A continuous geological profile of the Opalinus Clay from the Mont Terri rock laboratory is available from the 250 m deep inclined borehole BDB-1 since the beginning of 2014. Three main lithofacies types were encountered (Tab. 2-1). In this borehole, from bottom to top, 33 m of a shaly facies of Toarcian age with numerous of bioclastic material is followed by 15 m of shaly facies with large amounts of ammonites. The transition to this upper part marks the Toarcian/Aalenian boundary, which was thoroughly biostratigraphically investigated in Reisdorf et al. (2014). Further up, 4 m of sandy carbonate-rich facies with several distinct bioclastic limestone beds is present. At the bottom of this facies, two conspicuous pyrite horizons are present. The carbonate-rich sandy facies is followed by 13 m of sandy facies with a large amount of bioclastic lenses, 36 m of monotonous shaly facies, and the upper sandy facies with marly, sometimes sideritic, and sandy nodules. The top of the Opalinus Clay consists of a calcareous hardground with reworked limonitic intraclasts.

The next lithostratigraphic unit, the Passwang Formation, is composed of a series of parasequences reflecting a shallow, mixed siliciclastic and carbonate depositional environment (Burkhalter 1996) with a total thickness of about 70 m. Investigations on the BDB-1 core material yielded 11 m pertaining to Sissach Member at the base and 58 m undifferentiated to Passwang Formation (Hostettler et al. 2017 submitted). Finally, the Hauptrogenstein is present, consisting of shallow-water oolitic carbonates with some distinct coral horizons. Gonzalez & Wetzel (1996) described three shallowing-upward successions, which generally start with fine-grained marly beds and end with a maximum flooding surface or a hardground on top of oolitic or sparry bioclastic limestone. The Hauptrogenstein exhibits a total thickness of about 100 m and crops out in the northern overturned limb of the Mont Terri anticline just north of the drilling site. The end of the Middle Jurassic is characterized by shallow water deposits and iron-oolitic beds of the Ifenthal Formation (Bitterli 2012). The thickness of these deposits is estimated at 50 m in the region of the Mont Terri. It is overlain by deeper water clays (Gygi 1969) and nodular marls of the Bärschwil Formation, which mark the beginning of the Late Jurassic (Oxfordian). The following coral horizons and oolitic limestone with oncoids and patch reefs are remnants of a prograding reefal belt that extended over large areas. Well-bedded platy limestone and oncolithic beds of the Vellerat Formation are indicators of shallow water conditions. Furthermore, a continental influence of the marine sediments was present. Later, a shallow, fully marine carbonate platform evolved and led to the 50 m thick succession of micritic limestone of the Courgenay Formation. A total thickness of about 250 m can be attributed to the Oxfordian. During the Kimmeridgian, the platform intermittently emerged and water depth varied between 0 and 100 m. Numerous traces of dinosaurs were found in the micritic and oolitic limestone of the Reuchenette Formation (Marty 2008, Comment et al. 2011).

The wellhead of borehole BDS-5 is located on a gentle slope oriented towards WSW 500 m SW of the summit of the Mont Terri (Fig. 2-2). The bedrock at this location is overlain by colluvium, mostly consisting of angular components from the Hauptrogenstein. The uppermost bedrock is Opalinus Clay, constituting the strongly tectonized northern limb of the exposed core of the Mont Terri anticline. The anticline axis and, accordingly, the lithological contacts are

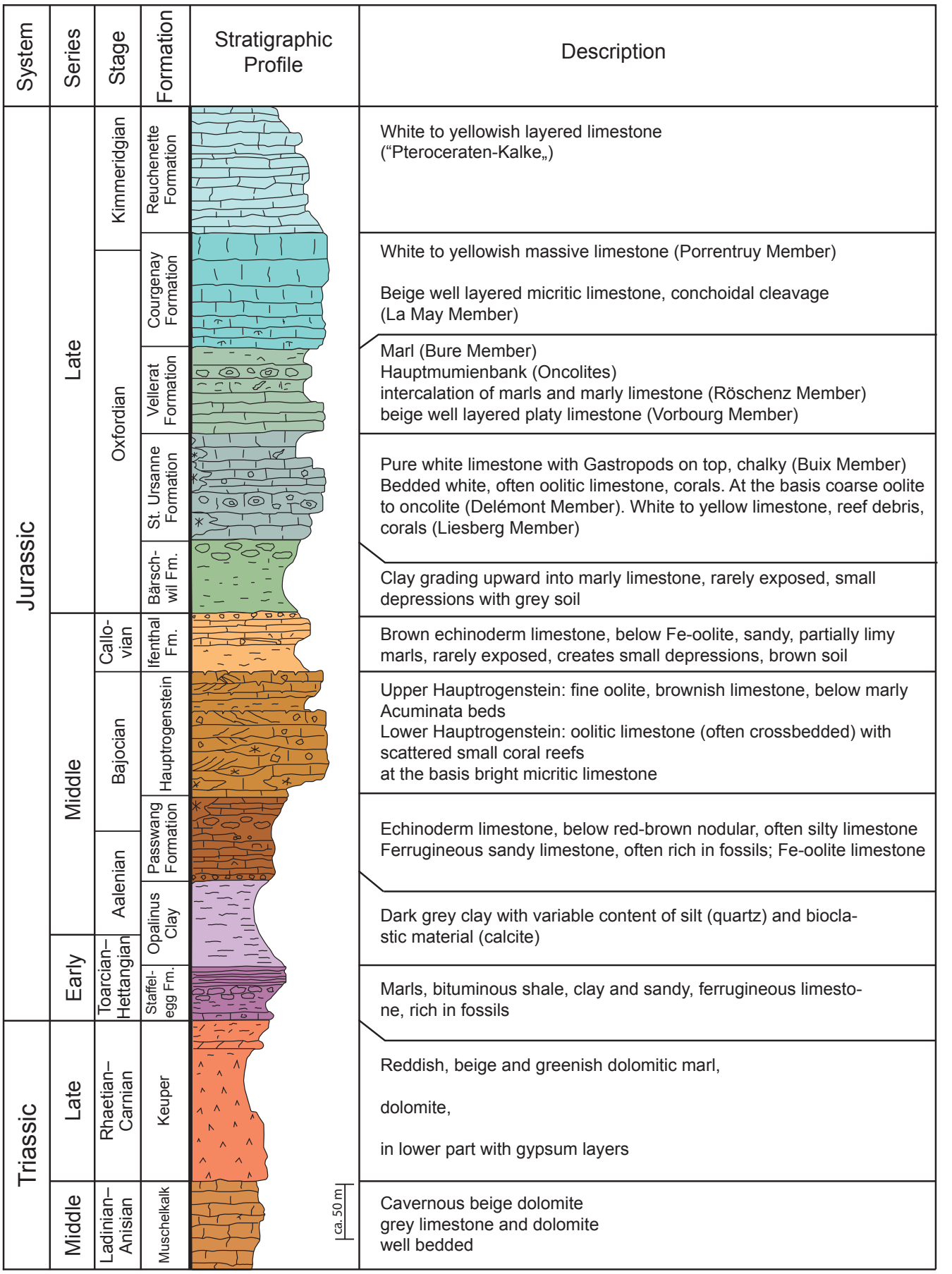

Fig. 2-1: Extract of the synthetic stratigraphic column of the study area encompassing Late Triassic and Jurassic strata, without Cenozoic (sketch after pers. comm. P. Jordan).

Table 2-1: *Subdivision of Opalinus Clay and bounding formations.*

Stage	Formation	Member/Facies (Hostettler et al. 2017, submitted)	Gallery meter along security gallery (Bläsi et al. 1996)	Depth/Thickness BDB-1 (Hostettler et al. 2017, submitted)	Description
Bajocian	Hauptrogenstein	on top facies of Rothenfluh Mb. present, below oolitic facies	–	0–37 m	Coral bearing oolitic lime-stone, in the upper part with marls, rich in bivalves and echinoderms
	Passwang Formation	Passwang Formation, non specified	–	37–57 m	Intercalation of sandy lime-stone and marls, on top with Fe-oolite
				57–95 m	Sandy limestone/marl-intercalation with Fe-oolites
Aalenian		Sissach Mb.	781– ca. 795 m	95–106 m	Silty clay and marl with layers of siltstone, limestone and Fe-oolite
	Opalinus Clay	Sandy facies	ca. 795–835 m	106–137 m 31 m	Silty clay and marl with lenses of silt, sideritic
		Shaly facies	835–869 m	137–173 m 36 m	Monotonous clay
		Sandy facies	869–890 m	173–186 m 13 m	Marly siltstone and silty clay, silty and bioclastic lenses
		Carbonate-rich sandy facies	890–900 m	186–190 4 m	Silty limestone, marly silt-stone and silty marl
		Shaly facies (Aalenian?)	900–930 m	190–(202?) m 12 m?	Silty clay and silty marl, numerous ammonites
Toarcian		Shaly facies (Toarcian?)	930–1024.5 m	(202?)–237 m 35 m?	Silty clay and marl, abundant bioclastic material
	Staffelegg Formation	Gross Wolf Mb.	–	237–243 m 6 m	Alternation of marl and clay
		Rietheim Mb.	–	243–248 m	Black bituminous shales

Sandy facies is highlighted in yellow, shaly facies in grey, and carbonate-rich sandy facies in blue. Data are from the BDB-1 borehole in the security gallery of the Mont Terri motorway tunnel (after Hostettler et al. 2017 submitted).

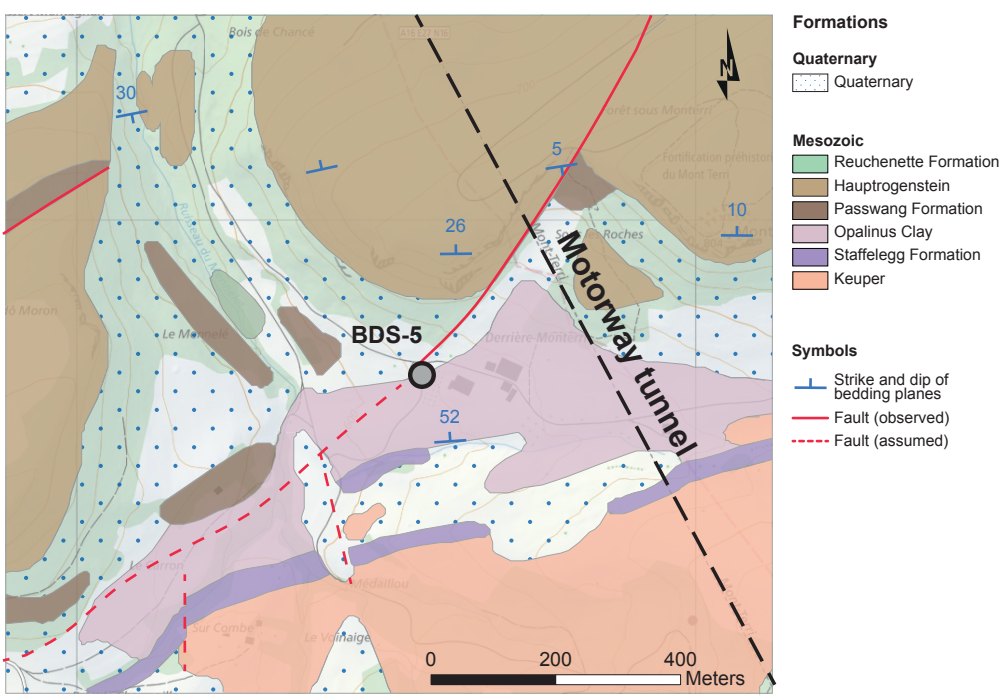

Fig. 2-2: Geological situation in the vicinity of borehole BDS-5, the black dashed line marks the axis of the Mont Terri motorway tunnel (modified after Laubscher 1963).

roughly striking WSW–ENE or even W–E a bit more to the east. Towards the north, the Hauptrogenstein crops out, forming the steep upper slopes of the Mont Terri. To the south, the gentle and highly eroded relief consists of soft rocks such as Opalinus Clay, Staffelegg Formation, and Keuper (Trias), which form the core of the Mont Terri anticline.

2.2 General tectonic situation

The region of the Mont Terri between Courgenay and St.Ursanne is located in the sinistral transfer zone, which connects the northern end of the Bresse Graben with the southern end of the Rhine Graben. This zone can be described as a diffuse transfer zone with both Rhenish (NNE–SSW striking) and Permo-Carboniferous (E–W and ENE–WSW striking) faults that were active during the European intra-continental rifting phase in the Paleogene (Picot et al. 2005, Ustaszewski et al. 2005). Oblique and frontal ramps developed during the Late Miocene Jura thrusting phase, triggered at these pre-existing faults. Whereas in the Folded Jura the Malm is detached, the Malm is regarded as autochthonous north of the main thrust in the Tabular Jura. Nevertheless, folding is observed in the region of Porrentruy as well, which suggests a slight detachment of the Malm (Fig. 2-3).

In early interpretations, the Mont Terri anticline was regarded as a fault-bend fold which had developed above a frontal ramp and features an overturned forelimb, leading to a complex pattern of thrust faults, normal faults, and tectonic slabs (Freivogel & Huggenberger 2003). However, Caer et al. (2015) recently proposed a detachment fold geometry. This new interpretation considers an episode of folding followed by an episode of thrusting (Fig. 2-4). In the first step of deformation, the SE dipping former normal fault localizes the development of a detachment fold with steep limbs above the evaporitic Muschelkalk. In a second phase it is crosscut

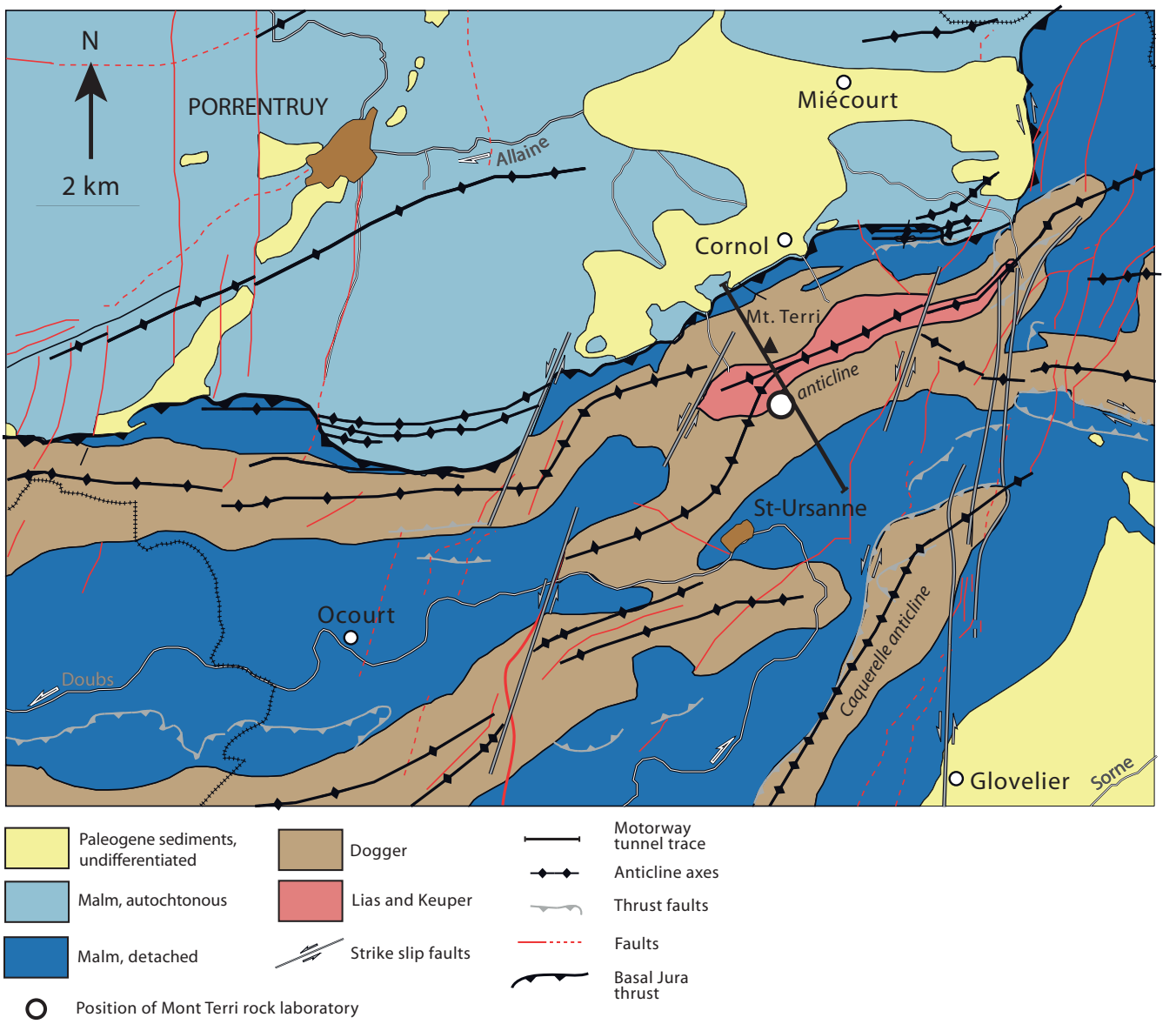

Fig. 2-3: Tectonic map of the area with indication of the drilling site and geological cross section (after Nussbaum et al. 2011).

by a low angle ramp and the hanging wall is passively transported over it. The main detachment occurred within the Middle Triassic evaporites (Anhydrite Group), which consists of sulphate beds and rock salt. Towards the WNW, the fold axis is more or less normal to the tectonic stress, which was present during the Jura thrusting phase in Late Miocene propagating from the SSE towards the NNW. Towards the WSW, the anticline splits up into two anticlines, of which the northern branch is intersected by a sinistral strike slip fault. The two branches form a lateral or oblique ramp towards the west. Whereas the Mont Terri rock laboratory is located in the southern limb of the Mont Terri anticline, the borehole BDS-5 is located in the northern limb, north of the ramp and the core of the anticline, and thus most likely above a Permo-Carboniferous graben, as postulated on the balanced section by Caer et al. (2015) (Fig. 2-4 and Appendix A).

For the prognosis of the borehole, it was not clear whether steeply or even overturned Liassic rocks would be encountered at depth or not. Another critical and uncertain issue relates to the potential occurrence of anhydrite or gypsum bearing rocks within the Keuper formation that could destabilize the borehole. From neighboring boreholes, the depth of the main thrust could be estimated with a high probability at a depth of 110 m near to the BDS-5 drill site, which equals 510 m a.s.l. Remains of strongly tectonized Paleogene rocks were expected within the main thrust fault zone, although no such zone was traversed by the motorway tunnel at the projected location. However, the tunnel crosses Paleogene rocks at its northern termination. Less information concerning the main thrust footwall was available for prognosis, since previous boreholes most often stopped right at the top of the Late Jurassic underneath the main thrust and barely retrieved more than 1 m of Late Jurassic cores. Due to outcrops in the Ajoie further to the north, it could be assumed that the bedding in the footwall of the thrust was more or less horizontal and the stratigraphy barely disturbed by tectonic processes. According to Caer et al. (2015), a thick accumulation of Muschelkalk is present below the Mont Terri anticline, and the nucleus for the initiation of the ramp was the pre-existing southern border of an assumed Permo-Carbon-

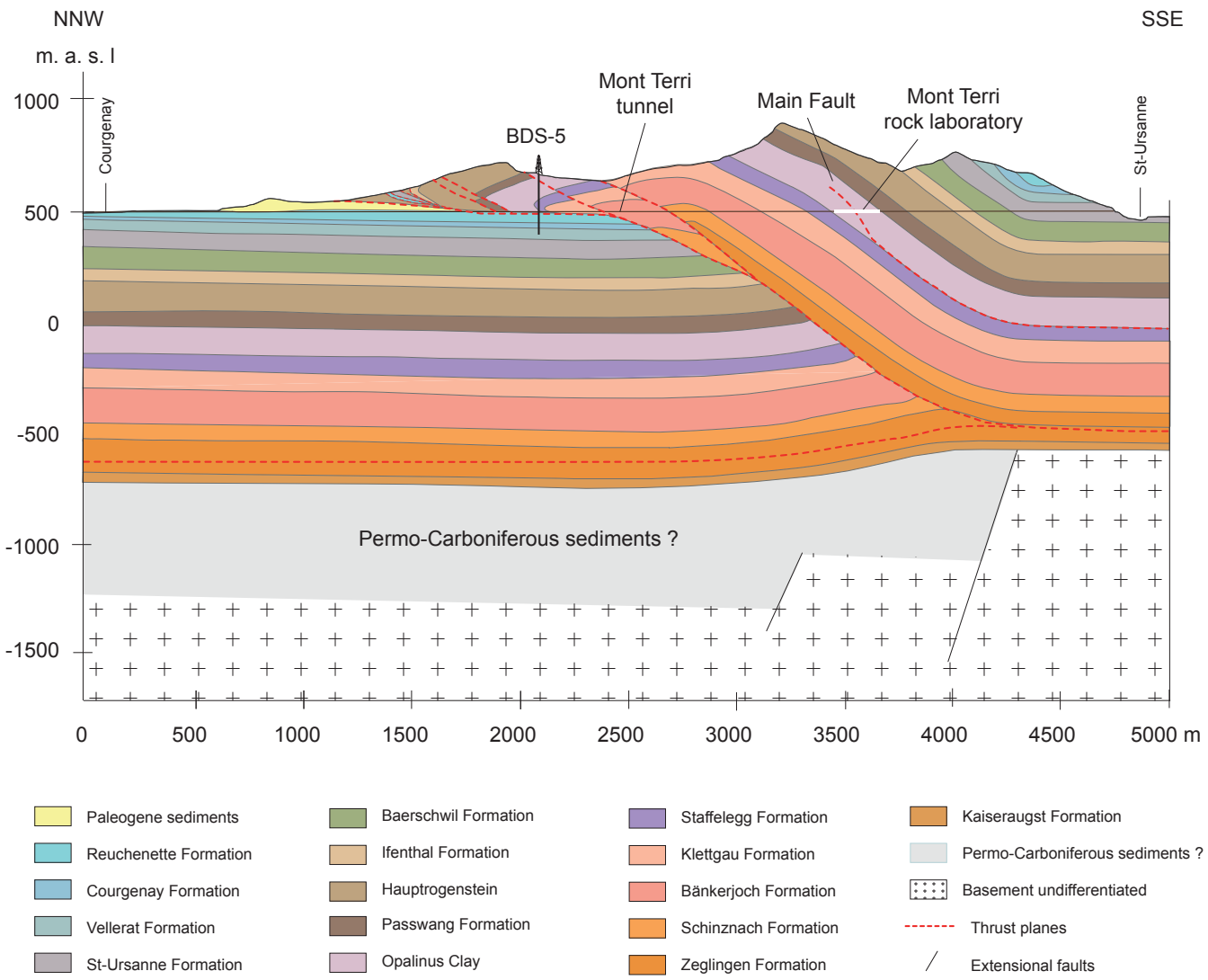

Fig. 2-4: Geological section of the Mont Terri anticline with the locations of borehole BDS-5 and the Mont Terri rock laboratory underneath the farm Outremont. Data from Freivogel & Huggenberger (2003) and Caer et al. (2015.) was used for this synthetic section, 250 m SSW of the Mont Terri motorway tunnel course.

iferous graben. The assumption of thick accumulation of Muschelkalk is based on a balanced section construction supported by mechanical analysis. The limit analysis determines the optimal deformation including faults considering the mechanical equilibrium and the Mohr-Coulomb criterion (Caer et al. 2015). Furthermore, in opposition to Freivogel & Huggenberger (2003), the footwall of the basal detachment developed a drag fold along the ramp, and the faults delimiting the imbricates of the hanging wall right in the core of the anticline are much steeper. On the original section of Caer et al. (2015), the northern limb of the Mont Terri anticline is overturned, which is a result of the extrapolation from the La Malcôte outcrop further to the east. Towards the west, the series of sections from Freivogel & Huggenberger (2003) clearly show that the strata of the northern limb are not inverted.

3. Stratigraphy, sedimentology and structural geology

D. Jaeggi, H. Bläsi, A. Morard, B. Hostettler, C. Nussbaum

3.1 Objective and methodology

The main objective of the core mapping was to get a continuous stratigraphic profile from the entirely cored borehole in order to:

- verify the completeness of the stratigraphic column and the thickness of the individual formations and members
- describe the microfacies of the individual rock types
- determine the facies distribution in the Opalinus Clay about 2 km off the Mont Terri rock lab
- determine the lateral variability of facies distribution and the possibility for regional correlation of marker horizons
- obtain the geometry and architecture of the basal detachment including the deformed rocks above and below

Core mapping was continuously performed during the drilling process. The core material was aligned, and if necessary, cut by the drilling staff with an angle grinder in order to fit into the core boxes. The PE-core boxes could be closed with a cover and were suitable for 5 m of core material. The core boxes were then carried to the core storage by the drilling staff, about 30 m away from the drill rig, and aligned there. The core material was turned axially into the position of dip direction according to the local trend observable in nearby outcrops and cleaned with a wet towel. After the approximate reorientation of the cores, a scan line was drawn on top of the core with depth marks every 20 cm and arrows indicating the direction of drilling. Once aligned, oriented, and marked, the core boxes were photographed for photo documentation (Jaeggi et al. 2012). Core mapping was performed using standard templates by the geologists D. Jaeggi, C. Nussbaum and P. Müller (all swisstopo) (Fig. 3-1). Support concerning stratigraphy was provided by H.R. Bläsi (University of Bern) (Bläsi 2011). Further support on specific formations was provided by K. Ramseier (University of Bern) for the Paleogene section and by A. Reisdorf (University of Basel) for the Middle Jurassic section.

The core material was extensively sampled by swisstopo, Nagra, University of Bern, University of Pau, and Solexperts-MeSy GmbH (Jaeggi et al. 2012). Samples were taken for thin section analysis of microfacies, structural analysis on shear zones and for measurements of magnetic properties. Argillaceous samples were immediately wrapped on-site into cellophane foil and stabilized at the Mont Terri rock laboratory with resin or vacuumed aluminum foil. Calcareous samples were not conditioned.

Fig. 3-1: Standard core mapping at the drilling site near Derrière-Monterri. (Photo © Comet Photoshopping GmbH)

3.2 Results from core mapping and thin section analysis

The detailed mapping on a scale 1:7.5 by swisstopo is provided in Appendix C. The summarized stratigraphy is provided in Appendix B and on Figure 3-2. Each formation or sub-facies encountered by the BDS-5 borehole is described below, starting with the units of the Tabular Jura in the footwall of the basal detachment.

3.2.1 Tabular Jura (footwall)

In the borehole BDS-5, the Tabular Jura is present between 216.5–102.4 m depth. The lowermost part of the borehole lies within the Vellerat Formation, followed by the Courgenay Formation and the Reuchenette Formation.

216.5–204.2 m: Vellerat Formation, Röschenz Member (Oxfordian)

From 216.5 to 204.2 m, the core material consists of beige and grey silty/sandy marls with well-cemented 5–10 cm thick calcareous lumachella beds containing a large amount of gastropods (*Natica* sp.) and oysters. Such a lumachella bed mainly consisting of gastropods with mm-size is displayed on photomicrograph P (Fig. 3-3). Apart from gastropods, bivalves and debris of echinoderms are present as well. Furthermore, foraminifera of the genus *Alveolina* are present within the Röschenz Member of the BDS-5 borehole (pers. comm. H.R. Bläsi, University of Bern). The matrix is a mudstone with clear signs of de-dolomitization. In the lowermost part of the borehole, from 215.0 to 216.5 m, some debris of a

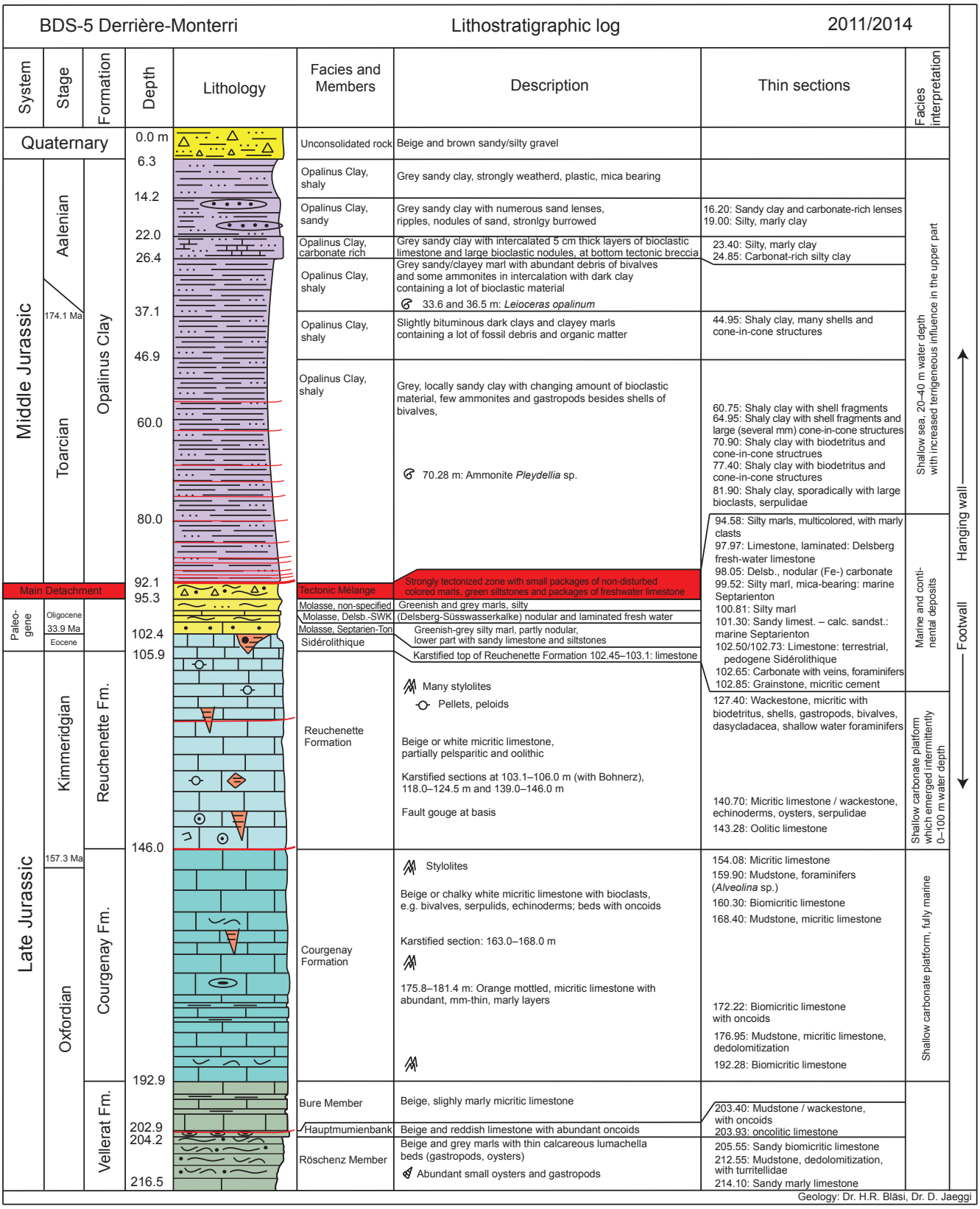

Fig. 3-2: Lithostratigraphy of borehole BDS-5 (modified after Bläsi 2011). The main detachment is highlighted in red. Folded Jura (hanging wall) is present above, Tabular Jura (footwall) below.

relatively homogeneous beige brown lime marl could be retrieved despite a significant amount of core loss. LAUBSCHER (1963) reported a total thickness of about 30 m for the Röschenz Member (former Natica Beds), with increasing content of limestone towards the bottom of the section. Considering these observations, the top of the well-bedded Vorbourg Member is expected about 15–20 m below the final depth of BDS-5. Near 214.0 m, a conspicuous layer of ooids and peloids was mapped. From 210.7 to 211.3 m, limonitic lime marl with small oysters and large amounts of biodetritic components is present.

204.2 – 202.9 m: Vellerat Formation, Hauptmumienbank Member (Oxfordian)

A conspicuous beige and reddish colored micritic limestone with large oncoids is typical for the Hauptmumienbank Member, which can reach up to 5 m thickness in the larger area. However, according to LAUBSCHER (1963), oncoids could be missing entirely in parts of the Ajoie, just north of the drill site. Photomicrograph O (Fig. 3-3) displays a mudstone to wackestone with a lot of large fossil debris with algal crusts, oncoids. The oncoids reach diameters of up to several mm. Bivalves and echinoderms are common as well.

202.9–192.9 m: Vellerat Formation, Bure Member (Oxfordian)

From 202.9 m upwards, 10 m of beige slightly marly micritic limestone of the Bure Member is present. Large, entirely preserved bivalves in their original living position brachiopods (*Zeillerina humeralis*), oysters and crinoids are present in this section. Furthermore, a layer of oncoids could be detected near 193.5 m. The lower section above the Hauptmumienbank Member consists of reddish sandy marls with a brecciated texture and with some large vugs filled with blocky sparite. Between 201.7 and 198.8 m, a marly limestone is present.

192.9–146.0 m: Courgenay Formation (Oxfordian–Early Kimmeridgian)

The Courgenay Formation is represented by beige and slightly reddish micritic limestone. From 192.9 to 173 m, thin marly layers are common, while the rock is more massive above. Near 179 m, some conspicuous, thin iron-oolitic layers are present. Photomicrographs L, M and N (Fig. 3-3) display mudstones which are strongly burrowed and which contain some fecal pellets. In photomicrograph L, large foraminifera of the genus *Alveolina* are present. Sporadically, large echinoderms and shells of bivalves occur. Photomicrograph M displays a pelmicrite (right hand side) with a reddish colored and brecciated fracture, probably still indicating some karstic influence from the Eocene Sidérolithique (laterite formation) (left-hand side). Photomicrograph N indicates small rhombohedra, which are the result of de-dolomitization. From 163–158 m, a lot of bioclastic material consisting of large oysters, gastropods and bivalves (*Cardium*) is present. The rock there consists of white chalky limestone, which is typical for the Courgenay Formation. At the depth interval from 168–163 m, first signs of karstification could be detected on the core material. Fillings of fractures there consist of greenish sandy clays with angular components. These first signs of karstification are more than 60 m below the former karstic surface the Eocene age.

146.0 –102.4 m: Reuchenette Formation (late Oxfordian – Kimmeridgian)

The Reuchenette Formation is very similar to the Courgenay Formation and also consists of beige micritic limestone with some layers of peloids or oolites. This formation marks the top of the Tabular Jura below the Mont Terri main detachment in this region. The bottom of this formation is marked by a 1 m thick fault gouge which most likely represents the filling of a major NE–SW striking normal fault dipping with 80° to the east. The fault gouge consists of angular components with diameters of up to 10 cm in a clayey/sandy matrix.

Accumulations of larger fossils and corals are present. Larger open vugs with idiomorphic calcite crystals covering the walls are typical. The rock is strongly neocrystic. Photomicrograph J (Fig. 3-3) indicates a wackestone or biomicrite with lots of larger biodetritus, bivalves, gastropods, and Dasycladaceae, a green algae and shallow water foraminifera such as *Miliolida*. On photomicrograph K a micritic limestone (wackestone) with large oysters covered with Serpulids is displayed. Small empty rhombohedras within the micritic matrix point to de-dolomitization. In some zones, the rock is slightly rose-colored and of a marble-like appearance. At 143 m, and again from 137–134 m, oolitic intervals are present. Unlike in the Courgenay Formation below, thin marly layers are only sporadically present. Near 120 m, a 60 cm thick tectonic breccia with angular components in a circumfluent clayey/sandy matrix is present and most likely marks a major fault. Vuggy porosity is predominantly present above 130 m, with increasing abundance and size towards the karstified top of the Tabular Jura. Vugs mainly developed from leached corals, which are sometimes partially preserved on the rims as recrystallized massive calcite.

3.2.2 Paleogene sediments and tectonic mélange (footwall)

In the core material of the BDS-5 borehole, Paleogene sediments including a tectonic mélange on top are present from 105.9 to 92.1 m. The former rock surface of the Kimmeridgian limestone in the footwall is located at 102.4 m. The upper part of the Kimmeridgian is strongly karstified and former cavities are completely filled up with residual deposits of Eocene age. They are followed by Septarien-Ton, Delsberg-Süsswasserkalk and a non-specified “molasse”-unit just below the tectonic mélange. The tectonic mélange builds the uppermost part of this Paleogene section.

The thickness of the Paleogene sediments (without the Eocene joint fillings) amounts to 7.1 m. A 3.2 m thick tectonic mélange of Paleogene components marks the transition to the hanging wall.

105.8–102.4 m: Sidérolithique infilling in the karstified top of Reuchenette Formation (Eocene)

The Eocene karst fills, consisting of reddish, greenish and beige clays and marls with limy components, mark a continental, non-marine depositional environment. Con-

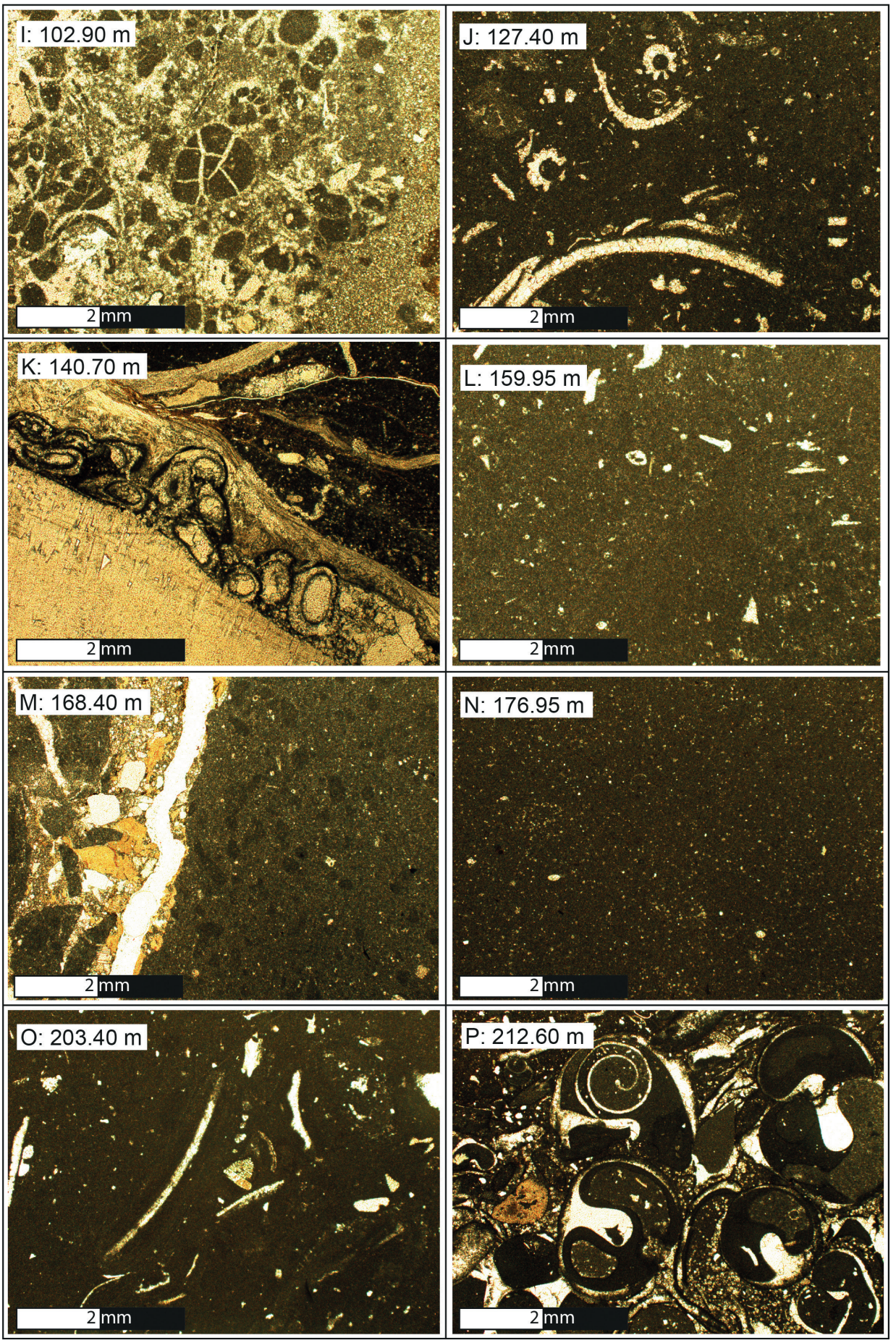

Fig. 3-3: Photomicrographs under plane light, Kimmeridgian (I–K) and Oxfordian (L–P) (see text for description).

glomerates and yellowish sandy bolus clay with abundant bean ore are present down to 104.8 m. Below that depth, a brownish karst filling with non-weathered components of Kimmeridgian limestone floating in a matrix of karstic residual clay is present. Photomicrograph H (Fig. 3-4) shows a grainy carbonate with foraminifera, conglomeratic components with pedogenic crusts, rhizocretions and components of Late Jurassic limestone including veins. The vuggy pore space is partly filled up with blocky sparite. Photomicrograph I (Fig. 3-3) shows a conglomerate with rounded components of Late Jurassic limestone and debris of echinoderms. Some of the components exhibit a remarkable mesh of veins. The conglomeratic components are covered with crusts of micritic cement.

No larger open cavities are present, causing the former karst system to be completely sealed off. The former corroded erosional surface, here the Reuchenette Formation, is conformably overlain by thin Paleogene sediments.

102.4–98.7 m: Septarien-Ton (Oligocene)

From 102.4 to 100.5 m, grey sandy limestone to fine-grained silty and calcareous sandstone is present. The rock is very well cemented; the grains are 50–200 µm in diameter, which is mostly in the fine sand fraction (photomicrograph G Figure 3-4). The glauconite and the foraminifera clearly indicate a marine environment. Then greenish-grey silty clayey and mica bearing nodular marls follow up to 98.7 m. The entire, barely 4 m thick succession clearly indicates a marine depositional environment.

98.7–97.7 m: Delsberg-Süsswasserkalk (Oligocene)

Beige crumbly, nodular, and laminated freshwater limestone originating from a lacustrine depositional environment is only about 1 m thick, but was determined by H.R. Bläsi as the Delsberg-Süsswasserkalk. The limestone is horizontally, at times even wavy layered and exhibits some calcite veins and vuggy pores filled with blocky sparite (photomicrograph F, Fig. 3-4). Small gastropods are typical, and on bedding planes, Mn-precipitations and Fe-carbonates are present. At 98.3 m and 98.5 m, two remarkable, very sharp horizontal and glassy shining contacts are present. These horizons could be of tectonic origin (probably indicative for seismic activity) and were sampled by C. Aubourg (University of Pau) in order to measure the magnetic susceptibility in the framework of the PS (Petrofabric and strain in Opalinus Clay) experiment of the Mont Terri Project (Aubourg et al. 2012). These conspicuous horizons are discussed extensively in chapter 6 of this report.

97.7–95.3 m: non-specified "molasse" unit (Oligocene?)

Above the Delsberg-Süsswasserkalk, a 2.4 m thick zone of grey and greenish silty marls is present, which most likely belongs to a molasse series. The precise stratigraphic attribution and age of this section could not be determined. It is also not clear whether this part and the strongly tectonized part above belong to the same stratigraphic unit. However, this section does indicate apparently normal stratigraphic succession above the Delsberg-Süsswasserkalk, which points towards a Paleogene age. Sensu stricto, this section of the borehole is still part of the main detachment's footwall.

95.3–92.1 m: Tectonic mélange

Just below the Opalinus Clay, a 3.2 m-thick tectonized zone with small packages of internally non-disturbed multi-colored marl, green siltstone and packages of freshwater limestone is present. The angular components are sometimes rotated and elongated to lenticular shape. The surfaces are very shiny, indicating shear planes that have undergone a high mechanical stress. The components most likely originate from Paleogene sediments, but cannot be attributed more precisely. Presumably, this part of the borehole represents the zone where the main shearing of the overthrust occurred.

3.2.3 Folded Jura (hanging wall)

Above the main detachment, the Folded Jura is present from 92.1 m up to the surface. The lowermost part of the Folded Jura is represented by strongly tectonized Opalinus Clay. Up to about 55 m, numerous faults and fault zones were encountered on the core material. The lowermost encountered part of the Opalinus Clay extends up to 46.9 m and is of the shaly facies type. Above and up to 37.1 m, slightly bituminous material is present with large amounts of bioclastics. Following that, a shaly facies very rich in ammonites is present up to 26.4 m, where 4.4 m of carbonate-rich sandy facies follow. From 22.0 to 14.2 m, a sandy facies was found, and the top is again marked by a shaly facies type.

92.1–46.9 m: Opalinus Clay, shaly facies (Toarcian)

From 92.1–46.9 m, a rather monotonous succession of grey, locally sandy clay with changing amounts of bioclastic material, some bivalves, gastropods, serpulids and ammonites is present. As photomicrograph D (Fig. 3-4) shows, large cone-in-cone structures of cm-size are present below large fossil debris. Macroscopically, those structures give the rock a nodular appearance. On photomicrograph E (Fig. 3-4) a biodetritic layer with associated cone-in-cone structures leads to a nodular appearance and to a harder level within the sedimentary record, which is solely of diagenetic origin, apart from the accumulation of large shell fragments. It is quite evident that more pyrite is present within the bioclastic layer than in the clay, which could be due to the presence of more organic matter during deposition. The pyrite is concentrated in aggregates of framboidal shapes.

From 92.1 to 82.0 m, the clay is strongly tectonized, which marks a somewhat gradual transition to the tectonic mélange below. Nevertheless, the rock above also remains strongly faulted up to a depth of about 55 m, where many C-type shear bands were encountered on core material (Appendix C), mostly with steep inclinations of 40–60° northwards.

Ammonites which were collected on core material are of the genus *Pleydellia* (Aalensis zone) and thus of Toarcian age (pers. comm. B. Hostettler).

46.9–37.1 m: Opalinus Clay, shaly facies (Toarcian–Aalenian)

In this section, slightly bituminous dark clays and clayey marls with large amounts of small dispersed fossil debris, mostly from bivalves (*Bositra buchi*), and organic matter are present. At several locations, bedding parallel spurs and grooves, as well as coal fragments, could be found on the

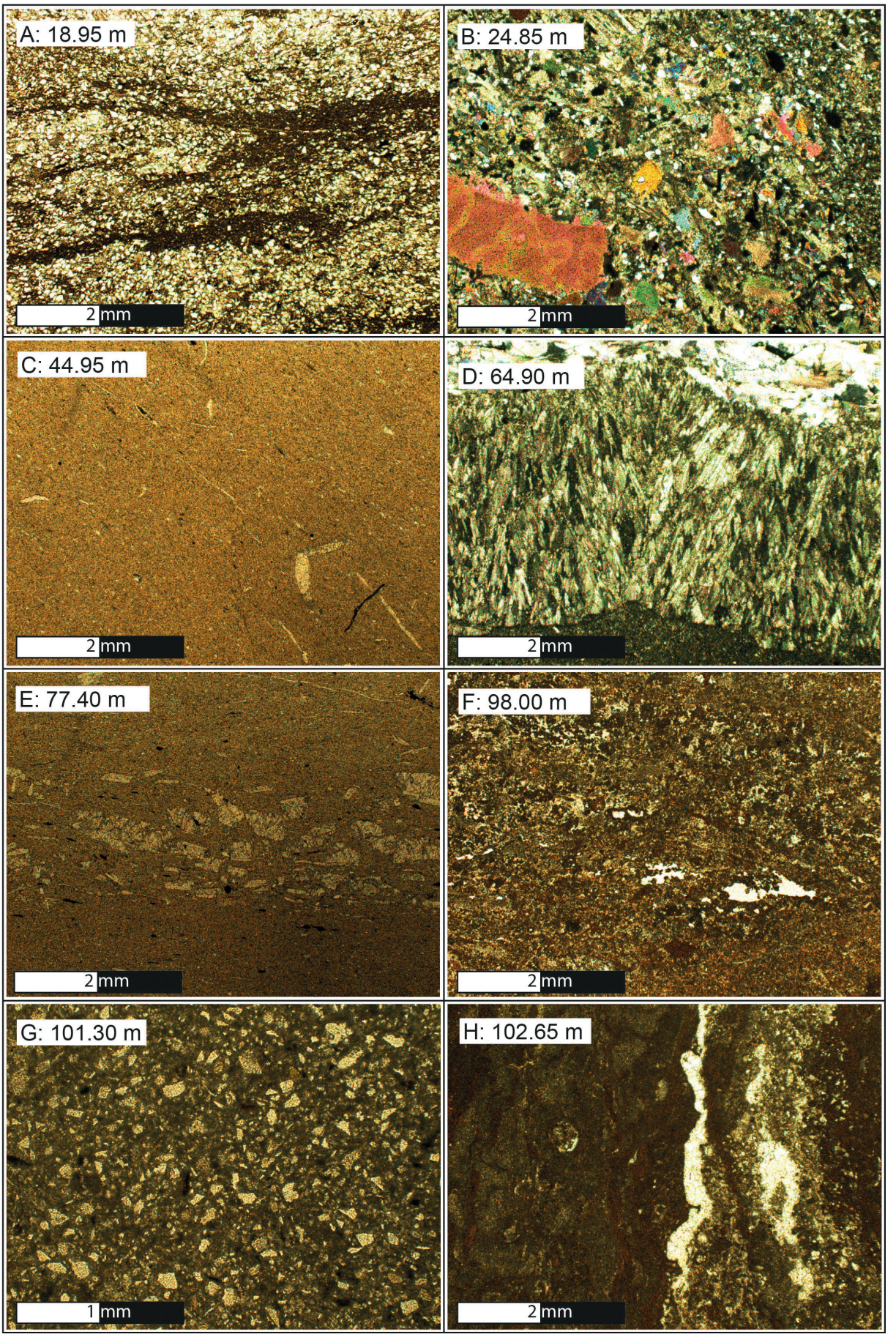

Fig. 3-4: Photomicrographs under plane light, except photomicrograph B, which is polarized, Aalenian (A, B), Toarcian (C–E), Paleogene (F–H) (see text for description of photomicrographs).

bedding planes. On the photomicrograph C (Fig. 3-4), many small and very thin shells of bivalves are visible. Furthermore, many cone-in-cone structures are present in the clay, often located below some larger fossil debris, e.g. bivalves. Faults are still present, although no conspicuous shear zones can be observed anymore. The first biostratigraphic evidence of the Torulosum subzone could be found (pers. comm. B. Hostettler) at 40.8 m, and is thus of Toarcian age. However, the transition to the Aalenian could be located some meters above as well. Due to the few documented ammonites in this section, the transition cannot be located more precisely.

37.1–26.4 m: Opalinus Clay, shaly facies (Aalenian)

The shaly clay can be described as a grey clayey silty marl with abundant debris of bivalves and echinoderms with intercalated m-thick dark sterile clays. Several ammonites with diameters up to 5 cm could be detected on the core material, which all belong to the genus *Leioceras* and thus clearly are part of the Opalinum zone. At 32.7 m and 27.2 m, conspicuous layers with idiomorphic pyrite crystals of 1 mm diameter are present. Characteristic nodules of pyrite, some of which even build cm-thick layers, are also known from boreholes in the Mont Terri rock laboratory, where they predominantly occur slightly below the carbonate-rich facies and thus in a comparable stratigraphic position.

At 26.4 m, a remarkable NE–SW striking tectonic breccia dipping with 60° to the east abruptly separates the shaly facies from the carbonate-rich facies above.

26.4–22.0 m: Opalinus Clay, carbonate-rich facies (Aalenian)

A grey sandy clay with intercalated 5–10 cm thick layers of bioclastic limestone and large bioclastic nodules is present between 26.4 and 22.0 m. Fragments of echinoderms up to 3 mm in diameter are evident on photomicrograph B (Fig. 3-4). The large fossil debris is often covered with pyrite. Lenticular accumulations of large fossil debris are typical for this facies type. Burrowing led to a nodular and irregular appearance of the rock. Due to the good cementation and high carbonate content, the rock is quite hard and the cores exhibit a characteristic white color.

22.0–14.2 m: Opalinus Clay, sandy facies (Aalenian)

Further up, the rock contains less carbonate, yet still a lot of quartz accumulated in numerous sandy lenses and small layers. The matrix of the rock exhibits a higher quartz content as well. The quartz content at photomicrograph A (Fig. 3-4) is about 30%. Carbonate is quite abundant as cement within the silty lenses but also in lenticular accumulations of bioclastic material. Some mica and greenish glauconite grains and opaque pyrite are present as well. Burrowing seems to be important and many sedimentary structures might have been wiped out. Nevertheless, sedimentary structures such as starved ripples and flat lenses are present at some locations. Burrowing furthermore led to a nodular appearance of the rock. Bedding plane orientation as recorded on core material seems to be at around 25° towards the north.

14.2–6.3 m: Opalinus Clay, shaly facies (Aalenian)

The grey argillaceous rock is brittle. Bedding or rather lamination is clearly visible and dips about 30° towards the north. Below 13 m, the rock is no longer weathered and structural features can be seen much more clearly. The number of thin sand lenses or even layers of silt increases with depth. Burrowing and even ripples are visible. Grey clay containing few strongly weathered, silty lenses, builds the top bedrock surface at a depth of 6.3 m. It can be assumed that the Quaternary deposits did slide on the weathered bedrock surface, and may still do so.

6.3–0.0 m: Quaternary deposits

Unconsolidated loose rock was encountered down to a depth of 6.3 m below ground. Directly above the rock surface, a beige gravel with lots of angular fragments of the Hauptrogenstein marks the transition to loose rock deposits, sitting on top of reworked and weathered Opalinus Clay. It is presumed that this colluvium could stem from a small landslide. From 3.2 to 3.0 m, an old, rather organic-rich topsoil is present.

Finally, beige silty made ground with lots of Hauptrogenstein components, some brick pieces and coal particles build the uppermost and youngest cover at the drilling location.

3.3 Geophysical logging

The borehole was extensively logged by the company Terratec from Heitersheim, Germany. During four logging campaigns (see Tab. 1-1) the following logs were performed: Gamma ray (GR), spectral gamma ray (SGR), resistivity (DIL/ELOG), full wave form sonic (FWS), temperature conductivity (TC), acoustic borehole imager (ABI), caliper (3 arms, non-oriented or 4 arms, oriented) (Klaudius et al. 2011). In the latter report, the raw files of all performed logs and the tool sheets are given as well. Only the most important results are summarized and given in a composite log in the present report (fold out in Appendix D).

The geometry of the borehole was measured with a 3-arm caliper during the first two logging campaigns and with a 4-arm caliper in the third and fourth one. The deviation of the borehole was determined from the built-in magnetometer and accelerometer of the acoustic borehole imager (ABI) tool.

All logs were carried out in the borehole filled up with inhibitive drilling mud (polymer guar gum). The drilled diameter of the logged borehole in the upper part (0–113.5 m) was 122 mm and in the lower part (113.5–216.5 m) 101 mm.

3.3.1 Gamma ray (GR)

The natural gamma ray measurement (GR), which is integrated in most logging tools, was used for measuring the counts per second (cps) of the natural total gamma radiation. The gamma counts have not been calibrated for American Petroleum Index (API).

The natural gamma ray measurement shows 75 cps in the upper weathered shaly facies of the Opalinus Clay, about

50–75 cps in the sandy facies of the Opalinus Clay, and about the same in the carbonate-rich facies, although there with minima below 50 cps. From 26.4 m down to 92.1 m, the shaly facies exhibits values of 75–100 cps, locally of up to 125 cps. At 73 m, for instance, more clayey intervals are present. Compared to the superficial shaly section, the rock here is not weathered, suggesting no influence of meteoric water and de-compaction due to swelling. The sandy and carbonate-rich sections of the Opalinus Clay clearly show lower values, which is due to a lower content of clay minerals.

50–75 cps could be measured within the tectonic mélange from 92.1–95.3 m. The freshwater limestone at 98 m showed very low values with 25 cps, whereas the rest of the molasse exhibited values of 50–75 cps.

Below the main detachment in the footwall, down to 130 m, counts of 10–25 cps were measured, increasing to 25–40 cps for the section between 130 and 146 m, indicating a slightly higher clay content below the oolitic section. Very constant values of 25 cps were measured from 146–160 m. The lithostratigraphic border from Reuchenette Formation to Courgenay Formation is present at 146 m. From 160 to 166 m, 20–40 cps and from 166 to 202 m, 10–30 cps were measured, indicating an alternation of rather pure limestone and slightly marly sections or thin marly layers. Below 202 m, the environment becomes marlier again, and the counts vary between 20 and 75 cps.

3.3.2 Spectral gamma ray (SGR)

In addition to the standard GR probe, a spectral gamma probe was used, measuring the full energy spectrum and allowing for the determination of the K, U and Th concentrations. The splitting of the total signal into these fractions is of special interest to the geological interpretation of transitions and boundaries between formations and members.

In sedimentary series, U-Th isotopes originate from weathering products of igneous origin. U-Th events (peaks or minima) often indicate sequence boundaries or horizons of reduced or missing sedimentary accumulation such as hardgrounds. For sedimentological studies, the Th/U-ratio is an indication of the degree of weathering.

At the borehole BDS-5, the spectral gamma ray is relatively high down to 102 m. Below that depth, it is in general quite low. About 16 events of increasing and decreasing U3O8 could be detected within the 86 m of Opalinus Clay, which are due to the cyclic depositional environment and which could be related to the coarsening upward cycles postulated by Wetzel & Allia (2003). However, due to the high tectonization, a sound interpretation of depositional cycles is not possible.

Below, within the limestone of the Malm, conspicuous U-Th peaks could be detected at 144.5–146.5 m, at 184–186 m, and near 202–204 m. At 144.5 to 146.5 m, the transition from Reuchenette Formation to Courgenay Formation is present, which can also be seen in the U-Th record. The event at 202–204 m is right at the location of the Hauptmumienbank Member.

3.3.3 Resistivity (DIL, ELOG)

Resistivity measurements were performed using both a dual induction (DIL) and a 16”–64” laterolog (ELOG) probe. Both probes use two different electrode spacings in order to measure the near and far field resistivity within the formation.

From 12–25 m the resistivity increases from 10–40 Ωm, indicating an increase of sand and carbonate content. Between 25–90 m within the lower shaly facies the resistivity is low. From 90–100 m within the tectonized zone about 10 Ωm are measured. In the Malm rocks, resistivities are remarkably higher at 100–5000 Ωm. However, the high resistivity near 130 m might be an artifact. There is no geological explanation for this remarkable peak (see Appendix D). The marly zone below 202 m shows a higher long normal (LN) resistivity than the short normal (SN) one, which could be due to the mud cake, which exhibits a higher electrical conductivity. In general, SN should be equal to LN in low permeable zones, and in permeable zones such as fractured limestone or sandstone, LN should be higher than SN due to the mud cake. However, since the borehole was drilled with polymer (guar gum), the conductivity near or at the borehole wall could be increased within marly zones as well, similiarly, for instance, to the area below 202 m.

3.3.4 Full wave form sonic (FWS)

With the full wave form sonic log (FWS), the full sonic wave-train at all three receivers, including the velocity of the first arrival, is recorded simultaneously. Elastic parameters of the surrounding rock mass can be estimated with this data.

The velocity profile deduced from the FWS log shows p-wave velocities (Vp) continuously increasing from 2000–3000 m/s for the depth range of 13 to 26 m. This increase of velocity is on the one hand due to the increasing content of sand and carbonate, but on the other hand also due to decreasing influence of weathering and decomposition of the rock mass with increasing depth. At 26 m, there is a peak of 4200 m/s. Below, values ranging between 2000 m/s and 2500 m/s are measured within the shaly facies of the Opalinus Clay. The limestone of the Malm exhibits values for Vp of about 5500 m/s, and while the marls of the Röschenz Member do so below 3000 m/s.

The elastic parameters were calculated using a density of 2.45 g/cm^3 for the clays above the main detachment and 2.6 g/m^3 for the Late Jurassic limestone below. Only values for Dynamic Poisson’s ratio and Young’s modulus are given on the composite log in Appendix D. Poisson’s ratio ranges from 0.2–0.3 in the Opalinus Clay, with an increasing tendency with depth, and 0.3 in the limestone of the footwall. Young’s modulus is at around 0.5–2 GPa in the Opalinus Clay and 40–60 GPa in the limestone of the footwall.

3.3.5 Temperature conductivity (TC)

Temperature and conductivity measurements were taken with a TC-probe.

The TC-logs do not indicate anything special. In general, the logging was performed right after the drill rods or the

packer systems were removed, and as such, the profile was always disturbed. Conductivity, which generally ranged between 1000 and 1100 µS/cm, was strongly influenced by the content of polymers (guar gum) in the upper section. In the lower section, conductivity ranged between 600 and 800 µS/cm. The general temperature trend is an increase with depth, and no anomalies can be observed on these disturbed profiles.

3.3.6 Acoustic borehole imager (ABI)

A continuous high resolution 360 degree image of the borehole wall could be created with the acoustic borehole imager (ABI). Orientations of structural features such as faults, fractures and bedding planes could be determined on the log directly, particularly by analyzing the amplitude image, which represents changes in the acoustic signal of the rock.

The acoustic hardness of the rock is represented by the amplitude image on the left side, showing mineralogical changes or differences in the cementation. On the right-hand side, locally washed out marly or less cemented layers exhibit a longer travel time, indirectly also highlighting changing rock types.

At a depth of 25 m, the change from a more carbonated facies of the Opalinus Clay to a sandier one below is well represented on the acoustic image (Fig. 3-5). The acoustic hardness of the rock decreases and a clear layering of clay and intercalated sand lenses becomes visible. Furthermore, due to some washing out of less cemented loose layers, the bedding is clearly represented in the travel time image. A 60° steep fault, consisting of a tectonic breccia, is known at 26.4 m from the core material. In the acoustic images, this structure is represented by both amplitude and travel time. The tectonically induced zone of weakness was washed out through the drilling process, leading to some topography on the borehole wall, which was detected with the acoustic probe. At greater depths, there is another remarkable change to a rather homogeneous shaly part of the Opalinus Clay.

Within the Paleogene section from 97.7 to 98.7 m, several horizontal limestone layers are present, causing a high amplitude on the acoustic image (Fig. 3-6). One of those hard limestone layers is marked in the figure (A). The more marly zones in between are slightly washed out, leading to enhanced travel times on the right hand side of the log.

The Delsberg-Süsswasserkalk is a laminated limestone, sometimes with wavy lamination, with some marly layers in between. The transition to the underlying Septarien-Ton is sharp on both acoustic images, the amplitude image as well as the travel time image. The mostly marly section contains larger nodules of calcareous components, probably well cemented concretions (feature B on Fig. 3-6). The nodular character of the rock is highlighted by high-amplitude reflections and low travel times. Within the Septarien-Ton bedding is no longer visible from the acoustic image alone.

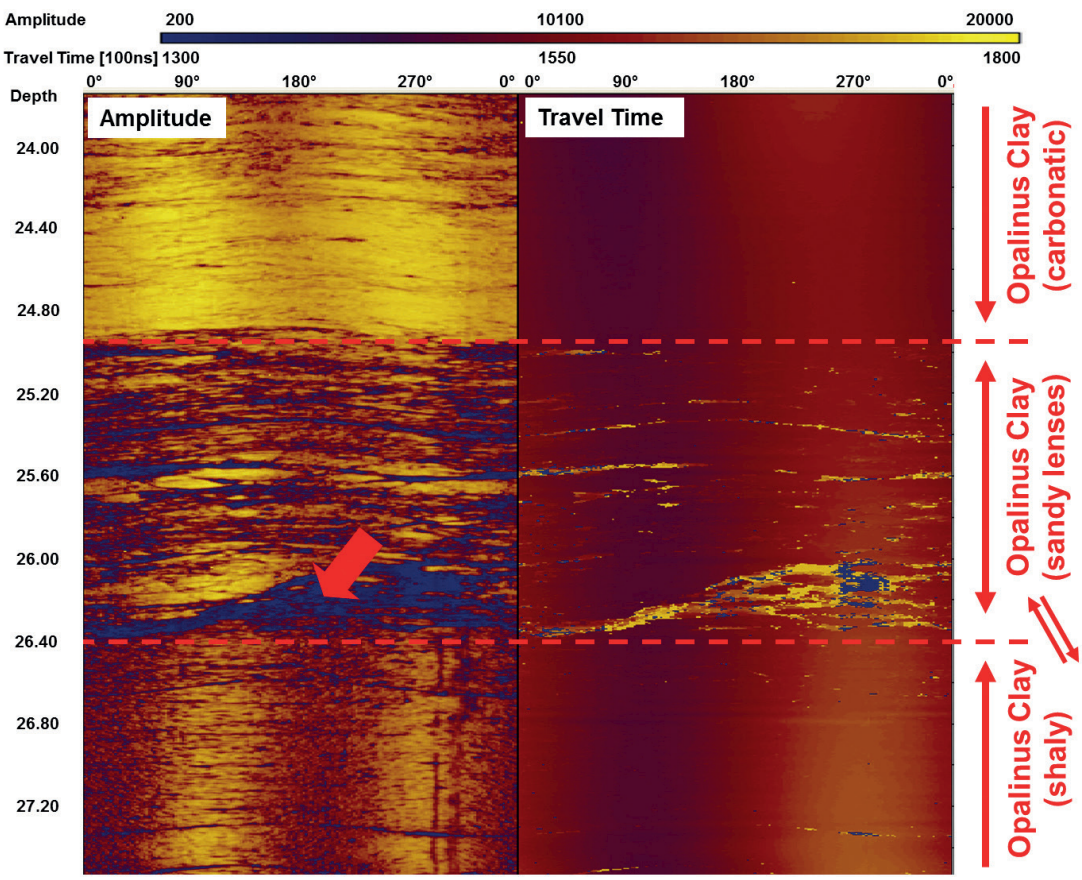

Fig. 3-5: Acoustic image of the interval 23.8–27.4 m with sharp transitions between the three different lithofacies types within the Opalinus Clay. Arrow indicates a 60° steep fault, consisting of a tectonic breccia.

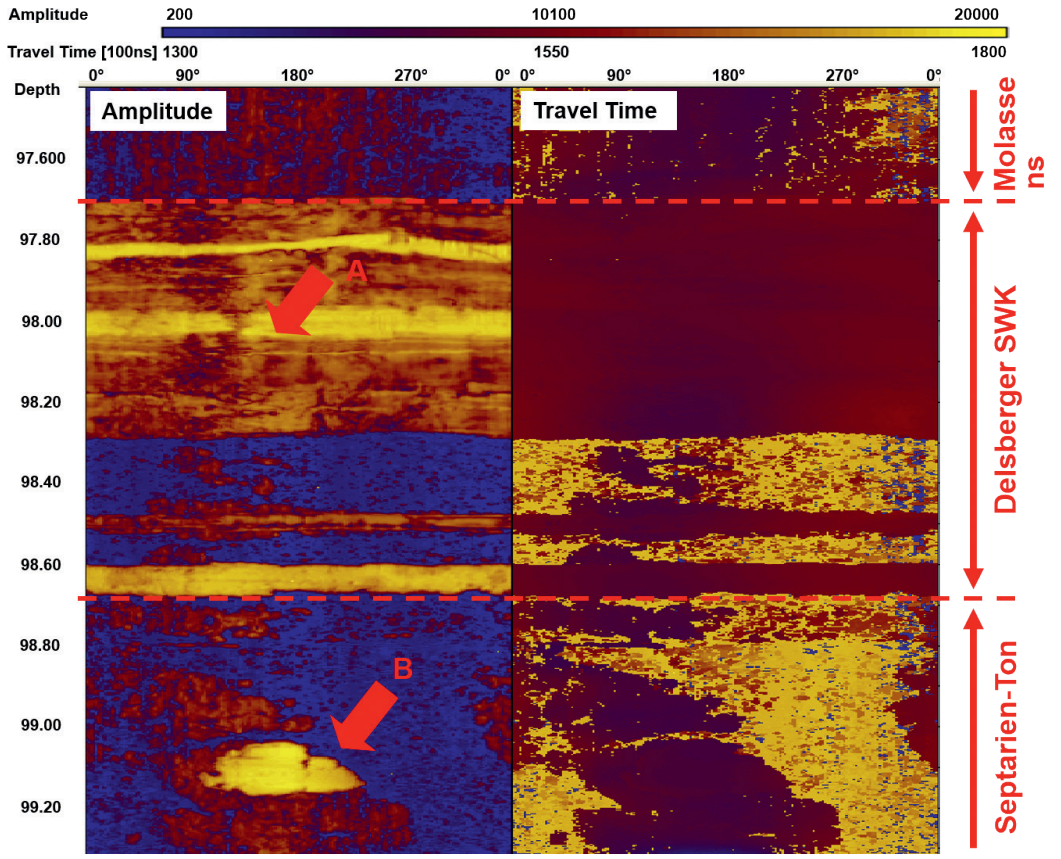

Fig. 3-6: Acoustic image of the interval 97.5–99.3 m with sharp transitions within the Molasse section. Molasse ns indicates non-specified Molasse..

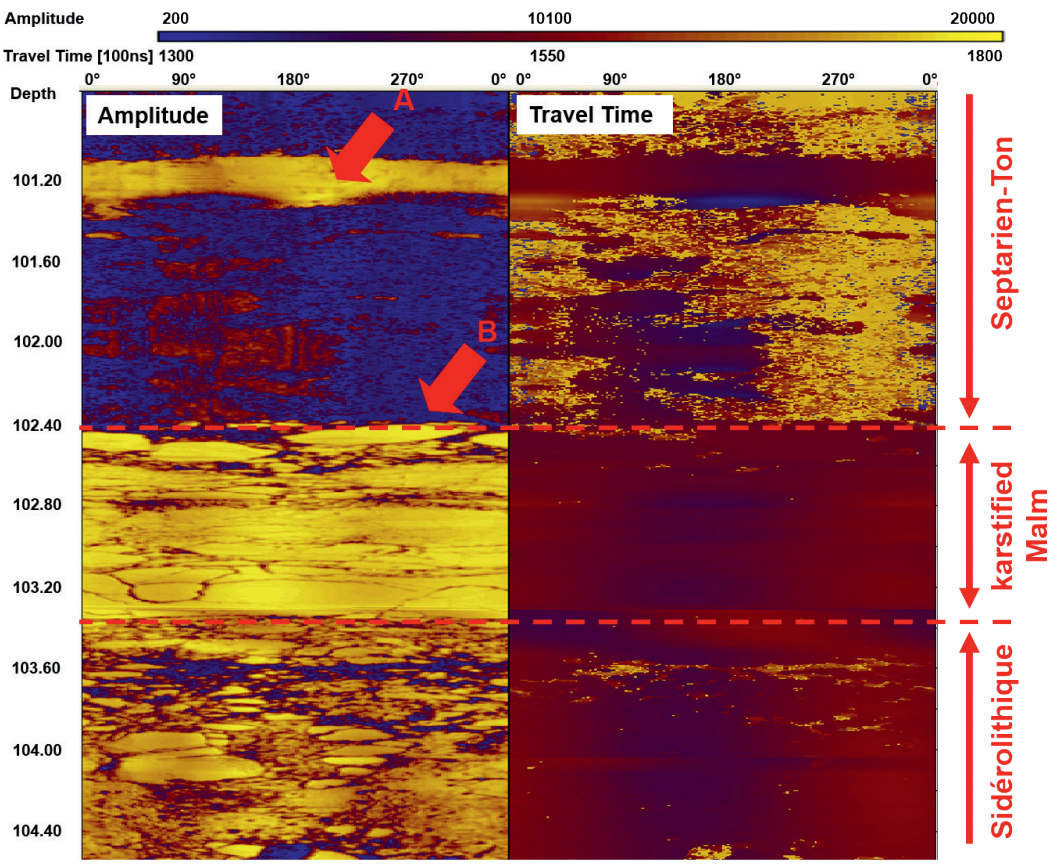

Fig. 3-7: Acoustic image of the interval 100.8–104.5 m with sharp transitions within the Molasse section and the transition to the karstified limestone of the footwall (Malm) (zoomed in).

The Septarien-Ton in the lower section exhibits some calcareous layers as well (feature A on Fig. 3-7), apart from the nodules observed above. The nodules in the lower part are rather elongated and a clear layering is visible, especially on the travel time part of the acoustic image.

At 102.4 m, the Septarien-Ton directly overlies the karstified top of the limestone in the footwall (feature B), which in this borehole consists of beige micritic limestone of the Reuchenette Formation. The limestone is strongly fractured, with most fractures being solution-enlarged and filled up with multi-colored residual clays, mostly bolus clay of Eocene age (Sidérolithique). However, the transition to the underlying Late Jurassic limestone is rather diffuse since (Sidérolithique) with bean ore (Bohnerz) – so-called bolus clay – is present from below 103.3 m down to a depth of 105.9 m, filling up a larger cavity within the limestone (Fig. 3-8).

The nodular character of the clayey to marly filling of the karst pocket within the Late Jurassic limestone is nicely represented, especially within the amplitude image of the acoustic log. The nodules mostly consist of non-weathered Late Jurassic limestone in a clayey matrix including abundant bean ore grains with diameters of up to 1 cm. When comparing the images of amplitude and travel time between the bolus clay section and the Septarien-Ton section, it becomes evident that the bolus clay is much better cemented and stiffer than the Septarien-Ton, where the drilling process obviously led to some borehole roughness (see travel time image for Septarien-Ton in Figure 3-8).

No clear difference can be seen on the acoustic image between karstified and non-karstified limestone. However, according to the observations from the core material, Eocene karst can be inferred down to several tens of meters below the top of the Late Jurassic. The limestone of the Late Jurassic is characterized by numerous fractures with thin clay coatings and fillings of residual clays. This leads to a clear shape of the fractures on the amplitude image, but does not result in a signal in the travel time image.

3.4 Structural data and observations on core material and ABI

Bedding within the upper part of the borehole down to 92 m varies between 30° and 40° towards the north. Further down, in the tectonized section within the Paleogene sediments, bedding is more or less horizontal. Below the basal detachment within the limestone of the Tabular Jura, bedding ranges between 10–15° towards NNE. These structures could be related to the deformation in the footwall of the Mont Terri anticline or to the Eocene–Oligocene flexure along the Rhine-Bresse transfer zone.

Within the Opalinus Clay, bedding parallel faults and small shear zones with various orientations towards NW and NE could be mapped with increasing amount with depth (see detailed geological mapping in Appendix C). Below 55 m, about 1 shear zone per meter was mapped. Most often, the shear zones are irregularly shaped, making it im-

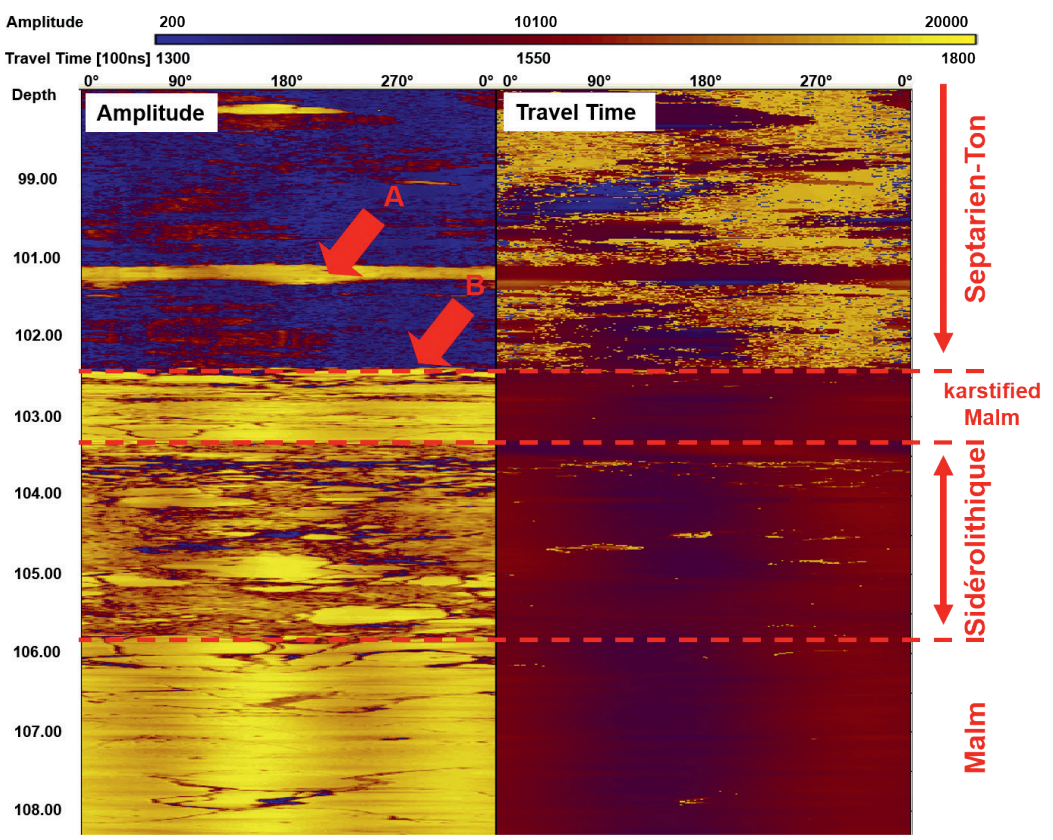

Fig. 3-8: Acoustic image of the interval 99–108 m showing the sharp transitions from Paleogene clays to karstified Malm, Eocene filling associated to palaeokarst and the non-karstified Malm (zoomed out).

possible to determine a clear orientation. At 41.8 m, however, a steeply inclined N–S striking calcite vein is present. It is presumed that this structure may be related to the formation of the Rhine Graben. Apart from this structure, normal faults or strike slip faults are not very common on the mapped core material of the BDS-5 borehole. Between 88 m and 95 m, the rock is strongly tectonized with various, mostly flat lying shear zones. As in the Opalinus Clay above, no fractures were observed in this section.

The limestones of the Late Jurassic that constitute the footwall of the basal detachment exhibit fractures as well as some larger tectonized zones such as tectonic breccias or fault gouges at 120, 130, 146 and 202 m depth. Most of them are probably related to normal faults or strike slip faults with N–S or SSW–NNE strikes and steep dips of 60–90°.

Figure 3-9 shows an example of a sub-vertical, N–S striking fault within beige micritic limestone of the Reuchenette Formation, most likely related to a strike-slip fault.

The observed fault gouges within the limestone of the Late Jurassic are mostly built of sandy/clayey, only weakly lithified material, which – due to its reduced stiffness – can be easily detected on the amplitude image of the acoustic borehole imager (Fig. 3-10). Due to the partially cohesionless sandy material, some roughness on the borehole wall is present, and consequently, the travel time image displays the shape of the tectonized zone as well.

Stereoplots of tectonic structures whose orientation could be determined were created for the hanging wall down to a depth of 92.1 m and, separately, for the footwall below 102.4 m. The hanging wall yielded a total number of 153 measurements (Fig. 3-11). The stereoplot of structures from the hanging wall shows two orientation maxima. The first set consists of bedding parallel faults dipping about 20–30° towards the north and some associated steeper dipping splays with approximately the same orientation. Those faults can be interpreted as back-thrust reverse faults in the northern limb of the Mont Terri anticline due to the thrusting of the Folded Jura onto the Tabular Jura (Aubourg et al. 2012). The faults of the second hanging wall set dip 20–40° towards E and most likely represent inherited normal faults of the Eo-Oligocene Rhine-Bresse graben system.

The second stereoplot which was created for the footwall below the basal detachment consists of 62 measurements (Fig. 3-12). Maximum density for this plot was reached at the orientation of 120°/56° (for the plane) reflecting N–S to NNE–SSW striking steeply dipping normal faults featuring fault gouges and tectonic breccias along the limestone of the Tabular Jura. As mentioned above, these faults, originally normal faults, most likely have been reactivated to sinistral strike slip faults (Ustaszewski & Schmid 2006, 2007). A second fracture set with orientations of 000°/20° is mostly related to bedding parallel faults.

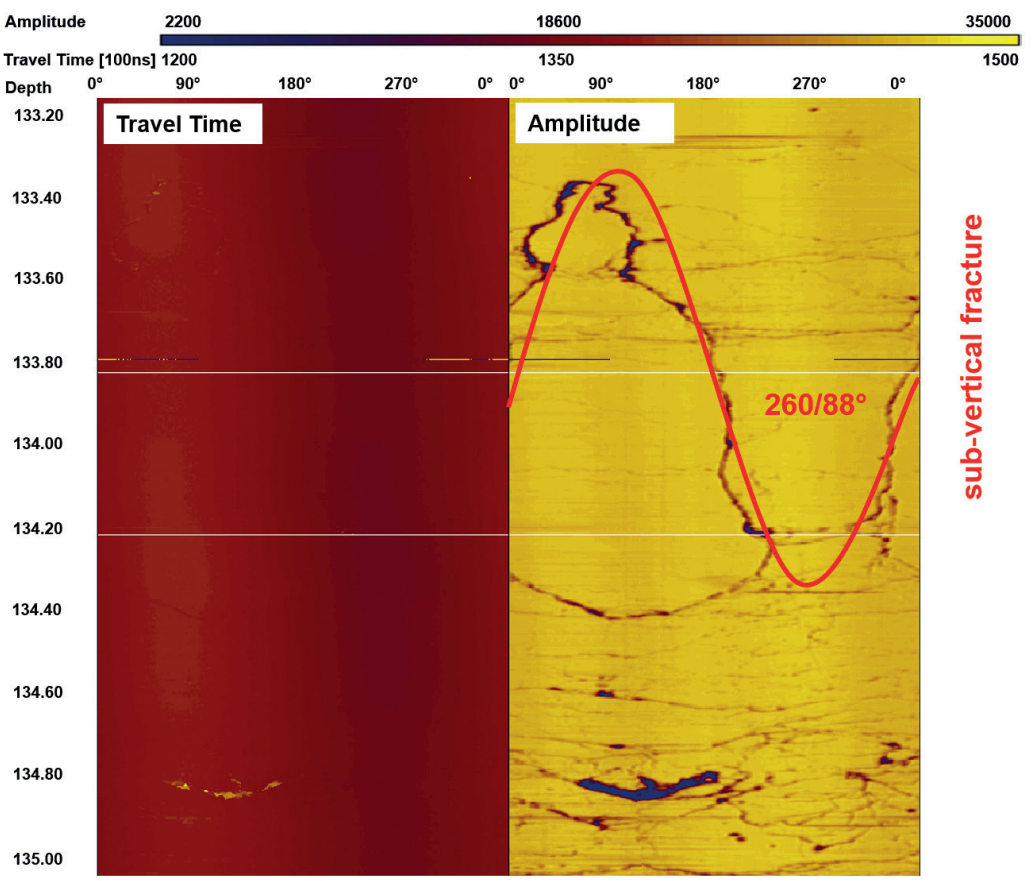

Fig. 3-9: Acoustic image of the interval 133.2–135.0 m showing a sub-vertical N–S striking fault with a thin clay filling, and is thus only displayed on the amplitude image. The white stripes are due to missing data from the log.

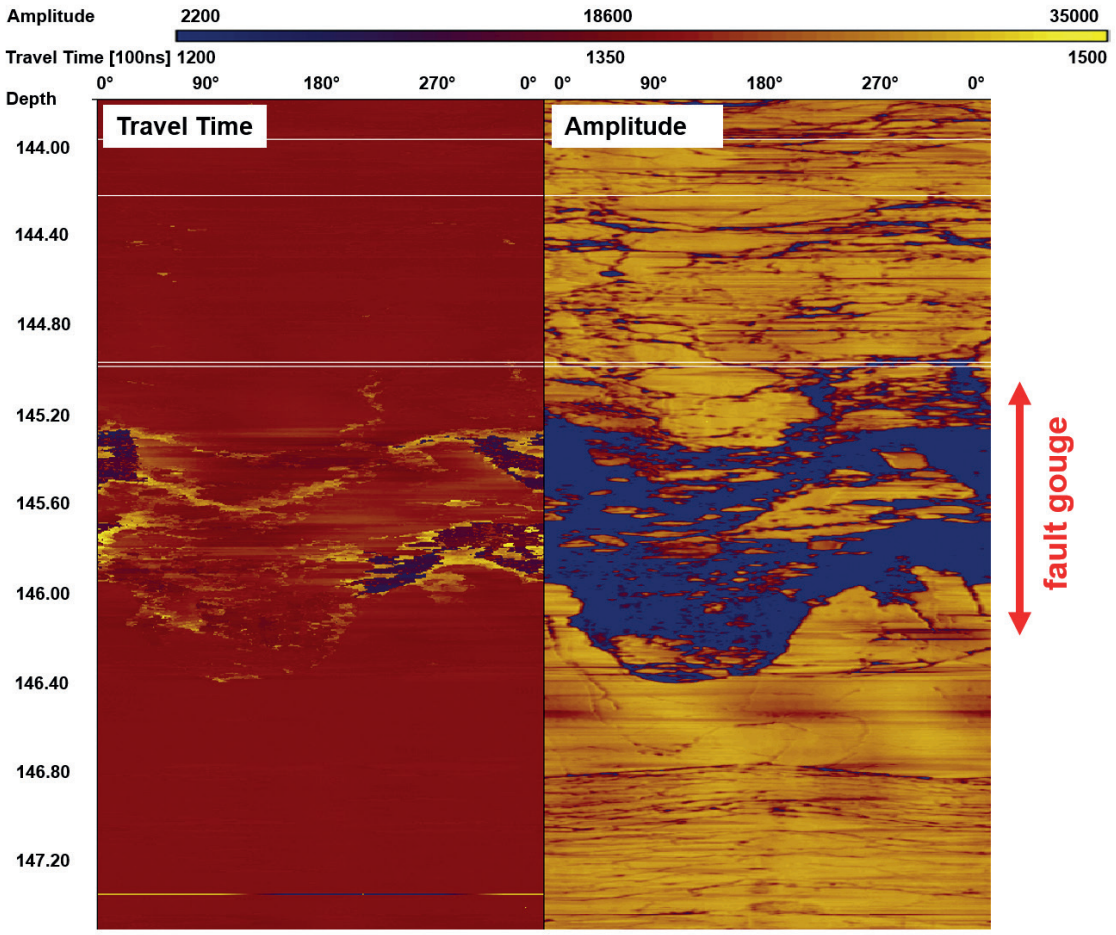

Fig. 3-10: Acoustic image of the interval 143.8–147.5 m showing a 0.8 m wide fault gouge with angular internal components of up to 10 cm diameter in a circumfluent fine-grained matrix. The zone is N–S striking with a dip of 80° towards W. The white stripes are due to missing data from the logging.

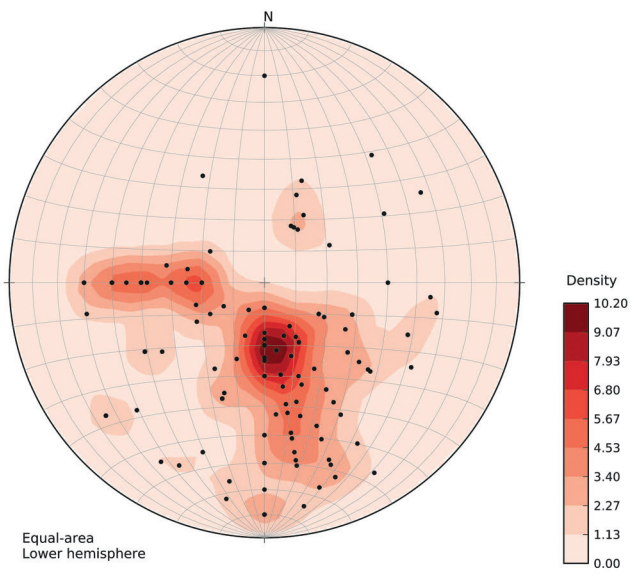

Fig. 3-11: Stereoplot (equal-area lower hemisphere) of mapped faults in the hanging wall. A total of 153 discontinuities are displayed on the plot. Maximum density: 10.2% at 180.0°/68.3° (pole) and 360.0°/21.7° (plane).

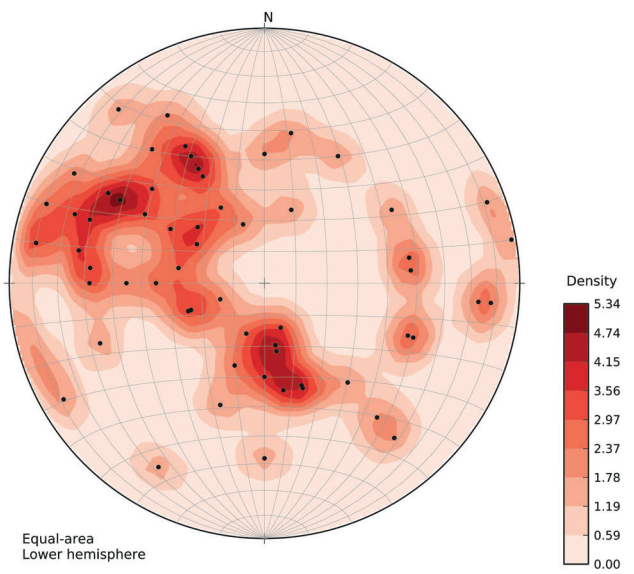

Fig. 3-12: Stereoplot (equal-area lower hemisphere) of mapped faults in the footwall. A total of 62 discontinuities are displayed on the plot. Maximum density: 5.3% at 300.0°/33.7° (pole) and 120.0°/56.3° (plane).

3.5 Key results and conclusions

The borehole consists of three main parts. Late Jurassic rocks in the footwall form the first part. On top, but still in the footwall, Paleogene rocks and a tectonic mélange just below the main detachment form the second part, which still belongs to the Tabular Jura. The third part consists of the Opalinus Clay and the capping loose rock in the hanging wall. The hanging wall corresponds to the overthrust sediments of the Folded Jura.

The footwall at the depth from 216.5–102.4 m is constituted by the Vellerat Formation with the marly Röschenz Member and the oncolithic Hauptmumienbank Member which builds an important marker horizon. On top, the micritic limestone of the Bure Member is present. Above 192.9 m, more than 45 m of beige or chalky white micritic limestone with bivalves, serpulids and echinoderms of the Courgenay Formation occurs. The upper part of this formation is karstified between the depth of 163 and 168 m, e.g. 66 m below the former topographic surface.

The transition to the overlying beige or white micritic shallow water platform carbonates of the Reuchenette Formation at a depth of 146 m is marked by a conspicuous fault gouge. This platform emerged intermittently several times, which is documented by algal mats and numerous sauropod and theropod traces (Marty 2008).

At 102.4 m, the surface of the Kimmeridgian is strongly karstified. Sidérolithique fillings of Eocene age such as bolus clay and bean ore are present. However, the former karst system is completely sealed off with residual clays. The former corroded erosional surface is conformably overlain by thin Paleogene sediments. From bottom to top the Paleogene sediments consist of the marine Septarien-Ton, the lacustrine Delsberg-Süsswasserkalk, and a thin cover of greenish and grey silty marls of non-specified sediments, most likely Paleogene as well. The total thickness of the Paleogene sediments is 7.1 m. The transition to the hanging wall is marked by a 3.2 m thick tectonic mélange.

Above the main detachment, in the hanging wall, the Folded Jura is present from 92.1 m up to the surface. The Opalinus Clay is strongly tectonized with numerous faults and fault zones up to a depth of about 55 m. Up to 46.9 m, the Opalinus Clay consists of dark, locally sandy clays with changing amounts of bioclastic material. Further up, the clay seems to be slightly bituminous with large amounts of spurs and grooves. The rock contains a lot of shells from the bivalve *Bositra buchi*. From 37.1 to 26.4 m, the clay contains large amounts of ammonites of Aalenian age as well as bioclastic material. The first indication for the transition to the Toarcian, however, was found at 40.8 m (ammonites of the Torulosum subzone). Two important pyrite horizons occur at 32.7 m and at 27.2 m. Those horizons could also be detected in several boreholes of the Mont Terri rock laboratory in a similar stratigraphic position (e.g. Reisdorf et al. 2014). Above these horizons a carbonate-rich facies (26.4 to 22 m) and a sandy facies (22 m to 14.2 m) were described on the core material. The top of the Opalinus Clay is formed by a weathered shaly facies type. The rock surface is located at 6.3 m.

Geophysical logging detected most of the lithological marker beds and furthermore indicated the nature of transitional boundaries. The eight most prominent marker horizons are listed in Table 3-1 below and are also marked on the composite log in Appendix D. Clear marks could be found on gamma ray, DIL/ELOG and FWS logs. The most prominent transitions are the intraformational boundaries from shaly to sandy to carbonate rich and once again shaly facies (marker A) in the Opalinus Clay and the transition from the Folded Jura in the hanging wall to the Tabular Jura in the footwall (marker B) at 92.1 m.

Within the Paleogene section, the Delsberg-Süsswasserkalk furthermore forms a strong lithological contrast to a rather marly section (marker C). The transition from the Paleogene to the Reuchenette Formation (marker D) leads to prominent contrasts in natural gamma count, velocity, and formation resistivity. At a depth of 130 m, an intraformational transition can be detected with the gamma ray and the resistivity, although after Hardenbol et al. (1998), no sequence boundaries or conspicuous facies changes should be present in the early part of the Kimmeridgian (marker E). Geophysical logging sometimes also detects very smooth transitions from one formation to the other (marker F). At a depth of 146 m on core material, the transition from Courgenay Formation (Late Oxfordian–Early Kimmeridgian) to the Reuchenette Formation (Kimmeridgian) was defined. It was an arbitrary definition rather than a true detection, since the boundary could only be set through knowledge of formation thickness at the regional scale. Down to a depth of 168 m, higher fluctuations of the total gamma mark the presence of Eocene karst (marker G). Further down, the signals are much smoother and no karst observations could be made on core material. The lowermost conspicuous transition was detected at 204 m, at the transition from the calcareous Bure Member and Hauptmumienbank Member (above) to the marly Röschenz Member (below) (marker H). While the total gamma count increases, remarkable decreases are recorded for resistivity and p-wave velocity.

Bedding in the hanging wall ranges between 30 and 40° northwards. Compared to the overturned beds at the same position a few 100 m eastwards, this is a very sharp change in the structural style and implies a different strain partitioning. A N–S or NNE–SSW striking fault which separates these two compartments is postulated. In the footwall, bedding ranges between 10–15° towards NNE. These structures could be related to the deformation in the footwall of the Mont Terri anticline or to the Eocene–Oligocene flexure along the Rhine-Bresse transfer zone. However, the direction is unexpected. It seems that large amplitude smooth undulations are present in the footwall. These could be linked to the folds observed in Late Jurassic rocks further north or to the presence of a Permo-Carboniferous trough. The observed dip towards NNE would then be due to the flexure of the trough fill along its southern boundary.

In the limestone of the Late Jurassic, some larger tectonized zones such as tectonic breccias or fault gouges could be detected. Most of them are probably related to normal faults with N–S or SSW–NNE strikes and steep dips of 60–90°. The structural analysis of 153 measurements in the hanging wall yielded two orientation maxima. Besides bedding parallel faults, which are related to the thrusting of the Folded Jura onto the Tabular Jura, a second set with average

Table 3-1: *The most important marker horizons encountered on the geophysical logs.*

Horizon	Depth [m]	Short description	Remarks on logging signals
A	26.4	OPA – transition carbonate-rich to shaly facies	GR increases from 50–75 cps to 75–100 cps, DIL increases from 10–40 Ωm and falls to 5–10 Ωm below, FWS reduced below by 1000 m/s
B	92.1	Transition OPA to tectonic mélange	GR decreases below from 75–100 cps to 50–75 cps
C	98	Delsberg-Süsswasserkalk	GR very low with 25 cps, FWS is increased by 1000 m/s
D	102.4	Transition Paleogene section to Reuchenette Formation	GR below is 10–25 cps, DIL increases from 10 to 100–5000 Ωm, FWS rises from 2500 to 5500 m/s
E	130	Reuchenette Formation Intraformational transition	GR increases from 10–25 cps to 25–40 cps, ELOG shows an abnormal peak of up to 5000 Ωm
F	146	Transition Reuchenette Formation to Courgenay Formation	GR below very constant at 25 cps
G	168	Courgenay Formation end of Sidérolithique karst fillings	GR higher fluctuations above (20–40 cps)
H	204	Bure Member to Hauptmumienbank Member to Röschenz Member	GR increases remarkably to 20–75 cps, high fluctuation below, DIL decreases from 100–5000 Ωm to 10 Ωm, FWS decreases from 5500 to 3000 m/s

The marker horizons are indicated on the fold-out in Appendix D.

dip 20–40° towards E most likely represent inherited normal faults of the Eocene-Oligocene Rhine-Bresse graben system. 62 measurements were performed below the basal detachment, which yielded a maximum density at the orientation of 120°/56° (for the plane) reflecting N–S to NNE–SSW striking steeply dipping normal faults featuring fault gouges and tectonic breccias along the limestone of the Tabular Jura. These faults, originally normal faults, most likely were reactivated to sinistral strike slip faults (Ustaszewski & Schmid 2006, 2007).

The lithostratigraphic data fits well into the regional setting. The Opalinus Clay encountered in the hanging wall, although strongly tectonized in the lower section, has a facies distribution comparable to the facies distribution known from the Mont Terri rock laboratory about 2 km towards the SSE. Structural data obtained from the borehole is also consistent with the data from the Mont Terri rock laboratory.

4. Hydrogeology and monitoring of pore water pressures

D. Jaeggi, J.M. Matray, D. Bailly, G. Klee

4.1 Objective and methodology

The borehole BDS-5 is located in a catchment area of superficial runoff into a small river which is hydraulically communicating with an exploited aquifer in fractured limestone about 1 km downstream. Furthermore, it is well-known that the fractured limestone of the footwall below the main detachment acts as a regional aquifer for the Ajoie plain north of the drill site. As such, the assessment of the hydrogeological situation was important for receiving permission to drill at the location Derrière-Monterri. Since the borehole was entirely drilled with polymer (guar gum) as drilling fluid, a survey of the water levels and drilling fluid losses was performed. Additionally, flux, electrical conductivity, temperature, pH and turbidity were measured regularly in sources and streamlets of the area.

At the end of the drilling activities on site, the casing of the borehole, which was installed after the first testing phase down to a depth of 113.5 m, was perforated in the depth range between 67.4–68.4 m with a 12 shot gun by BPC (Balance Point Control, Germany) in collaboration with Bereuter (Switzerland). Two absolute Keller pressure transducers PAA 36 XW were installed by swisstopo in collaboration with Stump Foratec AG at depths of 67 m and 125 m for long-term monitoring of pore pressures in the hanging wall and below the main detachment in the footwall. The two pressure transducers are connected to an autonomous GSMII data logger. The data is regularly retrieved by the swisstopo team and analyzed in the framework of the LP (Long-term monitoring of pore pressures) experiment of the Mont Terri Project. The completion of borehole BDS-5 is provided in detail in Figure 1-3.

The pressure data is regularly read out and plotted with precipitation data from the rainfall station Montenol of the Swiss meteorological service, located about 4 km to the south at a comparable altitude. The pressure data time series were analyzed on tidal effects by Matray & Bailly (2014). Generally, pore pressure time series show the occurrence of harmonics as a result of natural forcing tides. Tides are the response of the solid earth to the thermic and gravimetric stresses induced by the Sun-Moon couple. Tide harmonics with a pure gravimetric origin are the response of volumetric strain deformations of the earth crust by astronomic movement of the Moon. Their occurrence with amplitudes dominating other tides should indicate undisturbed conditions. The time series selected were first pre-processed in order to enhance or complete the signals due to data gaps, spurious values, and variable time steps. Afterwards they were processed by using statistical tools supplied by the MuStat algorithm (Bailly et al. 2012). The goals of processing were i) to verify the stationary behavior by detecting and characterizing in particular the amplitude of the selected semi-diurnal and diurnal tides on pore pressures spectra obtained by Fourier transform, ii) to assess their possible non-stationary behavior by wavelet decomposition of the time series in the time-scale domain and iii) to estimate hydraulic properties, such as the specific storage coefficient, by using simplified groundwater hydraulic models (Marsaud et al. 1993, Ababou et al. 2012). Matray & Bailly (2014) mainly focused on the four major tidal constituent's principal lunar semi-diurnal (M_2), principal solar semi-diurnal (S_2), lunar diurnal (K_1), and lunar diurnal (O_1). A listing of available semi-diurnal and diurnal harmonics is given in Appendix F. For the spectral analysis a recording rate of 15 minutes was necessary in order to obtain a sufficient resolution of the pore pressure time series.

4.2 Hydrogeological situation

The borehole is located within the superficial catchment area of an exploited communal source, located about 700 m downstream in fractured limestone of the Hauptrogenstein. The geological map of the area (Laubscher 1963) reveals (Fig. 2-2) that the borehole is located closely to colluvium deposits of the Passwang Formation and Hauptrogenstein, which form Mont Terri to the north. These loose rock deposits are mainly clayey gravels of low permeability. The rock surface at the drilling location is at a depth of 6.3 m and consists of Opalinus Clay, which builds a confined unit with permeability ranging between 1×10^{-12} m/s and 1×10^{-14} m/s (e.g. Bossart & Thury 2008). This Opalinus Clay, although strongly faulted in the lower part, can be regarded as an aquitard. The swelling minerals of the Opalinus Clay, such as illite-smectite-mixed layers, lead to self-sealing of faults or fractures. The Opalinus Clay of the faulted Jura (hanging wall) dips about 20–40° towards the NNW (Fig. 2-4). The aquifers of the Hauptrogenstein and potential water-bearing parts of the Passwang Formation are well sealed off towards the south and the borehole, and the water flows northwards or westwards, where the permeable formations crop out in the deeply incised valley. South of the borehole, mainly rocks with low permeability of the Staffelegg Formation and the Keuper are cropping out in the core of the Mont Terri anticline. These rocks are not encountered within the borehole. In the footwall, the borehole perforated strongly tectonized rocks of the Paleogene. Lugeon tests performed in the tectonic mélange during the construction of the nearby Mont Terri motorway tunnel yielded relatively low permea-

bility of 10^{-6} m/s (Norbert & Schindler 1988). Below 102.4 m, mainly carbonated series of the footwall are present in the borehole. These rocks act as regional aquifers in the Ajoie plain. Permeability there is commonly within the range of fractured carbonate rocks, although residual clays of the Eocene karst can seal off most of the accessible pore space.

The results of water level measurements during the drilling process imply that highest losses of drilling fluid (mixture of polymer based on guar gum and water) have occurred within the upper section of the borehole in the Opalinus Clay (Jaeggi et al. 2012). Another remarkable drop of the water level of about –10 m occurred at a depth of 93 m. Those losses all occurred within the clay-rich facies of the Opalinus Clay, where – from a geological point of view – no losses should occur. Macroscopically clear indications for weathering were observed in the superficial section down to about 13 m (Appendix C). Below, weathering and de-consolidation down to a depth of 30 m below surface with fracture-transmissivities ranging between 1×10^{-6} m²/s and 1×10^{-4} m²/s is possible and was reported by Hekel (1994) for superficial or exposed Opalinus Clay in southern Germany. According to this author, this zone of enhanced transmissivity is thicker on hills or at flanks. At BDS-5, enhanced hydraulic conductivities of 5.5×10^{-10} to 2.4×10^{-11} m/s have been recorded in the hanging wall, indicating, that the zone of weathering and decompaction reaches down to 90 m and consequently across the entire thickness of the Opalinus Clay. Borehole BDS-5 is clearly located in a flank position, and decompaction and rebound above the main detachment enabled a deep weathering and loosening of the clay formation.

Drilling fluid losses in the lower part of borehole BDS-5 were small. In fact, important fluid losses along this section, in particular the main thrust zone and the karstified Late Jurassic limestone, were expected and accounted for during the planning stage of BDS-5. In spite of these expectations no real permeable features could be detected along this section on cores or geophysical logs. The main reason for this observation was that solution-enlarged features and fractures were consistently clogged with clayey material.

4.3 In-situ pore water pressures

The two pressure transducers were programmed and connected to the data logger beginning August 2011. At interval 1 in the hanging wall the initial pressure (absolute pressure without compensation for air pressure) was 1.6 bar, continuously increasing to about 3.2 bar at the beginning of October 2011, without any recognizable cyclic influence. Two conspicuous sudden pressure drops in October and November 2011 occurred (Fig. 4-1). Since the end of November 2011, pressure has been continuously increasing again, although not as smoothly as before. Thus, the pressure signal within the Opalinus Clay at a depth of 67 m seems to have been influenced by external processes since then, maybe caused by a better coupling to the formation. The two sudden pressure drops after the first smooth pressurizing period are interpreted as breaktroughs of the pressure signal within the casing. The coupling to the formation at the upper interval is achieved over the 12 holes from the borehole perforation (Fig. 1-3). The sensor is located inside the casing in a gravel pack. As such, a temporary clogging of the holes could be a possible mechanism.

Even now, after three years with a current pressure of almost 4.6 bar, equilibrium has not yet been reached entirely. The pressure is still rising, although much slower than in the beginning. Taking the pressure evolution of the last three years into account, equilibrium will finally be reached at around 4.7 bar. This long-term behavior before pressure reaching equilibrium is typical for pressure measurements in very low-permeable, confined formations like the aquitard of the Opalinus Clay. A hydraulically disturbed zone is reported from the Mont Terri rock laboratory (Jaeggi & Nussbaum 2011), which is in the order of 15–20 m around the galleries. Intervals located deeper than 20 m generally exhibit a very similar pressure evolution until eventually reaching equilibrium after several years. Further effects, such as osmosis and diffusion due to the use of inappropriate fluid for saturation or borehole instability, can have an influence on long-term pressure evolution.

Interval 2, which is located in the footwall below the cemented casing at 125 m depth in the Late Jurassic limestone of the Tabular Jura, shows a very different behavior. Here, the pressure is in the order of 4.325±0.005 bar and thus varies only within a very narrow bandwidth of 0.01 bar. The variations of the pressure in this aquifer do not seem to be directly influenced by meteoric signals such as rainfall or temperature. However, regarding the hydrogeological situation, a large time shift between precipitation and pressure response seems possible (Appendix E). The aquifer between 102.4 and 204.2 m consists of Oxfordian and Kimmeridgian fractured limestone, which at least partially crops out in the Ajoie plain towards the north. Furthermore, the rocks there are not covered with an impermeable sediment cover anymore and are thus unconfined and in direct contact to the vadose zone. On a larger scale, annual periods with a minimum in spring seem to be present, even though the pressure time series is still too short for a conclusion (Fig. 4-1). If the pore pressure time series is zoomed in to a 10-day window, a clearly periodic behavior can be detected (Fig. 4-2). Two distinct peaks are present for every daily cycle, which strongly suggests an influence of diurnal or semi-diurnal tidal effects.

When comparing the heads of the two sensors to each other, there is a head difference of about 7 bar, with the higher head in the Opalinus Clay rather than in the Late Jurassic footwall. This considerable head difference suggests an overpressure in the aquitard Opalius Clay, which could be due to chemico-osmotic effects. The Opalinus Clay is bound by the surface, yielding a direct meteoric influence, and the aquifer of Late Jurassic limestone. Consequently, water with a very low salinity is transported from top and bottom by diffusion towards the aquitard Opalinus Clay, which itself exhibits a high pore water salinity. The driving process for this transport is most likely osmosis. Consequently, pore water pressure within the clay is enhanced. These effects are currently being studied in detail in the framework of the DB (Deep borehole) experiment in a 250 m long borehole at the Mont Terri rock laboratory.

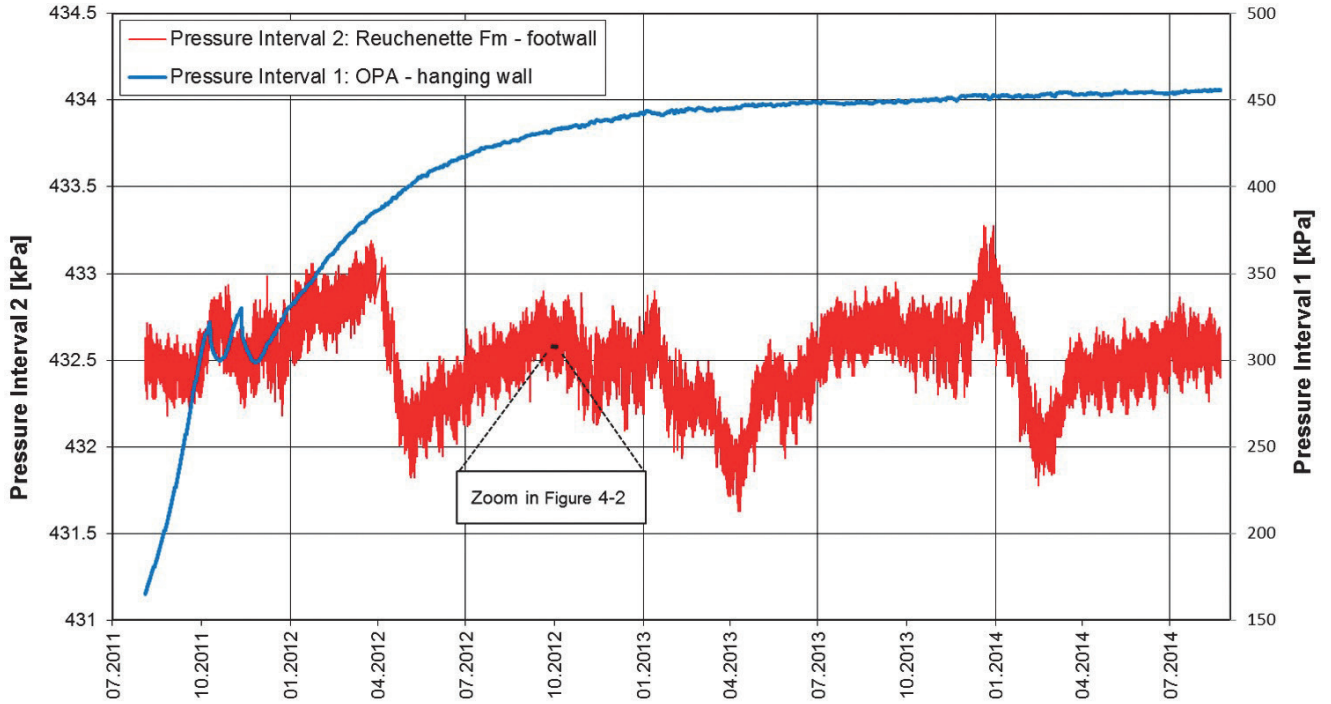

Fig. 4-1: Pore water pressure time series for interval 1 (67 m), blue curve, right axis and interval 2 (125 m), red curve left axis. Note 100× higher resolution of the left axis, red curve.

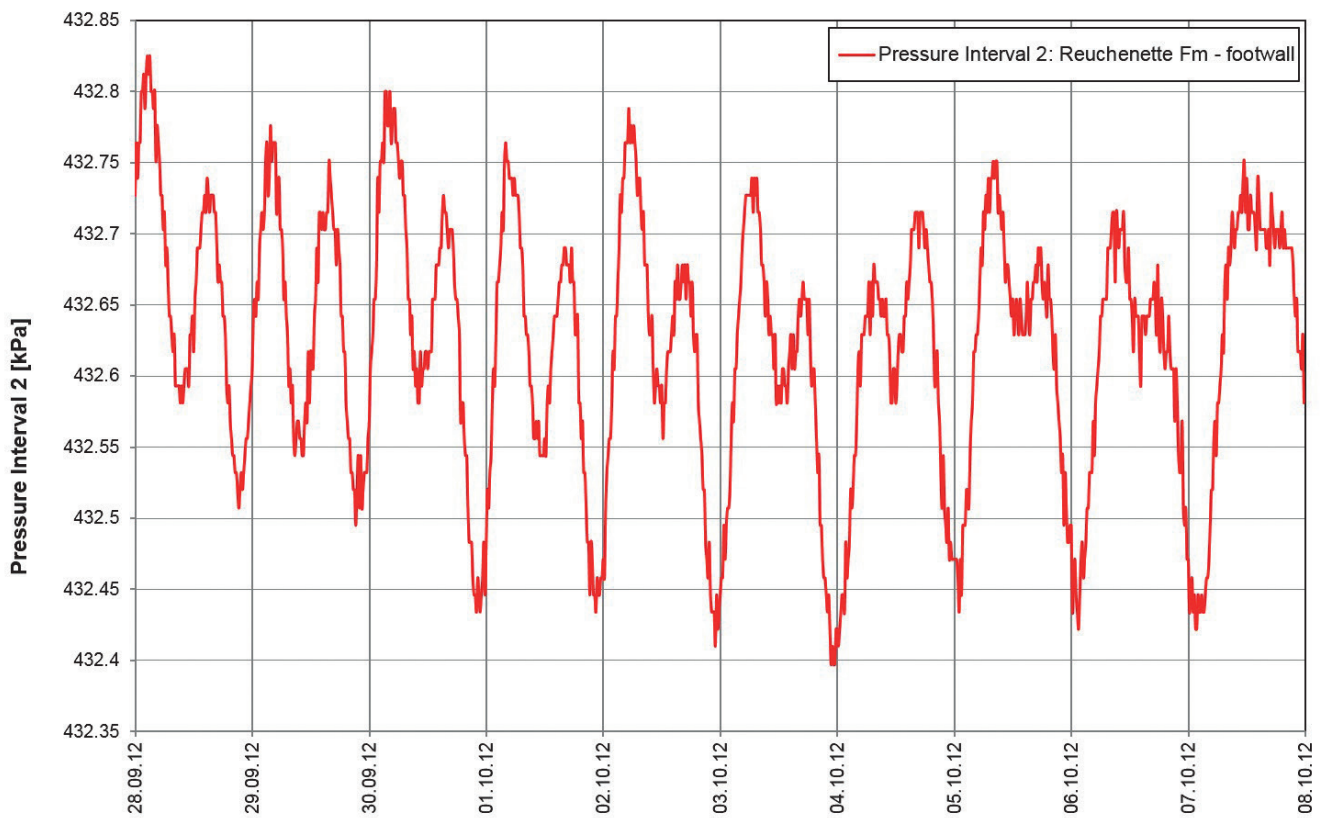

Fig. 4-2: Pore water pressure time series for interval 2 (125 m). The image shows a zoom in from Figure 4-1 to a 10-day window.

4.4 Spectral analysis of pore water pressure time series
(Matray & Bailly 2014)

For spectral analysis, selected signals are indicators of Earth crust deformation (displacements, strains) under Moon-Sun-Earth strains at the diurnal (K_1-lunar and O_1-lunar) and semi-diurnal (M_2-lunar, S_2-solar) tide components only, since the time series are not long enough to have access to annual harmonics. For the time series, a time step of 900 seconds was chosen as a good compromise between resolution and data storage.

According to the analysis of Matray & Bailly (2014) on the two pore pressure time series of borehole BDS-5, dimensional Root Mean Square (RMS) autospectra show that the four selected harmonics (K_1, O_1, M_2 and S_2) are only expressed in the carbonated footwall, below the main detachment at interval 2 (–125 m) (Appendix F). According to the authors, the occurrence and predominance of the three gravimetric harmonics (K_1, O_1 and M_2) over the solar one (S_2) strongly suggests that the porous medium is assumed to behave elastically to the effect of tidal dilatation (Fig. 4-3). Thus, all pore space is continuous and saturated with pore water. The time series of the footwall is assumed to be representative of undisturbed conditions. They could furthermore show that in the time series, pure gravimetric signals (M_2, K_1 and O_1) are very poorly influenced by atmospheric pressure. This result was deduced from the lack of M_2, K_1 and O_1 signals in the atmospheric pressure autospectra, and also from the very weak coherence function of pore-pressure versus atmospheric pressure cross-spectra at the M_2, K_1 and O_1 frequencies.

By using the very simplified Bredehoeft (1967) model, an estimate of the specific storage was attempted. This model takes into account that the magnitude of the hydraulic head fluctuation due to tidal effects is inversely proportional to the specific storage of the aquifer. This simplified model is given below:

$$\delta\epsilon_{Tidal} \approx S_s \delta H \qquad (4.1)$$

S_s specific storativity [m^{-1}]
$\delta\epsilon_{Tidal}$ amplitude for volumetric strain fluctuations related to the M_2 semi-diurnal earth tide [–]
δH amplitude of relative pressure fluctuations at the M_2-signal [m^{-1}]

Bredehoeft's model assumption neglects the grain compressibility and is thus only valid if one assumes that the medium is sufficiently consolidated. The model was applied to the Late Jurassic limestone in the footwall, which yielded a specific storativity of $2.7 \pm 0.1 \times 10^{-6}\ m^{-1}$. The calculation of S_s for the M_2-signal of interval 2 at a depth of 125 m is given in Appendix F.

In the Opalinus Clay of the hanging wall above the main detachment, results of RMS amplitude spectra indicate that the three main gravimetric harmonics (O_1, K_1 and M_2) (Appendix F) are either absent or – more likely – overwhelmed by background noise (Fig. 4-4). This result indicates that the time series is not representative of initial and undisturbed conditions. This is furthermore proven by the behavior of

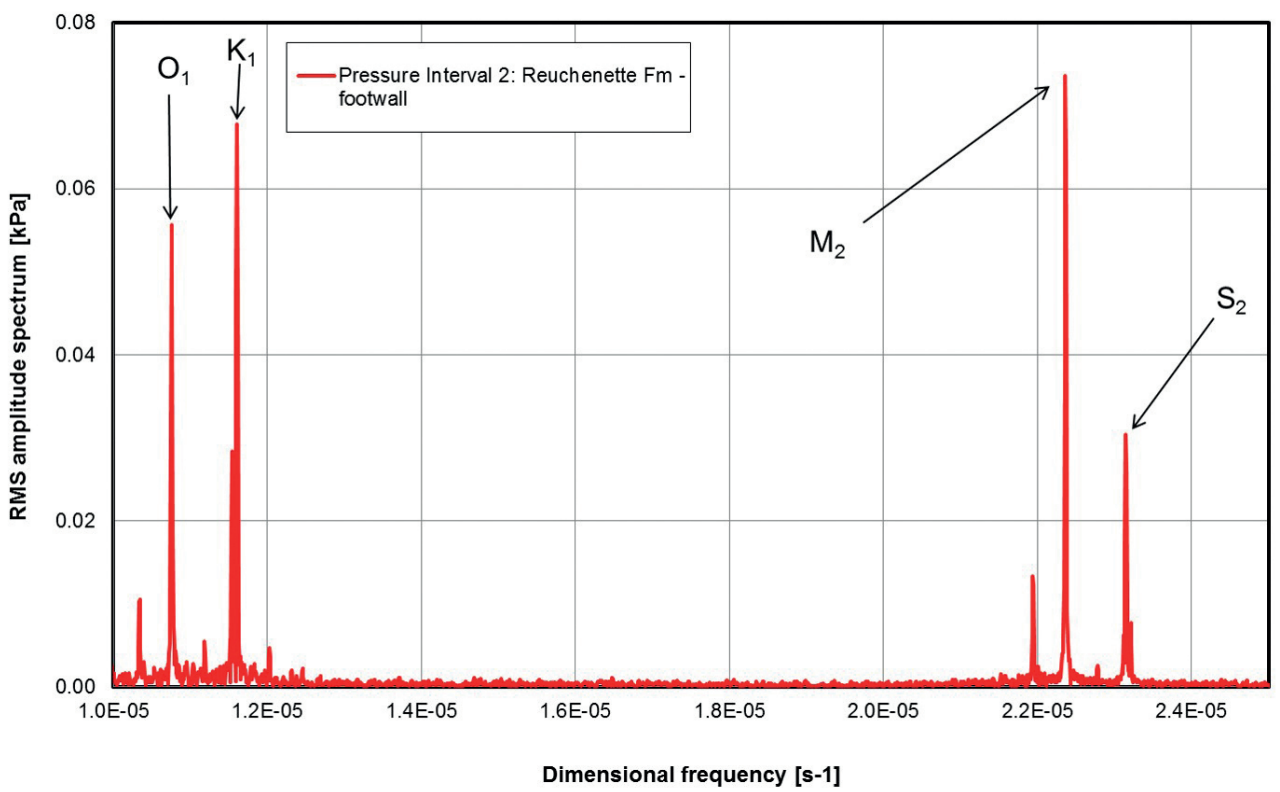

Fig. 4-3: Pressure of interval 2 (–125 m) preprocessed for the daily frequency domain. Note the occurrence of O_1 (lunar diurnal), K_1 (lunar diurnal), M_2 (principal lunar semi-diurnal) and S_2 (principal solar semi-diurnal) harmonics (from Matray & Bailly 2014).

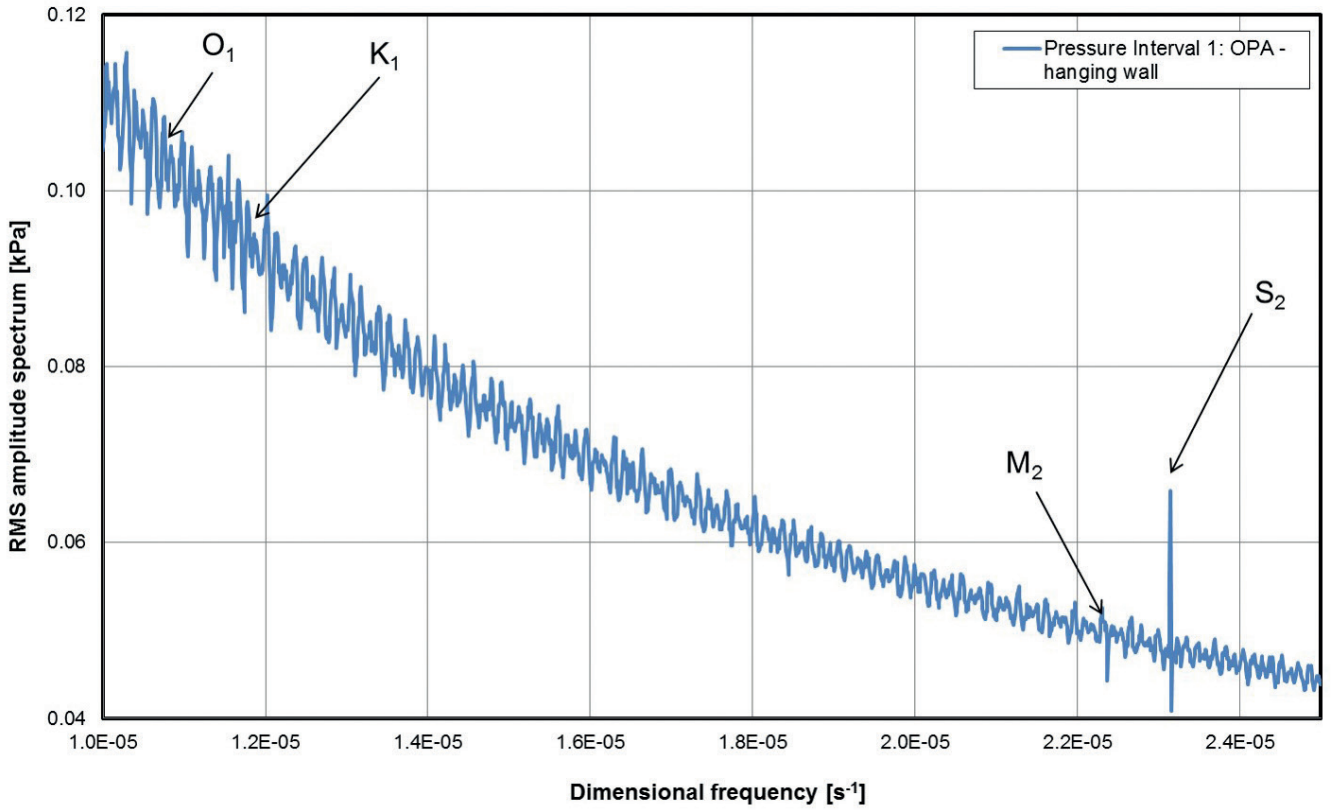

Fig. 4-4: Pressure of interval 1 (–67 m), preprocessed for the daily frequency domain. Note the occurrence of the S_2 harmonic (from Matray & Bailly 2014).

the pore pressure curve, which has not yet reached equilibrium, even after 3 years of recording. Using the model from Bredehoeft above, the specific storage for the Opalinus Clay can be estimated at 4.0×10^{-6} m^{-1}.

4.5 In-situ hydraulic tests during hydraulic fracturing

Prior to hydraulic fracturing (see chapter 5), short pressure pulse tests were carried out at 4 depth intervals in the hanging wall (Opalinus Clay) and at 7 depth intervals in the footwall (Late Jurassic rocks) (Klee 2012). The interval length tested in every individual test was 0.7 m. The tests were carried out in order to examine the suitability of the test sections for hydraulic fracturing and to determine the near-wellbore rock permeability of the test sections. The analysis of the tests is based on the classical method for slug tests (Cooper et al. 1967). The results were obtained by using the software code PERM, which uses an inversion procedure, to match the measured pressure decline with the theoretical one. The results of these tests are given in Table 4-1.

The tests yielded hydraulic conductivities between 2.4×10^{-11} m/s and 5.5×10^{-10} m/s with highest variability in the Opalinus Clay. Values for hydraulic conductivity in the Opalinus Clay obtained from 57 tests in the Mont Terri rock laboratory range from 1×10^{-14} to 1×10^{-12} m/s with a mean of 2×10^{-13} m/s (Bossart & Thury 2008). The much higher values for the Opalinus Clay at borehole BDS-5 can be explained with reference to its shallow position just above the main detachment. The hanging wall is entirely decompacted and rebound (see also chapter 4.2).

The values obtained in the fractured Late Jurassic rocks are probably too low and not representative for the hydraulic behavior of the entire formations since the tests were explicitly conducted in tight zones free of any discontinuities. Furthermore, clogging of fractures with residual clays and Eocene clayey karst infillings was observed on the mapped core material and could explain the extreme low values. The karst is thus entirely sealed. Generally, hydraulic conductivities in fractured limestone are in the range of 1×10^{-6} to 1×10^{-9} m/s.

The obtained values are most likely too high for the Opalinus Clay and too low for the Late Jurassic limestone in the footwall. However for checking the tightness of intervals suitable for hydraulic fracturing, values obtained from this simple hydraulic testing setup were sufficient.

4.6 Key results and conclusions

Pore water pressure monitoring and frequency analysis of time series revealed two hydraulically separated units, an upper confined aquitard in the Opalinus Clay which is not yet in equilibrium and a lower aquifer in the limestone of Oxfordian and Kimmeridgian age which is in equilibrium

Table 4-1: *Results of pressure pulse tests carried out in the course of hydraulic fracturing.*

Depth [m]	Hydraulic conductivity [m/s]	Formation/Facies	Interpretation of results
24.1	2.4×10^{-11}	Opalinus Clay/carbonate-rich sandy facies	Weathering decompaction rebound
63.2	1.9×10^{-10}	Opalinus Clay/shaly facies	
70.3	2.3×10^{-10}		
80.2	5.5×10^{-10}		
108.0	1.9×10^{-10}	Reuchenette Formation	Sealed karst tight limestone
110.5	8.4×10^{-11}		
128.5	1.2×10^{-10}		
148.0	1.2×10^{-10}	Courgenay Formation	
156.0	1.0×10^{-10}		
182.5	8.7×10^{-11}		
192.5	7.3×10^{-11}		

The tests were carried out in 0.7 m long intervals (depth gives the midpoint of interval) right before hydraulic fracturing. The different colors highlight the different facies types of the Opalinus Clay; carbonate-rich sandy facies (yellow), shaly facies (grey), and the different formations in the footwall below; Reuchenette Formation (turquoise), Courgenay Formation (blue) (data from Klee 2012).

and influenced by diurnal and semi-diurnal Lunar and Solar tides. The analysis of the pressure variations over the last three years shows an annual fluctuation of 0.010 bar or ±5 cm of head difference with a minimum in early April to early May. There is a large hydraulic head difference of about 7 bar between the Opalinus Clay in the hanging wall and the Late Jurassic limestone in the footwall. This difference is most likely due to chemico-osmotic effects and is currently being investigated in the Mont Terri rock lab, where the same phenomenon was observed.

Among the tides, four principal tidal signals were chosen and analyzed. Analysis of the two-year datasets show that the selected harmonics of the tides are only expressed in carbonated layers surrounding the Opalinus Clay and thus in the aquifer of the Malm limestone of the Tabular Jura, below the main detachment. The diurnal harmonics lunar diurnal, the principal lunar semi-diurnal, and the principal solar semi-diurnal were clearly detected on this dataset. For the aquifer in the footwall, the specific storage was estimated as $2.7\pm0.1\times10^{-6}\,m^{-1}$. The analysis of pressure time series in the hanging wall, the Opalinus Clay of the Folded Jura above the main detachment, showed that the main gravitational harmonics are absent, which is due to not yet having reached equilibrium. The specific storage for the Opalinus Clay can be estimated as $4.0\times10^{-6}\,m^{-1}$, which is within the range of values obtained from cross-hole hydraulic tests in the rock laboratory (Bossart & Thury 2008).

Matray & Bailly (2014) could furthermore show that in the time series, pure gravimetric signals (M_2, K_1 and O_1) are only very poorly influenced by atmospheric pressure. The conclusion is that correcting time series from the atmospheric pressure becomes unnecessary.

From the experience made with several boreholes analyzed in the Mont Terri rock laboratory and borehole BDS-5 for the analysis of pressure time series of confined units, several recommendations can be made:

The monitored intervals need to be at least 20 m away from galleries or the surface in order to be in a hydraulically undisturbed situation.

Short test intervals with a small volume decrease the time of equilibration. Furthermore, stiff packer systems need to be installed, e.g. stabilized with resin.

It is important to acquire the data with a recording rate of at least 15 minutes and to have a long enough time series in order to obtain sharp responses of the principal tides.

The results, e.g. the specific storage coefficients deduced from the analysis of the M_2 harmonic, should afterwards be tested by a series of hydraulic tests.

In order to have access to lower frequency semi-annual and annual harmonics and to the long-term behavior and properties of the Opalinus Clay, time temperature/pressure time series of >5 years have to be acquired.

The Opalinus Clay in the hanging wall is altered by weathering, decompaction, and rebound, which led to relatively high hydraulic conductivities. The Late Jurassic limestone in the footwall, on the other hand, exhibits extremely low hydraulic conductivities due to clogging of fractures and karst with residual clays. The results from short pressure pulse tests carried out in the framework of hydraulic fracturing are indicative rather for the tightness of intervals suitable for fracturing than for estimating the in-situ hydraulic conductivity. Generally, more sophisticated hydraulic tests are needed for reliable estimation of in-situ hydraulic conductivity.

5. Evaluation of in-situ stresses

D. Jaeggi, G. Klee, P. Bossart, C. Nussbaum

5.1 Objective and methodology

The knowledge of in-situ stresses is one of the most important boundary conditions for the excavation of underground facilities and especially for mechanical rock modeling of gallery behavior during and after the excavation process. The in-situ stress is the starting point of the stress path encountered by the rock mass in the vicinity of an underground excavation being built. Large stress changes are expected in the excavation vicinity. The stress at a particular location may represent the superposition of components from many different processes through time. In-situ stresses can be divided into gravitational stresses, tectonic stresses, residual stresses for instance due to diagenetic processes, metamorphism, magma cooling, and terrestrial stresses. The latter include seasonal temperature and pressure variations, tidal effects, Coriolis force and so on. In the Jura mountain range, tectonic stress on a regional scale generally has a dominating influence on the in-situ stress state. Major decoupling horizons will likely have a strong effect on the stress field as they may bound stress domains with different characteristics. At elevated locations and in the vicinity of the valleys bottoms, topographical effects (gravity driven) may dominate over tectonic stresses. Topography influences both magnitude and direction of principal stresses. The third and most local influence on in-situ stress are the contrasts of mechanical properties of the rocks themselves. Facies variation influences rock stiffness, anisotropy, strength, and rheology that in turn will impact in-situ stresses. All of these stress factors may be significant for the rock laboratory and the drill site of the BDS-5 borehole.

At the Mont Terri rock laboratory, in-situ stresses have been estimated since the very beginning of the rock laboratory in 1996. Different kinds of techniques were applied and tested in order to determine in-situ stress in the Mont Terri rock laboratory (Fig. 5-1 and Tab. 5-1). Stress relief methods, such as over- and undercoring methods, have been applied at various locations in the Opalinus Clay by Bigarré (1996, 1997), Bigarré & Lizeur (1997) and Bigarré et al. (1997). Between 2000 and 2004, BGR performed in-situ stress measurements based on the overcoring technique in 4 different niches and 9 boreholes in total (Heusermann et al. 2014). However, due to insufficient data quality in most of the boreholes, only maximum and minimum stress components in the plane perpendicular to the borehole axis could be determined. Although one could combine results from holes with different orientation to compute the complete stress tensor, it is not considered a solid approach in practice due to local heterogeneities in the stress field. Overcoring in-situ stress tests using an 8 elements strain gauge have been applied in the Lettenkohle towards the vent shaft, about 500 m NNW of the rock laboratory (Shin 2006, 2009). INERIS applied the overcoring technique as well, using CSIRO strain relief cells with 12 strain gauges in the northern part of the rock laboratory (Lahaye 2005). In-situ stress measurements using an Interfels® borehole slotter have been performed in the southern part of the Opalinus Clay (König & Bock 1997). Hydraulic methods have been performed at the same location by Evans et al. (1999) first. The volume of investigation is much smaller for stress relief methods such as overcoring, undercoring, and borehole slotter than for hydraulic fracturing technique. Whereas stress relief methods comprise volumes of about 10^{-3} to 10^{-2} m^3, the volumes of investigation for hydraulic methods range between 0.5 to 50 m^3, depending on rock quality and interval length. An extensive overview of different methods for in-situ stress measurements, together with an interpretation of the results, is provided in Bossart & Wermeille (2003). It is difficult to evaluate the in-situ stress state with standard approaches such as stress relief methods or hydraulic fracturing due to the specific properties of the Opalinus Clay. The Opalinus Clay is a transverse isotropic material in which stiffness and strength are constantly parallel to bedding, but not normal to it. Furthermore, hydro-mechanical coupled effects are particularly prominent in the rock mass response due to very low permeability at a relatively high porosity.

The most recent evaluations of the in-situ stress using the hydraulic fracturing method were conducted in the framework of the DS (Determination of stress) experiment, of which the BDS-5 borehole is also a part. Initial modeling exercises with the objective to determine the 3D in situ effective and total stress states in magnitude and orientation were conducted with drill core material from the BDS-1 borehole (Jahns 2011). This borehole is located in the Lettenkohle, NNW of the rock laboratory towards the vent shaft.

Hydraulic fracturing tests have been performed in borehole BDS-2 in the competent Hauptrogenstein SSE of the rock laboratory by Rummel et al. (2012) for the shallow part and by Enachescu (2011) for the lower part, who furthermore tested borehole BDS-4 in the Opalinus Clay. While from the shallow part of borehole BDS-2 only impression packer tests were used for the evaluation of the orientations of horizontal stresses, in the deeper section of BDS-2 and for borehole BDS-4 the orientations of the principal stresses were evaluated by using the impression packer method, optical borehole imager logging, and the analysis of borehole breakouts.

In 2011, the surface borehole BDS-5, located about 2 km NNW of the rock laboratory, was tested with hydraulic fracturing (Klee 2012). The main objective of the tests was the determination of magnitude and the orientation of principal

stresses (undisturbed by the presence of excavations) in the Mont Terri anticline, or in the vicinity of the Mont Terri rock lab, respectively. A further objective of this testing campaign was the evaluation of whether a decoupling of the principal stresses occurs across the main detachment or not. Note that the upper part of the borehole in the hanging wall consists of rather weak and ductile Opalinus Clay, while the lower part in the footwall consists of stiff limestone of the Kimmeridgian and the Oxfordian (Fig. 3-2). Thus, aside from a tectonically induced decoupling across the main detachment, the stiffness contrast might influence the orientation of the in-situ principal stresses as well. The borehole BDS-5 was tested with a total of 11 hydraulic fracturing tests and 10 impression packer tests between depths of 24.1 and 192.5 m. The main assumptions for hydraulic fracturing in a vertical borehole are that the overburden (vertical) stress is a principal stress, that the rock is homogeneous, isotropic, and initially impermeable, and that the induced fracture is perpendicular to S_h. At borehole BDS-5, stress magnitudes were evaluated from pressure signals and orientations were estimated by both, the impression packer method and by analyzing pre- and post hydraulic fracturing optical borehole imager logs. The theory in combination with the test sequence for borehole BDS-5 (Klee 2012) is provided in detail in chapter 5.3.2.

Lab tests on rock material yielded dynamic elastic parameters, fracture toughness and hydraulic tensile strength. Furthermore, simple hydraulic tests such as pressure pulse tests before hydraulic fracturing and step-rate injection tests after hydraulic fracturing were performed. The results of the hydraulic tests which were conducted in the course of hydraulic fracturing are provided in Table 4-1 and discussed in chapter 4.5.

Lab tests were performed on selected samples of the Kimmeridgian and Oxfordian limestone at the depth intervals from 127 to 197.5 m (Klee 2012). The test program consisted of the determination of density (ρ) and the measurement of ultrasonic velocity, p-wave velocity (v_p), and shear-wave velocity (v_s) which forms the basis for calculating the dynamic elastic parameters Young's modulus (E) and Poisson's ratio (υ). Furthermore, fracture toughness (K_{1c}) and hydraulic tensile strength (T) were measured. Fracture toughness K_{1c} is the critical stress intensity for fracture opening mode 1 (extensional). A summary of the results of these lab measurements is given in Table 5-4 and in chapter 5.3. Density was measured both on the core pieces by the buoyancy method in water and on mini-cores of about 30 mm diameter by simple volume and weight determination. Ultrasonic velocities were measured on mini-cores of 44–66 mm length and diameters of about 30 mm in close accordance with the ISRM standard (Rummel & van Heerden 1978). Dynamic Young's modulus (E) and Dynamic Poisson's ratio (υ) were calculated using the following formulas:

$$E = 2v_s^2\rho(1+\upsilon) \quad [\text{Pa}] \quad (5.1)$$

$$\upsilon = \tfrac{1}{2}\,(2-(v_p^2/v_s^2))/(v_p^2/v_s^2) \quad [-] \quad (5.2)$$

where

ρ density of the rock [kg/m³]
v_s shear-wave velocity [m/s]
v_p p-wave velocity [m/s]

The fracture mechanics parameter fracture toughness K_{1c} was measured by a 3-point bending test of Chevron-notched core pieces with a diameter D in close accordance with the ISRM standard (Ouchterlony 1988). The bending force was applied using a servo-controlled hydraulic testing machine with a constant piston displacement rate of 1×10^{-6} m/s. The fracture toughness was calculated from the peak bending load F_{max} and the Chevron notch depth a_0 with the formula:

Table 5-1: *Overview of in-situ stress testing carried out in the Mont Terri rock laboratory with the corresponding documentation.*

Experiment	Borehole	Method	Documentation
In-situ stress, over- and undercoring	BIS-A1	Overcoring, Undercoring	Bigarré (1996, 1997), Bigarré & Lizeur (1997), Bigarré et al. (1997)
In-situ stress, borehole slotter	BIS-B1	Dilatometer, Borehole slotter	Bühler (2000), König & Bock (1997)
In-situ stress, hydraulic fracturing	BIS-C1 and BIS-C2	Hydraulic fracturing	Evans et al. (1997)
EDZ cut-off	BEZ-A27 and BEZ-A28	Overcoring	Lahaye (2005)
Anisotropy and rock stress	BAS-1–BAS-6	Overcoring	Shin (2006, 2009)
Determination of stress	BDS-2 and BDS-4	Hyraulic fracturing	Enachescu (2011)
Determination of stress	BDS-1	Laboratory analyses using RACOS®-tests	Jahns (2001)
Determination of stress	BDS-1 and BDS-2	Hydraulic fracturing	Rummel et al. (2012)
In-situ stress, overcoring	BIS-D1–BIS-D9	Overcoring	Heusermann et al. (2014)
Determination of stress	BDS-3	Overcoring	Doe & Vietor (2015)

The locations of the boreholes or test sites can be found on Figure 5-1.

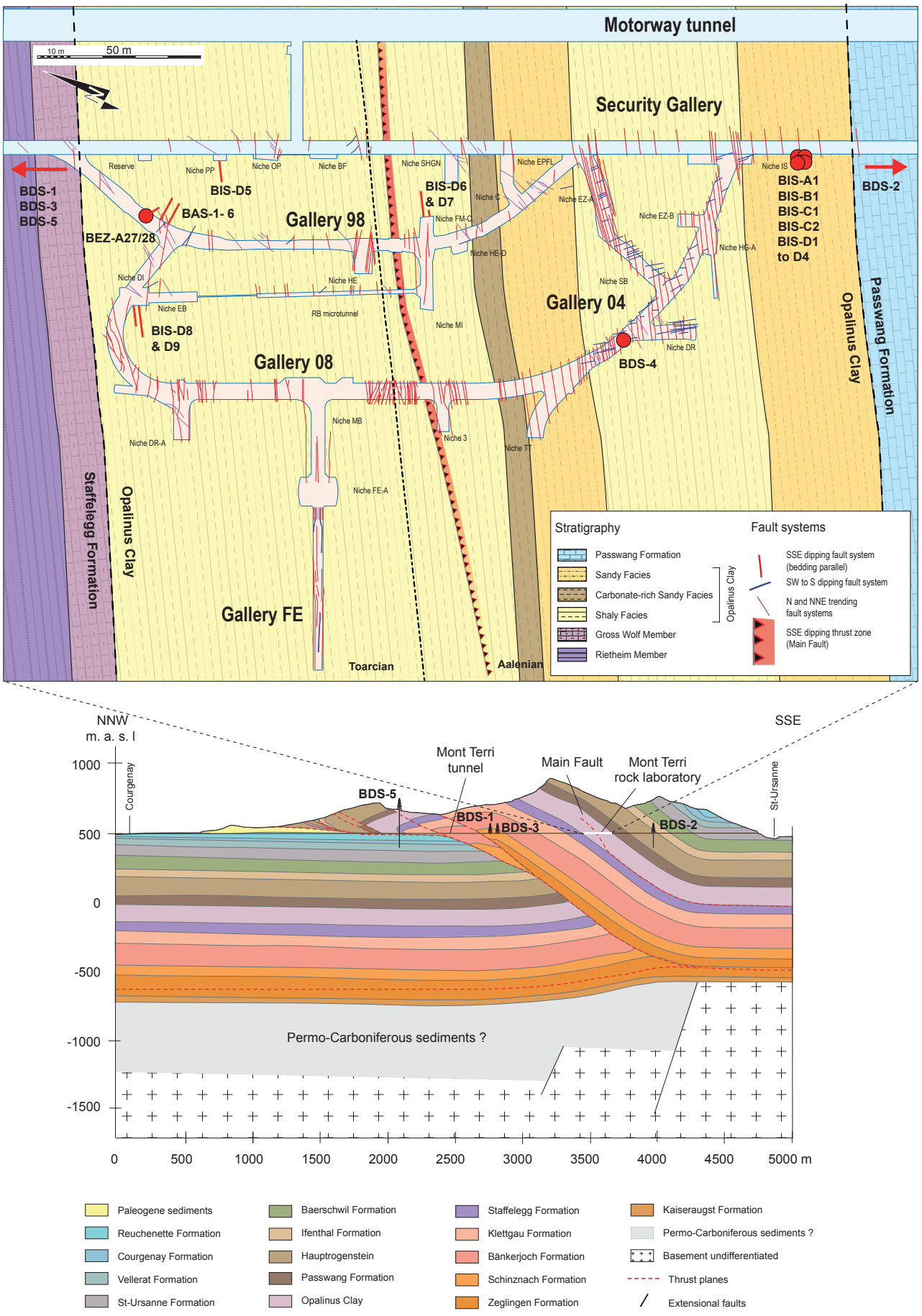

Fig. 5-1: Overview of campaigns for in-situ stress evaluation in and close to the Mont Terri rock laboratory. Authors and methods that were carried out methods are given for every borehole in Table 5-1.

$$K_{1c} = A_{min} F_{max} / D^{3/2} \quad [Nm^{-3/2}] \quad (5.3)$$

with

$$A_{min} = 3.33[1.835 + 7.15 a_0/D + 9.85(a_0/D)^2] \quad (5.4)$$

where

A_{min} geometric factor [–]
F_{max} peak bending load [N]
D diameter of core piece [m]
a_0 Chevron notch depth [m]

The hydraulic tensile strength T and the frack coefficient k were measured by hydraulic fracturing tests on mini-cores of 30 mm diameter and an axial hole of 3 mm diameter, subjected to a confining pressure between 1 and 15 MPa. The injection rate was about 1 ml per second. The injection fluid was hydraulic oil TELUS 32 with a viscosity of 25 cPoise.

5.2 Stress estimation in the Mont Terri rock laboratory

A good compilation of regional scale in-situ stress data is provided in Bossart & Wermeille (2003). From the Jura Mountain range, a whole variety of stress measurements at different depth levels and derived by different methods in different formations and tectonic units is available. The compilation of Bossart & Wermeille (2003) describes five methods which were used, mostly in deep boreholes in the Jura Mountain range. Techniques applied are the analysis of borehole breakouts by means of imaging logs (ABI and OBI) or with 4-arm caliper logs. This technique was mainly used in deep boreholes reaching the basement. S_H in these boreholes is generally NW–SE oriented. In the Schafisheim borehole, a shift of SH across the main detachment was observed. The corresponding S_H-directions change from NNE–SSW (above the main detachment) to NW–SE (below it). However, this change in direction was observed at a depth of 1400 m and thus far beyond the near-surface zone. Doorstopper measurements were applied in several quarries. They yield very heterogeneous near-surface data of in-situ stresses. Triaxial strain cell measurements were taken in four quarries and one tunnel. The results were also very heterogeneous in terms of the orientation of in-situ stresses. The borehole slotter method was widely used in shallow boreholes, mostly in Middle to Late Jurassic limestone. A compilation of stress data led to the distinction of five stress field provinces (Becker 1999, 2000). The Mont Terri area belongs to the central province, which is characterized by NNW–SSE to NNE–SSW S_H-directions. This province extends from the north of Basel to the Prealps front including the Rhine Graben and the Cantons of Basel, the west part of Aargau, Solothurn, Bern, and Fribourg. The last method which was used is the hydraulic fracturing method, which yielded a N–S direction of S_H at a test site in the Rheintal Graben NW of Basel.

More recently, analysis of borehole breakouts in two 5 km deep boreholes near Basel (Valley & Evans 2009) yielded the orientation of S_H. Borehole images are available through the sediment/basement interface where stress rotations of about 30° are observed. No images are available through evaporites layers of the Trias (assumed to be a main detachment level). However, accessory datasets which were analyzed in this publication suggest that another rotation takes place through this level with a N–S trend for S_H above the evaporites, and a NW–SE orientation in the basement, as inferred by borehole failure and earthquake data. Shallow earthquakes from the upper crystalline crust or even from the lowermost sedimentary rocks occurred several times in the region of St.Ursanne during the last few years. The focal mechanism of the strongest event suggests a thrust fault with a N–S oriented P-axis and thus coincides with the data from the borehole near Basel (pers. comm. N. Deichmann, ETH Zurich).

Early in-situ stress measurements in the Mont Terri rock laboratory were based on borehole slotting, the under-coring technique, and hydraulic fracturing. Further information was gathered from borehole breakouts and rock mechanical modeling (Bossart & Wermeille 2003). The stress directions deduced from borehole slotting seem to be controlled by the anisotropy due to the bedding planes. A major problem of the borehole slotter method is that most of the elastic response of the borehole wall takes place before the probe is inserted in the borehole. Consequently, only a small part of the elastic response can be measured, resulting in stresses that are too small. Furthermore, aspect ratios (σ_1/σ_3) of 20 are unrealistic (the rock mass would not be able to sustain such high differential stresses) and suggest that the obtained stress magnitudes are not very reliable. The results of the under-coring technique yield a vertical principal stress which is controlled by the overburden of about 250 m. The intermediate and minimum principal stresses do not coincide with the expected regional scale stress directions. However, stress magnitudes derived by the under-coring technique method, at least for the surroundings of the Mont Terri rock laboratory, seem to be more reliable, than those derived from the borehole slotting technique. Hydraulic fracturing (Evans et al. 1999) yielded a sub-vertically oriented σ_1 of 7 MPa, similar to the stress caused by overburden. σ_3 was 3 MPa in magnitude and NNW–SSE oriented parallel to the axis of the Mont Terri motorway tunnel. No value was given for the intermediate principal stress. The problem with hydraulic fracturing was that no stimulated axial fractures could be induced. Only bedding planes were opened, which implies that the assumption of mechanical isotropy is clearly not valid in the Opalinus Clay. Thus, the principal stresses could not be directly derived from shut-in pressures (P_{si}) and re-opening (P_r) pressures. A detailed analysis combined with numerical modeling led to the stress data presented above. Geological observations on galleries and boreholes in different orientations yielded further information about the in-situ stress field. Generally, stress-induced breakouts in an isotropic rock are recorded in the direction of σ_{min}. In the Opalinus Clay, rock anisotropy also has to be taken into account, which leads to additional breakouts controlled by strength anisotropy, termed here mechanical controlled breakouts (Bossart & Wermeille 2003; Fig. 5-2).

The observations from numerous mappings of galleries and boreholes show, that σ_{max} must be sub-vertically oriented and σ_{min} in a horizontal plane. Stress-induced breakouts

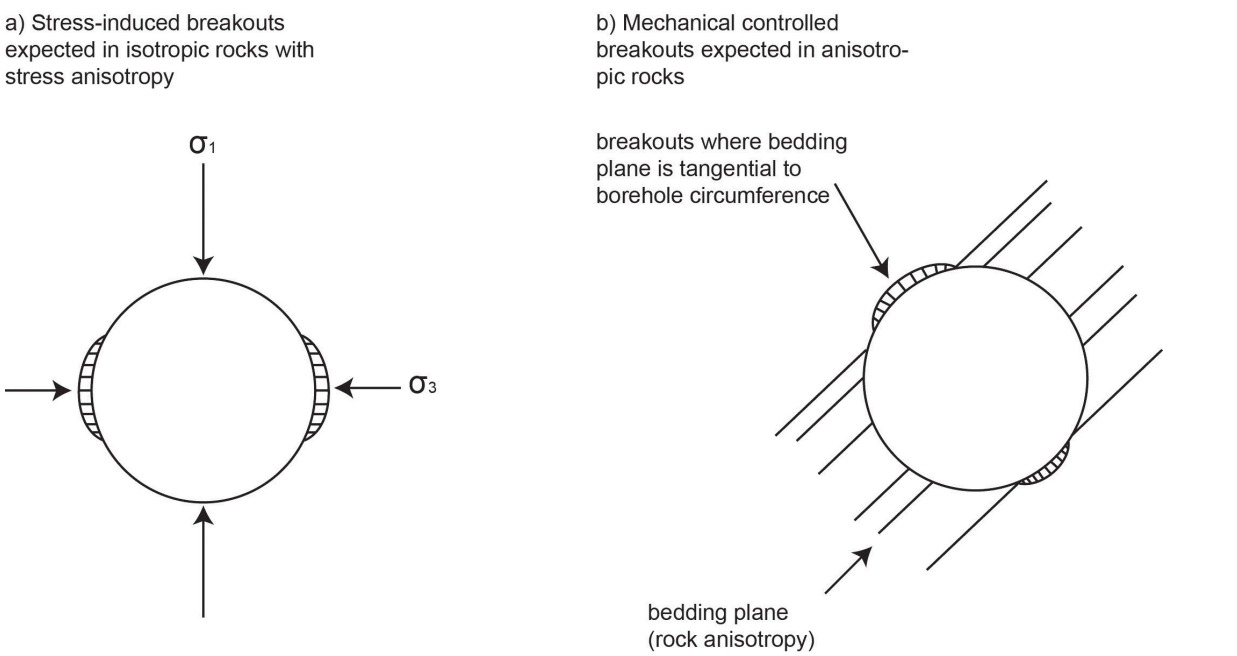

Fig. 5-2: Borehole breakouts due to a) stress redistribution around borehole in isotropic rocks and b) anisotropic rock fabric, e.g. pronounced bedding planes (from Bossart & Wermeille 2003). Breakouts controlled by strength anisotropy are termed mechanical controlled breakouts.

observed in the Opalinus Clay of the Mont Terri rock laboratory confirm the sub-vertical direction of σ_1 found with hydraulic fracturing and undercoring methods. σ_2 and σ_3 lie in a horizontal plane, although their direction is not very well constrained. The stress was further evaluated from rock-mechanical modeling carried out by Martin & Lanyon (2003). The modeling was performed using the boundary element code EXAMINE 3D. It has to be noted that the model used assumes linear elastic and isotropic conditions, which are very limiting assumptions for the Opalinus Clay. Data from boreholes instrumented to measure deformation and pore pressure responses during and after the excavation of new galleries was used as an input for the model. The idea was to find an initial stress tensor that fits the measured and calculated deformations and convergences during the excavation of a gallery. The result of this modeling is given in the table below (Tab. 5-2). According to this model, σ_1 is controlled by the overburden and σ_2 and σ_3 are in a sub-horizontal plane. Thoeni (2013) was able to show that the maximum principal stress proposed by Martin & Lanyon (2003) is in accordance with observations of the deformation of EDZ along Gallery 08. However, the magnitude for σ_3 of 0.6–2 MPa deduced from the modeling is not very well constrained and not realistic (Bossart & Wermeille 2003). A σ_3 below 2 MPa would lead to negative effective minimum principal stresses and to very high aspect ratios of 3–12, which would provoke tension fractures around boreholes and galleries. Bossart & Thury (2008) discussed this problem and suggest a more realistic σ_3 of 2–3 MPa. Taking these considerations into account and adapting the σ_3-magnitude of Martin & Lanyon (2003) to the magnitude suggested by Bossart & Thury (2008) yields the following stress tensor:

Table 5-2: *Stress tensor from modeling, after Martin & Lanyon (2003).*

Principal Stress	Magnitude [MPa]	Trend [°]	Plunge [°]
σ_1	6–7	210	70
σ_2	4–5	320	10
σ_3	2–3	50	15

The initial σ_3 of 0.6–2.0 MPa was adapted to a more realistic value.

From 2000 to 2004, BGR performed numerous in-situ stress tests in the sandy facies and the shaly facies (Fig. 5-1) in the Mont Terri rock lab using the overcoring technique (Heusermann et al. 2014). Due to insufficient quality of most of the 9 tested boreholes, only the stress components in a plane perpendicular to bedding and along the dip direction could be determined. The mean maximum component σ_{max} in this plane was 5.5 MPa, dipping 56° towards SSE, and thus more or less within the bedding plane. The mean minimum component σ_{min} was 2.6 MPa and normal to bedding. Unfortunately, no principal stresses can be deduced from this dataset. In 2004, INERIS conducted six in-situ stress measurements using the overcoring method and CISRO cells with 12 strain gauges (Lahaye 2005) in boreholes BEZ-A27 and BEZ-A28 in the northern part of the rock laboratory. Magnitudes were determined to be 10 MPa, 9–10 MPa and 3 MPa for σ_1, σ_2, and σ_3, respectively. The calculations took the transverse isotropy into account, but were still based on a linear elastic response which is not likely to be reliable for the Opalinus Clay. In addition, the elastic parameters they

used as input were much higher than as suggested in Bossart & Thury (2008). Interestingly, orientations of σ_1 and σ_2 from this analysis were located in the bedding plane with σ_3 normal to it, which suggests a strong effect of rock anisotropy on these results.

In 2009 hydraulic fracturing was carried out in a horizontal borehole BDS-1 near the ventilation cavern and a vertical borehole BDS-2 at the parking niche, south of the rock laboratory (Rummel et al. 2012). The horizontal borehole is located in dolomites and results could be cross-checked with overcoring techniques, which yielded principal stresses. The vertical borehole BDS-2 is located in the Hauptrogenstein of the parking niche and yielded an S_H oriented towards 070 or parallel to the fold axis of the Mont Terri anticline. According to Enachescu et al. (2014) it is not clear, whether these measurements are influenced by the gallery or not but given the stiff elastic properties of the Hauptrogenstein, the measurements are most probably not influenced. Unfortunately this interesting result for shallow measurements between 17 and 38 m depth in the carbonated Hauptrogenstein cannot be verified, since orientations were derived from impression packer tests only, without pre- and post-frack imaging logs.

In 2010, an additional hydraulic fracturing campaign was conducted, focusing on the undisturbed zone far outside of the galleries (Enachescu 2011). There, two deep boreholes, the prolonged borehole BDS-2 with 80 m depth in the Hauptrogenstein and BDS-4 with 55 m depth in the Opalinus Clay, were tested (Fig. 5-1). The tensile strength for the Opalinus Clay was assumed to be 0.67 MPa normal to bedding and 1.3±0.2 MPa parallel to bedding. Tensile strength for the limestone of the Hauptrogenstein was assumed to be 2 MPa. The hydraulic fracturing tests did not open any vertical fractures in either the carbonated Hauptrogenstein or the Opalinus Clay. Especially for the deeper part of BDS-2 in the Hauptrogenstein, this is a surprising result, since in the upper part axial fractures were identified on the impression packer tests (Rummel et al. 2012). Due to this obvious contradiction and the fact, that the analysis of the orientations of horizontal stresses was based on impression packers only, data of borehole BDS-2 is not considered and interpreted in the present study. The impressions in the Opalinus Clay-section indicate that only bedding planes opened, while pre-existing fractures were opened in the carbonates. This behavior is consistent with experience from previous attempts with hydraulic fracturing in which the fracturing mainly occurred along bedding planes (Evans et al. 1999). Without the initiation and propagation of newly created hydraulic fractures, the computation of maximum and minimum horizontal stresses is not possible by using standard hydraulic fracturing theory, except if multiple fractures with different orientations are available. Making some assumptions on depth evolution the stress ratios, HTPF (Hydraulic Tests on Pre-existing Fractures) (Cornet 1993) could then be applied. The orientations of pre-existing features in the Opalinus Clay are in most cases close to being parallel to bedding and are thus not useful for HTPF. However, additional logging data from borehole breakouts in borehole BDS-4 provided clear indications for S_H and S_h. Wellbore breakout directions indicate with high likelihood a trend for S_H of 033° and 123° for S_h. Furthermore, the inability of hydraulic fracturing to create vertical fractures suggests that the minimum principal stress acts in a direction close to normal to bedding, although this is likely influenced by the tensile strength anisotropy. The analysis of stresses in the $\sigma_1 - \sigma_3$ plane along with the breakouts led to estimates of stress state in the Opalinus Clay far outside of the influence of galleries given in Table 5-3 below:

Table 5-3: *Stress tensor deduced from a combination of hydraulic fracturing and analysis of borehole breakouts at the 55 m deep borehole BDS-4 after Enachescu (2011). Bedding is oriented 150°/45°.*

Principal Stress	Magnitude [MPa]	Trend [°]	Plunge [°]
σ_1	8.6	033	0
σ_2	6.7	123	70
σ_3	3.9	303	20

In order to summarize the available stress measurements from the Mont Terri rock laboratory, 33 available data from in-situ stress measurements have been compiled and plotted on a stereogram for the orientations of principle stresses and on a histogram for the magnitudes of those (Fig. 5-3). Details about the measurements are provided on a table in Appendix G.

According to Bossart & Wermeille (2003) the local stress field in the Opalinus Clay of the Mont Terri rock laboratory, which lies in the southern limb of the Mont Terri anticline, does not coincide with the expected regional stress field. The local maximum principal stress is sub-vertically oriented and does not coincide with the expected regional NW–SE directed principal stress direction. As a possible reason for this, they infer that the basal detachment, which is located below the rock laboratory in the Triassic evaporites, acts as a decoupling horizon. If we compare this suggestion to the latest overall dataset (Fig. 5-3), this could be the case for at least some of the shallow boreholes in the Opalinus Clay of the Mont Terri rock laboratory (green dots). σ_1 is sub-vertically oriented and σ_3 is parallel to the motorway tunnel. However, the intermediate and the minimum principal stresses are not very well constrained and interchanged compared to the orientations proposed by Martin & Lanyon (2003) (Tab. 5-2). Furthermore, if we have a closer look on the stereoplot, there are also data (green dots) where σ_1 is oriented NNW–SSE with a sub-vertical σ_3. This refers to data from shallow boreholes in the rock laboratory, where an overcoring campaign with CISRO cells (Lahaye 2005) yielded orientations of σ_1 and σ_3 located in the bedding plane. More consistent are data (blue dots) from in-situ stress measurements in competent dolomites of the Lettenkohle, north of the rock laboratory (Shin 2006, 2009 and Jahns 2011). They invariably show a NW–SE orientation of σ_1. There is only one datasets from the BDS-4 borehole in the Opalinus Clay (Enachescu 2011) for the attribute deep vertical borehole > 20 m. σ_1 there is trending towards 033° and σ_2 is subvertical, and its magnitude corresponds to the overburden (Tab. 5-3).

Recent numerical modeling of the Mont Terri anticline focused on the mechanisms which cause the present-day

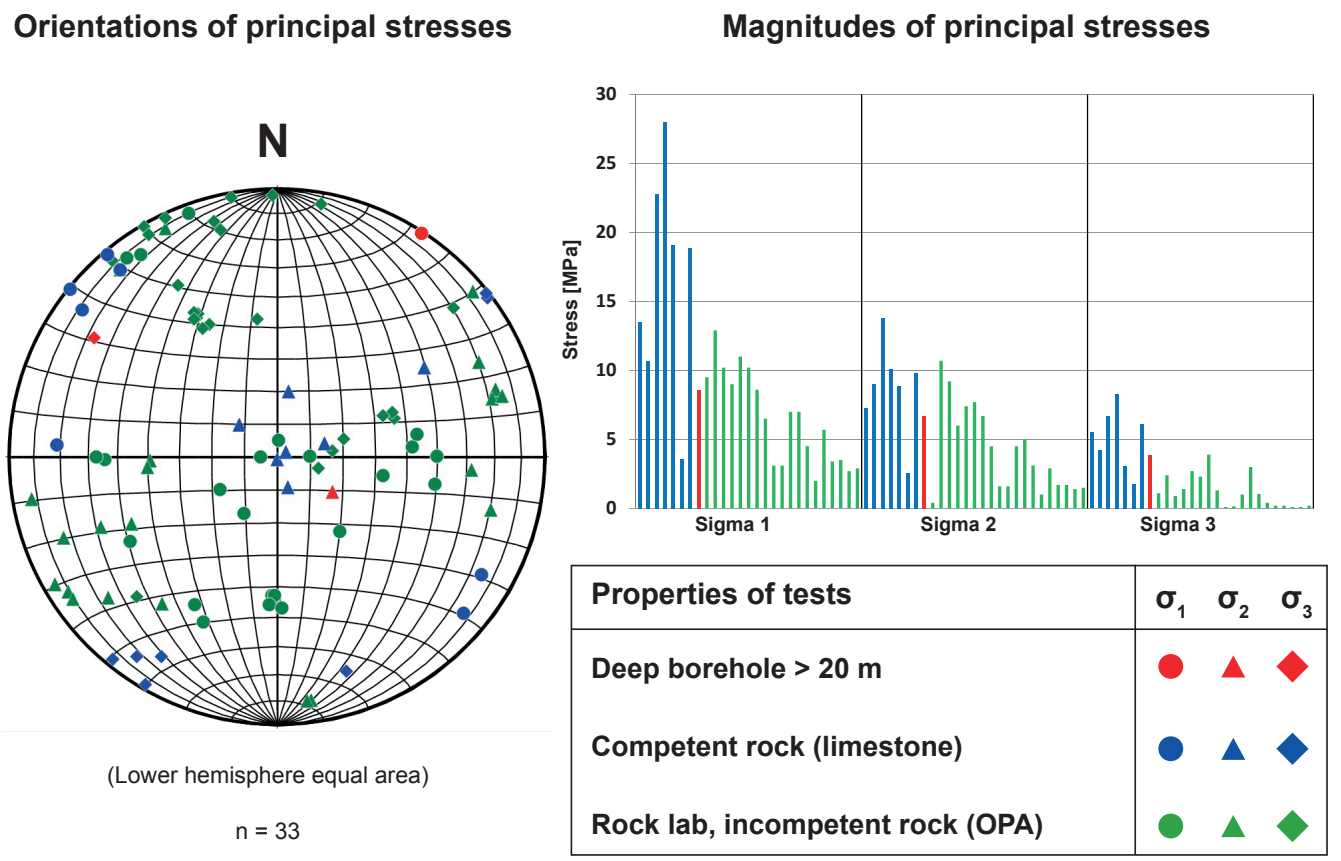

Fig. 5-3: Compilation of 33 (orientations) and 27 (magnitudes) in-situ stress measurements carried out in the rock laboratory of Mont Terri. The orientations are given on a stereoplot, the magnitudes are plotted on a histogram view. Stress data has been color coded for three attributes: red for the deep vertical borehole BDS-4 in Opalinus Clay, blue for boreholes carried out in the competent dolomite rocks of the Lettenkohle, north of the rock laboratory and green for shallow boreholes in the Opalinus Clay of the rock laboratory.

in-situ stresses. Petrini & Simpson (2008) distinguished tectonic and topographic control. In the model with pure tectonic control, higher stress levels of up to 15 MPa for σ_1 were observed. According to these authors, a purely gravitational case cannot explain the observed inclination of σ_1 for topography control (Tab. 5-2). The in-situ stress at rock lab level is dominated by gravitation, but there is still a signal of previous tectonic activity. Petrini & Simpson (2012) furthermore conclude from their model that stresses are affected by layering and that the influence of tectonic forces or topography is strongly dependent on material properties.

From the available data set of in-situ stress measurements, the following statements can be made: At Mont Terri, the stress filed is anisotropic and the rock is anisotropic as well, which as a combination make an interpretation of in-situ test data for stress evaluation a challenging task.

Three main influences or possible mechanisms which strongly affect the in-situ stress can be deduced from the available data:

The influence of the excavation of galleries affects the in-situ stress state in shallow boreholes at depths of <20 m. Here, the stress tensor proposed by Martin & Lanyon (2003) and Bossart & Wermeille (2003) applies, with σ_1 sub-vertical and controlled by the overburden (ρgh). σ_2/σ_3 are not well defined but lie more or less in a horizontal plane.

The second influence is whether the measurement is located in the "bench vice" of the "Fernschub" (tectonic dominated versus topography dominated) at lower levels or is influenced by topography at higher levels. The incised Doubs valley near St.Ursanne is located about 440 m a.s.l. and is thus deeper than the rock lab at 510 m a.s.l. Shallow boreholes at rock laboratory level or above are clearly located above the "bench vice" and thus controlled by topography and a vertical σ_1. Deeper boreholes such as the BDS-4 borehole with 55 m depth reach the influence of the "bench vice" (Fig. 5-4), where thin-skin tectonics and shortening above the detachment level of the Trias evapories dominate. Here, a N–S direction of the maximum principal stress is measured.

A third influence on the in-situ stresses is the competence or stiffness contrasts of the rock materials and the effects of anisotropy in both stiffness and strength, largely controlled by the orientation of the bedding planes. In limestone or dolomites north of the rock lab, N–S directions of σ_1 have been measured even at the level of the rock laboratory and are thus clearly above the "bench vice".

However, the measured in-situ stress in many situations is most likely a combination of all these influences. Chapter 5.4 attempts to highlight the complexity of the influences on a matrix-representation (Tab. 5-6). Finally, it is recommended that the stress tensor proposed by Martin & Lanyon (2003) and Bossart & Wermeille (2003) with a sub-vertical σ_1 and σ_2/σ_3 in the horizontal plane should be considered in the Mont Terri rock laboratory. Outside of the rock laborato-

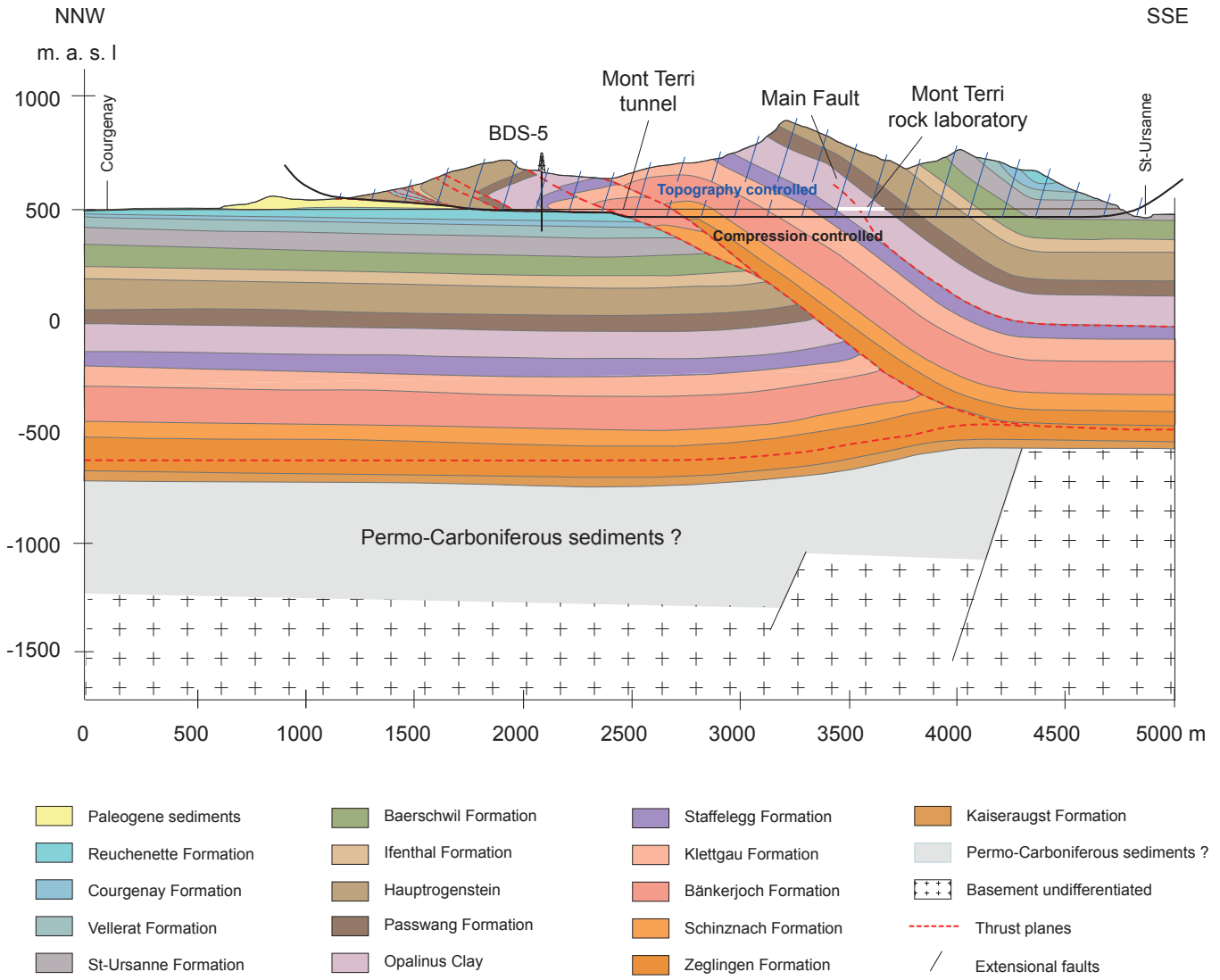

Fig. 5-4: Cross section of the Mont Terri anticline, showing topography and compression control on in-situ stress. The topography-controlled zone includes the vicinity of the rock lab (shallow boreholes with depths <20 m) and zones above. The influence of the compression-controlled zone starts well below the rock lab level and is linked to the elevation of the Doubs river valey. After Freivogel & Huggenberger (2003) and Caer et al. (2015).

ry, the stress tensor of Enachescu (2011) with a sub-horizontal σ_1 trending towards 030° and a sub-vertical σ_2 controlled by the overburden (ρgh) is recommended.

5.3 Hydraulic fracturing data of BDS-5

5.3.1 Lab testing

In the course of the hydraulic fracturing campaign, lab tests were performed on selected samples of the Kimmeridgian and Oxfordian limestone in depth intervals of 127 to 197.5 m (Klee 2012). The results are summarized in Table 5-4. The obtained values were used to cross-check the results from hydraulic fracturing by using them as input parameter for the fracture mechanics code FRAC (Rummel & Hansen 1989). According to Klee (2012), the simulation calculations with the code FRAC present an almost perfect match between the calculated and observed breakdown pressures Pc and the pressure decrease after fracture initiation of the in-situ hydraulic fracturing cycles. Thus, the simulation calculations may be considered as a quality control of the in-situ data analysis.

5.3.2 Hydraulic fracturing – theory and test sequence

The classical hydraulic fracturing analysis is based on Kirsch's (1898) solution for stress distribution around a circular hole. The Kirsch solution assumes a homogeneous isotropic and elastic rock mass, which is subjected to a far field compressive stress. Fracture initiation occurs, when internal fluid pressure (P_w) is equal to breakdown pressure (P_c) and thus $P_w = P_c$, then the simple force balance at the borehole wall is:

$$3S_h - S_H - P_c = -T, \text{ where} \qquad (5.5)$$

S_h minimum horizontal stress [Pa]
S_H maximum horizontal stress [Pa]
S_v vertical stress [Pa]

Table 5-4: *Summary of lab test results conducted for samples of Late Jurassic limestone (from KLEE 2012).*

Property	Value	Unit	Method
Density ρ	2.65±0.05	g/cm³	Buoyancy method
	2.65±0.02	g/cm³	Volumetric method
p-wave velocity V_p	5680±270	m/s	Ultrasonic measurements
Shear-wave velocity V_s	3240±150	m/s	Ultrasonic measurements
Youngs Modulus E (dynamic)	70±7	GPa	From ρ, V_p and V_s
Poisson's ratio υ (dynamic)	0.26±0.02	–	From V_p and V_s
Fracture toughness K_{1c}	1.03±0.35	$MN^{-3/2}$	3-point bending test
In-situ hydraulic tensile strength T	13.5±3.0	MPa	Hydraulic fracturing tests on minicores
Frack coefficient k	1.0±0.4	–	Hydraulic fracturing tests on minicores

The entire acquired dataset is provided in table G-3 in Appendix G.

P_c breakdown pressure or critical pressure [Pa]
P_w internal fluid pressure [Pa]
P_r re-opening pressure [Pa]
P_p pore pressure [Pa]
P_{si} shut-in pressure [Pa]
T tensile strength [Pa]

If the rock mass has a pore pressure P_p, then the effective stress law for tensile failure must be used. Thus, failure occurs if:

$$S_h < -(T-P_p) \quad [Pa] \quad (5.6)$$

Re-arranging equation 5.5 and substituting $(T-P_p)$ for T yields the maximum horizontal stress:

$$S_h = 3S_h - P_p - P_c + T \quad [Pa] \quad (5.7)$$

The shut-in pressure (P_{si}) is the pressure to merely keep open the fracture, after the pressurizing system is shut-in. It marks the transition between fast and slow pressure decay during the closure of the fracture and is also the pressure value at which the hydraulic flow out the fracture terminates. The re-opening pressure (P_r) is the pressure at which the pressure build-up of the second fracturing cycle deviates from the first cycle curve, and thus from linearity.

If one assumes that the minimum horizontal stress (S_h) is equal to the shut-in pressure (P_{si}) and that the vertical stress is a linear function of depth, then the stress components can be calculated as follows:

$$S_h = P_{si} \quad [Pa] \quad (5.8)$$

$$S_H = 3P_{si} - P_r - P_p \quad [Pa] \quad (5.9)$$

$$S_v = \sigma gh \quad [Pa] \quad (5.10)$$

$$P_r = P_c - T \quad [Pa] \quad (5.11)$$

Although the approach above is widely used, an uncertainty in the validity of the effective stress law for tensile failure remains. In rock with very low permeability, the P_p in eq 5.9 is multiplied by a factor which is < 1. Furthermore, there is a controversy around the re-opening pressure approach (EVANS et al. 1999 or RUTQVIST et al. 2000). Keeping these limitations in mind, it can be stated that the values of maximum horizontal stresses obtained by the procedure described in this report are only estimates and have to be treated with caution.

For the BDS-5 borehole, the general testing procedure was as follows (KLEE 2012):

The packers were inflated to a differential pressure of 8 MPa.

The testing interval was rapidly pressurized to a differential pressure of 3–5 MPa and the subsequent pressure decline was monitored for approximately 5 minutes (p-test on Fig. 5-5). Then, the interval pressure was released and the fluid volume recovered.

The test interval was pressurized with an injection rate of about 2 l/min until a drop in the interval pressure occurred or a constant injection pressure was reached (fracture opening on Fig. 5-5). Then, the injection was closed and shut in for about 3 minutes. Afterwards, the interval pressure was released and the fluid volume recovered.

The test interval was re-pressurized with injection rates of 2–5 l/min until constant injection pressures were reached (re-opening 1–3 on Fig. 5-6). Several repetitions of the re-frack cycles were performed, until the shut-in pressures could be reproduced.

During a stepwise increase of the injection flow-rate, the corresponding injection pressures were monitored (step-rate test on Fig. 5-5).

After the hydraulic fracturing, impression packer tests were performed. During 5 minutes, the packers were inflated to pressures of about 30% above the fracture re-opening pressure. Back at the surface, the oriented impressions on the rubber were extracted with plastic cover sheets wrapped around the packer. In addition, pre- and postfrack data from optical borehole imager logging (OBI) was available for the analysis of induced fractures.

For data analysis, breakdown pressure P_c (fracture initiation), re-opening pressure P_r (fracture re-opening), and shut-in pressures P_{si} or jacking pressure $P_{jacking}$ (step-rate test) are required. The entire procedure for the evaluation of the

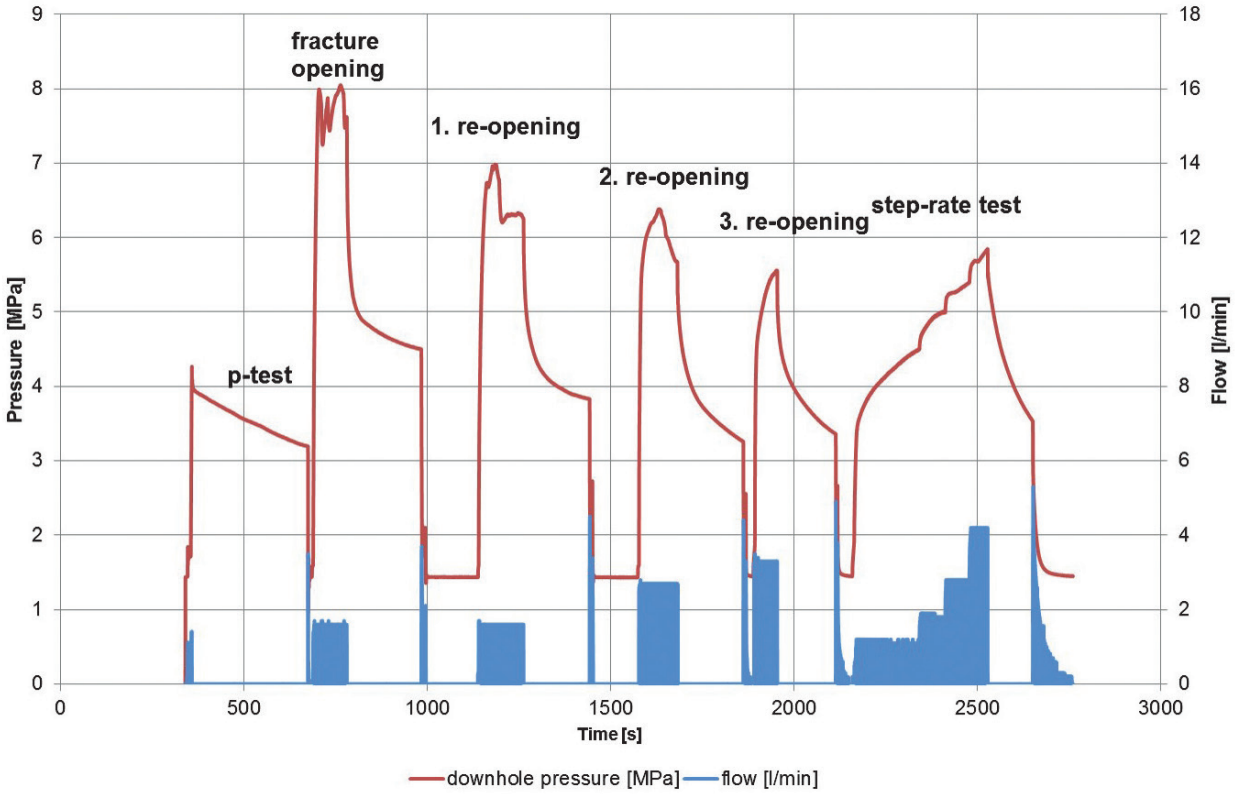

Fig. 5-5: Example of testing procedure for a hydraulic fracturing test at 148 m depth in borehole BDS-5. The pressure curve of the test is indicated in red (axis on left-hand side) and the integral of the flow in blue (axis on right-hand side) (from KLEE 2012).

magnitudes for a test at 148 m depth is provided in detail in Appendix G. Furthermore, the orientation of induced or stimulated fractures is required for the orientation of the stress components. In the study of KLEE (2012), this was done by means of impression packers and imaging logs (ABI/OBI).

5.3.3 Results of hydraulic fracturing

In the Opalinus Clay (hanging wall above the main detachment), four tests have been conducted, and in the Reuchenette and the Courgenay Formation (footwall below the main detachment), seven tests are available. According to KLEE (2012), the majority of the hydraulic fracturing tests indicated distinct fracture initiation events with breakdown pressure values ranging from 3.5–3.7 MPa (Fig. 5-6). Re-opening pressure values vary between 1.0 and 10.9 MPa. The corresponding in-situ hydraulic tensile strength for the Opalinus Clay ranges between 1.5 and 2.5 MPa with a mean value of 2.2 MPa. For the late Jurassic limestone below, in-situ hydraulic tensile strength varies between 3.3 and 8.3 MPa with a mean value of 4.8 MPa. This is much lower than the values obtained from hydraulic fracturing tests on 30 mm mini-cores, which yielded a hydraulic tensile strength of 13.5±3.0 MPa. According to KLEE (2012), considering the fracture mechanics size-dependency of the hydraulic tensile strength, the lab results are in agreement with the in-situ tests.

The author furthermore mentioned that the re-opening pressures in the clayey hanging wall were rather difficult to determine, since pressures did not linearly increase with injected fluid volume. The shut-in pressures varied between 0.7 and 9.75 MPa and were in the same order as the shut-in pressure derived from the step-rate injection tests. Despite some scatter, the re-opening and shut-in pressures show a systematic increase with depth. However, a thorough review of the data from impression packer tests and the pre- and post-frack data of imaging logs by swisstopo revealed that the four tests in the hanging wall only opened pre-existing features and that no axial fractures could be induced. In the case of the opening of a pre-existing feature, the only reliable information that can be derived is the normal stress across the fracture (given by P_{si}), which is not necessarily a principal stress. In the limestone of the footwall, axial or steeply inclined fractures dipping 73 to 90° which are not related to pre-existing features could be induced and detected in most cases with high confidence.

Due to the uncertainties in the Opalinus Clay (hanging wall above the main detachment) the data from above the main detachment is separated from the footwall data for further representation and interpretation.

The derived stress magnitudes with the orientations of S_H are given in Figure 5-7. Based on the data and assuming a rock density of 2500 kg/m³, a modified depth function for S_H, S_h and S_v can be derived for the footwall domain with z being the depth from the surface. The outliers at 110.5 and 156 m are not considered for the calculation of the depth function.

$$S_H\,[\mathrm{MPa}] = 0.036 \times z[\mathrm{m}] + 4.463 \qquad (5.12)$$

$$S_h\,[\mathrm{MPa}] = 0.039 \times z[\mathrm{m}] + 0.185 \qquad (5.13)$$

$$S_v\,[\mathrm{MPa}] = 0.025 \times z[\mathrm{m}] \qquad (5.14)$$

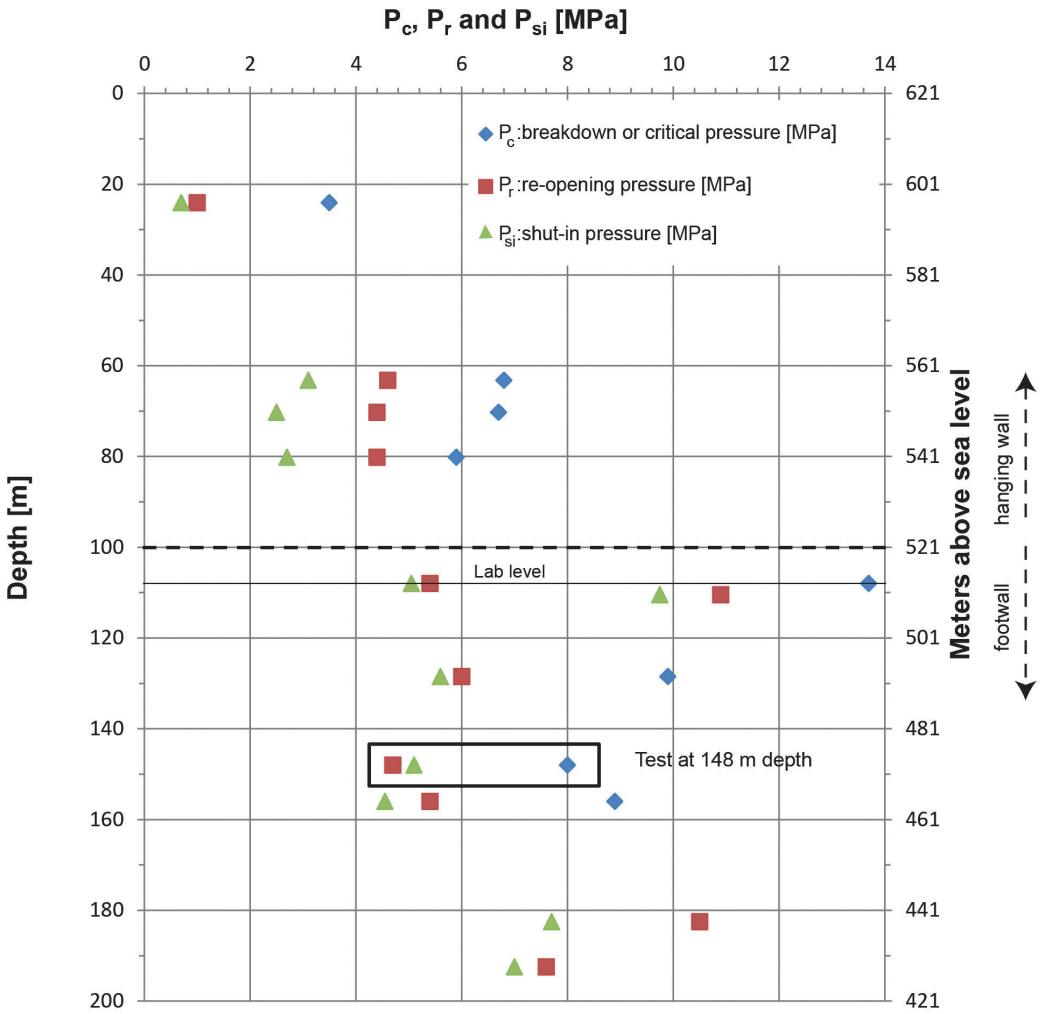

Fig. 5-6: Depth plot of breakdown pressure P_c, re-opening pressure P_r, and shut-in pressure P_{si} (modified after KLEE 2012). The numerical values of the pressures displayed in the figure are provided in Table G-4 in Appendix G. The test at a depth of 148 m is provided in Figure 5-5 and was analyzed in detail in Appendix G.

As mentioned above, for the two hydraulic fracturing campaigns in the hanging wall and the footwall of BDS-5, identification of induced or stimulated fractures was rather difficult on impression packers and image logs. In the hanging wall, only pre-existing features were opened and thus not considered for further interpretation. The most reliable test results of the tests in the footwall show N–S striking vertical to steeply inclined fractures. From these observations alone, the E–W orientation of S_H with 82°±19 for the hanging wall between depths of 24.1 and 80.2 m, as suggested by KLEE (2012), cannot be confirmed. Data from the deeper tests in the footwall between depths of 108 and 192.5 m suggest a N–S orientation of S_H with a mean of 14°±19° (Tab. 5-5).

Table 5-5: *Stress components at borehole BDS-5, modified after* KLEE *(2012).*

Stress components	Magnitude [MPa]	Stress direction (footwall) [°]
S_H	8.3	14±19
S_h	4.3	284
S_v	2.7	–

Considering only tests in the footwall and using the depth functions in eq. 5.12, 5.13 and 5.14, the horizontal stresses at rock laboratory level for z=107 m can be calculated. The evaluation of orientation was based on pre- and postfrack analysis of image logs.

The original interpretation of KLEE (2011) infers a decoupling of the tectonic stresses across the main detachment with a N–S orientation of S_H in the footwall and an E–W orientation in the hanging wall. However, the author reported difficulties in the identification of stimulated or induced fractures, as already reported by EVANS (1999) and ENACHESCU (2011), among others. A review of the test results from impression packer testing and pre- and postfrack analysis of im-

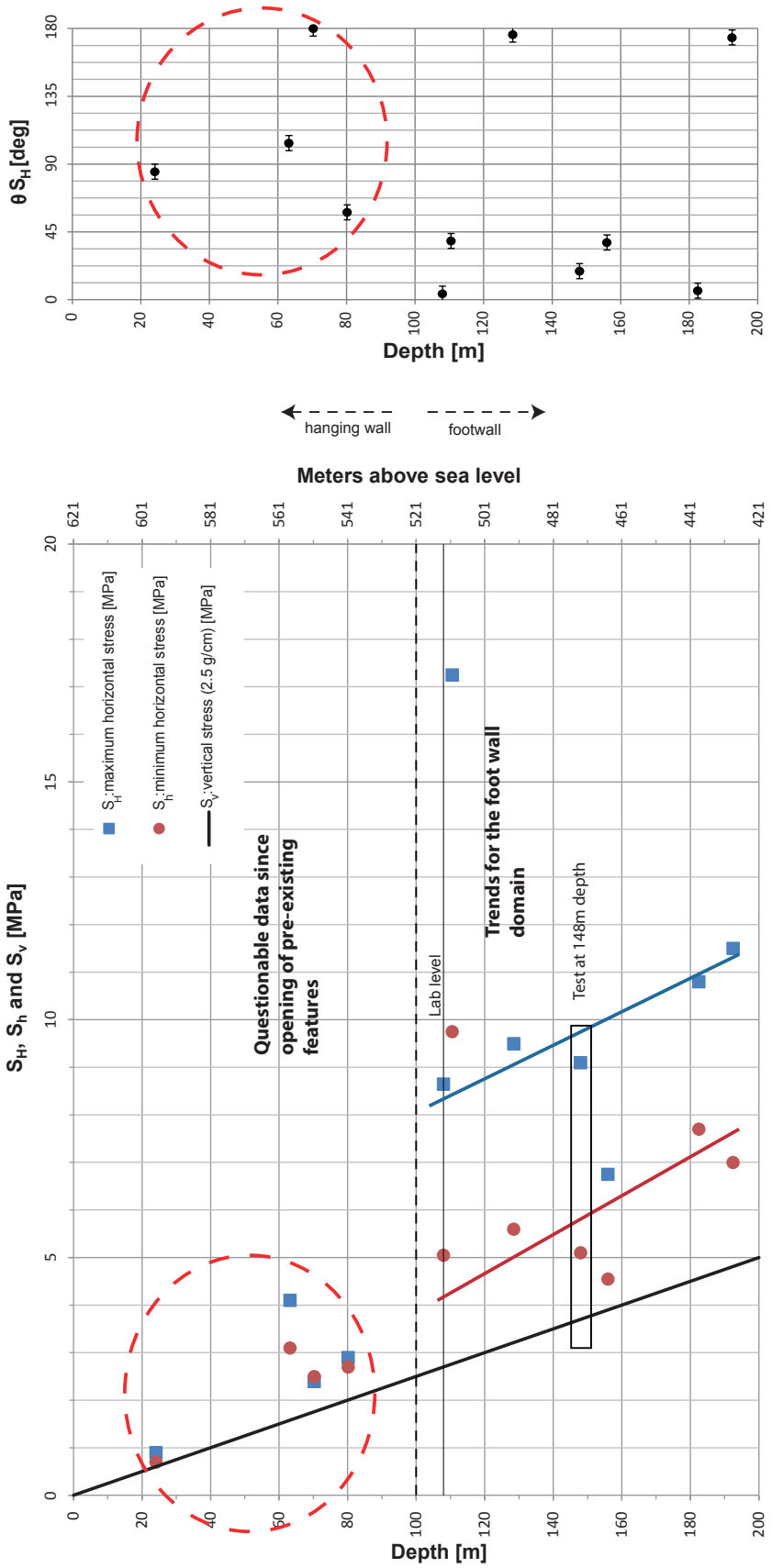

Fig. 5-7: Depth plot of stress magnitudes S_H, S_h, S_v and orientation of maximum horizontal stress S_H. The four tests in the hanging wall yielded questionable data due to missing induced axial features and are thus not included in the interpretation. The formula for the individual depth functions of S_H, S_h, S_v for the reliable tests in the footwall are given in equations 5.12, 5.13, and 5.14. For the calculation of the vertical stress a rock density of 2500 kg/m³ was assumed. The outliers at 110.5 m and 156 m are neglected for the calculation of the depth function. The well head is located at 621 m a.s.l. and the mean depth of the rock laboratory is 514 m a.s.l. The orientations of S_H were derived from pre- and postfrack analysis. The error bars for the direction of S_H show an uncertainty in the determination of ±5° (modified after KLEE 2012).

aging logs by swisstopo does not confirm the decoupling of tectonic stresses. The dataset in the hanging wall with Opalinus Clay at a very shallow position is too weak for an interpretation of magnitudes and orientations of horizontal stresses. In the Opalinus Clay, fractures with inclinations between 56° and 79° mostly northwards could be detected by comparing the optical logs. These are steeper than bedding, but with a comparable dip direction. From geological mapping (Appendix C) it is known that steep faults dipping northwards are common in the hanging wall. It is thus very probable that pre-existing features such as faults were opened during hydraulic fracturing. In the footwall, sub-vertical fractures with a strike direction N–S were induced. The features in the footwall can be regarded as axial features.

In theory, impression packer tests are needed in anisotropic argillaceous rocks such as the Opalinus Clay. After a hydraulic fracturing test, stimulated fractures tend to close again entirely and are hardly recognizable on optical logs. The induced fracture is opened again with the impression packers and produces a nice impression on the rubber. However, hydraulic fracturing in the Opalinus Clay generally opens pre-existing features such as bedding planes or faults. In the hanging wall of borehole BDS-5, no induced fractures could be observed on the impression packer tests. Axial features were all identified as scratches which most likely originated from the drilling process, e.g. retrieval of casing (Fig. 5-8). For an analysis of the borehole breakouts as performed by Enachescu (2011) the borehole is not deep enough. The Opalinus Clay in the hanging wall of borehole BDS-5 with depths shallower than 90 m did not show any evidence for a systematic orientation of borehole breakouts.

The orientation of the maximum principal stress axis in the hanging wall, as suggested by Klee (2011), is not consistent with the regional and large-scale stress tensor above the basal detachment within the Triassic evaporites (Nussbaum et al. 2011). Due to the superficial location of the Opalinus Clay and the position of borehole BDS-5 at the western flank of Mont Terri, topographic effects could dominate the stress field in the hanging wall. A decoupling across the main overthrust was reported from the Schafisheim borehole (Becker & Werner 1995), where the direction of S_H changed from a NNE–SSW direction in the sedimentary cover to a NW–SE direction below the main detachment in the basement. This decoupling, however, was observed there at a depth of 1400 m and thus cannot directly be compared to the BDS-5 borehole. In the footwall below, the stress state is consistent with the regional scale observations as well as with data obtained from the Mont Terri rock laboratory (Enachescu 2011), who proposed as best estimate an orientation of $S_H = 033°$ in the Opalinus Clay as well as in the Hauptrogenstein limestone of the back limb of the Mont Terri anticline.

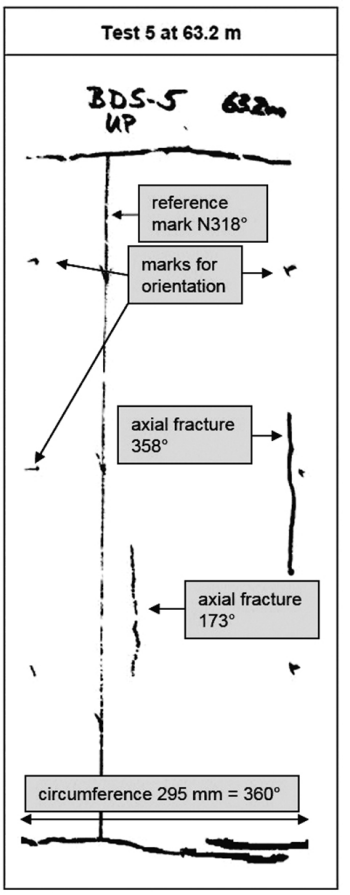

Fig. 5-8: Impression image of test no. 5 at 63.2 m depth. The circumference of 295 mm is equal to 360° (modified after Klee 2012).

5.4 Key results and conclusions

A total of 11 hydraulic fracturing tests and 10 impression packer tests were carried out in borehole BDS-5. Re-opening and shut-in pressures show a systematic increase with depth. There are indications that the tests in the hanging wall were likely dominated by the opening of pre-existing features (faults), while in the footwall, initiation and propagation of newly formed hydraulic fractures occurred. The interpretation of the footwall data can be done using standard hydraulic fracturing theory, which leads to depth-functions for maximum horizontal stress- and minimum horizontal stress-magnitudes yielding magnitudes of S_h 4.3 MPa and for S_H 8.3 MPa at a depth of 107 m or rock laboratory level. The analysis of the hydraulic fracturing orientation in the footwall suggest an S_H orientation of N14°±19° between depths of 108–192.5 m. In the hanging wall, the S_H orientation remains uncertain, since only the opening of pre-existing features a priori not aligned with any principal stress direction was achieved. The strike of these features is in average N82°±10°. The shut-in pressure represents the normal stress across these features and is an upper bound on the minimum principal stress. The shut-in pressures are relatively low in the hanging wall compared to the footwall. In the footwall a thrust regime ($S_v < S_h < S_H$) was measured, while in the hanging wall the nature of the stress regime remains uncertain, although it is likely controlled by superficial influences such as topography.

Numerous campaigns for the evaluation of the in-situ stress state have been conducted in and close to the Mont Terri rock laboratory. Early tests with borehole slotter as well as under- and overcoring yielded contradictory results (Bigarré 1996, 1997, Bigarré & Lizeur 1997, Bigarré et al. 1997). It was suspected that the rock mass close to boreholes

or galleries is affected by stress re-distribution (non-elastic response) and that future tests should be conducted with methods comprising larger rock volumes such as hydraulic fracturing methods and far out from the influence of the galleries (about 2–3 diameters). Bossart & Wermeille (2003) state that the stress field deduced from these early tests suggests a topographic control of the local stress field in the Mont Terri rock laboratory. The local maximum principal stress is sub-vertically oriented and does not coincide with the expected N–S orientation.

A set of in-situ stress measurements by overcoring, using CISRO stress cells, yielded magnitudes of 10 MPa, 9–10 MPa and 3 MPa for σ_1, σ_2, and σ_3 respectively (Lahaye 2005). Interestingly the orientations of σ_1 and σ_2 from this analysis were located in the bedding plane with σ_3 normal to it. This is not in accordance with other data from the rock laboratory and should be cross-checked with the latest values for rock elastic parameters since calculations were based on non-realistic elastic parameters. Further in-situ stress tests by using the overcoring technique also showed a maximum stress component oriented in the bedding plane with the same dip direction (Heusermann et al. 2014).

However, as Kupferschmied et al. (2015) have shown, the deformations in a drilled borehole in Opalinus Clay occur instantaneously and consequently with the development of a borehole disturbed zone (BDZ). Furthermore, the stress-release in-situ tests are based on the assumption that the rock behaves entirely elastic and in most studies even isotropic, which clearly is not the case. As a consequence, results from stress-release in-situ tests, such as borehole slotter and under- and overcoring, are inherently biased, a fact which should be taken into account for the interpretation of results.

Later hydraulic fracturing in the rock laboratory (Enachescu 2011) yielded more reliable data, although it suffered from the inability to clearly determine the orientations of the principal stresses. The experience with hydraulic fracturing in the Opalinus Clay has shown that predominantly pre-existing fractures and bedding planes are opened, all of which exhibit a much lower tensile strength than the intact rock mass. The last hydraulic fracturing campaign in the rock laboratory thus focused on deep boreholes in the Opalinus Clay and the Hauptrogenstein limestone south of the rock laboratory (Enachescu 2011). However, the same difficulties with the reactivation of pre-existing discontinuities were encountered. Despite this fact, an estimation of the orientation of the horizontal stress components could be made by means of an analysis of borehole breakouts and is now the reference for long vertical boreholes of >20 m depth in the Mont Terri rock lab (Tab. 5-3). In the footwall, evaluated stress data on borehole BDS-5 fits well into the regional scale dataset and the evaluated far field stress tensor.

The results of hydraulic fracturing campaigns in 2009 (Rummel et al. 2012) and 2010 (Enachescu 2011) in the Hauptrogenstein of borehole BDS-2 in the upper and the lower section are contradictory and not considered in the present study due to the impossibility to verify the obtained data of the first campagin.

Petrini & Simpson (2008) distinguished tectonic and topographic control in their numerical model of the Mont Terri anticline. For pure tectonic control they observed stress levels of up to 15 MPa for σ_1, which was also reported by Shin (2006, 2009) from the competent Muschelkalk and the Lettenkohle north of the rock laboratory. Petrini & Simpson (2012) furthermore conclude from their model that stresses are affected by layering and that the influence of tectonic forces or topography is strongly dependent on material properties.

The new compilation of all 33 in-situ stress measurements in and close to the Mont Terri rock laboratory has shown in general that, the stress field is anisotropic and the in-situ stress magnitudes and orientations are sometimes contradictory. An anisotropic stress field in combination with an anisotropic rock makes the interpretation of in-situ stress tests a challenging task.

Enachescu et al. (2014) proposed two major controls on stress for the in-situ tests conducted at the Mont Terri rock laboratory. The first control is the depth of the measurement with respect to topography and the second one is the location of the measurement with respect to rock types and their geometric distribution. In the present study a more refined concept is suggested, leading to a matrix of controls on in-situ stresses and mechanisms for three different cases. In spite of a highly scattered image for the principal stresses (Fig. 5-3), several groups of in-situ tests can be differentiated.

Deep boreholes in the Opalinus Clay, shallow boreholes in the Mont Terri rock lab, and boreholes located in the dolomites and limestone north of the rock laboratory can be separated from each other. In-situ stresses may be controlled by (Tab. 5-6):

- A. Excavation controlled stresses, where a primary stress field and a secondary stress field (influenced through excavation) can be distinguished. Generally, a distance of 2–3 tunnel-diameters is needed for undisturbed in-situ stress measurements. In-situ stress data in the Opalinus Clay of the rock laboratory are generally shallower than 20 m depth.
- B. Depth-controlled stresses, where at shallow levels topography plays an important role and at deeper levels the "Fernschub" leads to a bench-vice-situation, where horizontal tectonic forces dominate the stress field.
- C. Lithology-controlled stresses, where the rock competence (UCS, rock elastic parameters) builds an important control on the stress field. Stiff rocks act as a backbone and tend to transfer horizontal stresses and carry most of the load.

For every in-situ test, the stress field is a combination of these three controlling factors. In Table 5-6 the influences are indicated for three cases, and based on the existing dataset with 33 in-situ measurements, a best guess stress tensor is recommended:

1. Short boreholes (<20 m) on rock laboratory level and in Opalinus Clay

These boreholes can be influenced by both the primary and the secondary stress field. The depth level is shallow at rock lab level and thus topography-controlled. The rock is incompetent Opalinus Clay, yet for the sandy and also the carbonate-rich sandy facies rock stiffness can be up to three

Table 5-6: *Matrix of controls on in-situ stress and mechanisms for three different cases.*

Case	Mechanism / Control on stresses	Primary stress field	Secondary stress field	Deep level, "Fernschub"	Shallow level, topography influenced	Competent (UCS and E) high	Incompetent (UCS and E) low	Proposed stress tensor
1 Short boreholes <20 m rock lab level, Opalinus Clay	**A. Excavation**	+	+					σ_1 6–7 MPa 210°/70° subvertical $\sigma_{2/3}$ 4–5 MPa 320°/10° subhorizontal $\sigma_{3/2}$ 2–3 MPa 050°/15° subhorizontal
	B. Depth			–	+			
	C. Lithology					–	+	Martin & Lanyon (2003), Bossart & Wermeille (2003) – $\sigma_{2/3}$ in plane but not well defined
2 Long vertical borehole >20 m, in rock lab, Opalinus Clay	**A. Excavation**	+	–					σ_1 8.6 MPa 033°/0° horizontal σ_2 6.7 MPa 123°/70° subvertical σ_3 3.9 MPa 303°/20° subhorizontal
	B. Depth			+	–			
	C. Lithology					–	+	Enachescu (2011)
3 Boreholes in competent rock, N of rock lab, limestones and dolomites	**A. Excavation**	+	–					σ_1 15 MPa 320°/0° subhorizontal σ_2 8 MPa 070°/0° subhorizontal σ_3 4 MPa subvertical
	B. Depth			+	–			
	C. Lithology					+	–	Shin (2006, 2009)

+	applicable
–	not applicable
	not relevant
UCS	Uniaxial compressive strength
E	Elastic modulus

For every case the best guess stress tensor is proposed. The white fields are valid, where the symbols + or – mark whether a mechanism applies or not.

times higher. The proposed stress tensor for this group of boreholes is the one from Martin & Lanyon (2003) and Bossart & Wermeille (2003), where σ_1 is sub-vertical with a magnitude of 6–7 MPa and σ_2 and σ_3 lie in the horizontal plane but the directions are not well defined (Tab. 5-2). It has to be noted that the secondary stress field varies a lot, depending on the location relative to the excavations.

2. Long vertical borehole (>20 m) in the rock lab and in Opalinus Clay

A borehole such as this one is influenced by the primary stress field since it reaches zones far out of the rock-lab-influence, which is at least 2–3 tunnel diameters or >20 m. The depth level of such a borehole (e.g. BDS-4 55 m deep and vertical) reaches the bench vice of the "Fernschub"-influenced zone below the rock lab. The rock is incompetent Opalinus Clay. For BDS-4, an estimation for the stress tensor was carried out by Enachescu (2011), yielding a horizontal σ_1 trending towards 033° of 8.6 MPa, a sub-vertical σ_2 of 6.7 MPa dominated by the overburden (ρgh) and a sub-horizontal σ_3 trending in NW–SE direction with a magnitude of 3.9 MPa (Tab. 5-3).

3. Boreholes in competent rock, such as limestone and dolomites

For those boreholes, the primary stress field applies. Competent rock, such as dolomite or limestone acts as a back bone. They tend to transfer horizontal stresses and carry most of the loads. In competent rock, such as Lettenkohle and Muschelkalk north of the rock laboratory, σ_1 is sub-horizontally oriented towards NNW with a magnitude of about 15 MPa, σ_2 is sub-horizontal as well, and σ_3 is sub-vertical with a magnitude of 4 MPa (Shin 2006, 2009).

The following conclusion can be drawn for the BDS-5 borehole: Under the assumption that the evaluated stress components coincide with the principal stresses (which is the inherent assumption of the hydraulic fracturing method), the evaluated in-situ stresses in the footwall fit reasonably well with the stress tensor of Enachescu (2011) and also with the data from recent focal mechanisms (pers. comm. N. Deichmann, ETH Zurich). Thus, for the footwall in the competent rock of Late Jurassic limestone, case 3 (borehole in competent rock, such as limestone or dolomites) is representative. For the hanging wall in the Opalinus Clay above the main detachment, case 1 applies. The in-situ stress there is most likely controlled by topography.

6. Magnetic study on selected samples

C. Aubourg, R. Alzaruk

6.1 Objective and methodology

During the geological mapping of the drill cores, several fault gouges or shear zones have been encountered on core material, especially in the lower part of the Opalinus Clay section towards the basal thrust. Furthermore, a conspicuous black layer was detected within the Delsberg-Süsswasserkalk just a few meters below the basal detachment. Macroscopically, the surface was first interpreted as a tectonic or even seismic event which could be proof for recent seismic activity in the Mont Terri area. The surface greatly resembled an earthquake slip zone as reported from Taiwan by Hirono et al. (2007). Furthermore, Chou et al. (2012) have demonstrated that a gouge has the capability to record the earth's magnetic field during an earthquake.

The core material was sampled and analyzed on its magnetic susceptibility, the black layer characterized, and the possibility of tectonic origin tested (Aubourg et al. 2012). The study on this core material aimed to check whether the black layers are of tectonic or sedimentary origin and to check whether the fault zone is potentially active or not. The core material was wrapped into aluminum foil and put under vacuum on-site. In the laboratory, the samples were analyzed using optical and scanning electron microscope (SEM), measuring its magnetic susceptibility (magnetic fabric) and analyzing its palaeomagnetic record. Two samples of the BDS-5 borehole were analyzed and are briefly described below:

BDS5-79 (79.4–79.6 m), fault gouge, Opalinus Clay, Toarcian, hanging wall (Fig. 6-1)

The Opalinus Clay at that location is strongly deformed with lots of faults and fault zones or shear zones. The sample is located about 13 m above the main detachment in the hanging wall. On core material from 79.40–79.70 m, a shear zone with the orientation 360°/20° has been encountered within the Opalinus Clay, rich in biodetritic material and exhibiting a bedding orientation of 330°/45°. The rock contains a lot of framboidal pyrite, as a thin section analysis has shown.

BDS5-98 (98.3–98.8 m) black layer, Delsberg-Süsswasserkalk, Oligocene, top of footwall (Fig. 6-2)

The Delsberg-Süsswasserkalk extends from the depth of 97.7–98.7 m and consists of horizontally laminated crusty limestone with veins and gastropods and dark grey clayey marls from a lacustrine depositional environment. A more or less uniform clayey and sandy marl follows below, the Septarien-Ton. The sample originates from a rather marly

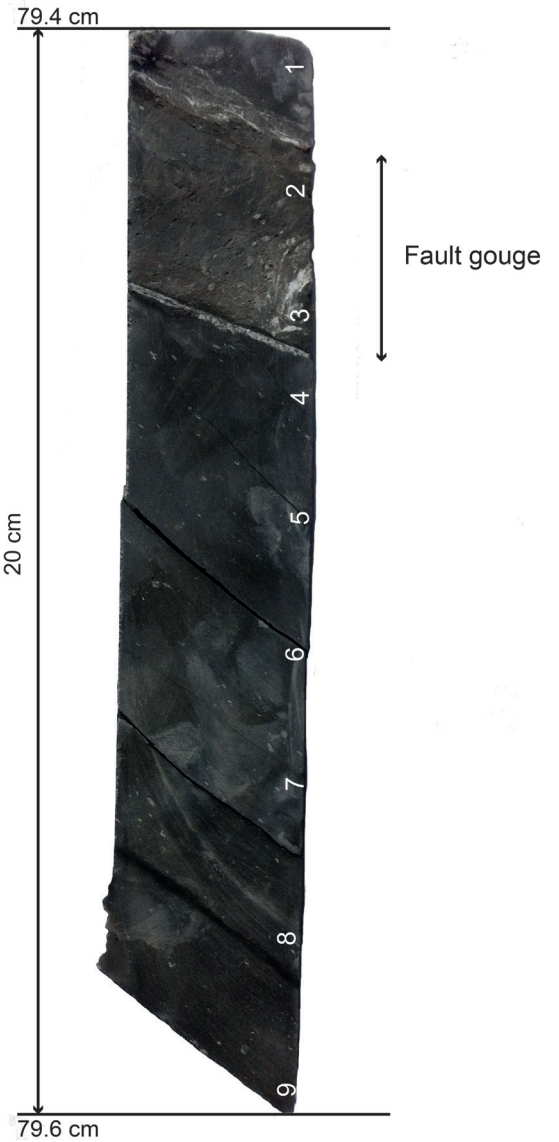

Fig. 6-1: Image of core sample BDS5-79 in the shaly facies of the Opalinus Clay. The numbers 1–9 correspond to the subsamples taken (after Aubourg et al. 2012).

section with an intercalated limestone bed from a depth of 98.6–98.7 m. Steeply inclined joints and veins are present above 98.3 m. At least three conspicuous polished horizontal contacts with shining glassy surfaces are present.

The methods that were applied are extensively described in Aubourg et al. (2012). Only some of the most important characteristics of these methods are mentioned in the following.

For microscopic analysis, scanning electron microscopy (SEM) coupled with energy dispersive spectrometry (EDS)

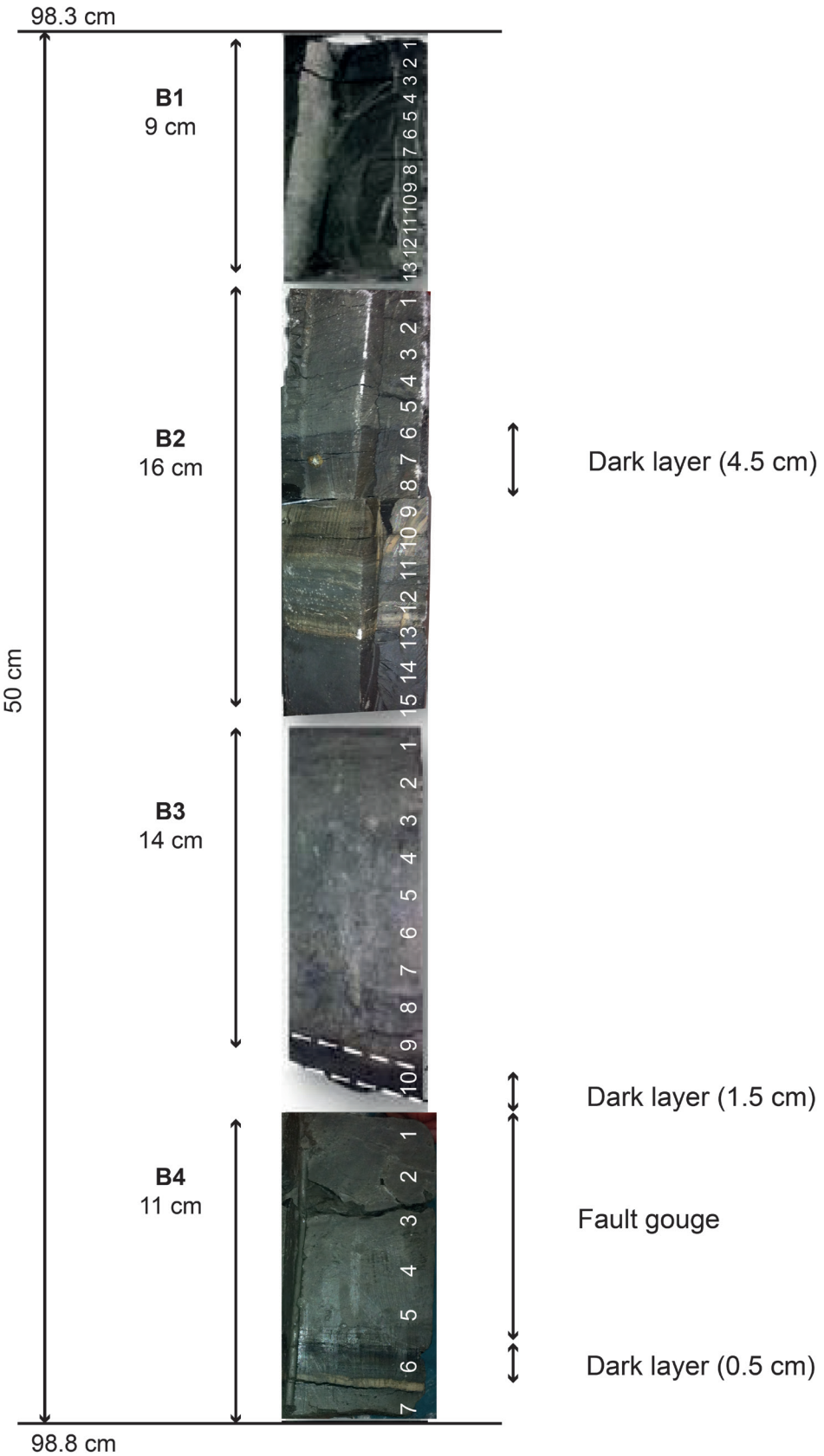

Fig. 6-2: Image of core sample BDS5-98 divided into four parts and the three remarkable dark layers with shining surfaces of 4.5 cm, 1.5 cm, and 0.5 cm thickness in the Delsberg-Süsswasserkalk, at a depth of 98 m. The numbering on the right side of the core corresponds to the subsamples taken (after Aubourg et al. 2012).

on a Zeiss Sigma SEM was used. Furthermore, binocular and reflected-light polarizing microscopes were used.

The evaluation of the anisotropy of the magnetic susceptibility (AMS) measurements was done by measuring cubic samples with an anisometer Kappabridge AGICOA MFK. This model allows measurements at different frequencies and different fields and has a rotary device for measuring anisotropy. Its sensitivity is 3×10^{-8} SI (dimensionless in SI system) for a nominal volume of 10.8 cm^3.

The anisotropy of magnetic susceptibility is determined by measuring low-field magnetic susceptibility in different directions along a sample. An AMS measurement of one rock specimen results in an ellipsoid of magnetic susceptibility (K) defined by the three principal axes K1 (max), K2 (int), and K3 (min). The long axis K1 represents the magnetic lineation, while the short axis K3 defines the pole of magnetic foliation. From the magnitude of these axes, three classical anisotropy parameters can be calculated:

Mean susceptibility: $Km=(K1+K2+K3)/3$ [SI] (6.1)

Degree of anisotropy: $P=Kmax/Kmin$ [–] (6.2)

Shape parameter: $T=(\ln F-\ln L)/(\ln F+\ln L)$ [–] (6.3)

where
$F=K2/K3$ and $L=K1/K2$

The mean susceptibility (Km) provides an indication of the content of magnetic minerals. The degree of anisotropy P is sensitive both to the degree of alignment of magnetic minerals (texture) and the intrinsic properties of magnetic minerals. The shape parameter (T) provides an indication whether the magnetic fabric is planar ($0<T\leq 1$) or linear ($-1\leq T<0$). AMS was selected as the key technique to assess the strain imprint in core samples.

Palaeomagnetic measurements of the natural remanent magnetization (NRM) were performed with a 2G Enterprise SQUID magnetometer. The NRM of U-channels (archive halves) and cubic samples have been analyzed in the automated stepwise AF demagnetization process (up to 40 mT). Two methods were applied for isolating the primary magnetization. The thermal demagnetization by heating a specimen to an elevated temperature below the Curie temperature of the constituent ferromagnetic minerals and then cooling to room temperature in zero magnetic fields. The second method is alternating magnetic field (AF) demagnetization by applying an alternating field of progressively higher magnitude.

6.2 Results from the magnetic study

6.2.1 Microscopic observations

The core sample BDS5-79 in the Opalinus Clay exhibits a well-defined fault gouge with a thickness of about 5 cm (sections 2+3 on Fig. 6-1). Both limits of the fault gouge are built by mm-thick Calcite fillings. Above and below, the Opalinus Clay remains undeformed with visible bedding.

Three remarkable, very sharp contacts are present in core BDS5-98 (Fig. 6-2). In the middle of core BDS5-98 (B2), a 4.5 cm thick zone of non-cohesive muddy black material was observed. In the lower part of BDS5-B3, a 1.5 cm thick oblique black layer is present, and in the lower part of BDS5-98 (B4), a 5 mm thick horizontal and glassy shining black layer with sharp boundaries could be found. On the sample BDS5-98 (B4) with the conspicuous glassy layer, the microscopic analysis was extended. The optical analysis of the black zones and layers revealed black elongated bodies of 1500–2280 µm in size (Fig. 6-3 a, b, c). All the black bodies have the same shape and are concentrated in the middle of the black zone. The elongated bodies are interrupted by sub-vertical calcite veins (Fig. 6-3 d).

The chemical analysis (EDS) of the black bodies revealed that they are mainly composed of organic matter with small amounts of quartz and sulfur. A few percent of pyrite is present in the black layers, which is a common mineral in anoxic sediments. Well preserved framboidal pyrite was observed, as well as pyrite grains accumulated in layers. Thus,

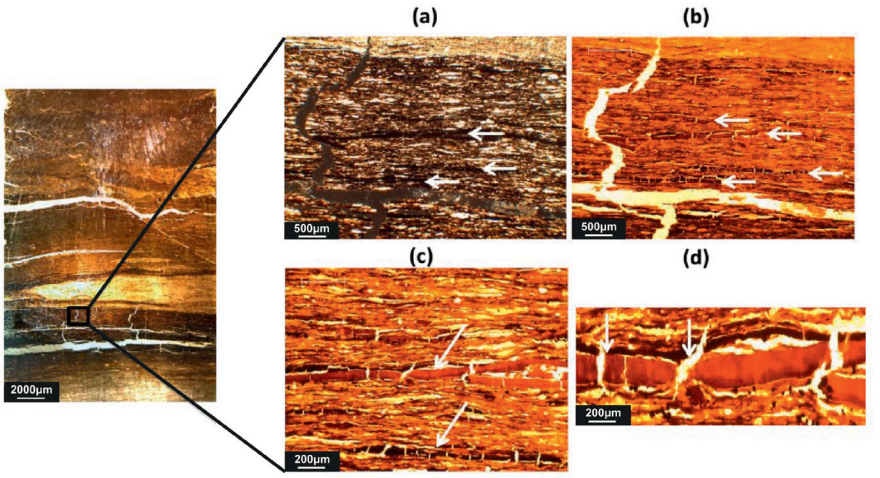

Fig. 6-3: Thin section from the black layer in sample BDS5-98 (B4) under optical microscope (a) plane light (b, c+d) polarized light. The white arrows indicateg the black bodies (from Aubourg et al. 2012).

the microscopic observations clearly indicate that these black layers are not of tectonic, but most likely sedimentary origin. The pyrite in the black layers appears well preserved and undeformed, which indicates that no major deformation process besides extension occurred recently. The extension led to a boudinage of the black layers where the gaps are filled up with calcite. The estimated extension is in the order of 8–10%.

However, just above these layers, gouge-like wavy structures are present with crushed pyrite framboids, indicating creep motion (Fig. 6-4). While the framboids from the rock wall are not deformed, the framboids in the gouge are either relatively undeformed or partly crushed. The transition from the wall rock to the gouge is very sharp with non-presence of fault breccia or cataclasites. Furthermore, Aubourg et al. (2012) observed patches of gypsum in some places, which can be interpreted as result of complete dissolution of pyrite. The gouge most likely formed under anoxic conditions since no chemical changes can be observed on the framboids. This indicates the absence of fluids in the gouge.

6.2.2 Observations on anisotropy of magnetic susceptibility

Anisotropy of magnetic susceptibility (AMS) was selected as the key technique to detect the strain imprint in core samples. AMS data from core BDS5-79 indicate that the Opalinus Clay displays a well-defined magnetic lineation which is more or less parallel to the fold axis. However, data from the fault gouge (sections 2+3) on Figure 6-5a show the same AMS as well.

The samples from cores BDS5-98 indicate either horizontal layering or gouges with no clear foliation (Fig. 6-5 b–e). Magnetic lineations all show a rather flat SW–NE orientation. The magnetic foliations for B1, B2 and B4 are rather poorly defined and sub-horizontal. Magnetic foliation is only well defined in the B3 sample and steeply dipping towards SE.

In the majority of the cores, the magnetic fabric shows oblate ellipsoids with positive T-factors and thus planar magnetic fabric. The degree of anisotropy is low, as expected for sedimentary rocks, ranging between 1.085 and 1.014, while the mean magnetic susceptibility ranging from 34 to 1 µSI.

6.2.3 Palaeomagnetic analysis

Orthogonal plots of alternating magnetic field (AF) demagnetization of U-channels (continuous core halves) were measured where both horizontal (X–Y) and vertical component (X–Z or Y–Z) are plotted (X=north, Z=vertical). Results from the BDS5-B4 core are given in Figure 6-6, where a creep-like gouge (samples 1–5) and horizontal black layers (samples 6 and 7) could clearly be identified. The magnetic record is generally fine and not noisy in the gouge. There are at least two components of normal polarity and probably some reverse components. This suggests that the gouge does not have recent activity and that remagnetization took place at least >0.78 Ma, and is thus older than the last magnetic chron of normal polarity (Brunhes chron). While some components are pointed northwards, some components deviate to the east in gouge samples (3, 4 and 5). The components in the wall rock (sample 6) resemble to the gouge. The measured magnetization of sample 6 is probably averaged by the neighboring gouge. On the course of demagnetization, distinct components between gouge samples and undeformed sediments can be observed. This proves that gouge samples, in spite of their strongly deformed nature, had the capability to record the Earth magnetic field.

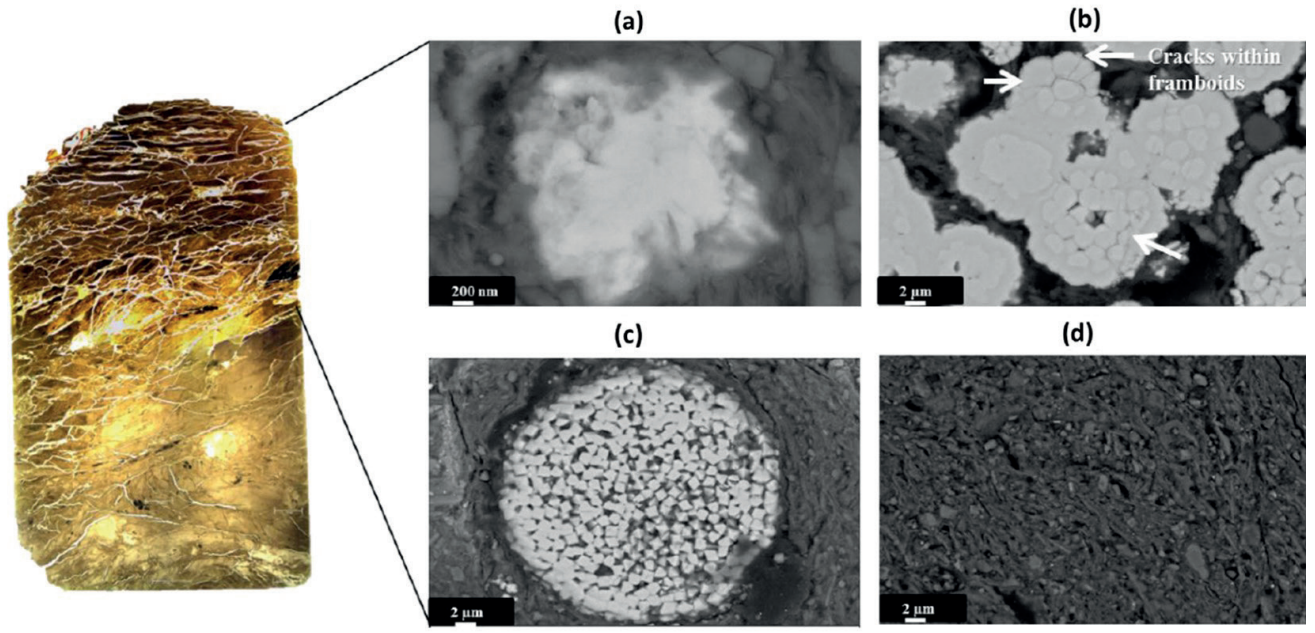

Fig. 6-4: Sample BDS5-98 (B4), upper part: SEM images showing three types of framboids in fault gouge. (a) pyrite totally crushed, (b) framboid partially crushed with cracks within framboids, (c) framboid preserved, wrapped by clays, (d) gouge matrix filled with clay minerals and calcite grains. On the left side, a thin section from the gouge is displayed (from Aubourg et al. 2012).

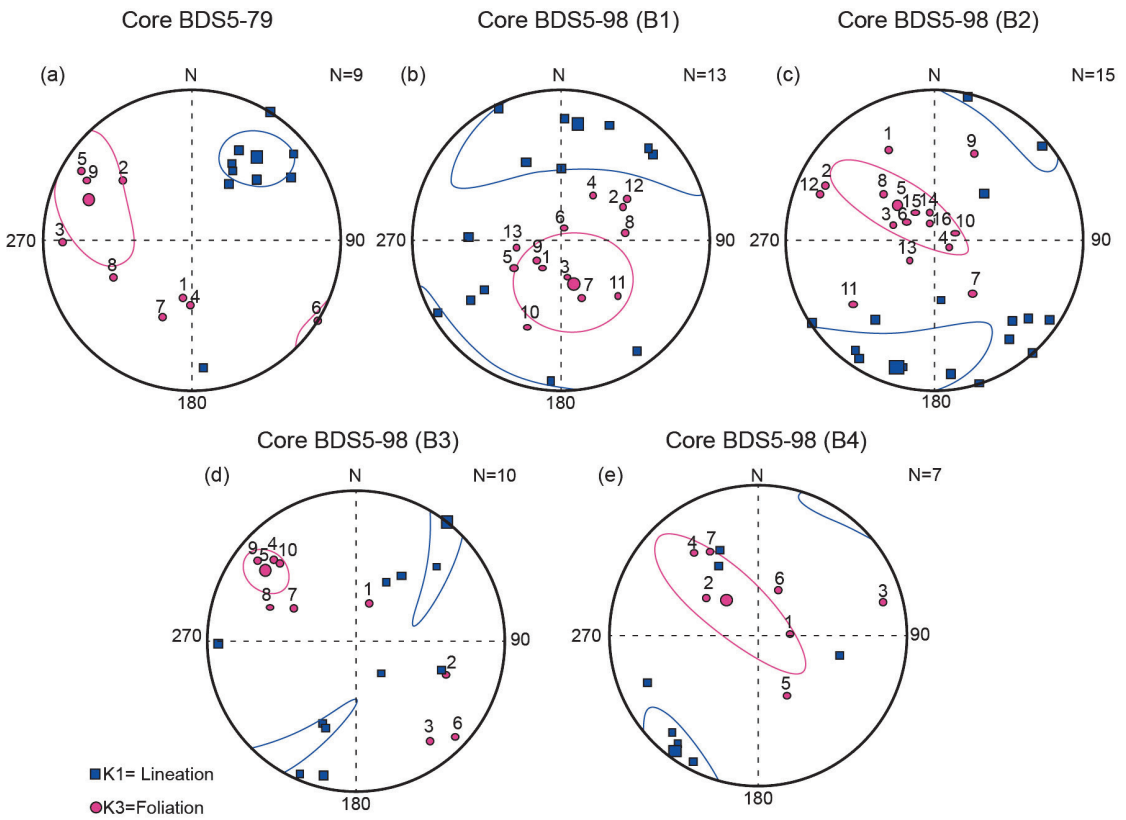

Fig. 6-5: The magnetic fabrics of core samples. BDS5-79 sections 2+3 are from a fault gouge and samples 1 and 4–9 are from undeformed Opalinus Clay. Samples BDS5-B1 to B3 predominantly consist of horizontal layers. In sample BDS5-B4, sections 1–5 can be assigned to a fault gouge and sections 6+7 to a horizontal black layer. Squares represent K1 axes and circles K3 axes. Their size corresponds with the confidence ellipse (from Aubourg et al. 2012).

6.3 Key results and conclusions

The most important results of the three different methods applied are listed in the following.

Microscopic data

- The black layers within the Delsberg-Süsswasserkalk are clearly of sedimentary origin.
- The fault gouge in the Opalinus Clay above shows a demonstrable evolution of pyrite minerals as observed and reported by Chou et al. (2012) from a gouge in Taiwan. It was formed by aseismic fault creep. Two observations indicate that the fault gouge does not result from recent activity. There is evidence of extensional tectonics which took place after the compressional phase. Furthermore, magnetic analysis reveals that the gouge retains a complex assemblage of palaeomagnetic components >0.78 Ma.

AMS data

- A magnetic lineation is developed parallel to the direction of the fold axis and thus normal to the tectonic compression. This observation could be made in the Opalinus Clay, in the Cenozoic rocks, and in the fault gouges as well. Therefore, the magnetic lineation is interpreted as having formed contemporaneously with the Mont Terri anticline.
- A steep magnetic foliation is present in the gouges which probably has a tectonic significance. The results are consistent with a SE–NW direction of compression. According to Aubourg et al. (2012), this fabric is contemporaneous with the displacement along the flat ramp.

Palaeomagnetism

- The data indicate that the gouge has the capability to record a magnetization after its formation. The mechanism for this process remains unclear. Aubourg et al. (2012) propose shear heat as a plausible mechanism. However, since no seismic event has been encountered on core material in this study, only slow deformation rates were present in the past, which hardly has sufficient heat potential.

Two samples have been analyzed from the lower part of the Opalinus Clay in the hanging wall and the Delsberg-Süsswasserkalk just below the main detachment in the footwall. The chemical analysis of the black bodies within the freshwater limestone at a depth of 98.5 m revealed that they are mainly composed of organic matter. Consequently, these are undeformed accumulations of organic matter within a lacustrine environment and not “pseudotachylites”, which would infer a seismic origin. No seismic event was detected on the rock material and the two analyzed samples.

Anisotropic magnetic susceptibility data indicate a stretching along the fold axis of the Mont Terri anticline,

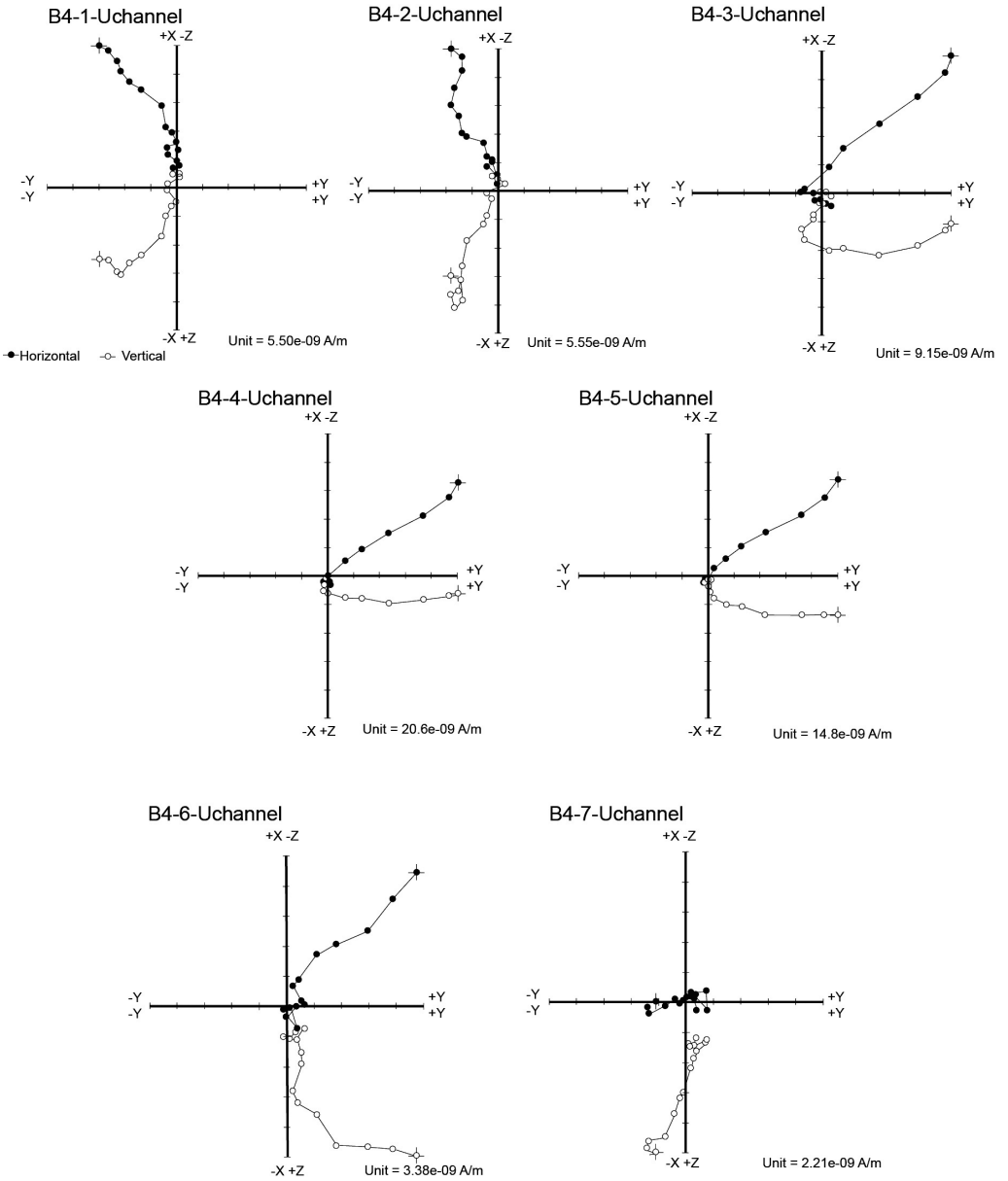

Fig. 6-6: Plots of NRM components during AF demagnetization from 7 sections of BDS5-B4. Sections 1–5 are from a gouge and sections 6+7 from a black layer. Black symbols lie within the horizontal plane (X-Y with X parallel to north) and open symbols lie within the vertical plane (Y-Z with Z positive upward) (from Aubourg et al. 2012).

which is consistent with the tectonic compression normal to the fold axis. Palaeomagnetic data suggest that the gouges do not originate from recent activity and that remagnetization took place before 0.78 Ma or earlier. The palaeomagnetic record exhibits well-defined components in the gouge, indicating that a physical process – chemical or thermal, for instance – is responsible of the magnetic imprint after the gouge formation.

7. Interpretation and discussion

D. Jaeggi, P. Bossart, C. Nussbaum

The borehole consists of three main parts. Late Jurassic rocks in the footwall form the first part. On top of that, but still in the footwall, Paleogene rocks and a tectonic mélange just below the main detachment form the second part, which still belongs to the Tabular Jura. The third part consists of the Opalinus Clay and the capping unconsolidated sediment in the hanging wall. The hanging wall corresponds to the overthrust sediments of the Folded Jura. The top part of the Opalinus Clay, comprised from top to bottom of shaly facies, sandy facies and carbonate-rich sandy facies and again shaly facies, is clearly of Aalenian age (Opalinum zone). At a depth of around 40 m, a transition from Aalenian to Toarcian (Torulosum subzone Aalensis zone) could be identified. This transition was also identified in the Mont Terri rock laboratory in a similar stratigraphic position of about 15 m below the bottom of the carbonate-rich sandy facies. The initial prognosis of the borehole corresponded well with the encountered situation concerning the depth-level of the overthrust and the transition to the Reuchenette Formation in the footwall. In terms of its geological section, the borehole is thus already located in the flat of the detachment fold. However, it was not clear from the prognosis whether the Staffelegg Formation, or even multicolored dolomitic marls of the Keuper, would be encountered or not. The main reason for this was that the prognosis was based on geological knowledge from the Mont Terri motorway tunnel and thus from a section about 250 m to the east. In the complex core of the Mont Terri anticline, the structures are especially not cylindrical and thus difficult to extrapolate. The thickness of the thrust zone is 3.2 m and comprised of tectonic mélange. The Paleogene sediments below remained more or less undeformed. The Opalinus Clay above, however, is affected by brittle deformation in the lower 40 m.

The bedding in the hanging wall rather steeply (30–40°) dips northwards. Compared to the overturned beds at the same position (dipping 60° towards S) a few 100 m towards the east, this is a very sharp change in its structural style and implies a different strain partitioning. A N–S- or NNE–SSW-striking Rhenish fault, which separates these two compartments is postulated. In the footwall, bedding ranges between 10–15° towards NNE (Appendix C), which could be related to the deformation in the footwall of the Mont Terri anticline or to the Eocene-Oligocene flexure along the Rhine-Bresse transfer zone. It seems that some large amplitude smooth undulations are present in the footwall, which could be linked to the folds observed in Late Jurassic rocks further north and/or to the presence of a Permo-Carboniferous trough.

Hydraulic fracturing data of borehole BDS-5 (Klee 2012) was reviewed and re-interpreted by swisstopo. Taking into account only reliable data of the footwall, an S_H of 8.3 MPa, S_h of 4.3 MPa and an S_v of 2.7 MPa at rock lab level (514 m a.s.l.) can be calculated. The analysis of the stress directions suggests for the tests a N–S orientation of S_H with 14°±19° in the footwall between depths of 108 and 192.5 m. This direction of S_H is consistent with regional scale data and data from deep boreholes of the Mont Terri rock laboratory. A decoupling of the principal stresses across the main detachment, as suggested by Klee (2011), cannot be confirmed after a review of the available dataset. Data quality in the hanging wall is too weak for reliable interpretation of test results.

Generally, induced axial fractures can be detected with impression packer tests. In this case, however, no induced features could be found with the technique in the Opalinus Clay. The analysis of stress orientation in the hanging wall performed by Klee (2011) relies entirely on the analysis of pre- and postfrack imaging logs, which only detected preexisting features. Furthermore, borehole breakouts suitable for analysis of stress directions are not present in such a shallow borehole, with the Opalinus Clay entirely located at a depth shallower than 90 m. Numerical modeling (Petrini & Simpson 2008, 2012) showed that the stress field in the upper part of the Mont Terri anticline, including the Opalinus Clay in the Mont Terri rock laboratory, is mainly dominated by topographical control (Fig. 5-4), which most likely is also the case for the Opalinus Clay section in the hanging wall of borehole BDS-5. A recent review of the in-situ stress data of the DS experiment by Enachescu et al. (2014) came to the same conclusion, however, by considering the results of shallow hydraulic fracturing data in the Opalinus Clay of borehole BDS-5. The stress field below the main detachment in the Late Jurassic rocks is consistent with regional scale data and fits reasonably well with both the stress tensor of Enachescu (2011) and data from recent focal mechanisms of the region which indicate a N–S compression. However, the new compilation of all available 33 in-situ stress measurements in and close to the Mont Terri rock laboratory showed that the stress field is generally anisotropic and the in-situ stress tests are sometimes contradictory. An anisotropic stress field together in combination with anisotropic rock makes the interpretation of in-situ stress tests a challenging task. Petrini & Simpson (2012) could furthermore show with their numerical model that stresses are affected by layering and that the influence of tectonic forces or topography is strongly dependent on material properties. Based on the compilation of the 33 in-situ stress measurements (Fig. 5-3) together with the results from numerical modeling and the latest data from borehole BDS-5, a conceptual model of controls on in-situ stress and mechanisms for three different cases could be elaborated (Tab. 5-6). The three different

controls excavation, depth, and lithology were cross-checked with the mechanisms stress field, depth level and rock competence or stiffness, and finally led to three distinct cases:

Case 1 concerns short boreholes of <20 m depth located in the Mont Terri rock laboratory. Here, the stress tensor from Martin & Lanyon (2003) and Bossart & Wermeille (2003) is proposed, where σ_1 is sub-vertical with a magnitude of 6–7 MPa and σ_2 and σ_3 lie in the horizontal plane, although the directions are not well defined. Case 2 concerns the long, vertical boreholes with depths of >20 m drilled vertically down in the Mont Terri rock laboratory. Here, the stress tensor proposed by Enachescu (2011) applies, with a horizontal σ_1 of 8.6 MPa, trending towards 033°. σ_2 is 6.7 MPa, sub-vertical and dominated by overburden, and σ_3 is sub-horizontal trending NW–SE with a magnitude of 3.9 MPa. Case 3 concerns boreholes in competent rock, such as limestone or dolomites. In the Lettenkohle and the Muschelkalk NNW of the Mont Terri rock laboratory, a sub-horizontal σ_1 of 15 MPa was found by Shin (2006, 2009). This stress concentration in stiff, competent rocks was satisfyingly confirmed by numerical modeling (Petrini & Simpson 2008). σ_2 is also sub-horizontal, while σ_3 is 4 MPa and sub-vertical.

Case 3 (borehole in competent rock, such as limestone or dolomites) is representative for the Late Jurassic rocks in the footwall of borehole BDS-5. For the hanging wall in the Opalinus Clay above the main detachment, case 1 (shallow boreholes in the Opalinus Clay or at rock lab level) applies.

No indications of Neotectonics could be found on core material. The two analyzed conspicuous horizons from the Delsberg-Süsswasserkalk were identified as accumulations of organic matter in a lacustrine depositional environment. Furthermore, gouges were analyzed with Alternating Field (AF) demagnetization on their palaeomagnetic footprint. The data suggest that the gouges do not originate from recent activity and that remagnetization took place before 0.78 Ma or earlier. A physical process such as chemical or thermal overprinting is responsible of the magnetic field after the gouge formation. Gouges are thus capable to preserve geomagnetic information during their formation. The encountered magnetic foliation in the analyzed gouges is consistent with a SW–NE compression of the Mont Terri anticline.

Indications for karst could be found down to 66 m below the Eocene palaeosurface. This proves that the former rock surface of the Late Jurassic rocks was deeply affected by karst processes, such as dissolution of carbonate, collapse and disintegration of the rock and precipitation of residual clays. It seems that these residual clays have entirely clogged the solution-enlarged fractures and cavities since permeability of the rock is not enhanced, as it could be shown with hydro tests and water level measurements during drilling. However, pore water pressure monitoring and frequency analysis of pore pressure time series revealed two hydraulically separated units: an upper confined unit in the Opalinus Clay not yet in equilibrium and a lower aquifer in the limestone of Oxfordian and Kimmeridgian age which is in equilibrium and influenced by diurnal and semi-diurnal Lunar and Solar tides. The overpressure in the Opalinus Clay compared to the aquifer in the footwall suggests the occurrence of chemico osmotic effects. Despite the still transient pressure signals in the Opalinus Clay, the M_2-signal was sufficiently robust for calculating specific storage, which is $4.0 \times 10^{-6}\,m^{-1}$ and within the range of values obtained from cross-hole hydraulic tests in the rock laboratory (Bossart & Thury 2008).

8. Conclusions

D. Jaeggi, P. Bossart, C. Nussbaum

The borehole was drilled without any influence on the catchment area of sources. No loss of fluid that could pollute any potential aquifers was recorded during the drilling operation. Compared to the aquifer below, the Opalinus Clay was clearly identified as a confining unit with an overpressure. In this aquifer of Late Jurassic limestone, fractures were completely clogged with residual clays from Eocene karst.

No exploitable resource was encountered in the 216 m deep borehole. Even the suitability of Late Jurassic rocks as a reservoir rock must be questioned in regards to the low permeability encountered during various investigations (core mapping, water level survey while drilling, hydraulic pressure pulse tests, pressure signal analysis). Opalinus Clay as well as at least the upper part of the footwall, clogged with residual clays, can be termed cap rocks.

The evaluation of in-situ stresses in the Opalinus Clay remains a challenging task and needs to be developed further. Stress-release in-situ stress tests in the Opalinus Clay are biased and not suitable for this type of rock. Hydraulic fracturing also proved to be problematic in the Opalinus Clay. A best guess stress tensor for boreholes out of the rock-lab-influence is given in Enachescu (2011), with σ_1 horizontal and trending towards N or NNE, and σ_2 controlled by the overburden. In the rock lab for boreholes shallower than 20 m, the stress tensor of Martin & Lanyon (2003) and Bossart & Wermeille (2003) is suggested, with σ_1 sub-vertical and controlled by the overburden (6–7 MPa at rock-lab-level). σ_2 and σ_3 are either parallel or perpendicular to the Mont Terri motorway tunnel, but not well defined in their orientation. Even after 33 measurements in the Mont Terri rock laboratory the data set remains very heterogeneous and the interpretation of the tests a challenging task. A matrix which could act as an orientation for the planning and interpretation of future in-situ stress tests and furthermore build an important planning tool for geothermal boreholes, CO_2-sequestration and shale gas was elaborated. For fracking purposes, boreholes should be drilled in the σ_1/σ_3-plane, which is based on the results from the footwall of the BDS-5 borehole, a vertical plane striking towards N or NNW. The highest borehole stability can be granted in this plane for boreholes similar to BDS-5.

From the hydraulic fracturing data available in BDS-5, no reliable analysis of the in-situ stress magnitudes or directions is possible in the hanging wall. A decoupling of the in-situ stresses as postulated by Klee (2011) thus cannot be confirmed. The analysis results in the footwall are consistent with regional scale data and focal mechanisms from recent, very shallow seismic activity in the St.Ursanne region. The Opalinus Clay in the hanging wall is located well above the influence of tectonic compression and thus most likely mainly controlled by topographical effects.

References

Ababou, R., Fatmi, H. Matray, J. M., Nussbaum, C. & Bailly, D. (2012): Statistical analysis of pore pressure signals in claystone during excavation works at the Mont Terri Underground Research Laboratory. Characterization of clay stone at the Mont Terri Underground Research Laboratory dedicated to research on radioactive waste disposal: statistical analyses of pore pressure signals, hydrogeologic properties and evolution of excavation disturbed zone (EDZ). – Radioactive Waste, tech. open Access Publ. *17*, 373–418.

Aubourg, C., Alzaruk, A. & Nussbaum, C. (2012): PS Experiment: Magnetistudy of gouge from Borehole BDS-5. – Mont Terri Proj. intern. tech. Note. 2012-40. swisstopo, Wabern/CH.

Bailly, D., Matray, J. M. & Ababou, T. (2012): Statistical pre-processing and reconstruction methods for subsurface hydro-meteorological and crack aperture time series. – XIX International Conference on Water Resources CMW, University of Illinois at Urbana-Champaign, June 17–22.

Becker, A. (1999): In situ stress data from the Jura Mountains. New results and interpretation. – Terra Nova *11*/1, 9–15.

— (2000): The Jura Mountains: An active foreland fold-and-thrust belt? – Tectonophysics *321*, 381–406.

Becker, A. & Werner, D. (1995): Neotectonic state of stress in the Jura Mountains. – Geodin Acta *8*/2, 99–111.

Bigarré, P. (1996): In situ stress measurements (IS), Design of experiment IS-A (combined over- and under-coring technique). – Mont Terri Proj. intern. tech. Note. 1996-28. swisstopo, Wabern/CH.

— (1997): In-situ Stress measurement IS-A: Raw data report (rough measurements). – Mont Terri Proj. intern. tech. Note. 1997-10. swisstopo, Wabern/CH.

Bigarré, P., Camus, P. & Guinard, E. (1997): In-situ stress measurement (IS-A): Long term measurements. – Mont Terri Proj. intern. tech. Note. 1997-40. swisstopo, Wabern/CH.

Bigarré, P. & Lizeur, A. (1997): In-situ stress measurement (IS-A): Results of the in-situ experiment: calculation of the stress. – Mont Terri Proj. intern. tech. Note. 1997-14. swisstopo, Wabern/CH.

Bitterli, P. (2012): Die Ifenthal-Formation im nördlichen Jura. – Swiss Bull. angew. Geol. *17*/2, 93–117

Bläsi, H.R. Peters, T.J. & Mazurek, M. (1991): Der Opalinus – Ton des Mont Terri (Kanton Jura): Lithologie, Mineralogie und physikochemische Gesteinsparameter. – Nagra intern. Ber., 90-60.

Bläsi, H.R. (2011): DS-Experiment, Stratigraphy of the BDS-5 borehole. – Mont Terri Proj. intern. tech. Note. 2011-55. swisstopo, Wabern/CH.

Bollinger, T., Engesser, B. & Weidmann, M. (1993): Première découverte de mammifères pliocènes dans le Jura neuchâtelois – Eclogae Geol. Helv. *86*, 1031–1068.

Bossart, P. & Thury, M. (2008): Mont Terri Rock Laboratory. Project, programme 1996 to 2007 and results. – Rep. swiss geol. Surv. *3*.

Bossart, P. & Wermeille, S. (2003b): The stress field in the Mont Terri region – data compilation. In: Heitzmann, P. & Tripet, J.-P. (Ed.): Mont Terri Project – Geology, paleohydrology and stress field of the Mont Terri region (p. 65–92). – Rep. FOWG, geol. Ser. *4*.

Bredehoeft, J.D. (1967): Response of well aquifer systems to earth tides. – J. appl. Res. *72*/12, 3075–3078.

Bühler, C. (2000): IS-B Experiment: Results of long-term dilatometer measurements. – Mont Terri Proj. intern. tech. Note. 1997-41. swisstopo, Wabern/CH.

Burkhalter, R.M. (1995): Ooidal ironstones and ferruginous microbialites: origin and relation to sequence stratigraphy (Aalenian and Bajocian, Swiss Jura mountains). – Sedimentology *42*, 57–74.

— (1996): Die Passwang-Alloformation (unteres Aalénien bis unteres Bajocien) im zentralen und nördlichen Jura. – Eclogae geol. Helv. *89*, 875–934.

Caer, T., Maillot, B., Souloumiac, P., Leturmy, P., De Lamotte, D.F. & Nussbaum, C. (2015): Mechanical validation of balanced cross-sections: the case of the Mont Terri anticline at the Jura front (NW Switzerland). – J. struct. Geol. *75*, 32–48.

Chou, Y.-M., Song, S.-R., Aubourg, C., Song, Y.-F., Boullier, A.-M. & Lee, T.-Q. (2012): Pyrite alteration and neoformed magnetic minerals in the fault zone of the Chi-Chi earthquake (Mw 7.6, 1999): Evidence from frictional heating and co-seismic fluids. – Geochemistry, Geophysics, Geosystems, AGU and the geochem. Soc., *13*/8.

Comment, G., Ayer, J. & Becker, D. (2011): Deux nouveaux membres lithostratigraphiques de la Formation de Reuchenette (Kimméridgien, Ajoie, Jura Suisse) – Nouvelles données géologiques et paléontologiques acquises dans le cadre de la construction de l'autoroute A16 (Transjurane). – Swiss Bull. angew. Geol, *16*/1, 3–24.

Cooper, H.H., Bredehoeft, J.D. & Papadopulos, I.S. (1967): Response of a finite diameter well to an instantaneous charge of water. – Water Resources Research *3*, 263–269.

Cornet, F.H. (1993): The HTPF and the integrated stress determination methods. In: Hudson, J.A. (Ed.): Comprehensive Rock Engineering (p. 413–432). – Pergamon Press, Oxford.

Enachescu, C. (2011): DS experiment: fracking tests in BDS-2 and BDS-4 at the Mt. Terri Underground Research Facility. FMT DS experiment phase 15. – Mont Terri Proj. intern. tech. Note. 2010-53. swisstopo, Wabern/CH.

Doe, T. & Vietor, T. (2015): Review of in situ stress measurements and their context. – Mont Terri Proj. intern. tech. Report. 2012-06. swisstopo, Wabern/CH.

Evans, K., Piedevache, M. & Portmann, F. (1999): IS Experiment: Hydrofracture stress tests in boreholes BIS-C1 and BIS-C2. – Mont Terri Proj. intern. tech. Note. 1999-55. swisstopo, Wabern/CH.

Freivogel, M. & Huggenberger, P. (2003): Modellierung bilanzierter Profile im Gebiet Mont Terri - La Croix (Kanton Jura). In: P. Heitzmann & J.P. Tripet (Ed.), Mont Terri Project – geology, paleohydrology and stress field of the Mont Terri region (p. 7–44). – Rep. FOWG, geol. Ser. *4*.

Gonzalez, R. & Wetzel, A. (1996): Stratigraphy and paleogeography of the Hauptrogenstein and Klingnau Formations (middle Bajocian to late Bathonian), northern Switzerland. – Eclogae geol. Helv. *89*, 695–720.

Gygi, R.A. (1969): Zur Stratigraphie der Oxford-Stufe (oberes Jura-System) der Nordschweiz und des süddeutschen Grenzgebietes. – Beitr. geol. Karte Schweiz [N.F.] *136*.

Hardenbol, J., Thierry, J., Farley, M.B., Jacquin, T., De Graciansky, P.-C. & Vail, P.R. (1998): Jurassic chronostratigraphy. In: De Graciansky, P.C., Hardenbol, J., Jacquin, T. & Vail, P.R. (Ed.): Mesozoic and Cenozoic sequence stratigraphy of European basins (p. 763–781).

Hekel, U. (1994): Hydrogeologische Erkundung toniger Festgesteine am Beispiel des Opalinustons (Unteres Aalenium). – Tübinger geowiss. Arb. (TGA) *C*/18, 1–170.

Heusermann, S., Lege, C. & Küchemann, W. (2014): Rock stress measurements at the Mont Terri Rock Laboratory (IS-D). – Mont Terri Proj. intern. tech. Report. 2014-08. swisstopo, Wabern/CH.

Hirono, T., Yeh, E.-C., Lin, W., Sone, H., Mishima, T. & Soh, W. (2007): Nondestructive continuous physical property measurements of core samples recovered from hole B, Taiwan Chelungpu-Fault Drilling Project. – J. geophys. Res. *112*, B07404.

Hostettler, B., Reisdorf, A.G., Jaeggi, D., Deplazes, G., Bläsi, H.R., Morard, A., Feist-Burkhardt, S., Waltschew, A., Dietze, V. & Menkveld-Gfeller, U. (2017 submitted): Litho- and biostratigraphy of the Opalinus Clay and bounding formations in the Mont Terri rock laboratory (Switzerland). – Swiss J. Geosci.

Ito, T., Evans, K., Kawai, K. & Hayashi, K. (1999): Hydraulic fracture reopening pressure and the estimation of maximum horizontal stress. – Int. J. Rock Mech. Min. Sci. *36*/6, 811–826.

Jaeggi, D., Müller, P. & Nussbaum, C. (2012): DS (determination of stress) experiment: Report about the drilling activities and the geology/hydrogeology encountered at borehole BDS-5, Location: Derrière Mont Terri, Courgenay (Switzerland). – Mont Terri Proj. intern. tech. Report. 2012-05. swisstopo, Wabern/CH.

Jaeggi, D. & Nussbaum, C. (2009): DS determination of stress borehole BDS-2: visual core description and interpretation of facies. – Mont Terri Proj. intern. tech. Note. 2009-58. swisstopo, Wabern/CH.

— (2011): LP Experiment: Long term monitoring of pore pressures – Data report of Phases 13–15. – Mont Terri Proj. intern. tech. Note. 2008-73. swisstopo, Wabern/CH.

Jahns, E. (2011): DS Experiment: BDS-1: Determination of the 3D total and effective stress using RACOS®, final report. – Mont Terri Proj. intern. tech. Note. 2011-02. swisstopo, Wabern/CH.

Jordan, P. (2007): Sammelprofile der Sedimentgesteine der verschiedenen geologisch-tektonischen Einheiten der Schweiz. – Nagra Arbeitsber. NAB 07-35.

Kälin, D. (1993): Stratigraphie und Säugetierfaunen der obersten Süsswassermolasse der Nordwestschweiz. – Ph. D. thesis 10152, ETH Zürich.

Klaudius, J., Gracia, M., Fischer, D. & Pohl, C. (2011): Borehole logging in Derrière-Mont Terri, in the hole BDS-5 15th of June – 1st of July 2011. – Mont Terri Proj. intern. tech. Note 2011-42. swisstopo, Wabern/CH.

Klee, G. (2012): Determination of stress (DS) experiment: hydraulic-fracturing stress measurements in BDS-5 borehole at Derrière-Mont Terri. – Mont Terri Proj. intern. tech. Note. 2011-45. swisstopo, Wabern/CH.

König, E. & Bock, H. (1997): IS-B experiment, phase 2 in-situ stress measurements with the INTERFELS borehole slotter method along boreholes BIS-B1, BIS-B2 and BIS-B3. – Mont Terri Proj. intern. tech. Note. 1997-15. swisstopo, Wabern/CH.

Kupferschmied, N., Wild, K.M., Amann, F., Nussbaum, C., Jaeggi, D. & Badertscher, N. (2015): Time-dependent fracture formation around a borehole in a clay shale. – Int. J. Rock Mech. Min. Sci *77*, 105–114.

Lahaye, F. (2005): EZ-A Experiment: Stress measurements campaign by overcoring in the Mont Terri Laboratory using CISRO cells. – Mont Terri Proj. intern. tech. Note. 2004-86. swisstopo, Wabern/CH.

Laubscher, H.P. (1963): Blatt 1085 St-Ursanne. – Geol. Atlas Schweiz 1:25 000, Erläut. 40.

Marsaud, B., Mangin, A. & Belc, F. (1993): Estimation des caractéristiques physiques d'aquifères profonds à partir de l'incidence barométrique et des marées terrestres. – J. Hydrol. *144*, 85-100.

Martin, C.D. & Lanyon, G.W. (2003): Measurement of in situ stress in weak rocks at Mont Terri Rock Laboratory. – Int. J. Rock Mech. Min. Sci *40*, 1077–1088.

Martin, C.C., Lanyon, G.W., Bossart, P. & Blümling, P. (2004): Excavation Disturbed Zone (EZD) in clay shale: Mont Terri. – Mont Terri Proj. intern. tech. Report. 2001-01. swisstopo, Wabern/CH.

Marty, D. (2008): Sedimentology, taphonomy, and ichnology of Late Jurassic dinosaur tracks from the Jura carbonate platform (Chevenez – Combe Ronde tracksite, NW Switzerland): insights into the tidal-flat palaeoenvironment and dinosaur diversity, locomotion, and palaeoecology. – PhD Thesis, GeoFocus *21*, Univ. Fribourg.

Matray, J. M. & Bailly, D. (2014): LP Experiment: Statistical analysis of pressure signals measured on boreholes BDS-5 and BDS-2 and BGP-6. – Mont Terri Proj. intern. tech. Note. 2012-50. swisstopo, Wabern/CH.

Norbert, J. & Schindler, B. (1988): Tunnel du Mont Terri, Rapport géologique après exécution des forages de reconnaissance. – Consortium d'étude IJA-BG

Nussbaum, C., Bossart, P., Amann, F. & Aubourg, C. (2011): Analysis of tectonic structures and excavation induced fractures in the Opalinus Clay, Mont Terri underground rock laboratory (Switzerland). – Swiss J. Geosci *104*, 187–210.

Ouchterlony, F. (1988): ISRM Suggested methods for determining fracture toughness. – Int. J. Rock Mech. Min. Sci. *25*, 71–96.

Petrini, K. & Simpson, G. (2008): Determination of stress (DS) experiment: Continuation of 2D modelling of the stress distribution in the Mont Terri anticline. – Mont Terri Proj. intern. tech. Note. 2007-39. swisstopo, Wabern/CH.

— (2012): Determination of stress (DS) experiment: 2D modelling of the stress distribution in the Mont Terri anticline. – Mont Terri Proj. intern. tech. Note. 2008-39. swisstopo, Wabern/CH.

Picot, L., Becker, D., Lapaire, F., Ustaszewski, K. ,Hug, W.A. & Berger, J.P. (2005): Sédimentologie, paléontologie et paléoenvironnements côtiers de la région de Porrentruy (Sud-Rhénan, Paléogène, Jura, Suisse): Implications géodynamiques. – Eclogae geol. Helv. *98*, 281–296.

Reisdorf, A., Hostettler, B., Waltschew, A., Jaeggi, D. & Menkveld, U. (2014): SO (Sedimentology of Opalinus Clay) experiment: Biostratigraphy of the basal part of the Opalinus-Ton at the Mont Terri rock laboratory, Switzerland. – Mont Terri Proj. intern. tech. Report. 2014-07. swisstopo, Wabern/CH.

Reisdorf, A.G., Wetzel, A., Schlatter, R. & Jordan, P. (2011): The Staffelegg formation: a new stratigraphic scheme for the Early Jurassic of northern Switzerland. – Swiss J. Geosci. *104*/1, 97–146.

Rummel, F. & Hansen, J. (1989): Interpretation of hydrofrac pressure recordings using a simple fracture mechanics simulation model. – Int. J. Rock Mech. Min. Sci. *26*/6, 483–488.

Rummel, F. & van Heerden, W.L. (1978): ISRM suggested methods for determining sound velocities. – Int. J. of Rock Mech. Min. Sci. *15*, 53–58.

Rummel, F., Klee, G., Weber, U. (2012): DS experiment: DS (determination of stress): Results from the hydro-fracturing and hydro-jacking in BDS-1 and BDS-2 boreholes. – Mont Terri Proj. intern. tech. Note. 2009-43. swisstopo, Wabern/CH.

Rutqvist, J., Tsang, C.F. & Stephansson, O. (2000): Uncertainty in the maximum principal stress estimated from hydraulic fracturing measurements due to the presence of the induced fracture. – Int. J. Rock Mech. Min. Sci. *37*, 107–120.

Schaeren, G. & Norbert, J. (1989): Tunnels du Mont Terri et du Mont Russelin. La Traversée des Roches à Risques: Marnes et Marnes à Anhydrite. –SIA D *037*, 19–24.

Shin, K. (2006): AS experiment: Resuls from in-situ tests. Short report about the current state of AS experiment. – Mont Terri Proj. intern. tech. Note. 2006-33. swisstopo, Wabern/CH.

— (2009): DS (Determination of stress) experiment: Overcoring stress measurement by CCBO. Data report. – Mont Terri Proj. intern. tech. Note. 2009-57. swisstopo, Wabern/CH.

Thoeni, R. (2013): Geomechanical analysis of excavation-induced rock mass behavior of faulted Opalinus Clay at the Mont Terri Underground Rock Laboratory (Switzerland). – Eng. Geol. *194*, ETH Zürich.

Thury, M. & Bossart, P. (1999): Mont Terri Rock Laboratory. – Results of the hydrogeological, geochemical and geotechnical experiments performed in 1996 and 1997. – Geol. Rep. Swiss natl. hydrol. geol. Surv. *23*.

Ustaszewski, K. & Schmid, S.M. (2006): Control of preexisting faults on geometry and kinematics in the northernmost part of the Jura fold-and-thrust belt. – Tectonics *25*, TC5003.

– (2007): Latest Pliocene to recent thick-skinned tectonics at the Upper Rhine Graben-Jura Mountains junction. – Swiss J. Geosci. *100*, 293–312.

Ustaszewski, K., Schumacher, M.E. & Schmid, S.M. (2005): Simultaneous normal faulting and extensional flexuring during rifting: an example from the southernmost Upper Rhine Graben. – Int. J. Earth Sci. *94*, 680–696.

Valley, B. & Evans, K.F. (2009): Stress orientation to 5 km depth in the basement below Basel (Switzerland) from borehole failure analysis. – Swiss J. Geosci. *102*, 467–480.

Wetzel, A. & Allia, V. (2003): Der Opalinuston in der Nordschweiz: Lithologie und Ablagerungsgeschichte. – Eclogae geol. Helv. *96*, 451–469.

Appendix A

Geological section of the Mont Terri area

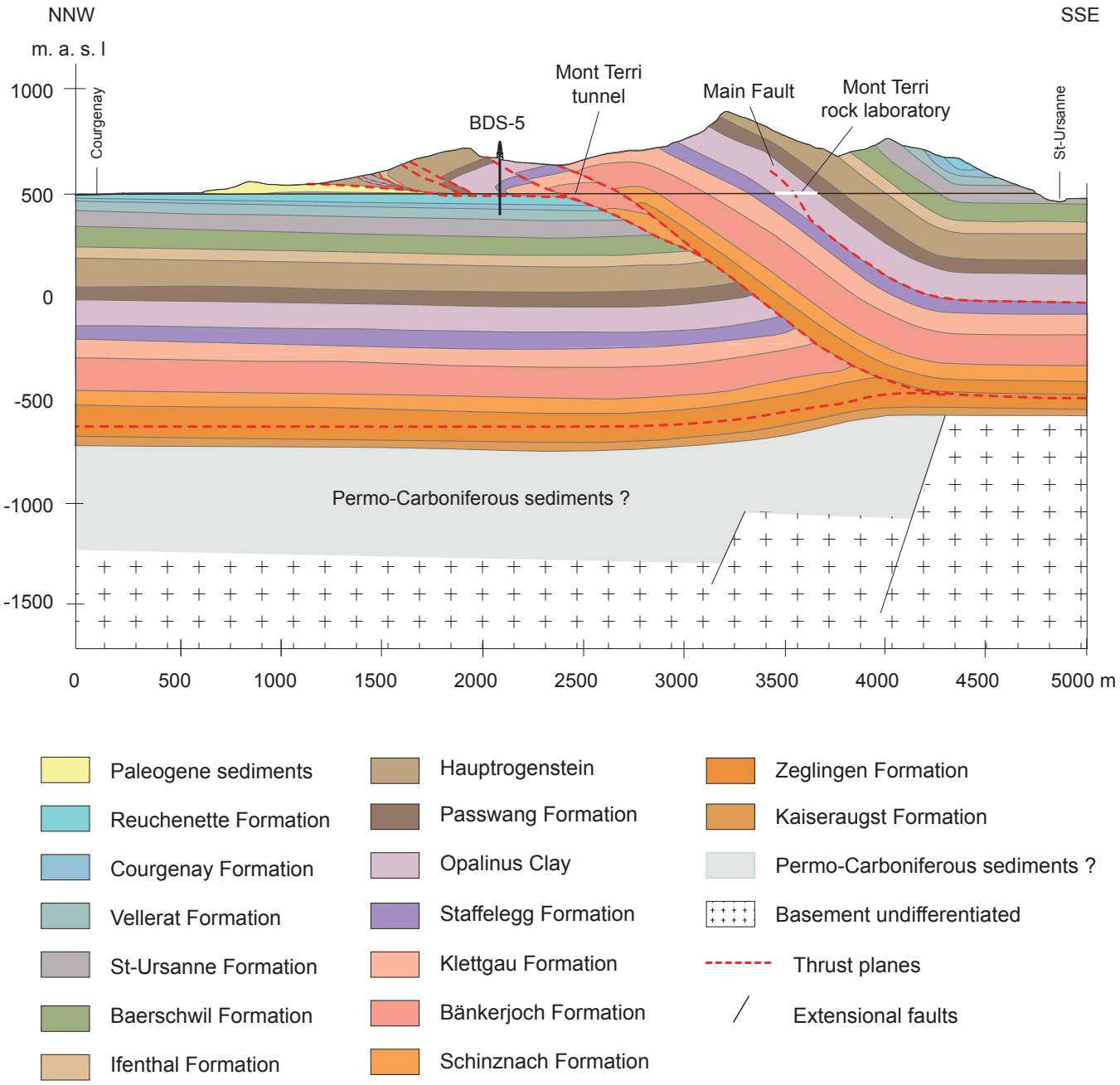

Fig. A-1: Geological section of the Mont Terri area with the Folded Jura on the right hand side and the Tabular Jura on the left hand side. Borehole BDS-5 was drilled through the Folded Jura in the hanging wall and the Tabular Jura in the foot-wall. Whereas the Mont Terri rock laboratory is located in the southern limb of the Mont Terri anticline, borehole BDS-5 is located in the northern limb, north of the ramp and the core of the anticline and thus probably above a Permo-Carboniferous graben, as postulated on the balanced cross section by Caer et al. (2015). These authors proposed a detachment fold geometry for the Mont Terri anti-cline. This new interpretation considers an episode of folding followed by an episode of thrusting. In the first step of deformation, the SE dipping former normal fault localizes the development of a detachment fold with steep limbs above the evaporitic Muschelkalk. In a second phase, it is crosscut by a low angle ramp and the hanging wall is passively transported over it. The main detachment occurred within the Middle Triassic evaporates (Anhydrite Group), which consists of sulphate beds and rock salt. According to Caer et al. (2015), a thick accumulation of Muschelkalk is present below the Mont Terri anticline and the nucleus for the initiation of the ramp was the pre-existing southern border of an assumed Permo-Carboniferous graben. The assumption of thick accumulation of Muschelkalk is based on balanced section construction supported by mechanical analysis.

Appendix B

Summarized stratigraphy encountered on drillcores

BDS-5 Derrière-Monterri — Lithostratigraphic log — 2011/2014

System	Stage	Formation	Depth	Facies and Members	Description	Thin sections	Facies interpretation
Quaternary			0.0 m	Unconsolidated rock	Beige and brown sandy/silty gravel		
Middle Jurassic	Aalenian	Opalinus Clay	6.3	Opalinus Clay, shaly	Grey sandy clay, strongly weatherd, plastic, mica bearing		Shallow sea, 20–40 m water depth with increased terrigeneous influence in the upper part
			14.2	Opalinus Clay, sandy	Grey sandy clay with numerous sand lenses, ripples, nodules of sand, stronlgy burrowed	16.20: Sandy clay and carbonate-rich lenses 19.00: Silty, marly clay	
			22.0	Opalinus Clay, carbonate rich	Grey sandy clay with intercalated 5 cm thick layers of bioclastic limestone and large bioclastic nodules, at bottom tectonic breccia	23.40: Silty, marly clay 24.85: Carbonat-rich silty clay	
			26.4	Opalinus Clay, shaly	Grey sandy/clayey marl with abundant debris of bivalves and some ammonites in intercalation with dark clay containing a lot of bioclastic material 33.6 and 36.5 m: *Leioceras opalinum*		
	174.1 Ma		37.1	Opalinus Clay, shaly	Slightly bituminous dark clays and clayey marls containing a lot of fossil debris and organic matter	44.95: Shaly clay, many shells and cone-in-cone structures	
	Toarcian		46.9	Opalinus Clay, shaly	Grey, locally sandy clay with changing amount of bioclastic material, few ammonites and gastropods besides shells of bivalves, 70.28 m: Ammonite *Pleydellia* sp.	60.75: Shaly clay with shell fragments 64.95: Shaly clay with shell fragments and large (several mm) cone-in-cone structures 70.90: Shaly clay with biodetritus and cone-in-cone structrues 77.40: Shaly clay with biodetritus and cone-in-cone structures 81.90: Shaly clay, sporadically with large bioclasts, serpulidae	
			60.0				
			80.0			94.58: Silty marls, multicolored, with marly clasts 97.97: Limestone, laminated: Delsberg fresh-water limestone 98.05: Delsb., nodular (Fe-) carbonate 99.52: Silty marl, mica-bearing: marine Septarienton 100.81: Silty marl 101.30: Sandy limest. – calc. sandst.: marine Septarienton 102.50/102.73: Limestone: terrestrial, pedogene Sidérolithique 102.65: Carbonate with veins, foraminifers 102.85: Grainstone, micritic cement	Marine and continental deposits
	Main Detachment		92.1	Tectonic Mélange	Strongly tectonized zone with small packages of non-disturbed colored marls, green siltstones and packages of freshwater limestone		
Paleo-gene	Oligocene		95.3	Molasse, non-specified	Greenish and grey marls, silty		
	33.9 Ma			Molasse, Delsb.-SWK	(Delsberg-Süsswasserkalke) nodular and laminated fresh water		
	Eocene		102.4	Molasse, Septarien-Ton	Greenish-grey silty marl, partly nodular, lower part with sandy limestone and siltstones		
				Sidérolithique	Karstified top of Reuchenette Formation 102.45–103.1: limestone		
Late Jurassic	Kimmeridgian	Reuchenette Fm.	105.9	Reuchenette Formation	Many stylolites Pellets, peloids Beige or white micritic limestone, partially pelsparitic and oolithic Karstified sections at 103.1–106.0 m (with Bohnerz), 118.0–124.5 m and 139.0–146.0 m Fault gouge at basis	127.40: Wackestone, micritic with biodetritus, shells, gastropods, bivalves, dasycladacea, shallow water foraminifers 140.70: Micritic limestone / wackestone, echinoderms, oysters, serpulidae 143.28: Oolitic limestone	Shallow carbonate platform which emerged intermittently 0–100 m water depth
	157.3 Ma		146.0				
	Oxfordian	Courgenay Fm.		Courgenay Formation	Stylolites Beige or chalky white micritic limestone with bioclasts, e.g. bivalves, serpulids, echinoderms; beds with oncoids Karstified section: 163.0–168.0 m 175.8–181.4 m: Orange mottled, micritic limestone with abundant, mm-thin, marly layers	154.08: Micritic limestone 159.90: Mudstone, foraminifers (*Alveolina* sp.) 160.30: Biomicritic limestone 168.40: Mudstone, micritic limestone 172.22: Biomicritic limestone with oncoids 176.95: Mudstone, micritic limestone, dedolomitization 192.28: Biomicritic limestone	Shallow carbonate platform, fully marine
		Vellerat Fm.	192.9	Bure Member	Beige, slighly marly micritic limestone	203.40: Mudstone / wackestone, with oncoids 203.93: oncolitic limestone	
			202.9	Hauptmumienbank	Beige and reddish limestone with abundant oncoids		
			204.2	Röschenz Member	Beige and grey marls with thin calcareous lumachella beds (gastropods, oysters) Abundant small oysters and gastropods	205.55: Sandy biomicritic limestone 212.55: Mudstone, dedolomitization, with turritellidae 214.10: Sandy marly limestone	
			216.5				

Hanging wall — Footwall

Geology: Dr. H.R. Bläsi, Dr. D. Jaeggi

Fig. B-1: Summarized stratigraphy encountered on borehole BDS-5.

Appendix C

Drillcore mapping of borehole BDS-5 Derrière-Monterri

BDS-5
Derrière-Monterri

Drillcore mapping
scale 1:7.5

Drilling:	Stump Foratec AG, Bern	
Date:	31.05.2011 – 05.07.2011	
Drillmaster:	K. Mano (Stump Foratec AG)	
Mapping by:	D. Jaeggi, C. Nussbaum, P. Müller (all swisstopo)	
Technique:	Wireline drilling, inhibitive (polymer)	
	0–7.7 m	Ø 168 mm
	7.7–113.5 m	Ø 122 mm (PQ)
	113.5– 216.5 m	Ø 101 mm
Completion:	Steel casing Ø 105/115 mm from 0 to 113.5 m	
Installation:	2 pressure transducers at 67 m and 125 m	
	2 x Keller PAA-36 X W, 30 bar, GSM-II module	

Legend:

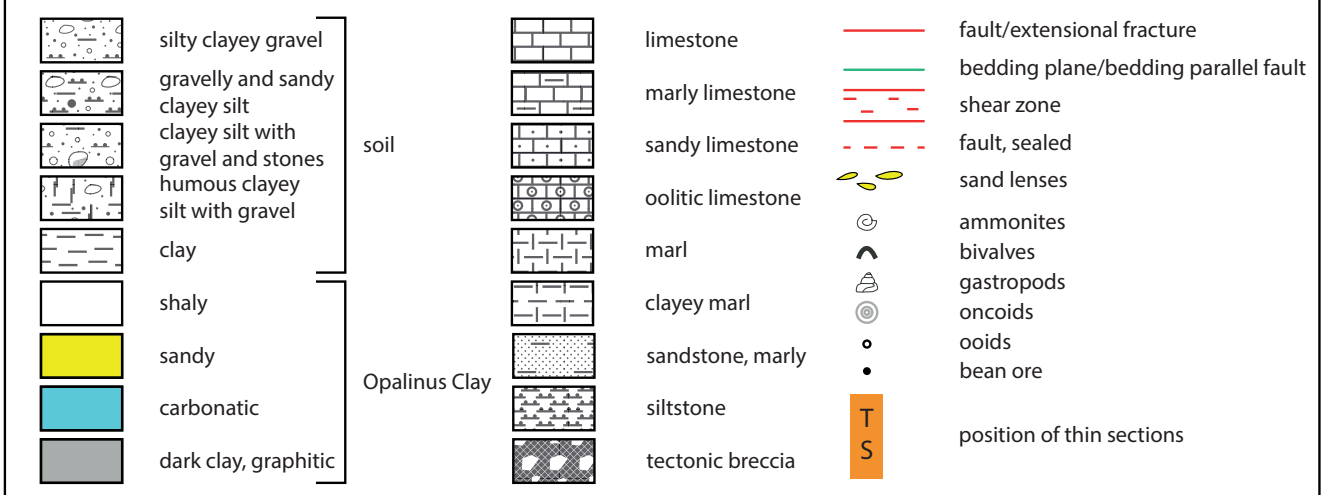

borehole BDS-5 drillcore mapping: jad/mpe page: 1

from 0 m to 3 m date of drillcore mapping: 01.06.2011 scale: 1 : 7.5

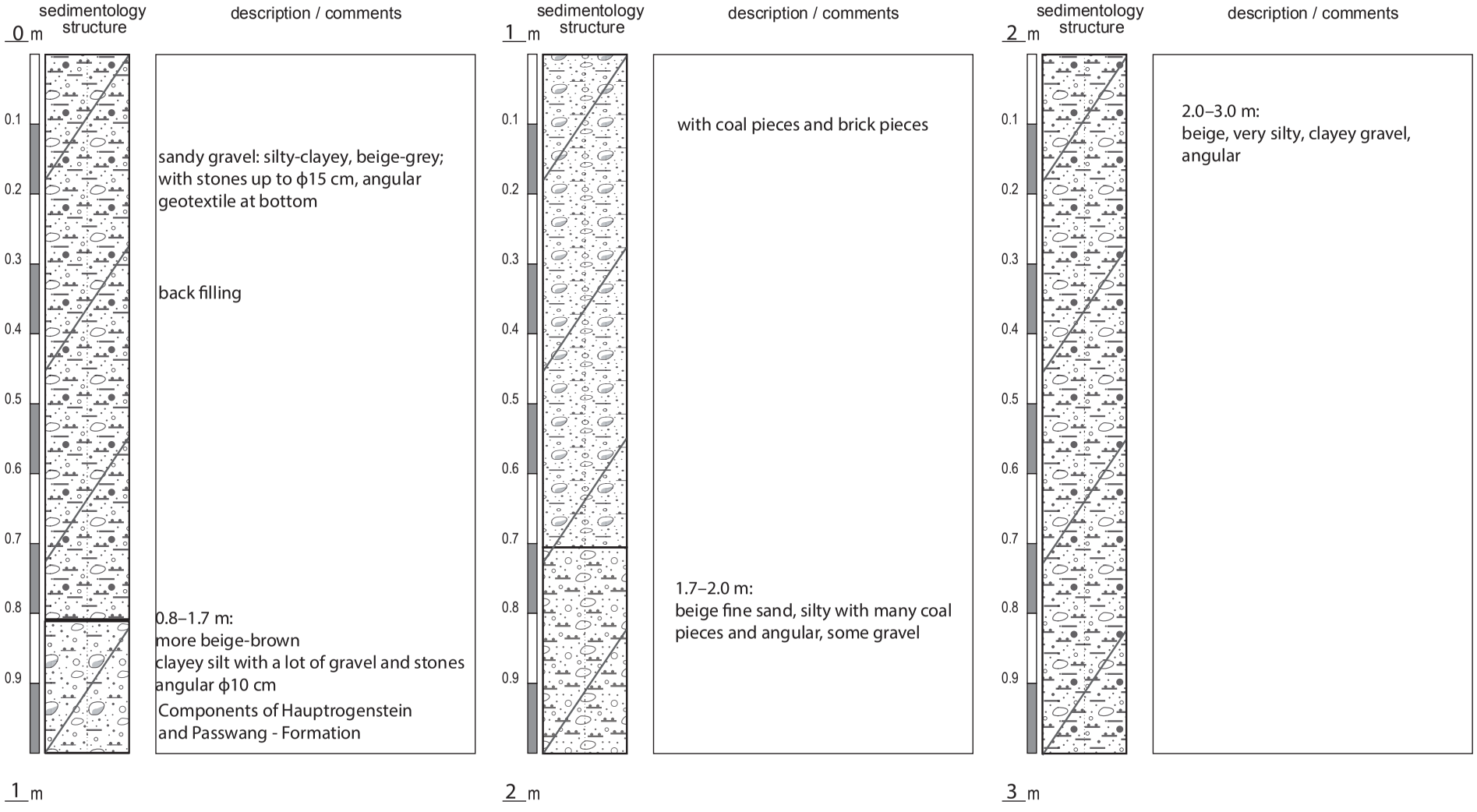

- Interpretation of facies/formation:

0–1.7 m	backfilling
1.7–3.0 m	backfilling

borehole BDS-5 drillcore mapping: jad/mpe page: 2

from 3 m to 6 m date of drillcore mapping: 01.06.2011 scale: 1 : 7.5

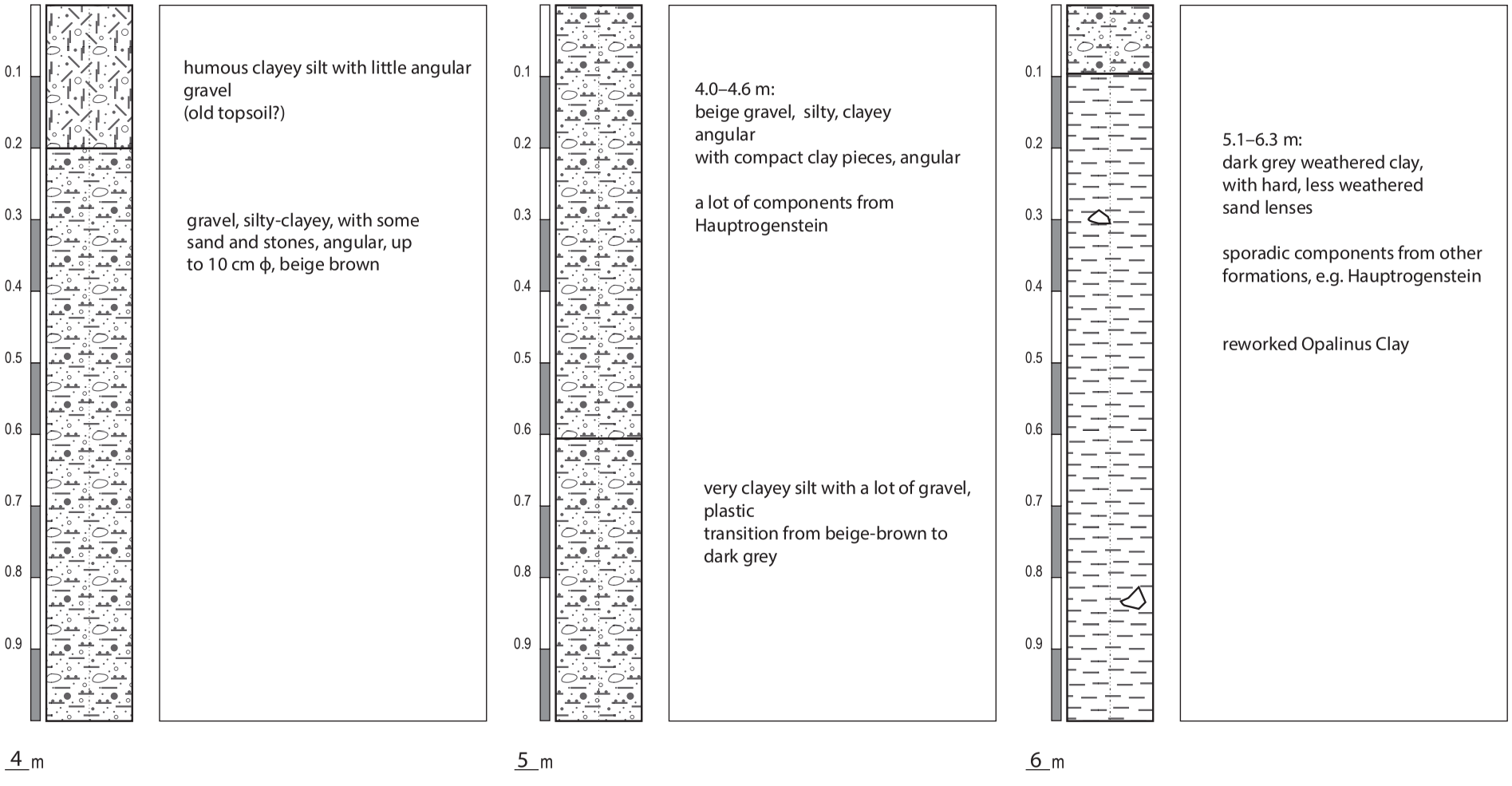

- Interpretation of facies/formation:

3.0–4.6 m:	colluvial deposits
4.6–6.3 m:	reworked Opalinus Clay (earth slip)

borehole BDS-5 drillcore mapping: jad/mpe page: 3

from 6 m to 9 m date of drillcore mapping: 01.06.2011 scale: 1 : 7.5

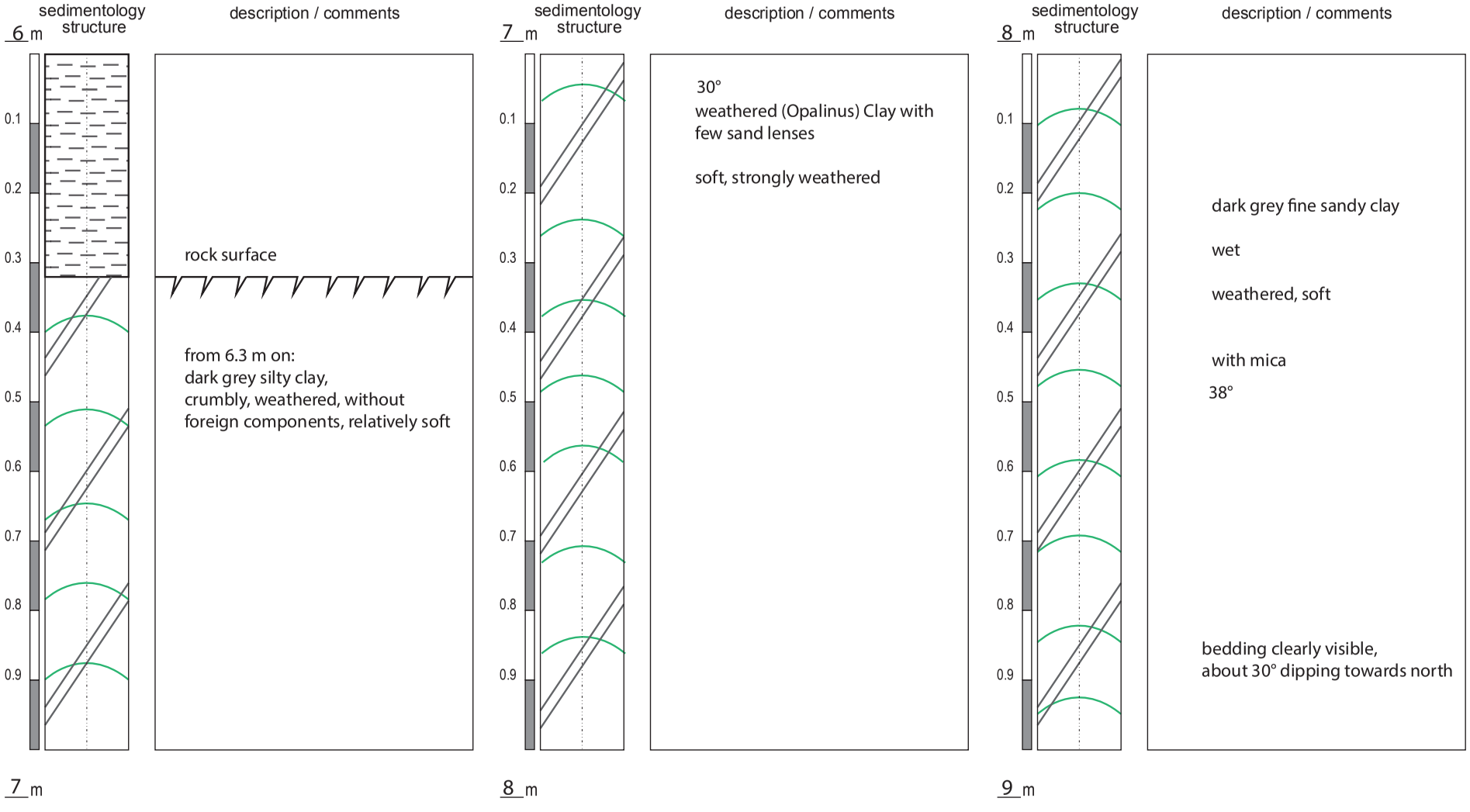

- Interpretation of facies/formation:

4.6–6.3 m:	reworked Opalinus Clay
6.3–13.0 m:	weathered Opalinus Clay

borehole BDS-5 drillcore mapping: jad page: 4

from 9 m to 12 m date of drillcore mapping: 07.06.2011 scale: 1 : 7.5

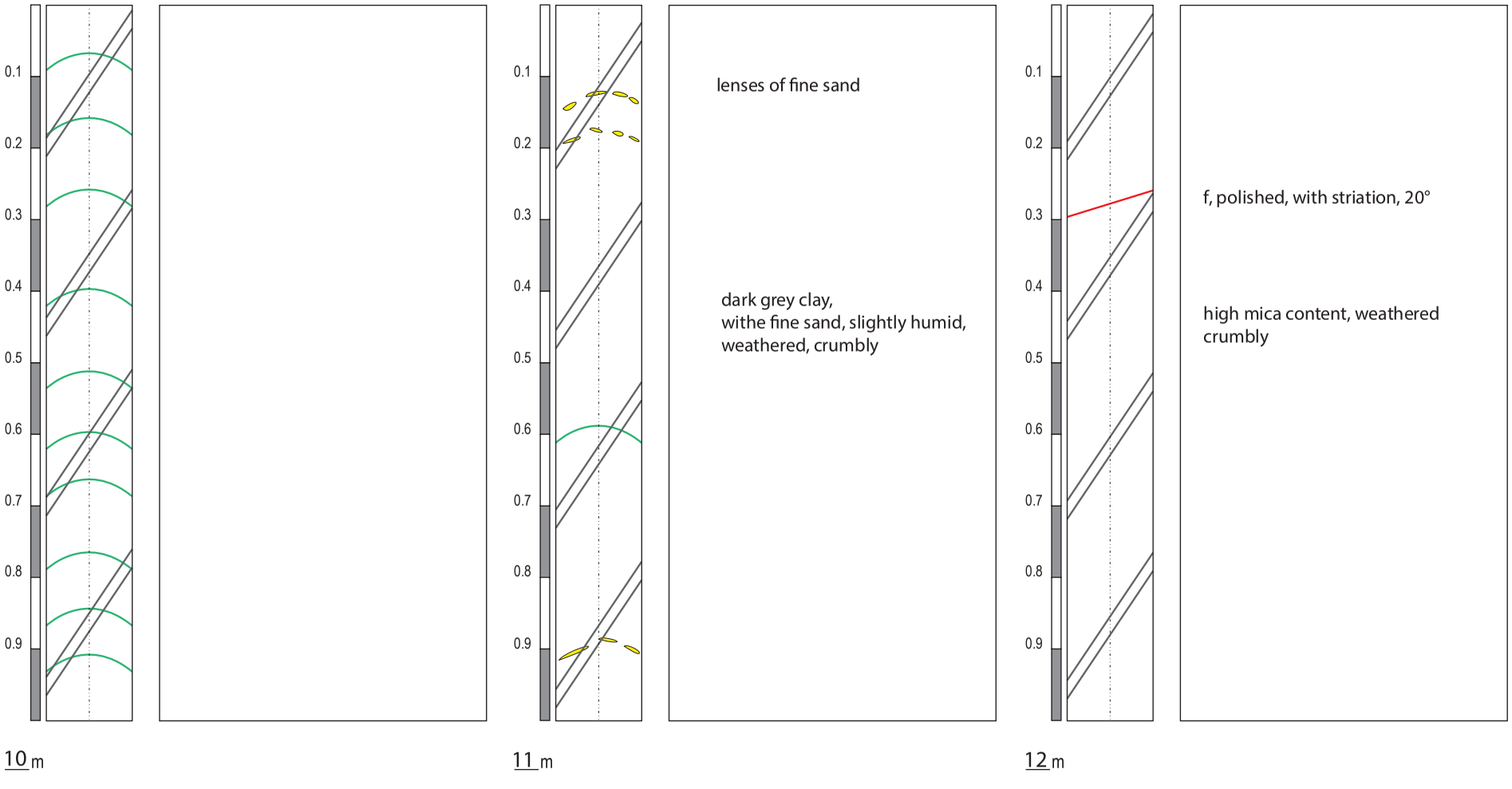

- Interpretation of facies/formation:

Opalinus Clay: shaly facies

borehole BDS-5 drillcore mapping: jad page: 5a

from 12 m to 13 m date of drillcore mapping: 07.06.2011 scale: 1 : 7.5

sedimentology structure	description / comments
12 m	
0.1	
0.2	
0.3	
0.4	fine sand lenses in weathered Opalinus Clay, crumbly
0.5	
0.6	
0.7	
0.8	
0.9	
13 m	

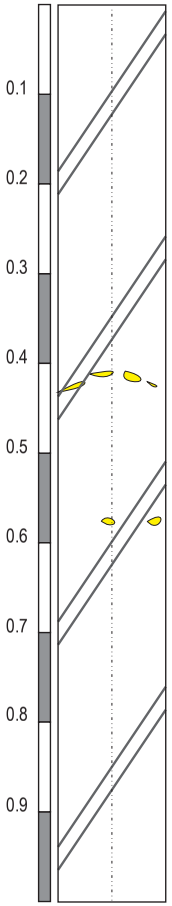

- Interpretation of facies/formation: Opalinus Clay: shaly facies

borehole BDS-5 drillcore mapping: jad page: 5b

from 13 m to 16 m date of drillcore mapping: 07.06.2011 scale: 1 : 7.5

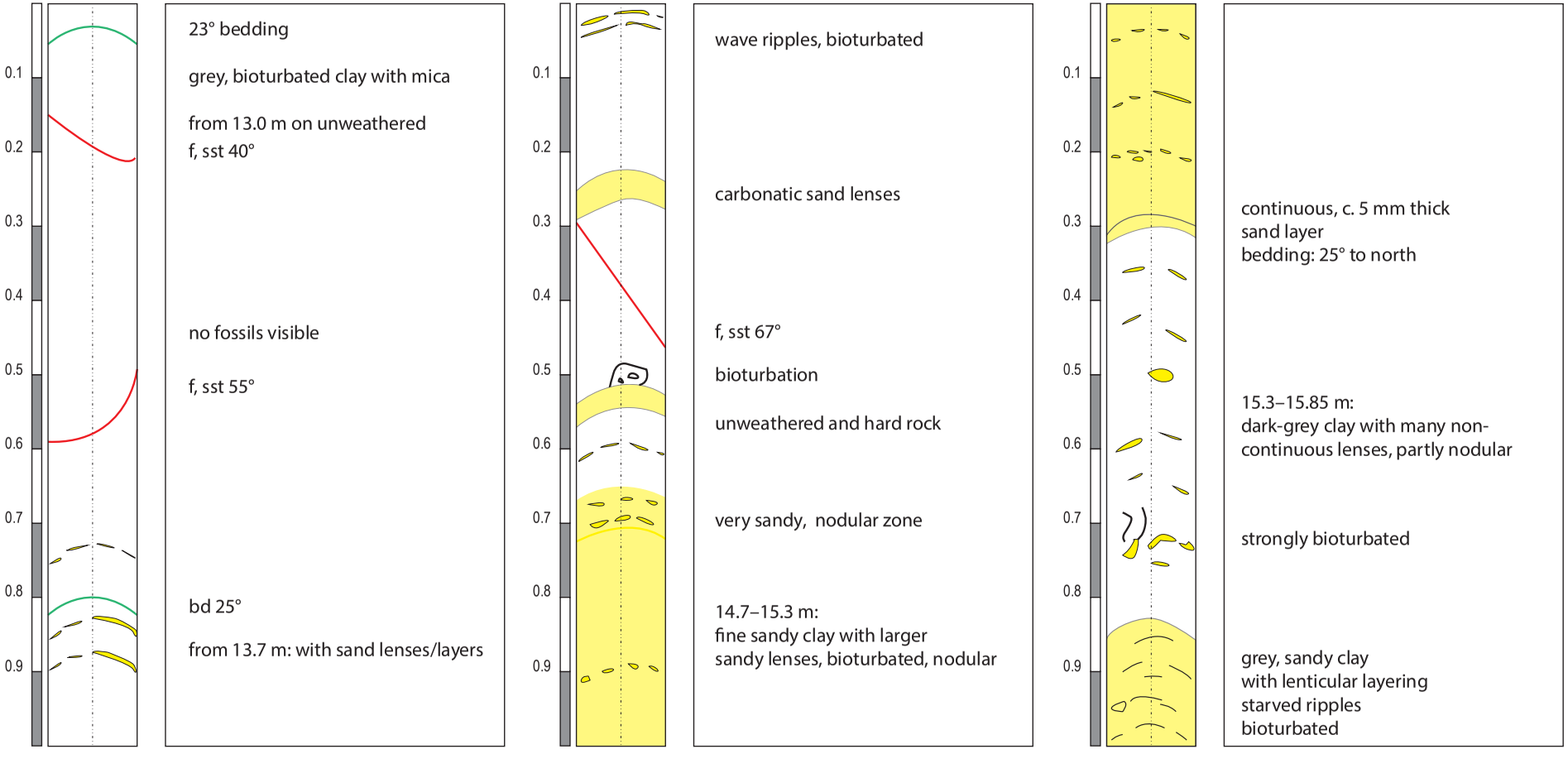

14 m 15 m 16 m

- Interpretation of facies/formation:

–14.2 m:	Opalinus Clay: shaly facies
from 14.2 m on:	Opalinus Clay: sandy facies

borehole BDS-5 drillcore mapping: jad page: 6

from 16 m to 19 m date of drillcore mapping: 07.06.2011 scale: 1 : 7.5

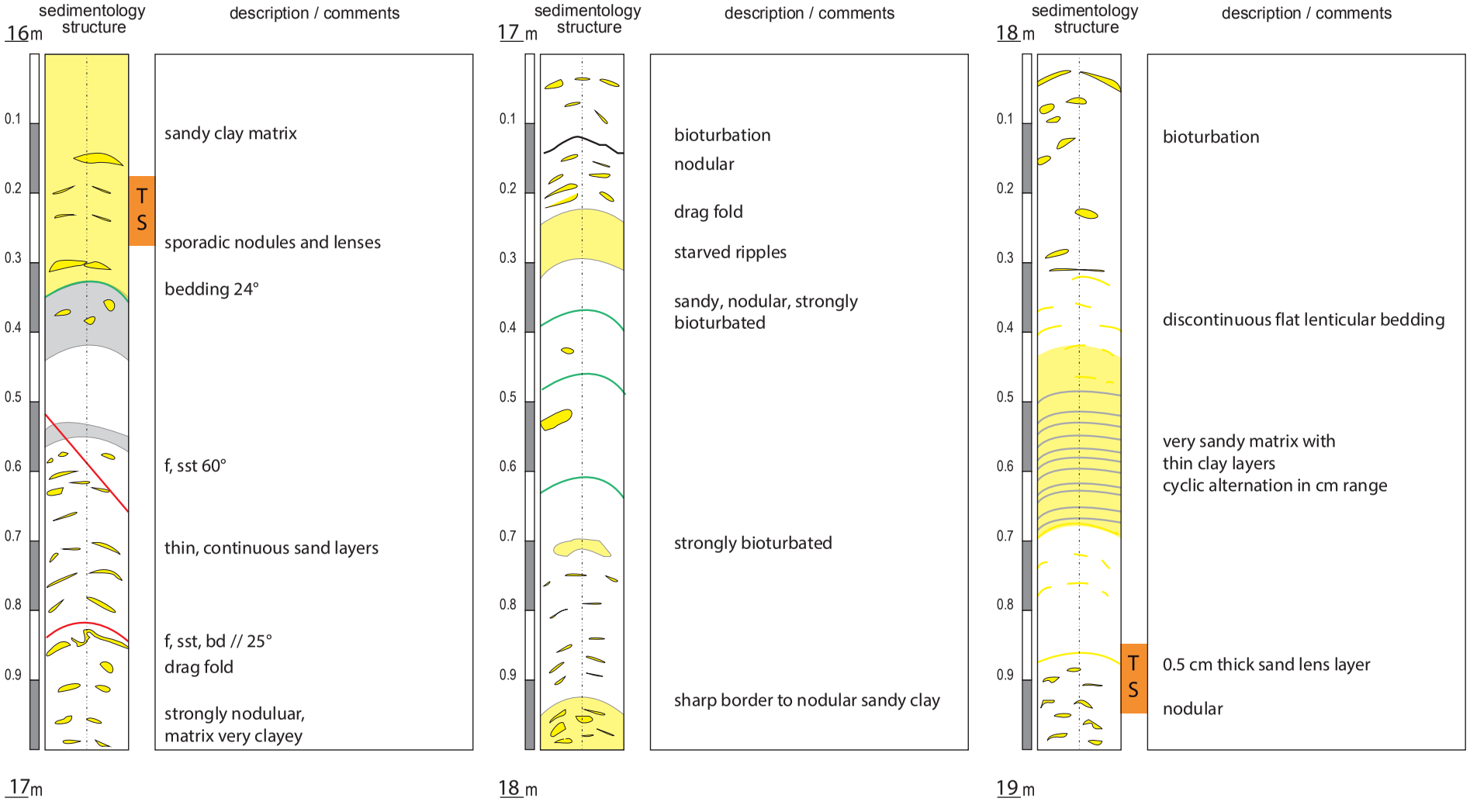

- Interpretation of facies/formation:

Opalinus Clay: sandy facies

silty, marly clay, grey with some biodetritus

borehole BDS-5 drillcore mapping: jad page: 7

from 19 m to 22 m date of drillcore mapping: 07.06.2011 scale: 1 : 7.5

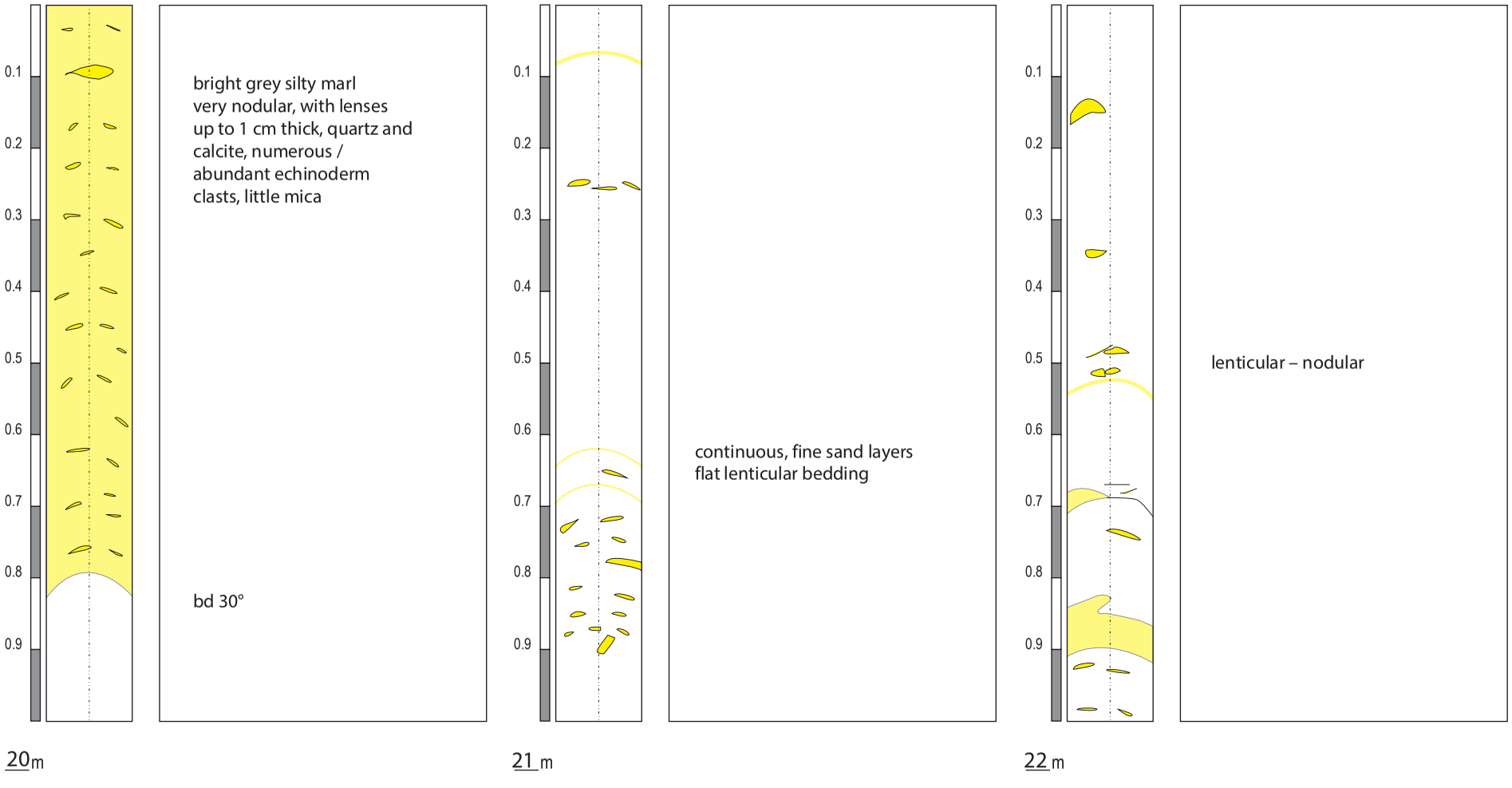

- Interpretation of facies/formation: Opalinus Clay: sandy facies

borehole BDS-5 drillcore mapping: jad page: 8

from 22 m to 25 m date of drillcore mapping: 07.06.2011 scale: 1 : 7.5

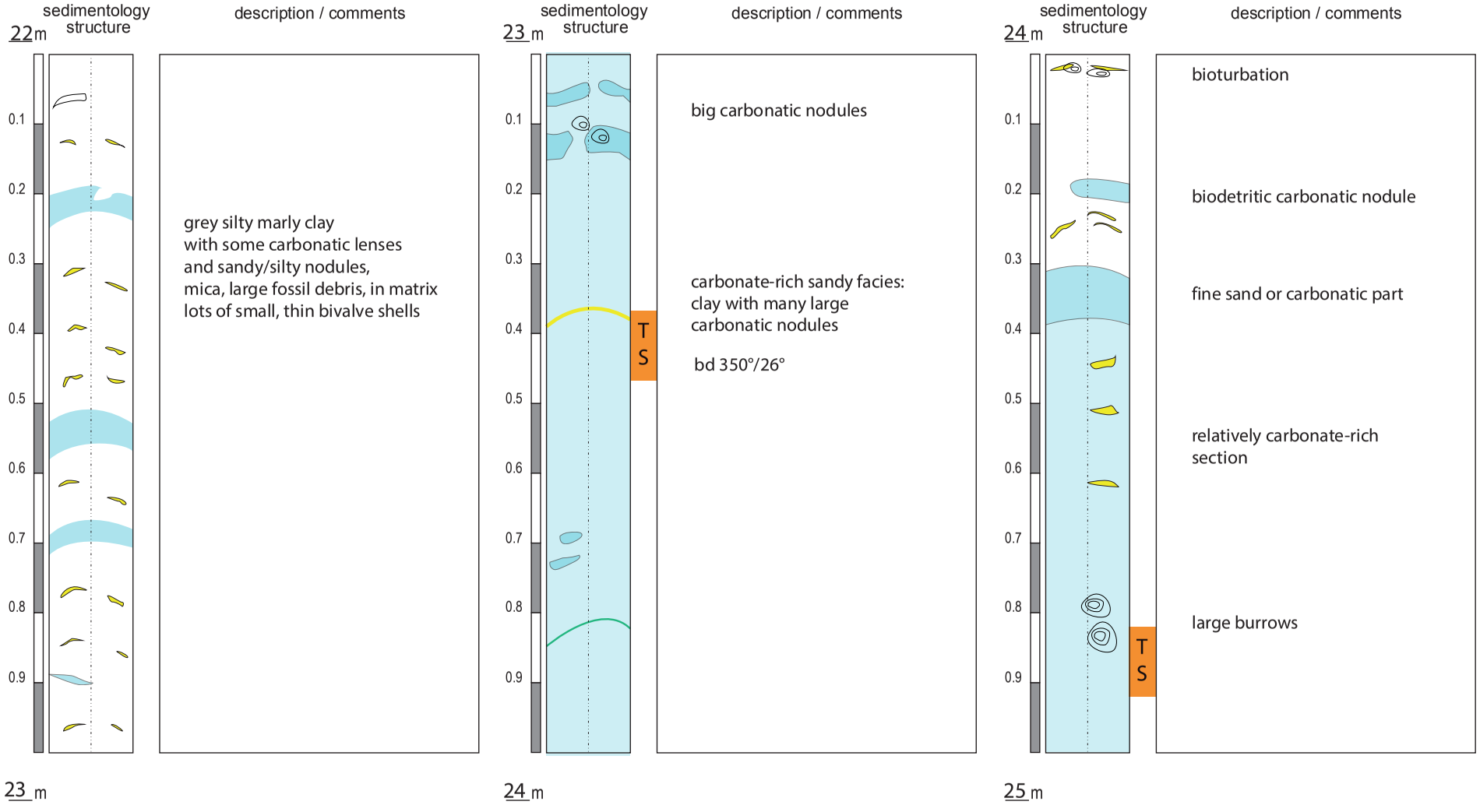

- Interpretation of facies/formation: Opalinus Clay: sandy – carbonate-rich sandy facies

borehole BDS-5 drillcore mapping: jad page: 9

from 25 m to 28 m date of drillcore mapping: 07.06.2011 scale: 1 : 7.5

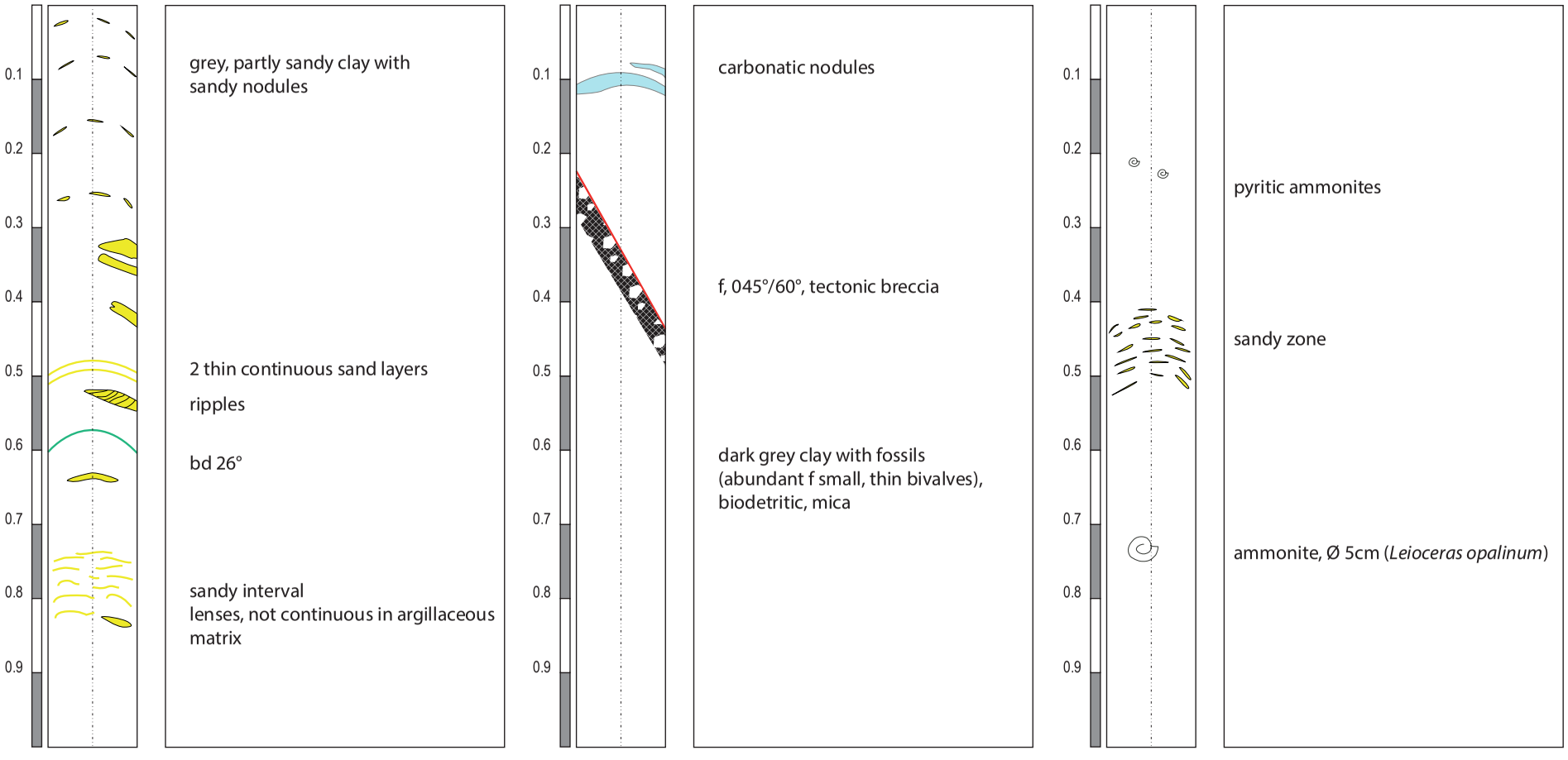

- Interpretation of facies/formation:

–26.35 m:	Opalinus Clay, carbonate-rich sandy facies
from 26.35 m:	Opalinus Clay, shaly facies

borehole BDS-5 drillcore mapping: jad page: 10

from 28 m to 31 m date of drillcore mapping: 07.06.2011 scale: 1 : 7.5

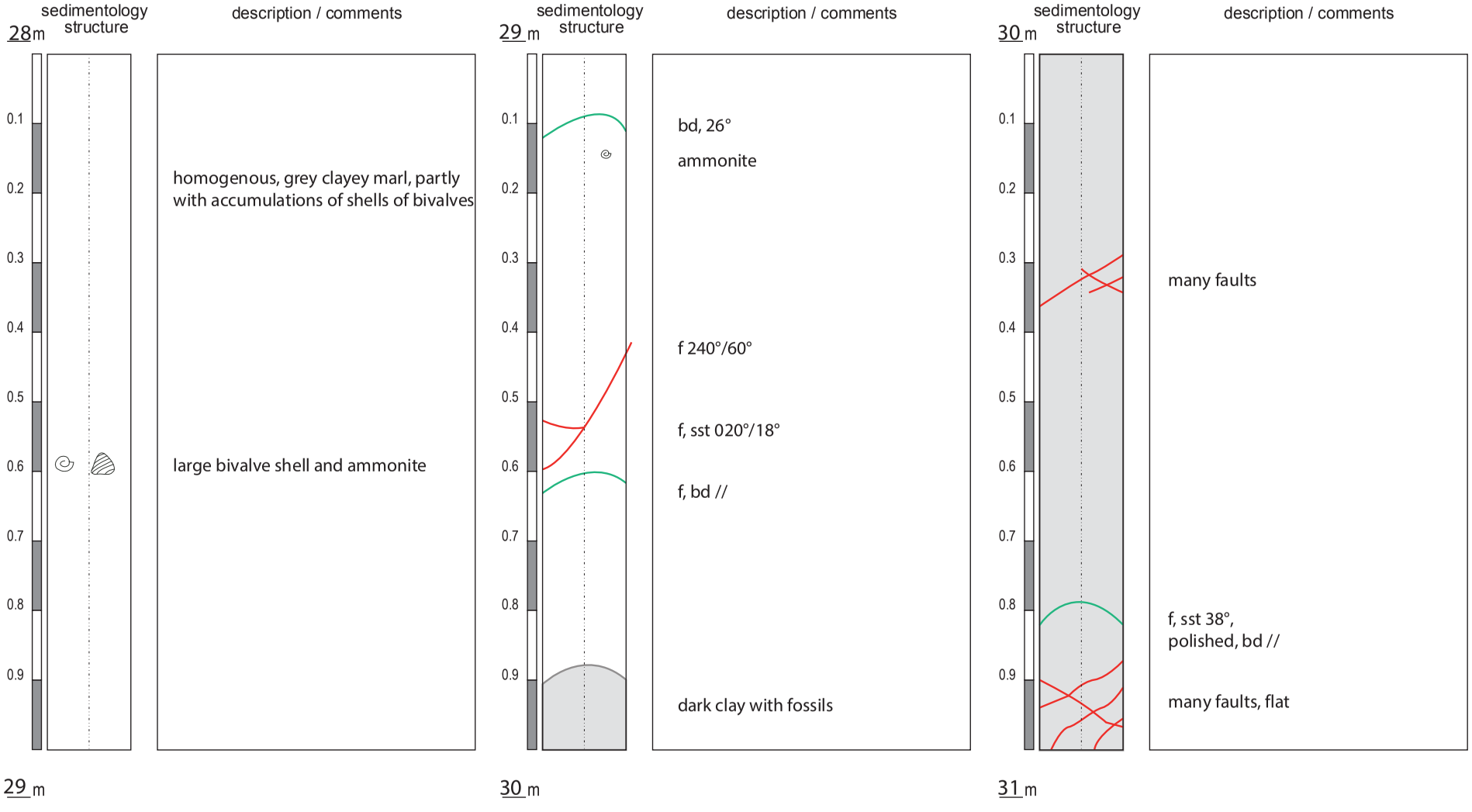

- Interpretation of facies/formation:

Opalinus Clay: shaly facies

borehole BDS-5 drillcore mapping: jad page: 11

from 31 m to 34 m date of drillcore mapping: 07.06.2011 scale: 1 : 7.5

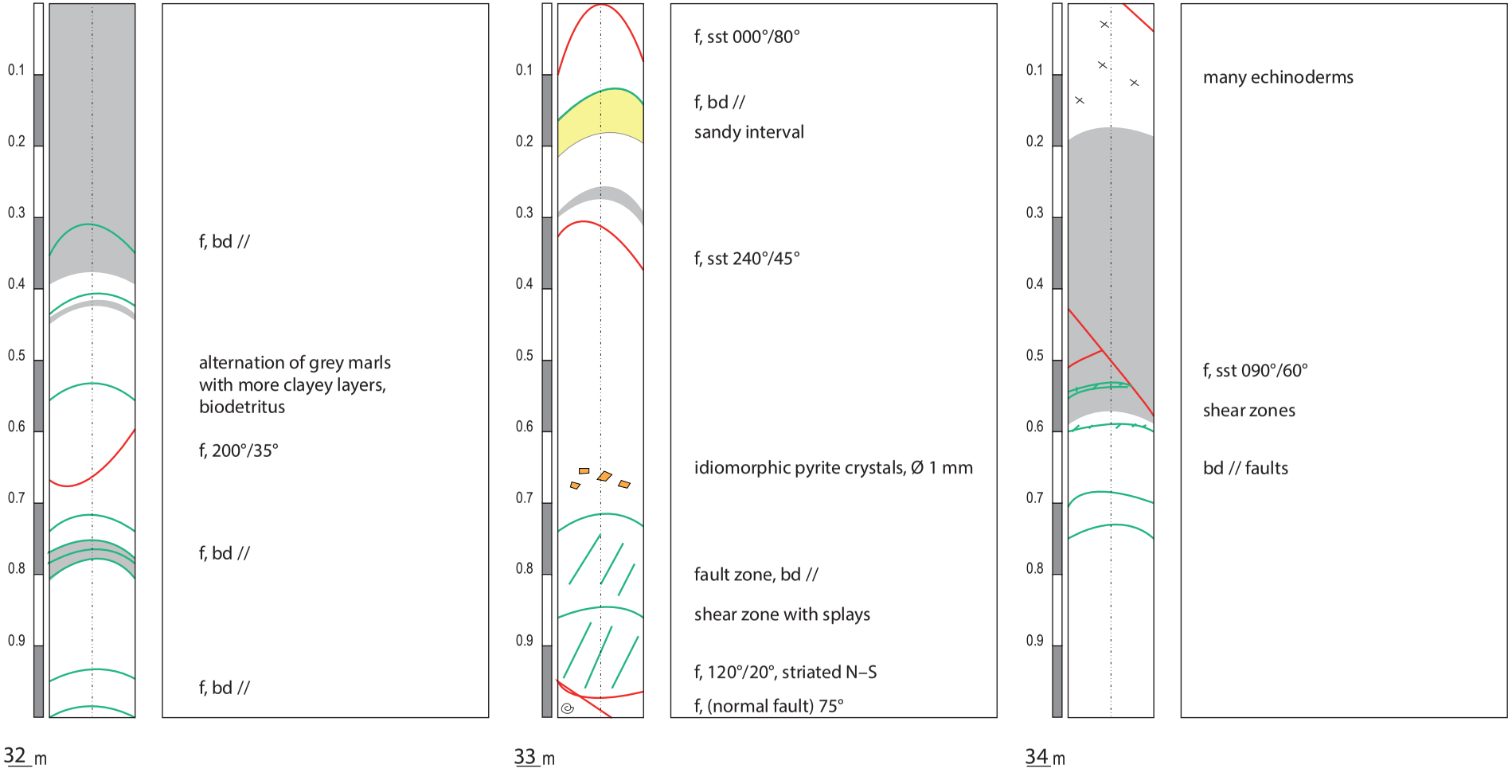

- Interpretation of facies/formation:

Opalinus Clay: shaly facies

borehole BDS-5 drillcore mapping: jad page: 12

from 34 m to 37 m date of drillcore mapping: 07.06.2011 scale: 1 : 7.5

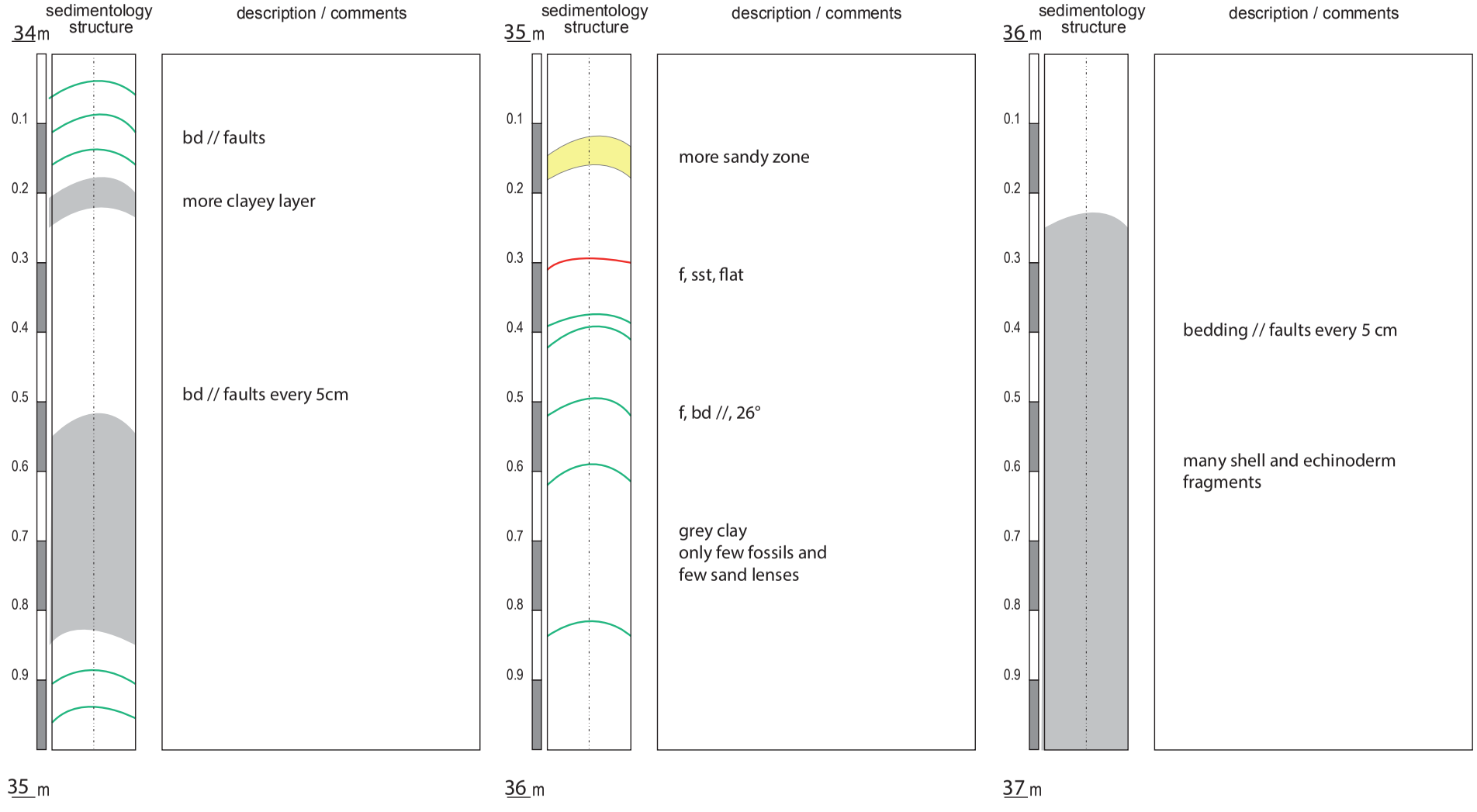

- Interpretation of facies/formation:

Opalinus Clay: shaly facies

borehole BDS-5 drillcore mapping: nuc, mpe page: 13

from 37 m to 40 m date of drillcore mapping: 08.06.2011 scale: 1 : 7.5

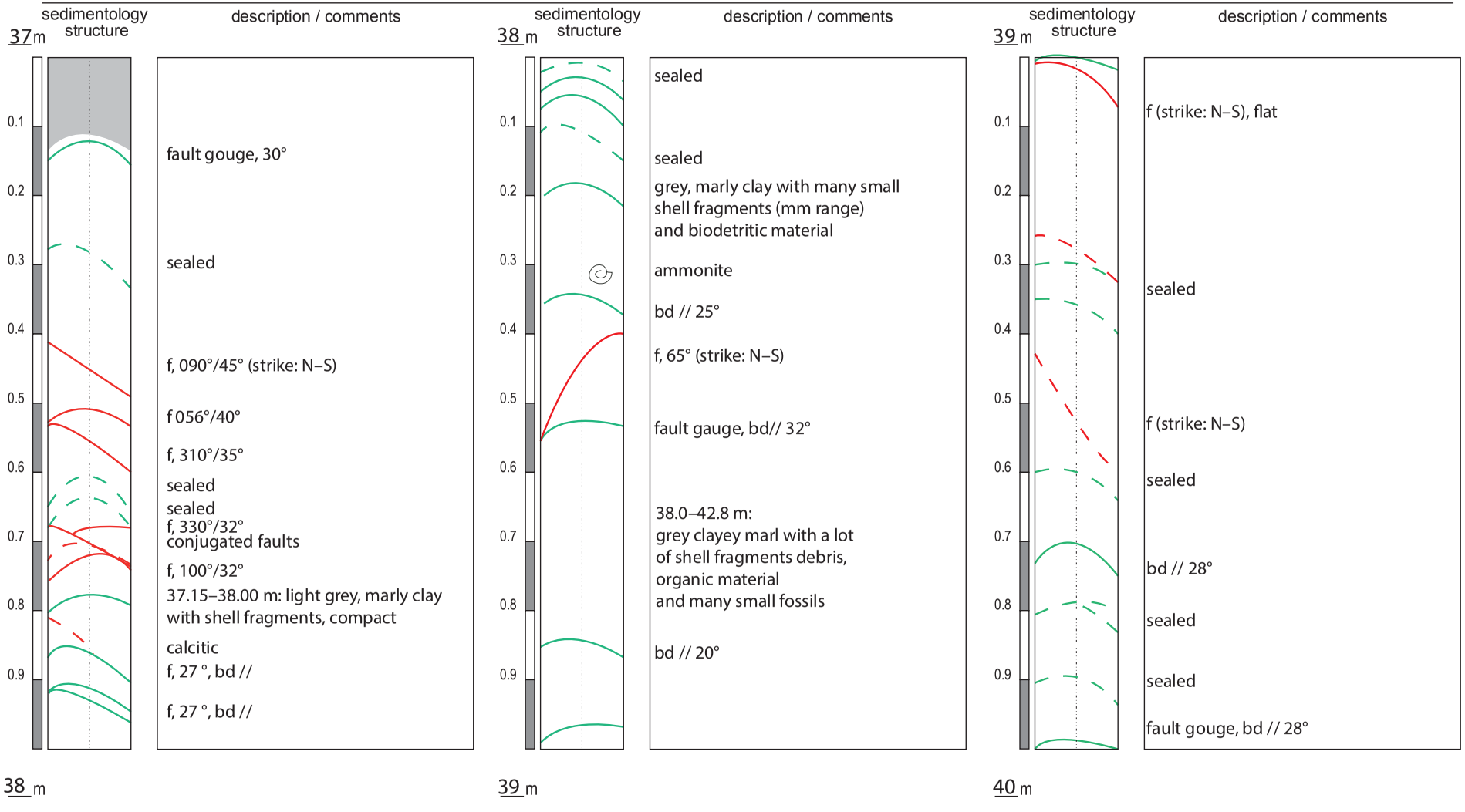

- Interpretation of facies/formation:

Opalinus Clay: shaly facies

borehole BDS-5 drillcore mapping: nuc, mpe page: 14

from 40 m to 43 m date of drillcore mapping: 08.06.2011 scale: 1 : 7.5

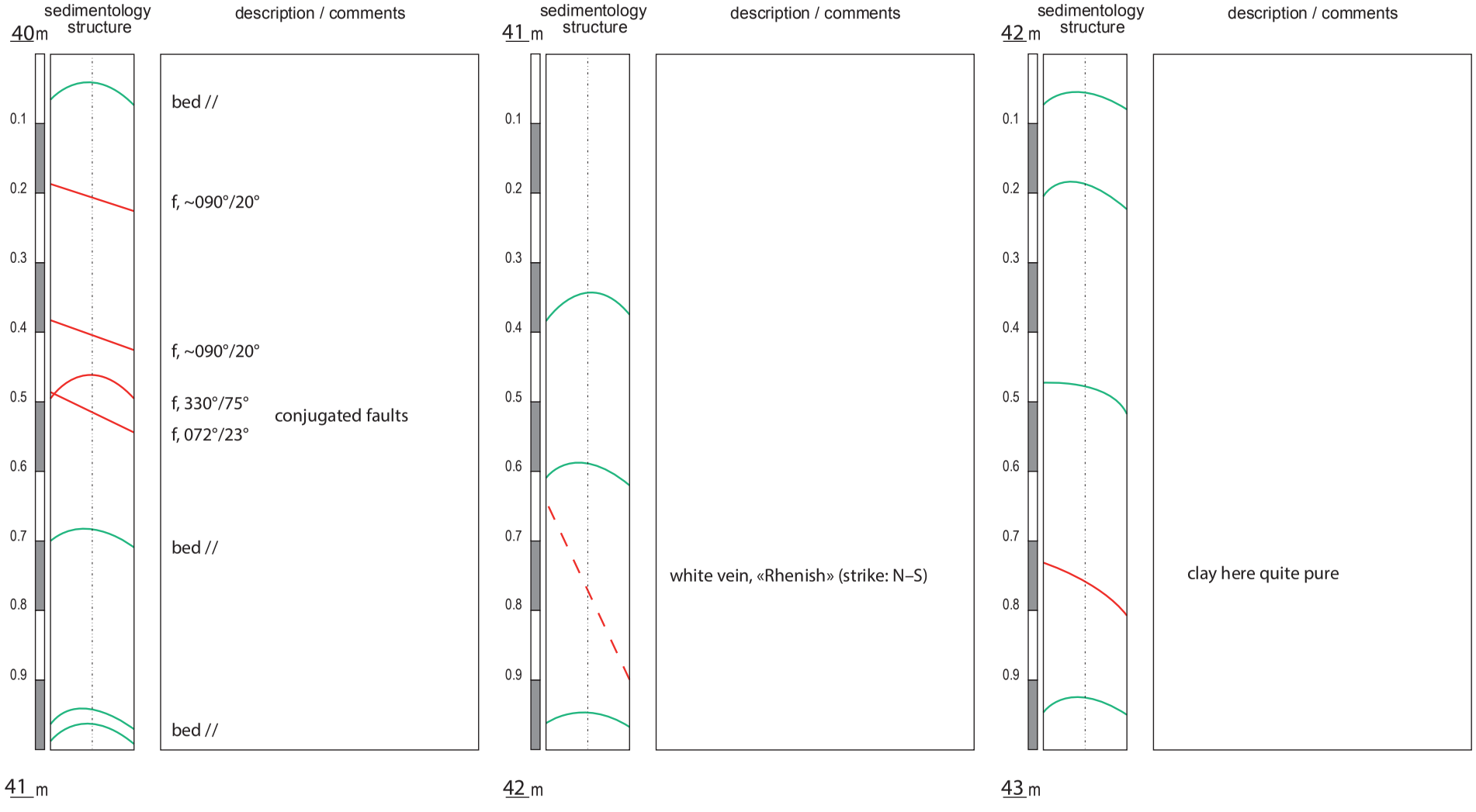

- Interpretation of facies/formation: Opalinuis Clay: shaly facies

borehole BDS-5 drillcore mapping: nuc page: 15

from 43 m to 46 m date of drillcore mapping: 09.06.2011 scale: 1 : 7.5

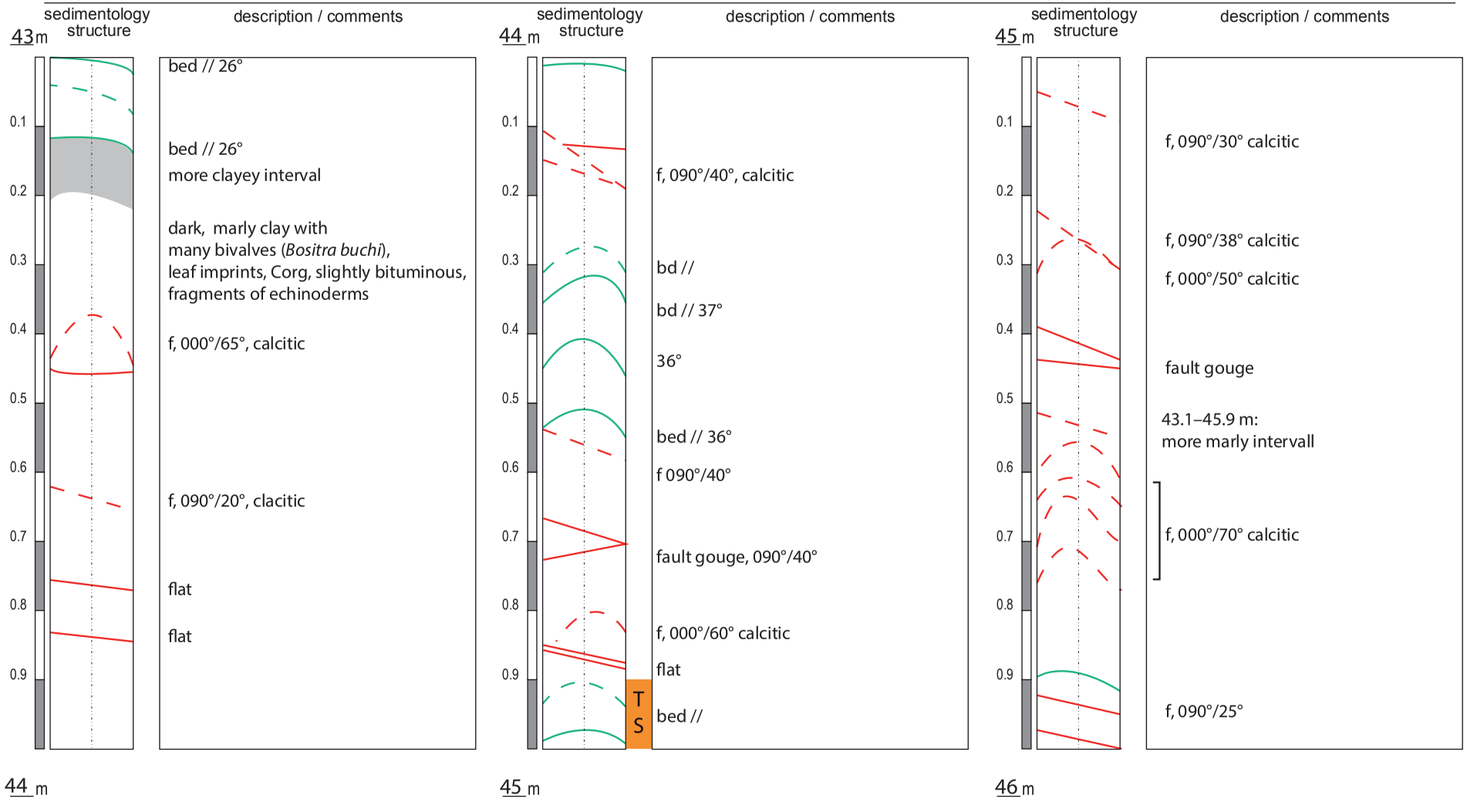

- Interpretation of facies/formation:

Opalinus Clay: shaly facies

borehole BDS-5 drillcore mapping: jad, nuc page: 16

from 46 m to 49 m date of drillcore mapping: 10.06.2011 scale: 1 : 7.5

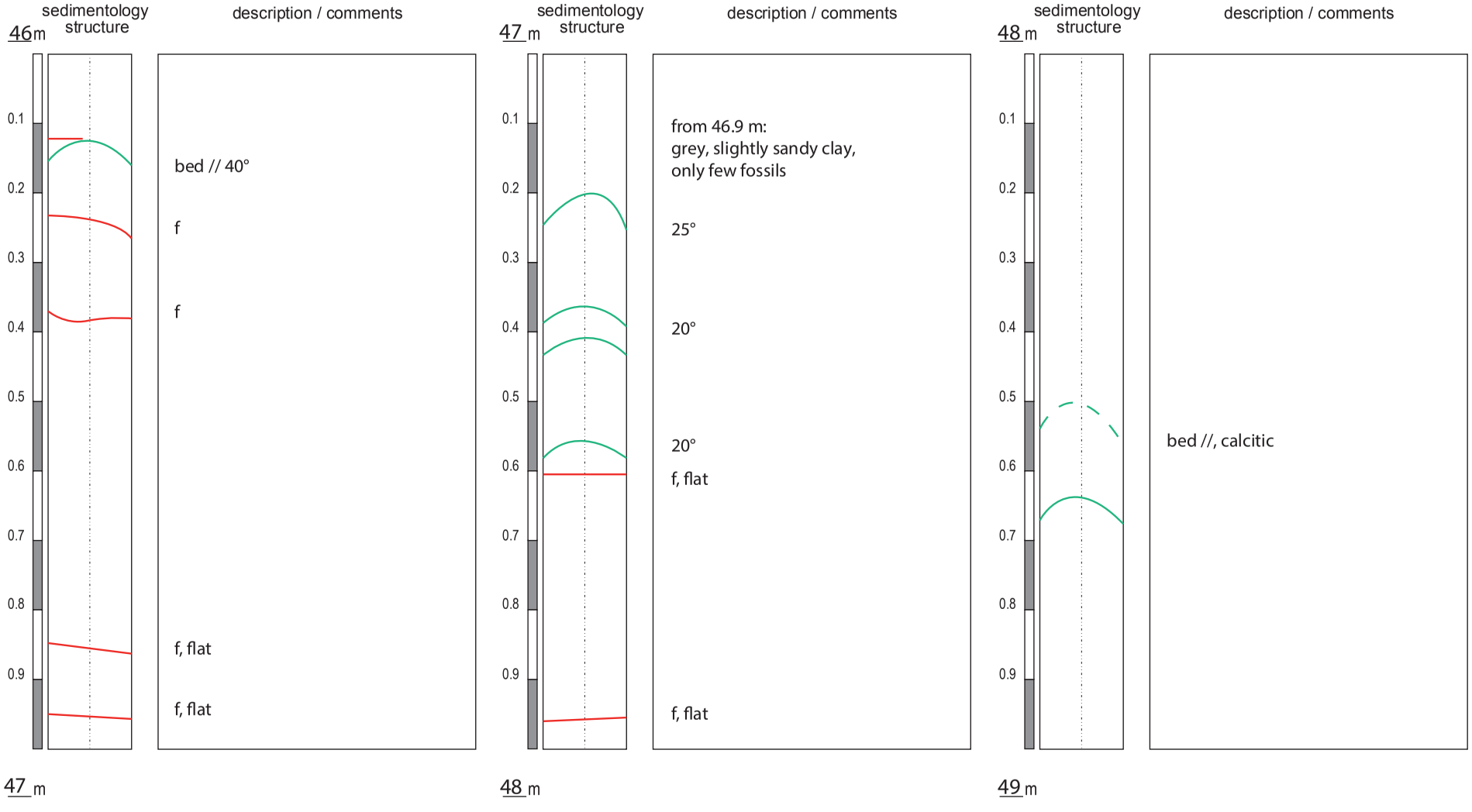

- Interpretation of facies/formation: Opalinus Clay: shaly facies

borehole BDS-5 drillcore mapping: jad, nuc page: 17

from 49 m to 52 m date of drillcore mapping: 10.06.2011 scale: 1 : 7.5

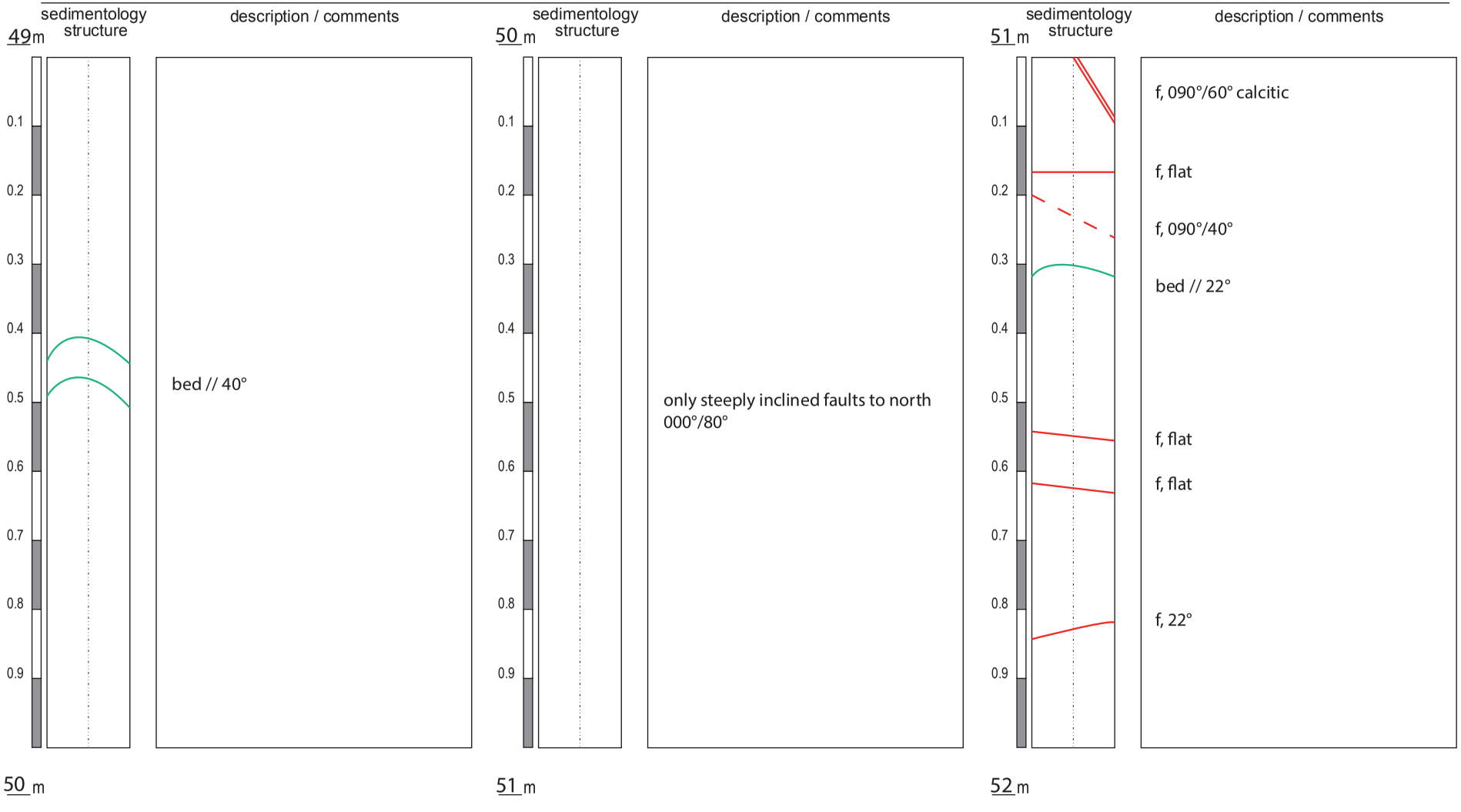

- Interpretation of facies/formation:

Opalinus Clay: shaly facies

borehole BDS-5 drillcore mapping: jad, nuc page: 18

from 52 m to 55 m date of drillcore mapping: 10.06.2011 scale: 1 : 7.5

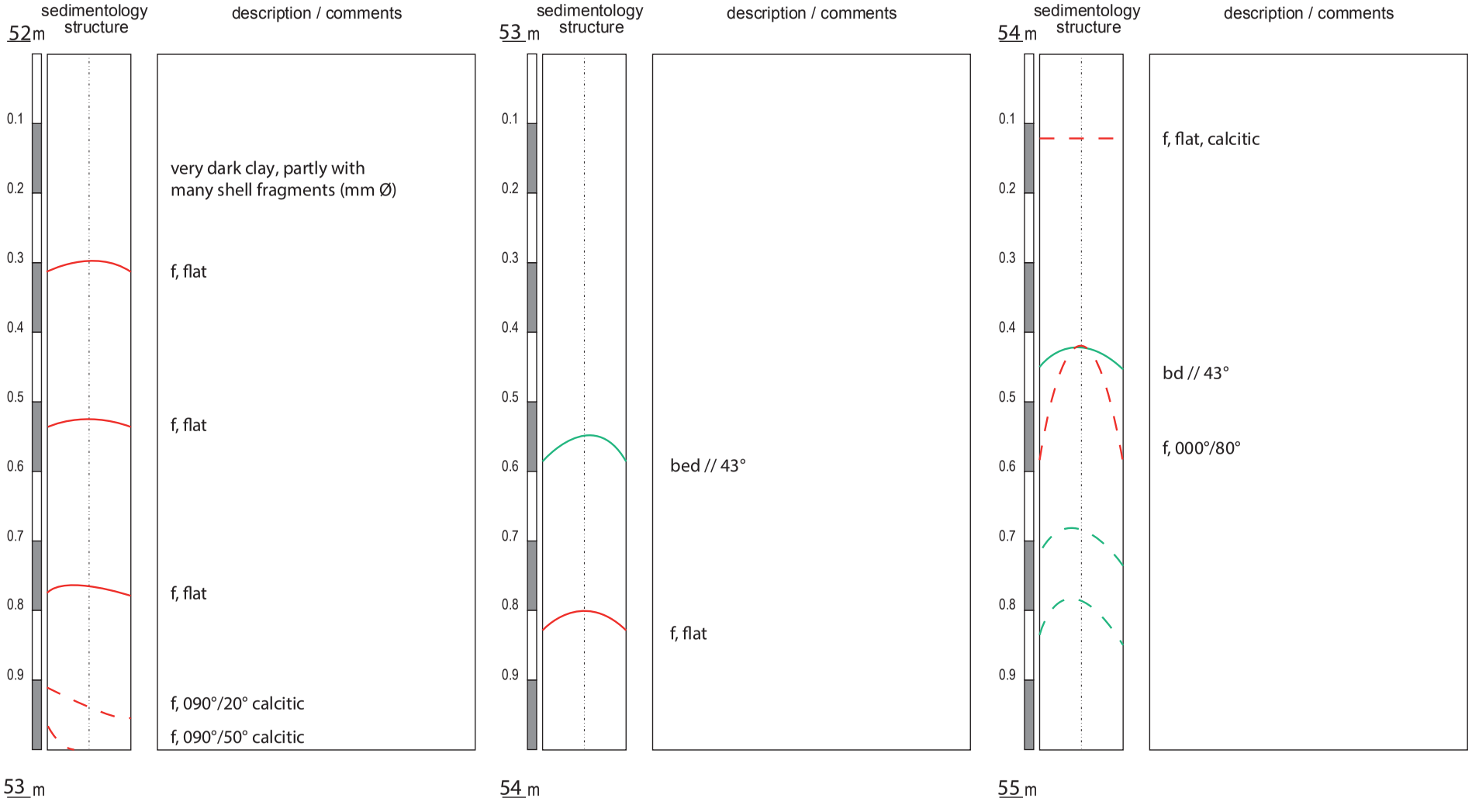

- Interpretation of facies/formation: Opalinus Clay: shaly facies

borehole BDS-5 drillcore mapping: jad page: 19

from 55 m to 58 m date of drillcore mapping: 10.06.2011 scale: 1 : 7.5

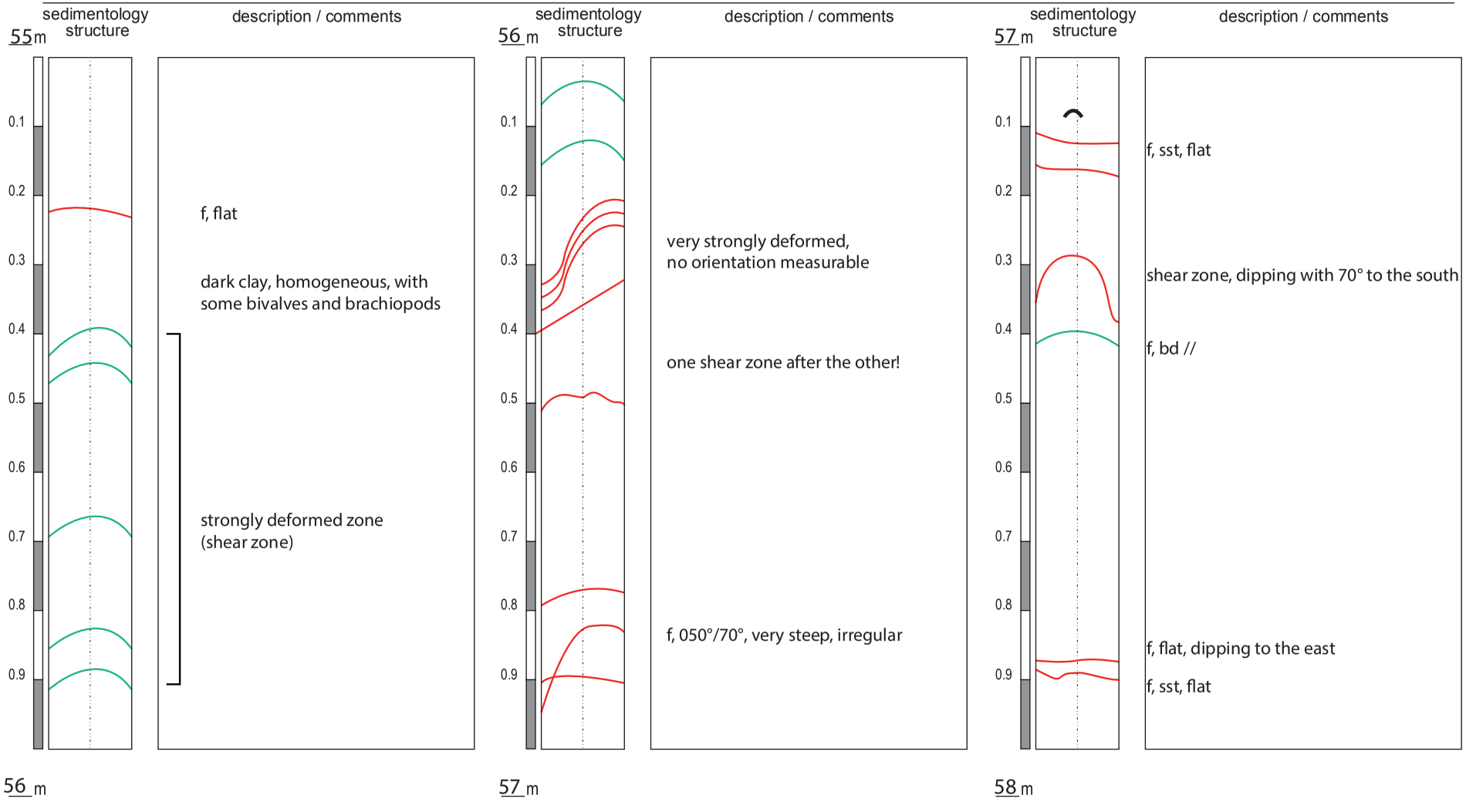

- Interpretation of facies/formation: Opalinus Clay: shaly facies

borehole BDS-5 drillcore mapping: jad page: 20

from 58 m to 61 m date of drillcore mapping: 10.06.2011 scale: 1 : 7.5

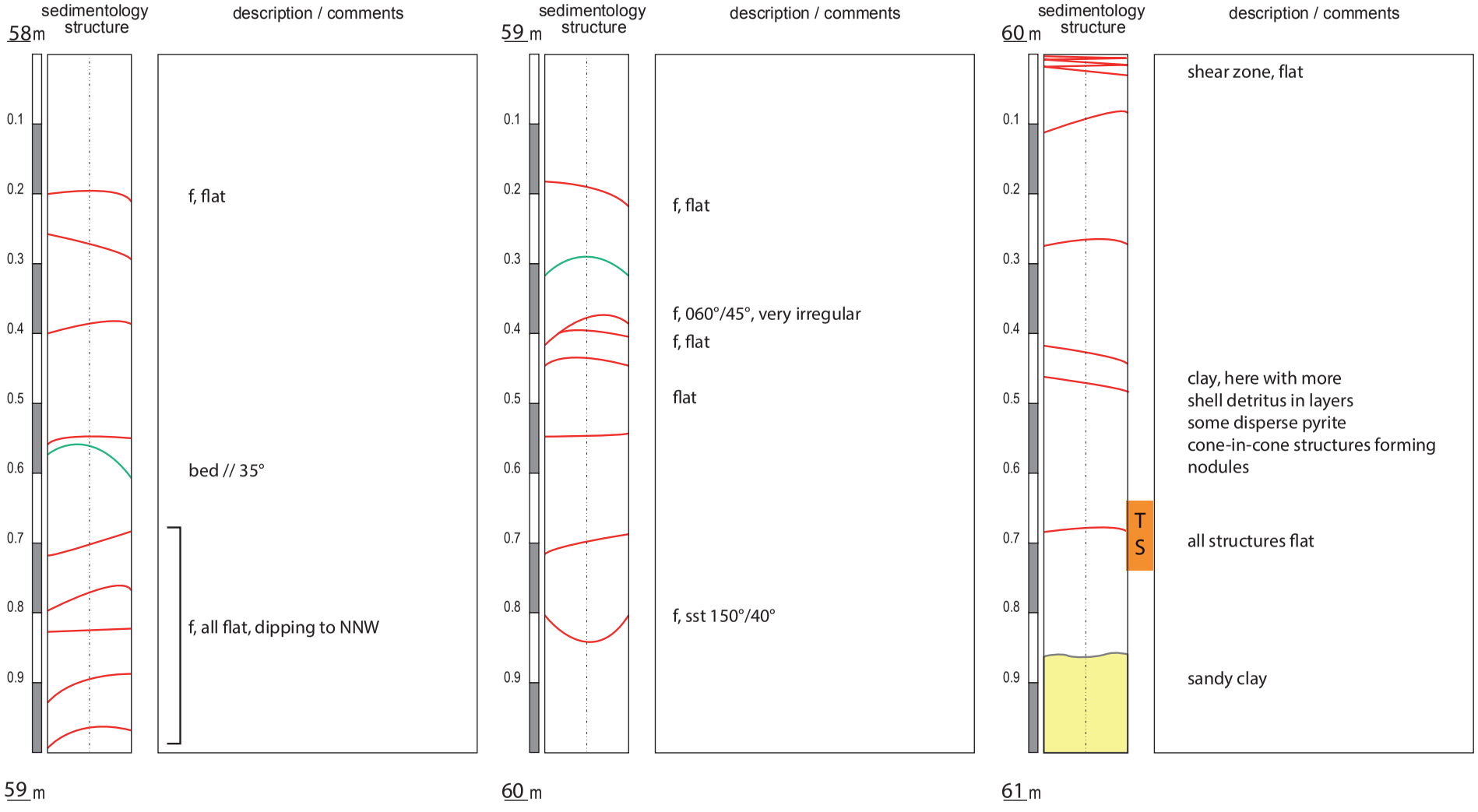

- Interpretation of facies/formation:

Opalinus Clay: shaly facies

borehole BDS-5 drillcore mapping: jad page: 21

from 61 m to 64 m date of drillcore mapping: 10.06.2011 scale: 1 : 7.5

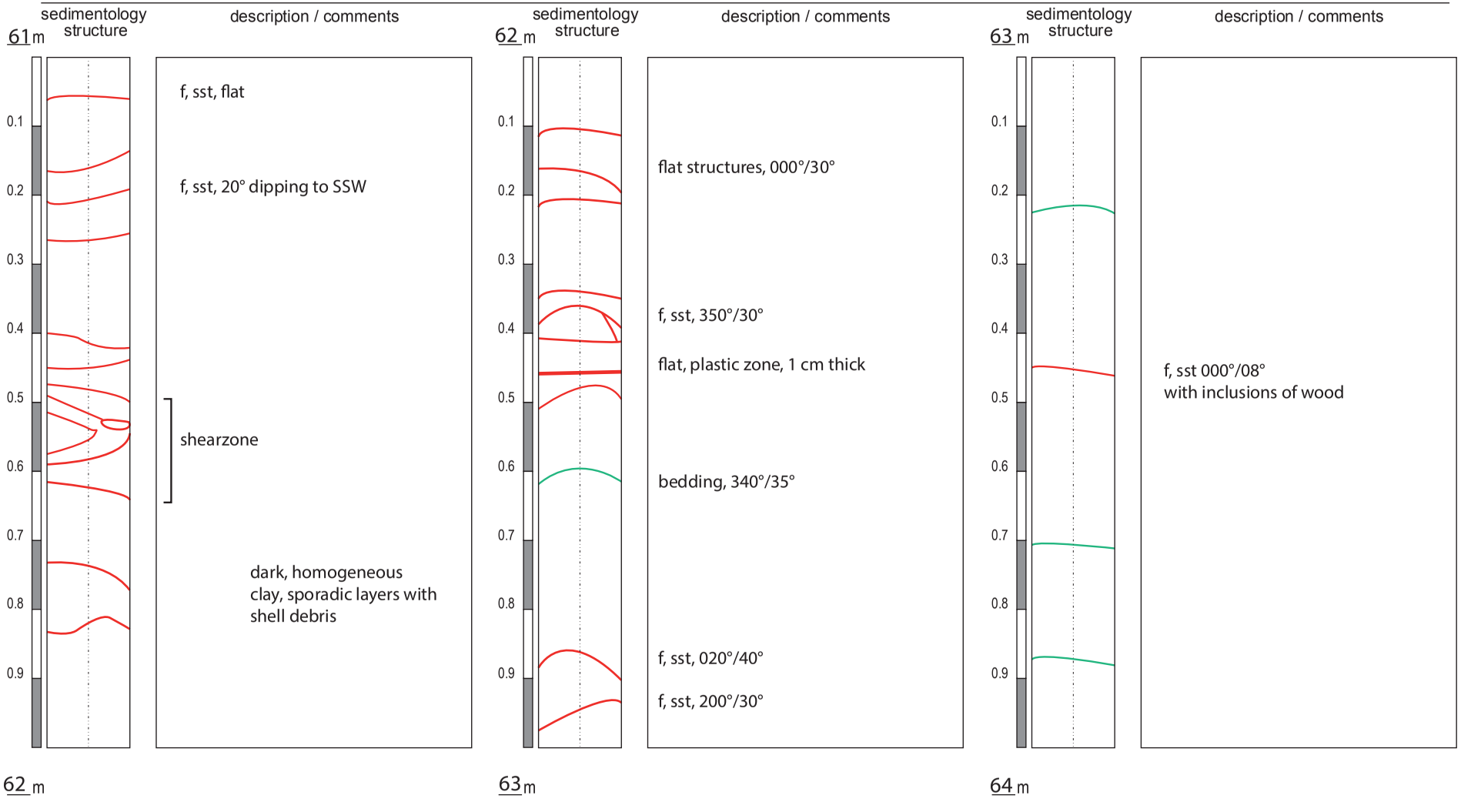

- Interpretation of facies/formation: Opalinus Clay: shaly facies

borehole BDS-5 drillcore mapping: jad page: 22

from 64 m to 67 m date of drillcore mapping: 10.06.2011 scale: 1 : 7.5

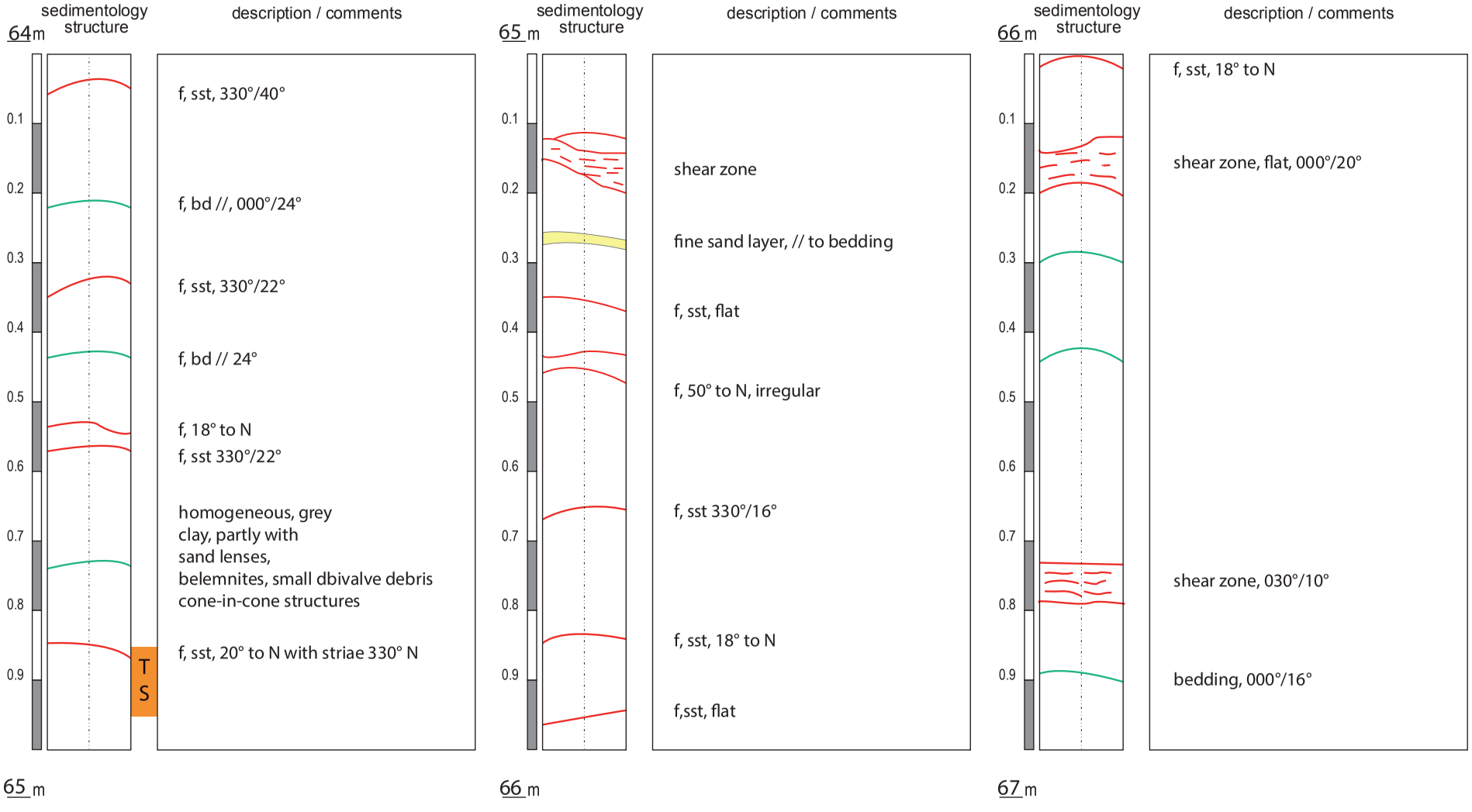

- Interpretation of facies/formation:

Opalinus Clay: shaly facies

borehole BDS-5 drillcore mapping: jad page: 23

from 67 m to 70 m date of drillcore mapping: 10.06.2011 scale: 1 : 7.5

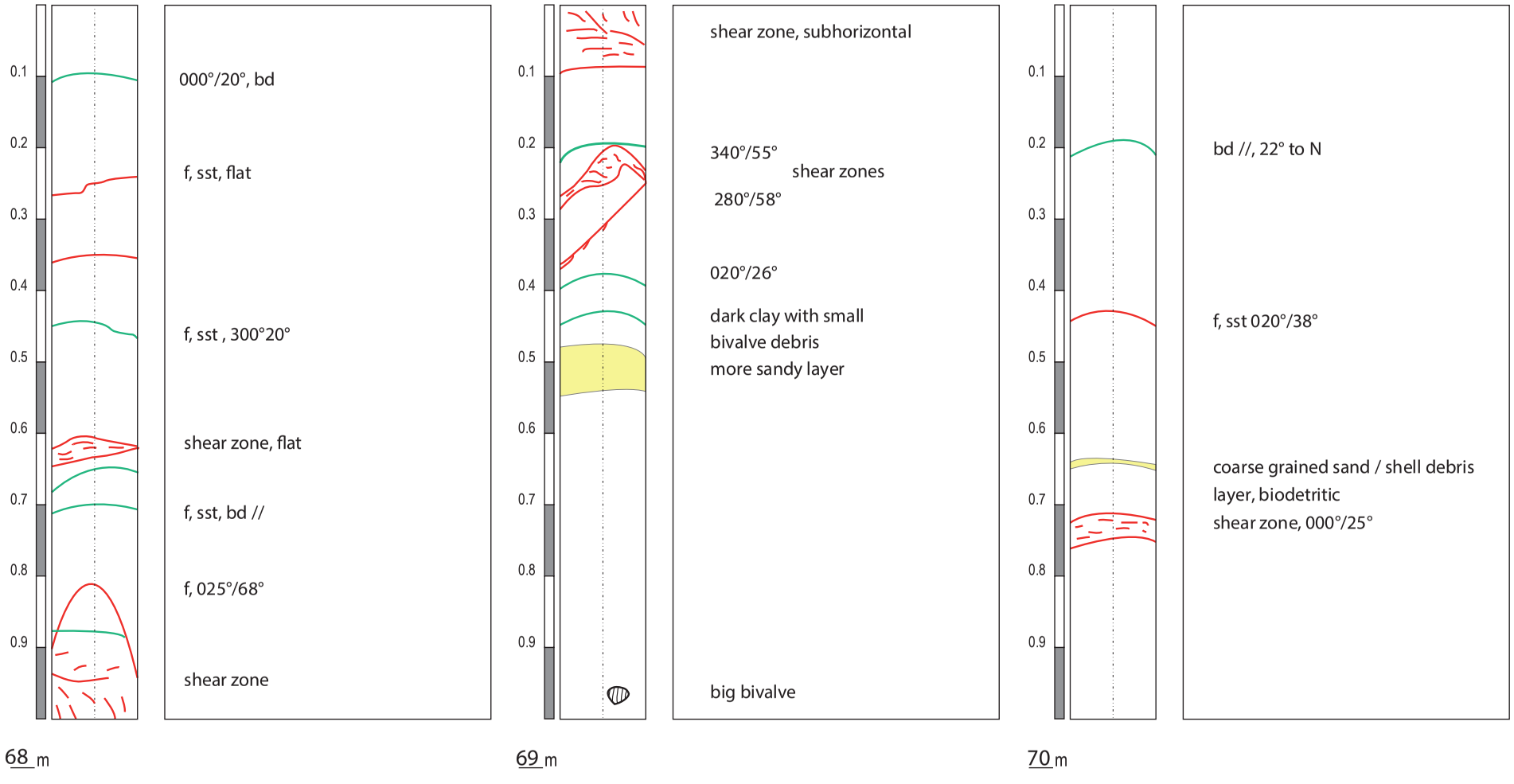

- Interpretation of facies/formation:

Opalinus Clay: shaly facies

borehole BDS-5 drillcore mapping: jad page: 24

from 70 m to 73 m date of drillcore mapping: 10.06.2011 scale: 1 : 7.5

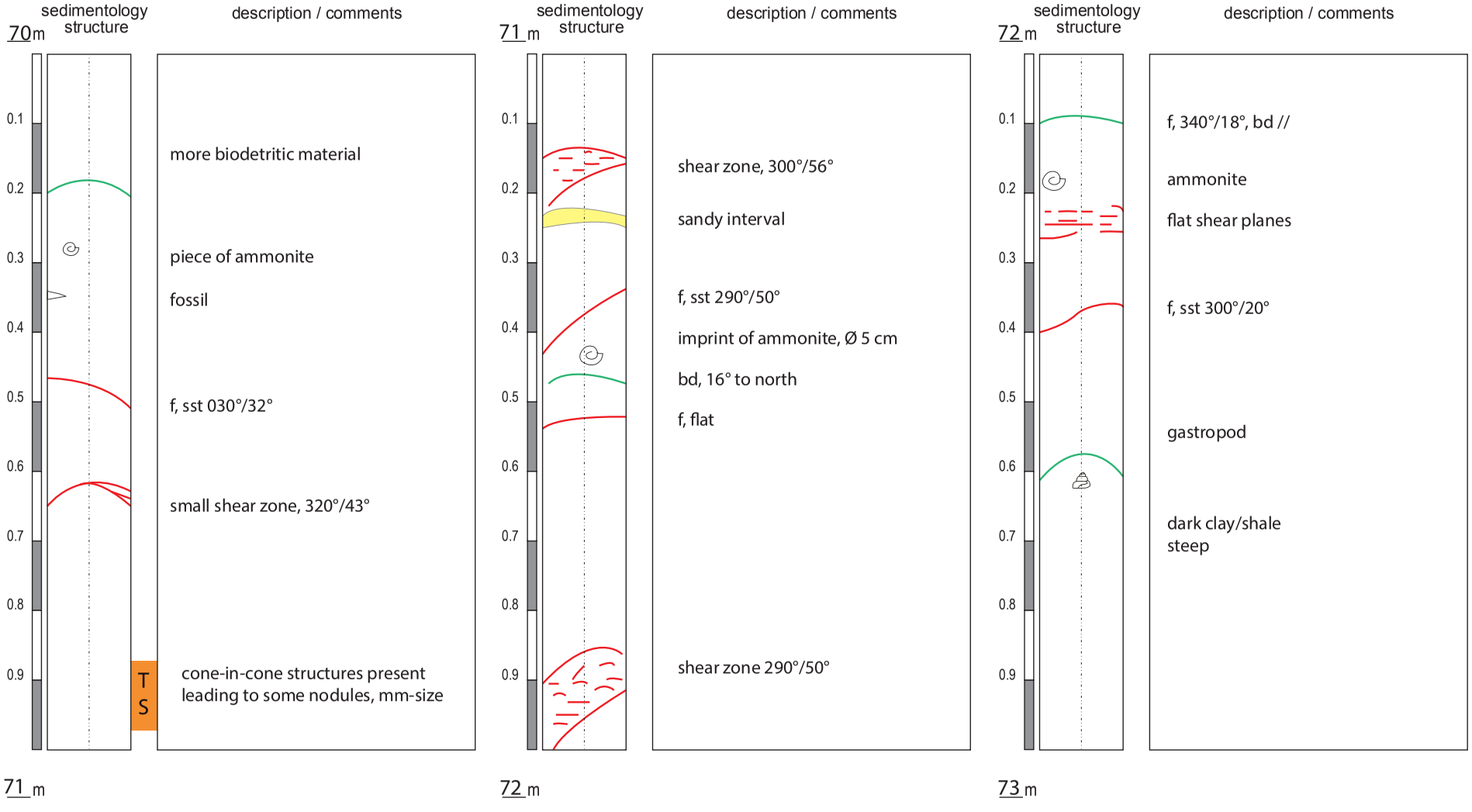

- Interpretation of facies/formation:

Opalinus Clay: shaly facies

borehole BDS-5 drillcore mapping: jad page: 25

from 73 m to 76 m date of drillcore mapping: 14.06.2011 scale: 1 : 7.5

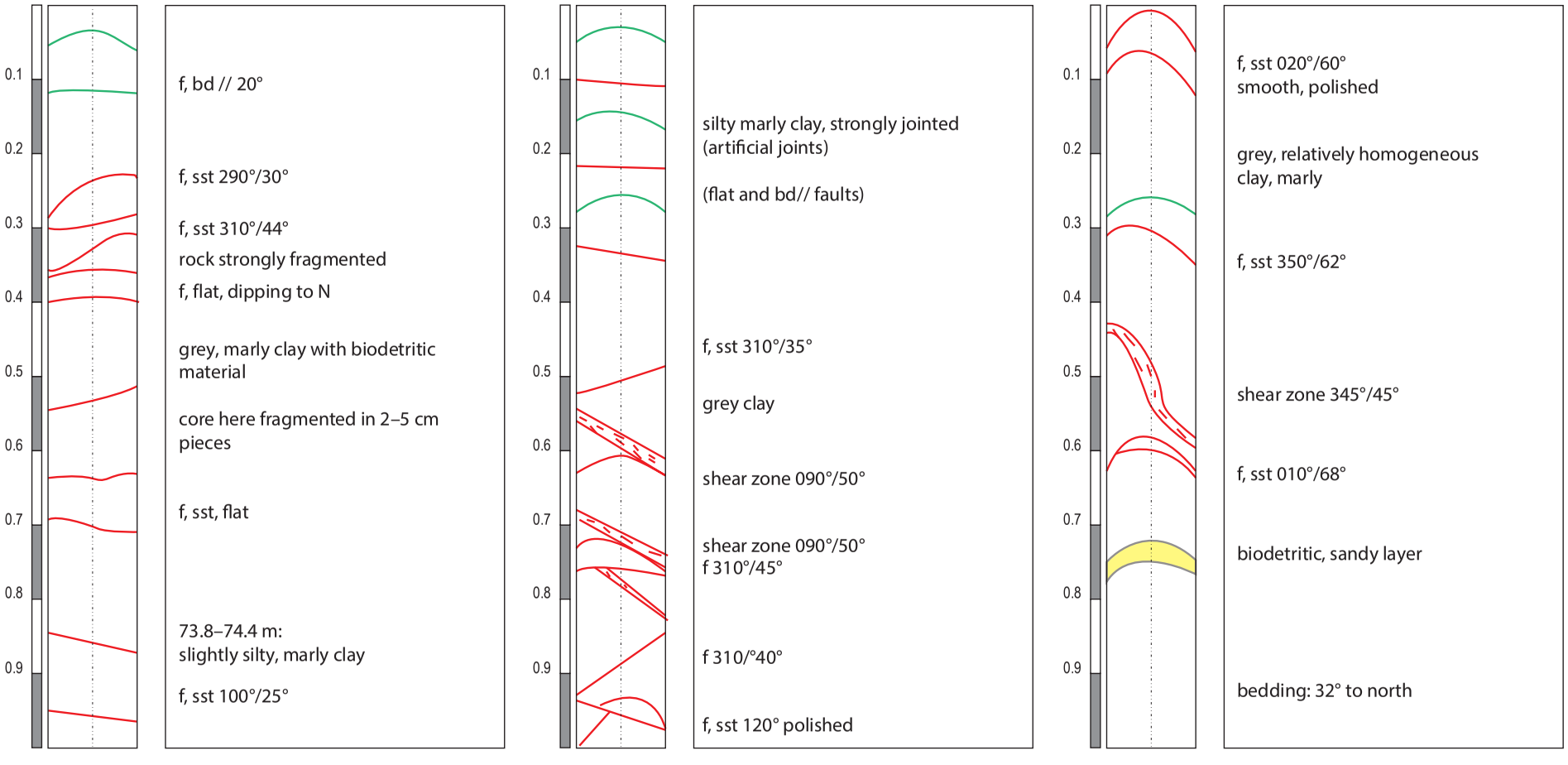

- Interpretation of facies/formation:

Opalinus Clay: shaly facies

borehole BDS-5 drillcore mapping: jad page: 26

from 76 m to 79 m date of drillcore mapping: 14.06.2011 scale: 1 : 7.5

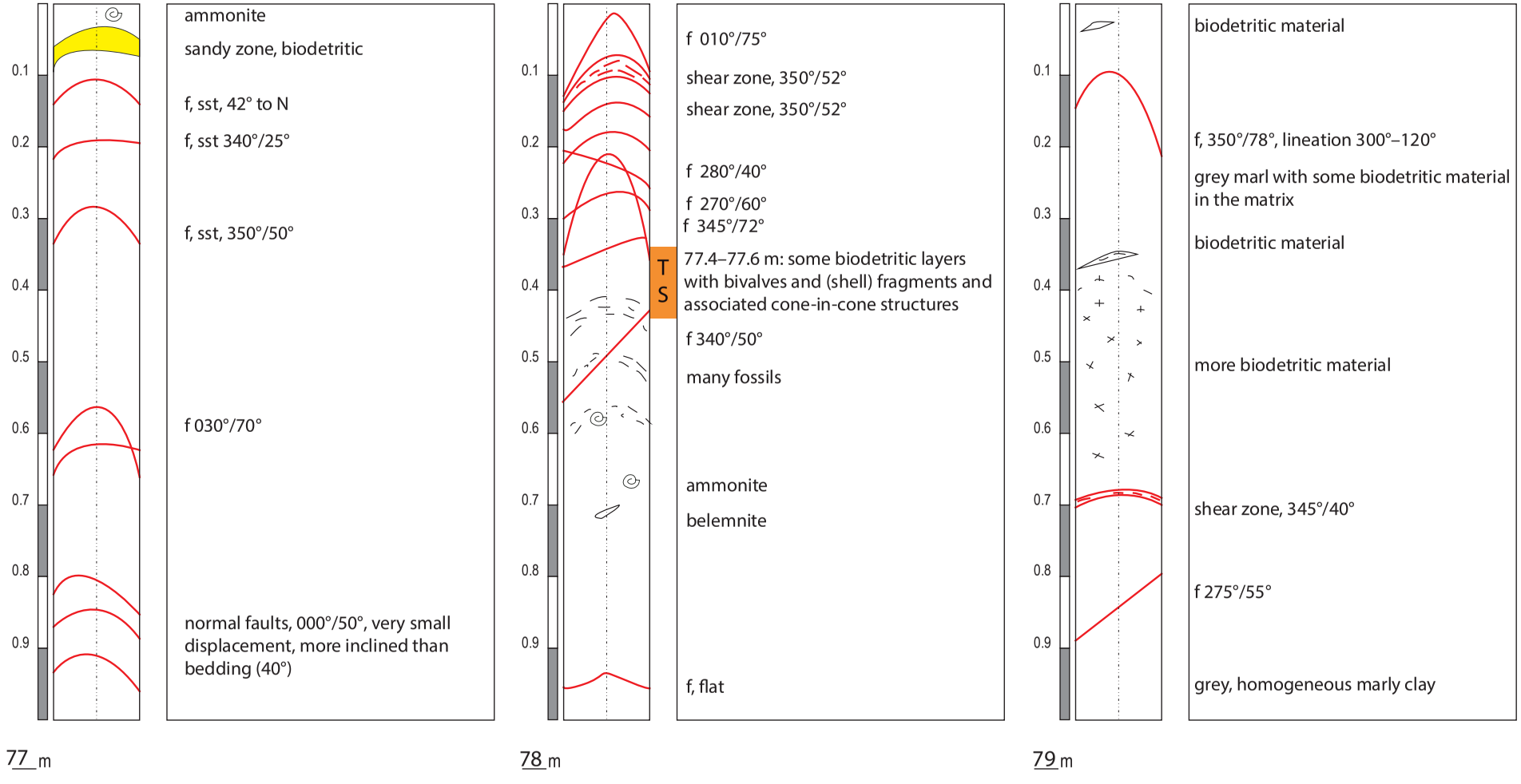

- Interpretation of facies/formation: Opalinus Clay: shaly facies

borehole BDS-5 drillcore mapping: jad page: 27

from 79 m to 82 m date of drillcore mapping: 14.06.2011 scale: 1 : 7.5

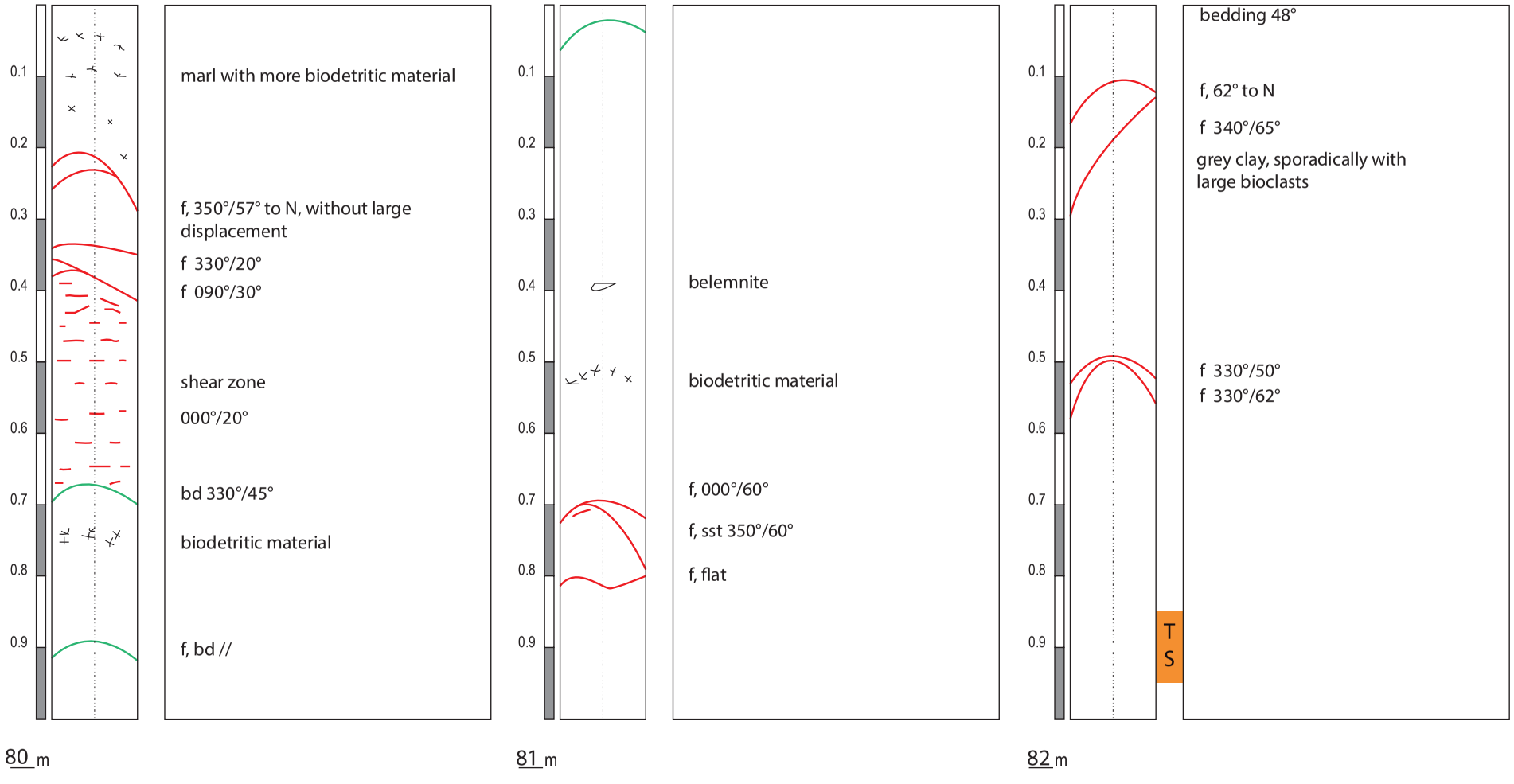

- Interpretation of facies/formation:

Opalinus Clay: shaly facies

borehole BDS-5 drillcore mapping: jad page: 28

from 82 m to 85 m date of drillcore mapping: 14.06.2011 scale: 1 : 7.5

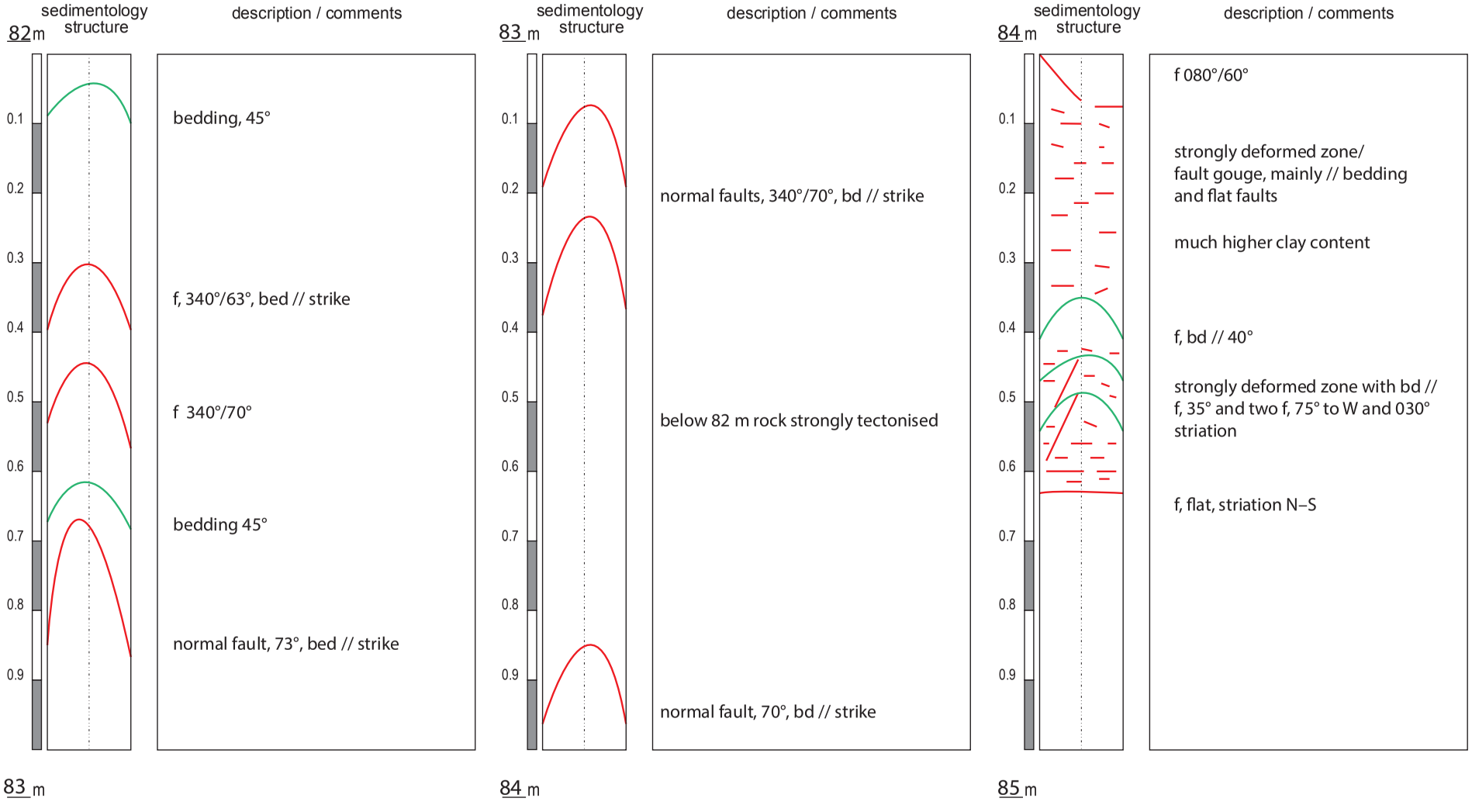

- Interpretation of facies/formation: Opalinus Clay: shaly facies

borehole BDS-5 drillcore mapping: jad page: 29

from 85 m to 88 m date of drillcore mapping: 14.06.2011 scale: 1 : 7.5

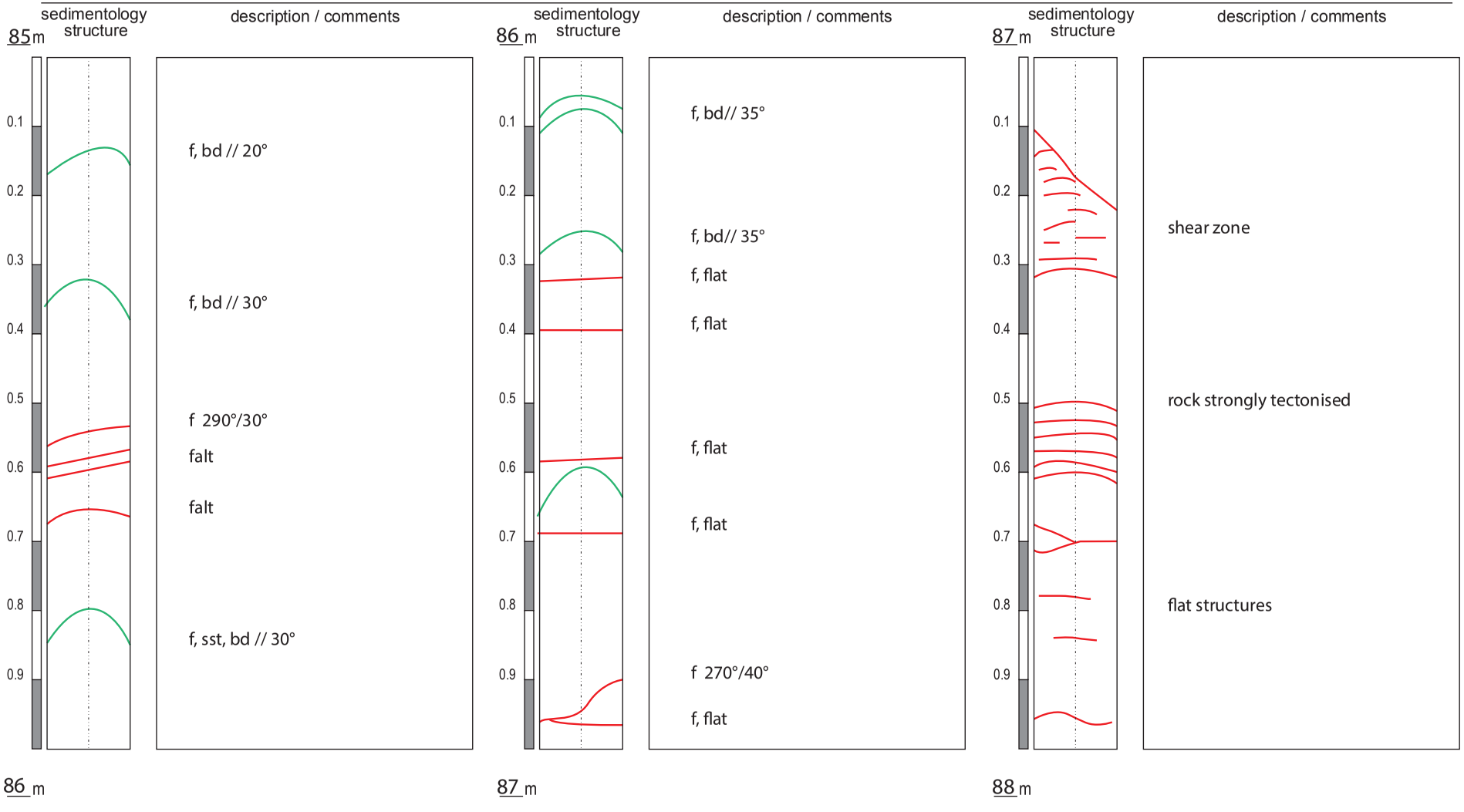

- Interpretation of facies/formation:

Opalinus Clay: shaly facies

borehole BDS-5 drillcore mapping: jad page: 30

from 88 m to 91 m date of drillcore mapping: 14.06.2011 scale: 1 : 7.5

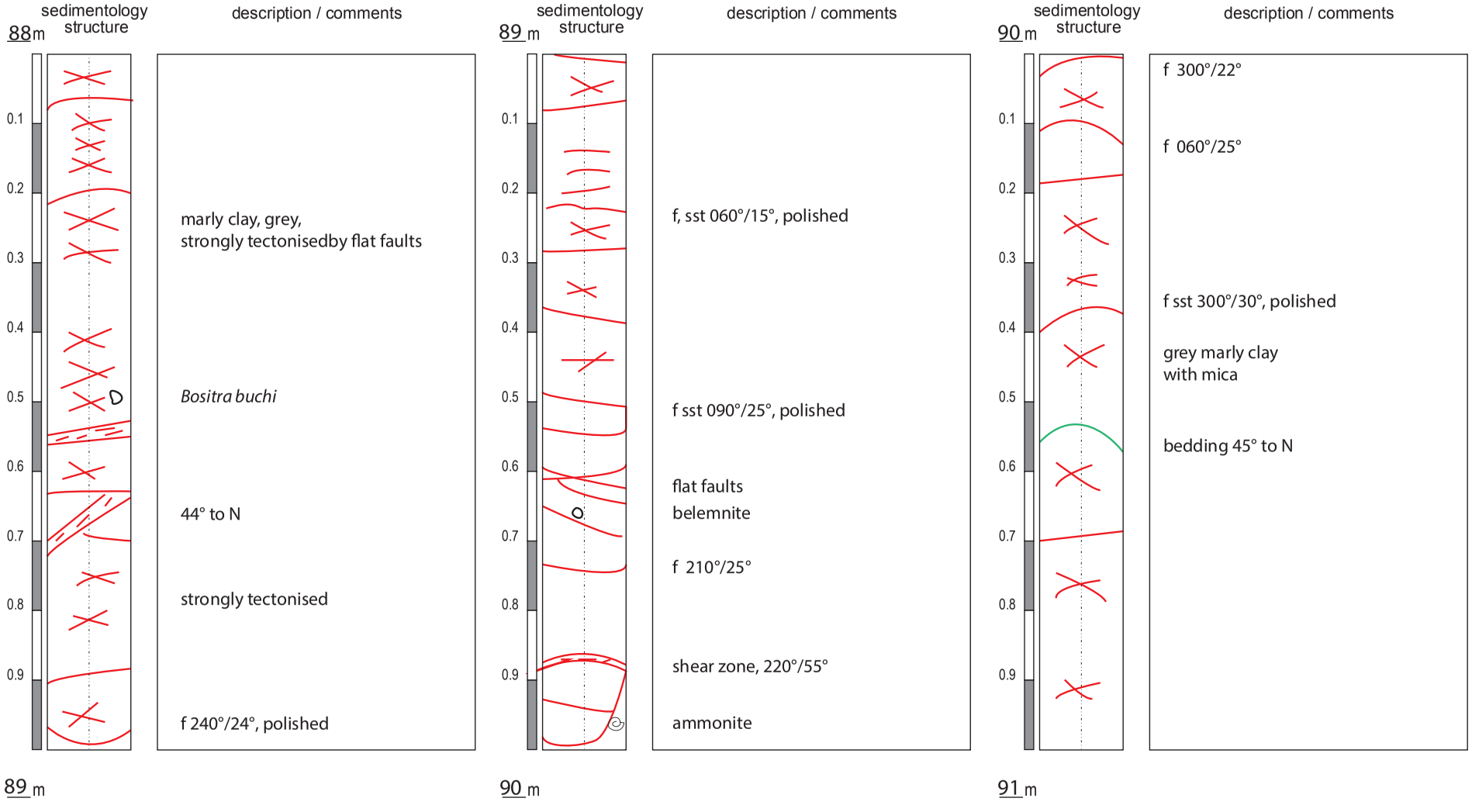

- Interpretation of facies/formation:

Opalinus Clay: shaly facies

borehole BDS-5 drillcore mapping: jad page: 31

from 91 m to 94 m date of drillcore mapping: 14.06.2011 scale: 1 : 7.5

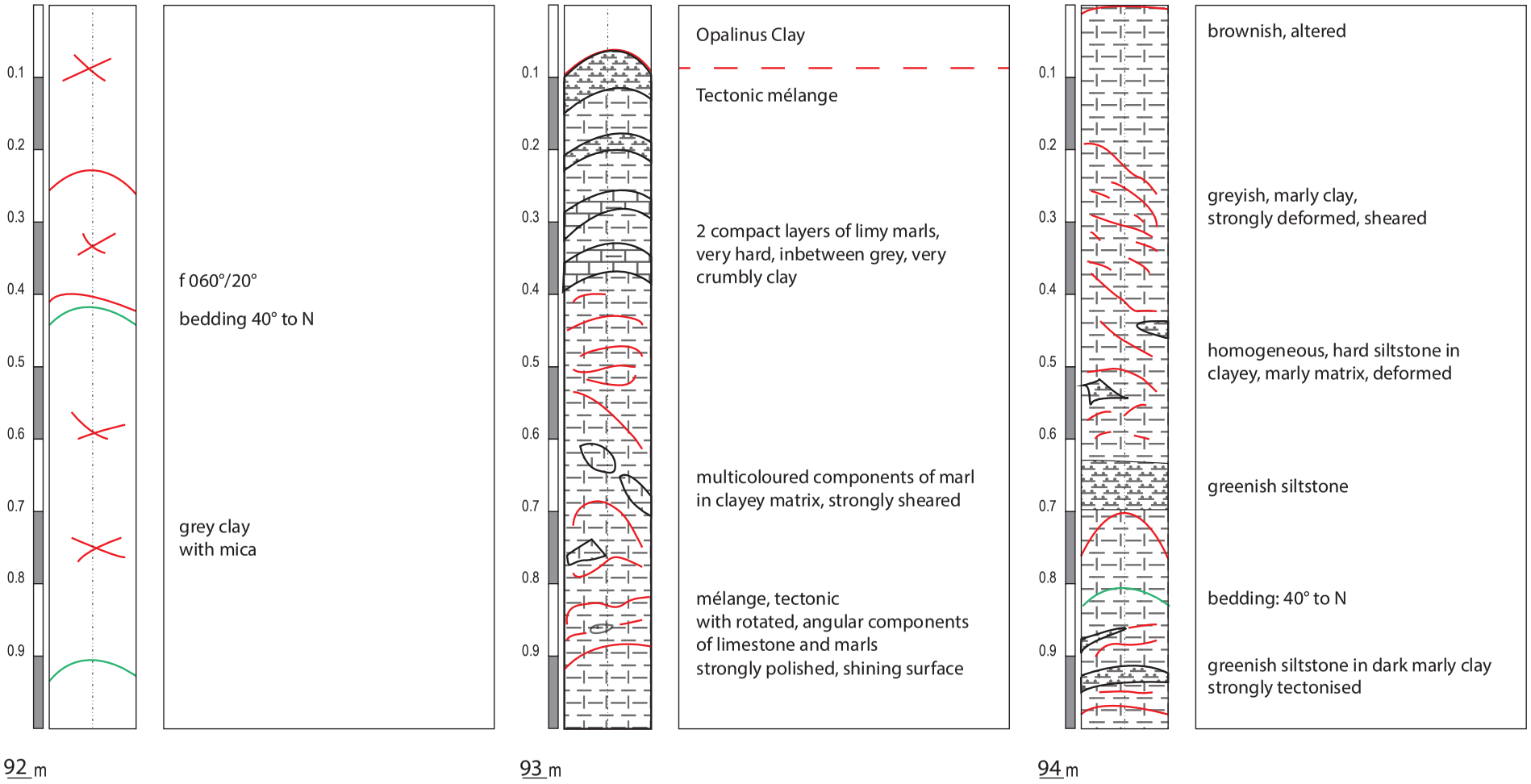

- Interpretation of facies/formation:

–92.1 m:	Opalinuns Clay, shaly facies
from 92.1 m on:	Tectonic mélange, multicoloured

borehole BDS-5 drillcore mapping: jad page: 32

from 94 m to 97 m date of drillcore mapping: 14.06.2011 scale: 1 : 7.5

94 m	sedimentology structure	description / comments
0.1		mainly brownish marl, silty
0.2		
0.3		
0.4		broken, compact lime layer on movement plane (large movements), phyllitic clay with lenticular, hard components
0.5		f, bd // 34°
0.6		
0.7		
0.8		
0.9		
95 m		

95 m	sedimentology structure	description / comments
0.1		95.3–97.7 m: greenish, grey silty marl
0.2		
0.3		
0.4		bedding // sheared
0.5		
0.6		
0.7		
0.8		
0.9		
96 m		

96 m	sedimentology structure	description / comments
0.1		f, bd // 34° to N
0.2		
0.3		
0.4		mainly grey silty marls
0.5		
0.6		
0.7		
0.8		
0.9		
97 m		

- Interpretation of facies/formation:

–95.3 m:	tectonic mélange, multicoloured marls
from 95.3 m on:	greenish and grey marls (Paleogene)

borehole BDS-5 drillcore mapping: jad page: 33

from 97 m to 100 m date of drillcore mapping: 14.06.2011 scale: 1 : 7.5

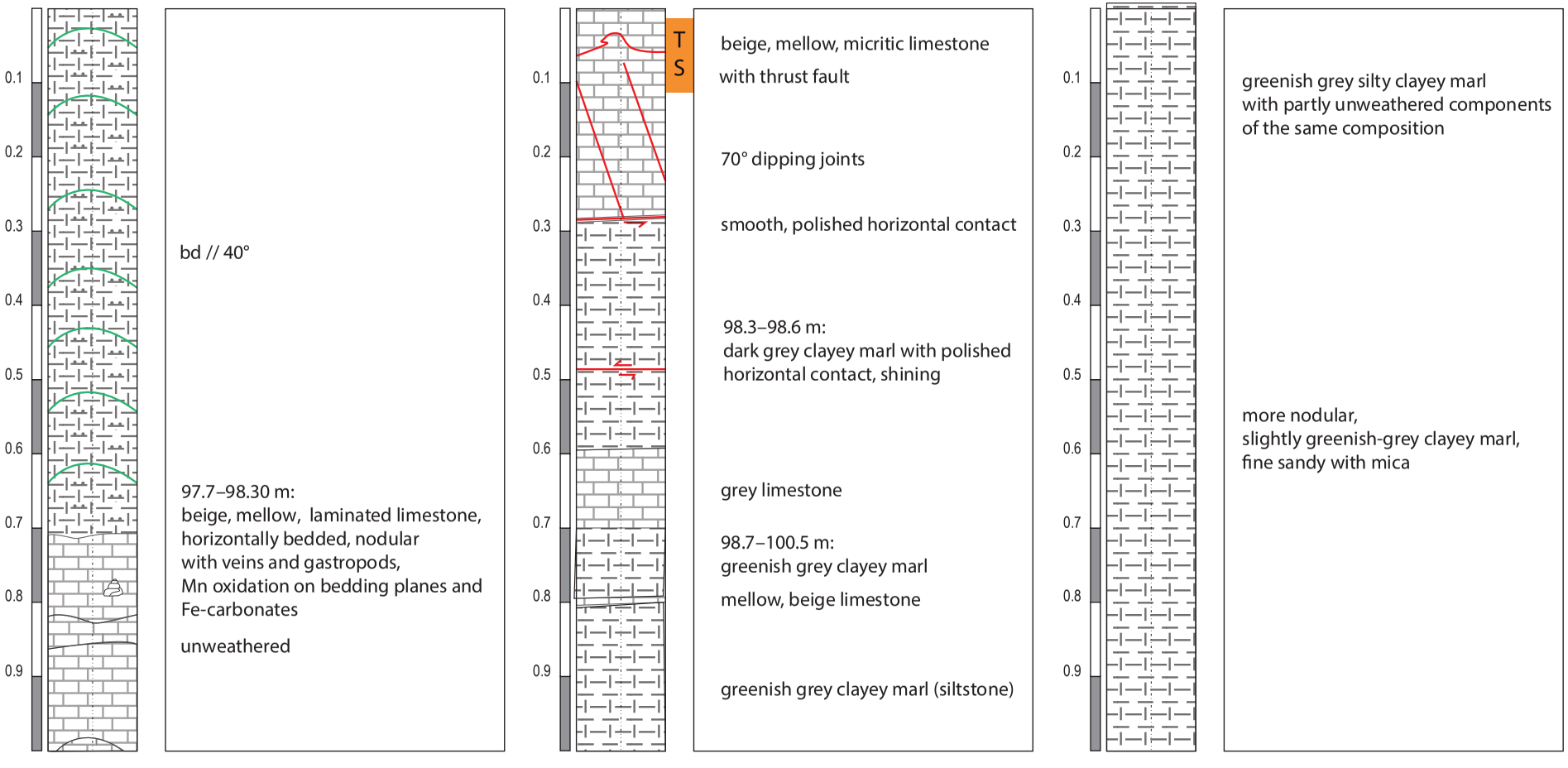

- Interpretation of facies/formation:

–97.7 m:	greenish and grey marls (Paleogene)
97.7–98.7 m:	freshwater limestone (Delsberg-Süsswasserkalk, Paleogene)
98.7–100.5 m:	mica bearing silty marl (Septarien-Ton, Paleogene)

borehole BDS-5 drillcore mapping: jad page: 34

from 100 m to 103 m date of drillcore mapping: 14.06.2011 scale: 1 : 7.5

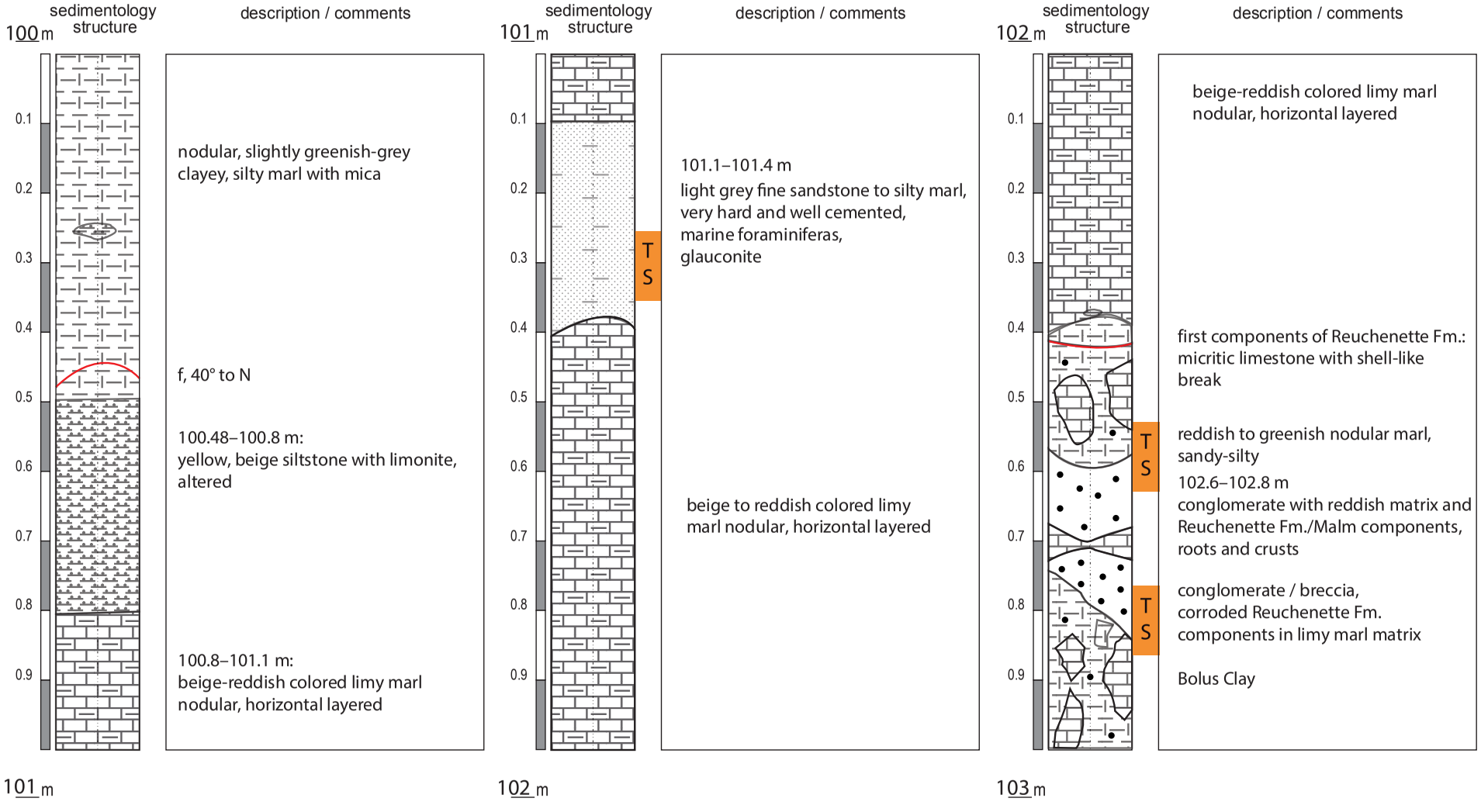

- Interpretation of facies/formation:

100.5–102.4 m: sandstones, siltstones, nodular marls (Septarien-Ton, Oligocene)
from 102.4 m on: Bolus Clay (Eocene)

borehole BDS-5 drillcore mapping: jad page: 35

from 103 m to 106 m date of drillcore mapping: 15.06.2011 scale: 1 : 7.5

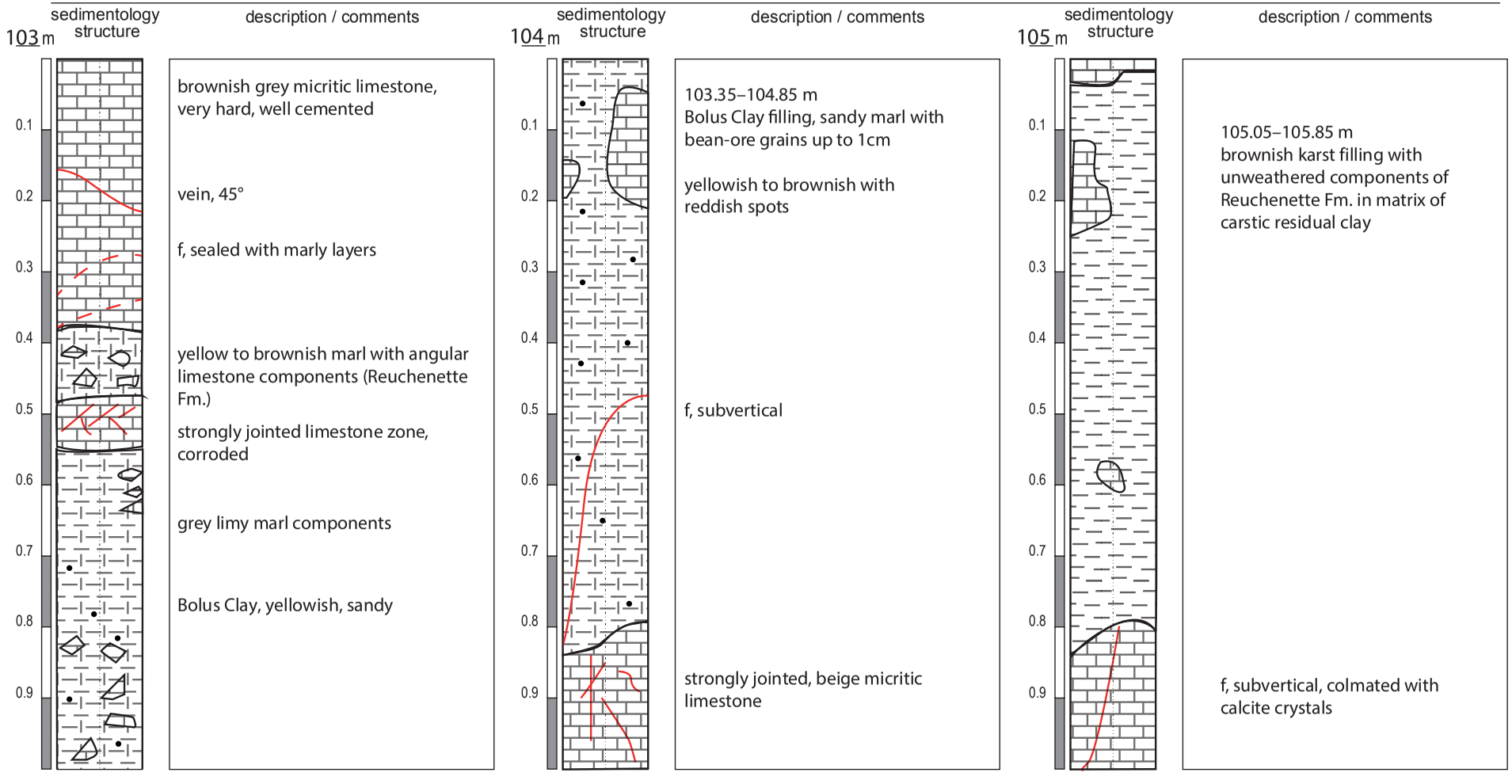

- Interpretation of facies/formation:

–105.85 m:	Bolus Clay (Eocene)
at 103.0 m:	top of limestone (Reuchenette Formation, Kimmeridgian)

borehole BDS-5 drillcore mapping: jad page: 36

from 106 m to 109 m date of drillcore mapping: 15.06.2011 scale: 1 : 7.5

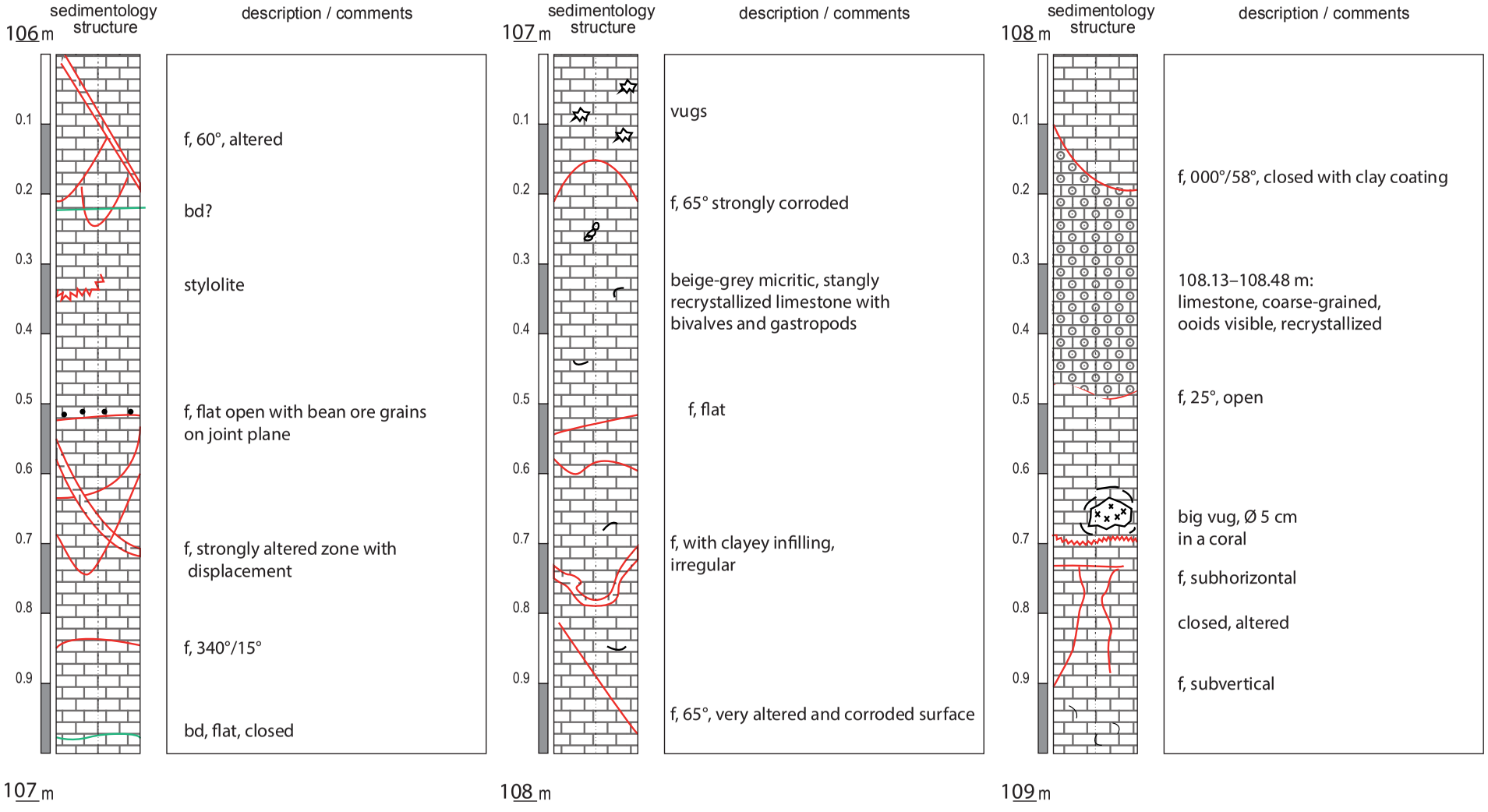

- Interpretation of facies/formation:

beige micritic limestone

Reuchenette Formation

borehole BDS-5 drillcore mapping: jad page: 37

from 109 m to 112 m date of drillcore mapping: 15.06.2011 scale: 1 : 7.5

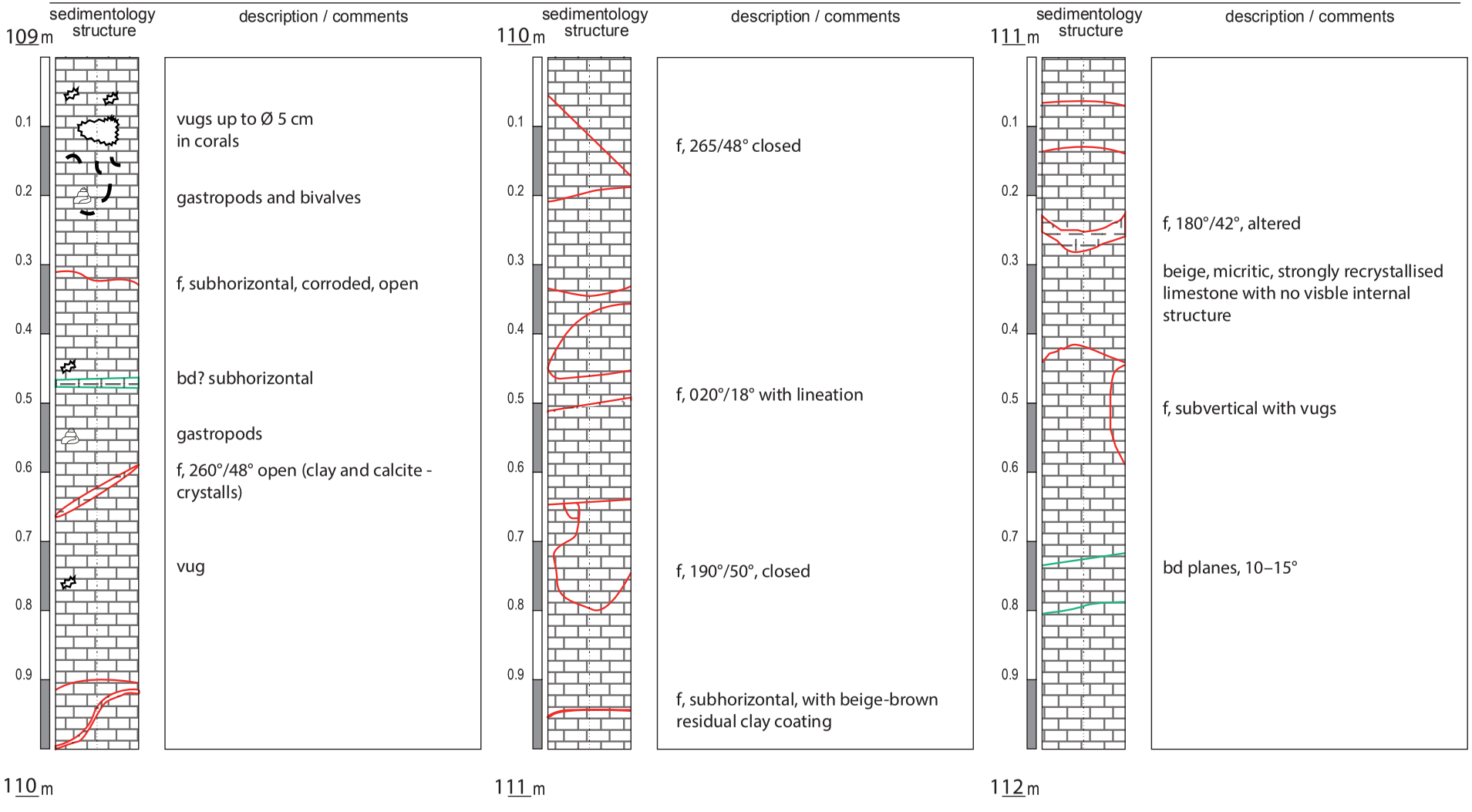

- Interpretation of facies/formation:

beige, micritic limestone

Reuchenette Formation

borehole BDS-5 drillcore mapping: jad page: 38

from 112 m to 115 m date of drillcore mapping: 15.06.2011/ 22.06.2011 scale: 1 : 7.5

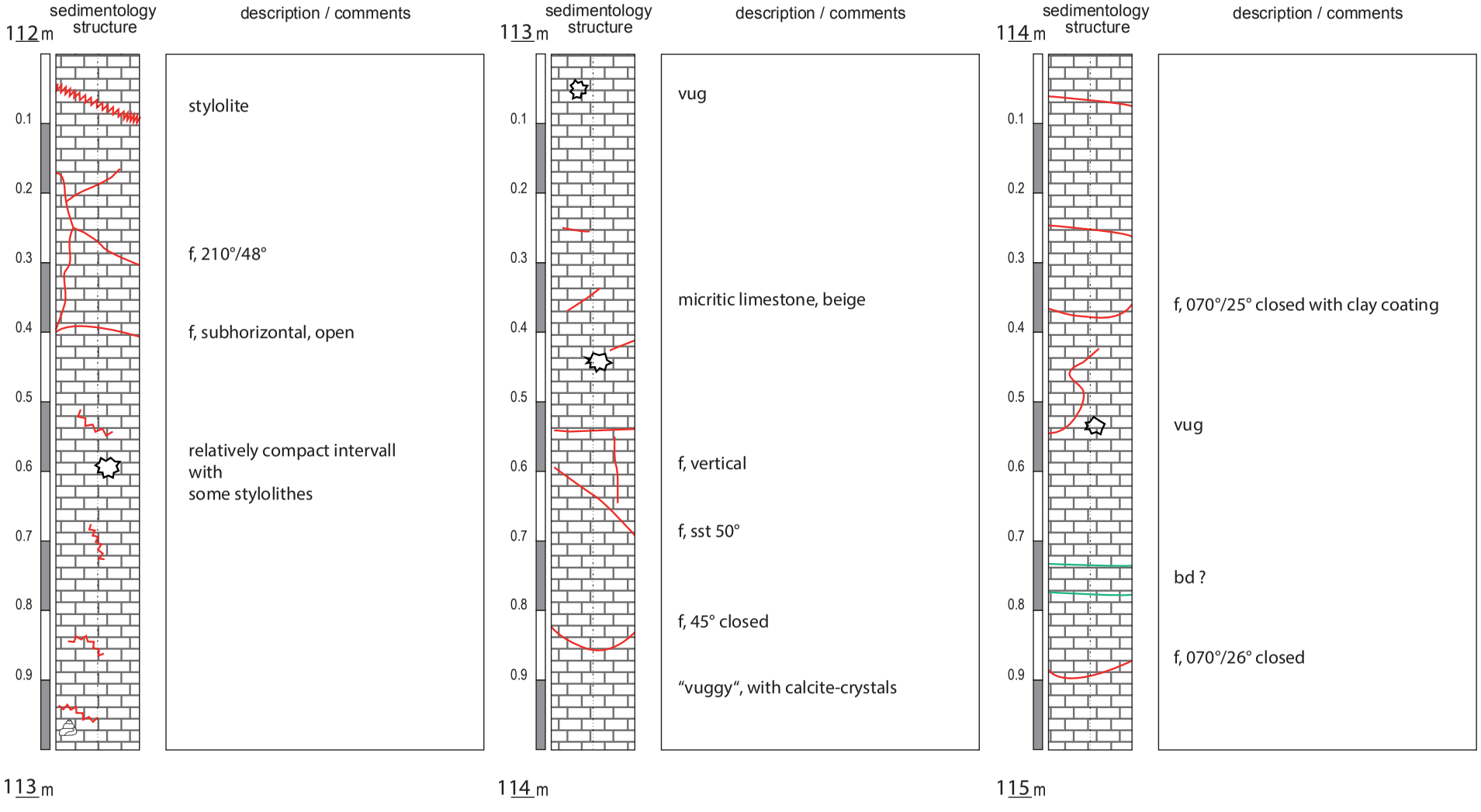

- Interpretation of facies/formation:

113.6 m: drillcore diameter changes from 85 to 63 mm
(borehole diameter from 122 to 101 mm)
beige micritic limestone

Reuchenette Formation

borehole BDS-5 drillcore mapping: jad page: 39

from 115 m to 118 m date of drillcore mapping: 22.06.2011 scale: 1 : 7.5

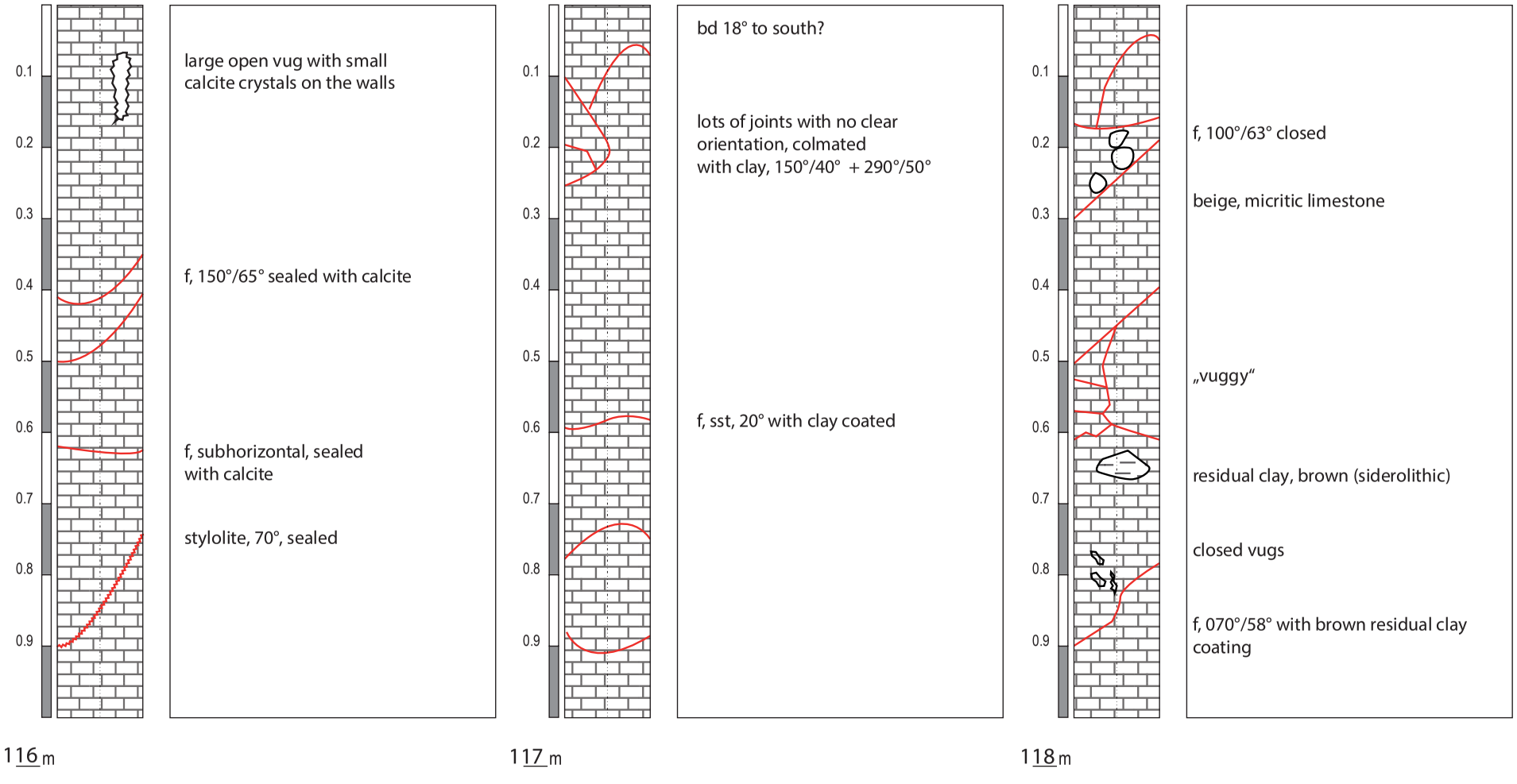

- Interpretation of facies/formation:

beige micritic limestone

Reuchenette Formation

borehole BDS-5 drillcore mapping: jad page: 40

from 118 m to 121 m date of drillcore mapping: 24.06.2011 scale: 1 : 7.5

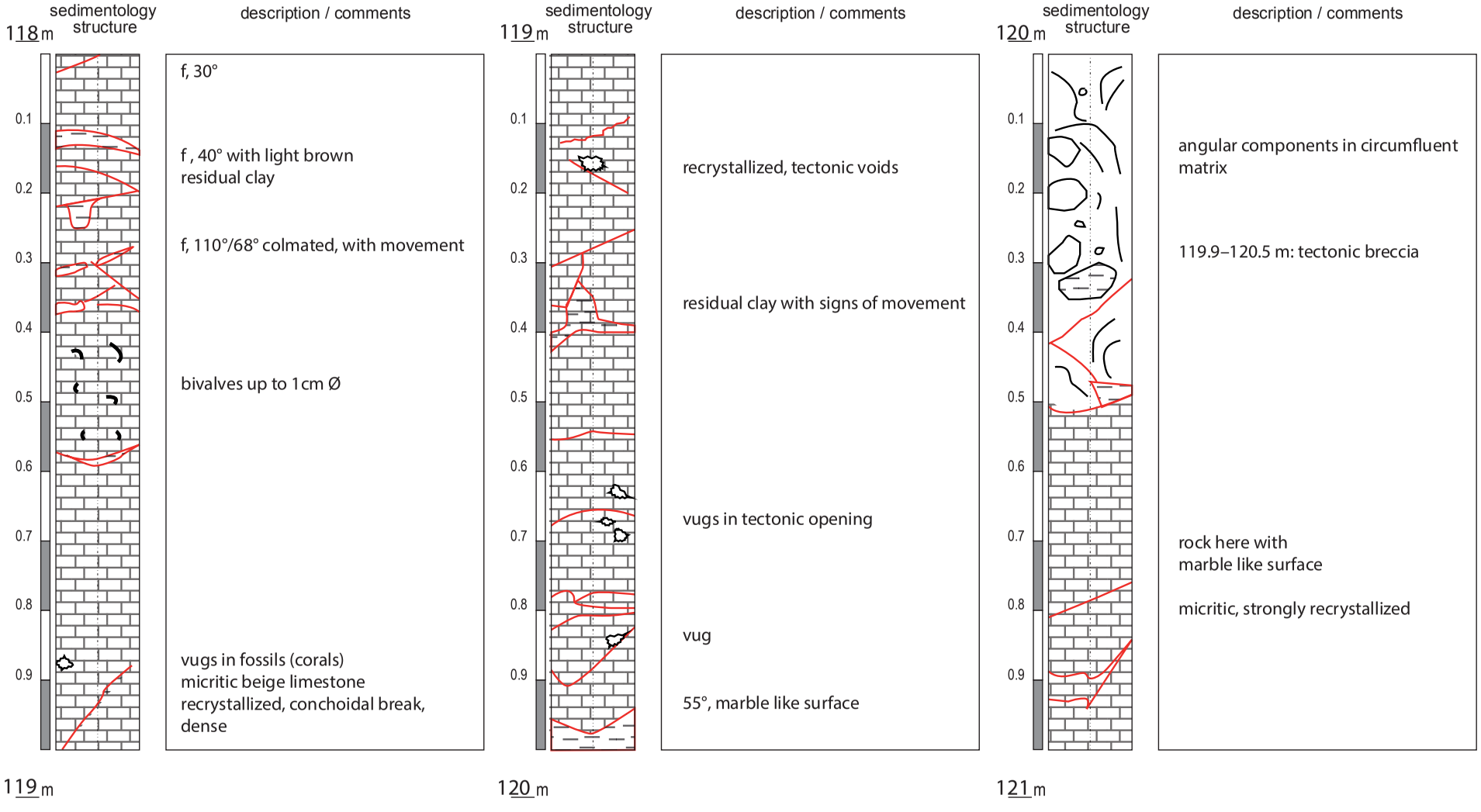

- Interpretation of facies/formation:

beige micritic limestone

Reuchenette Formation

borehole BDS-5 drillcore mapping: jad page: 41

from 121 m to 124 m date of drillcore mapping: 24.06.2011 scale: 1 : 7.5

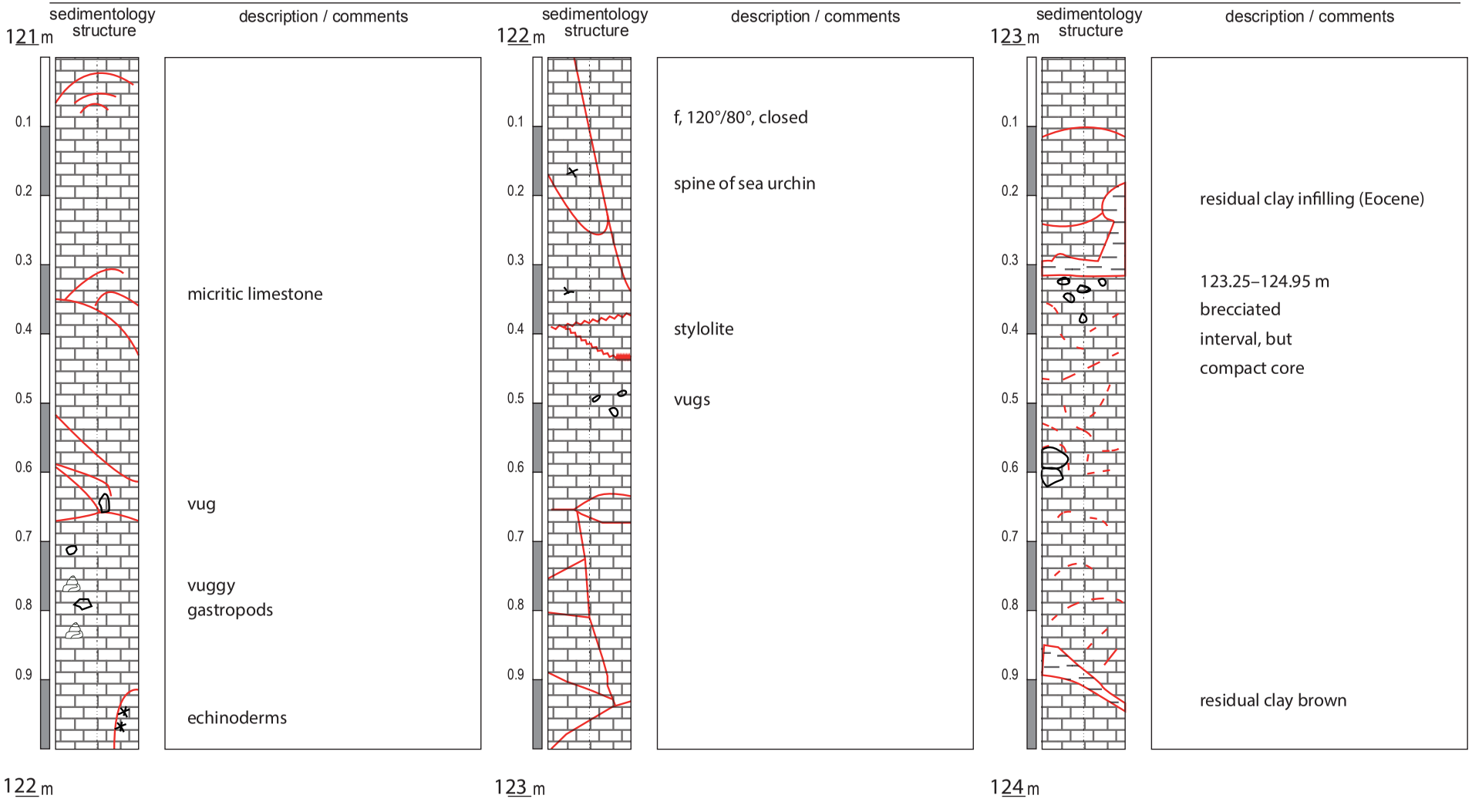

- Interpretation of facies/formation:

beige micritic limestone

Reuchenette Formation

borehole BDS-5 drillcore mapping: jad page: 42

from 124 m to 127 m date of drillcore mapping: 24.06.2011 scale: 1 : 7.5

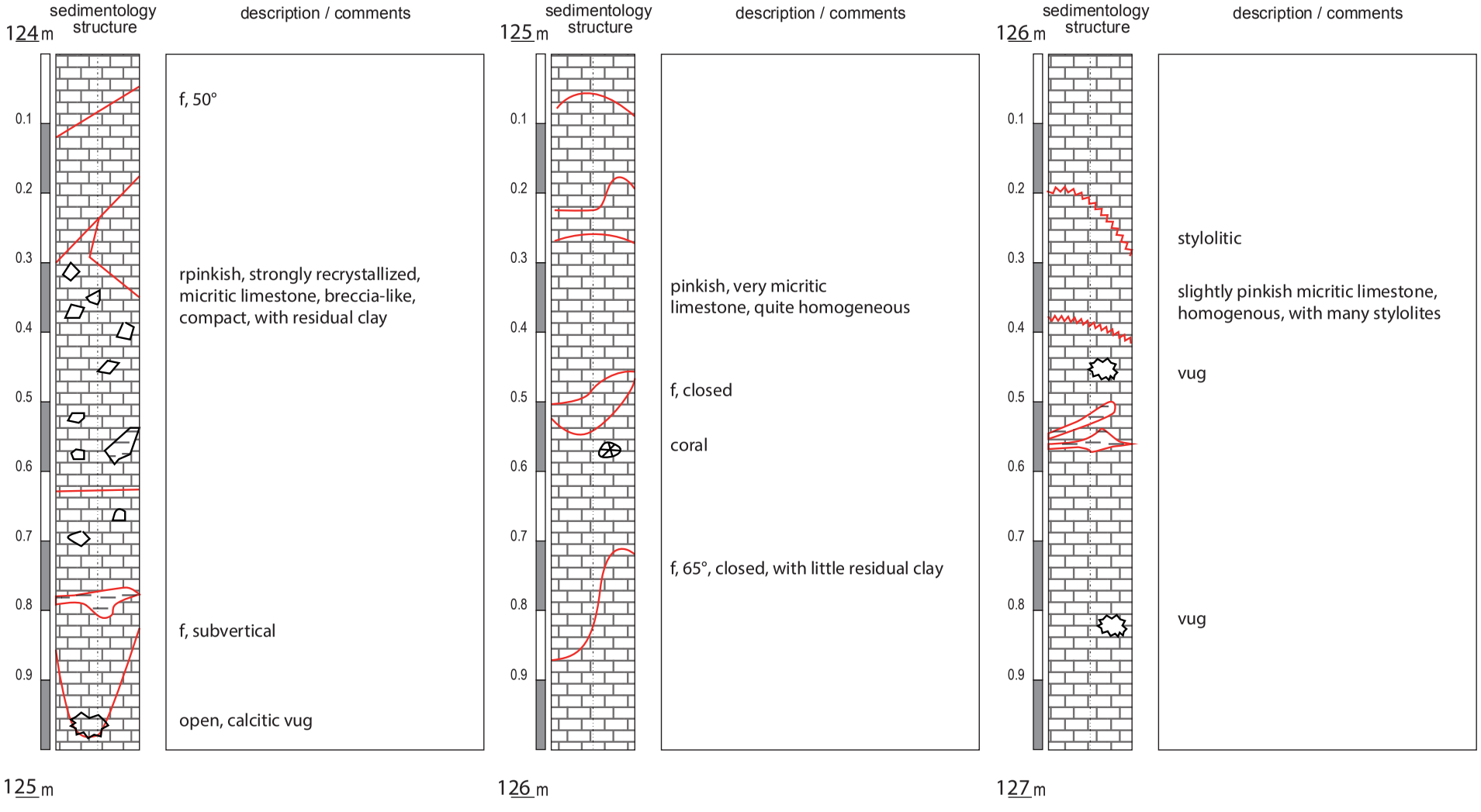

- Interpretation of facies/formation:

rose to beige micritic limestone

Reuchenette Formation

borehole BDS-5 drillcore mapping: jad page: 43

from 127 m to 130 m date of drillcore mapping: 24.06.2011 scale: 1 : 7.5

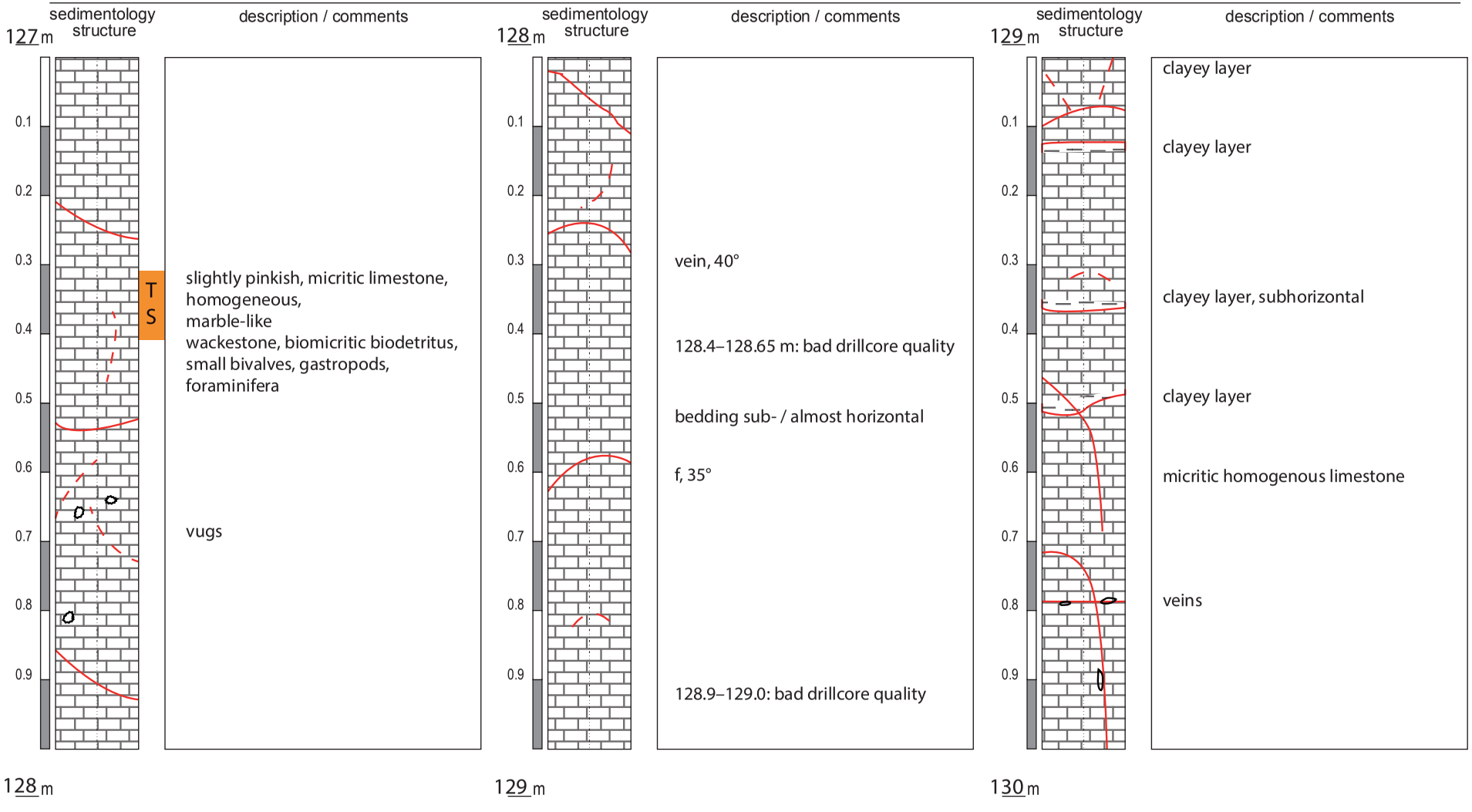

- Interpretation of facies/formation:

rose to beige micritic limestone

Reuchenette Formation

borehole BDS-5 drillcore mapping: jad page: 44

from 130 m to 133 m date of drillcore mapping: 24.06.2011 scale: 1 : 7.5

130 m	sedimentology structure	description / comments
0.1		
0.2		130.15–130.20 m: brecciated zone, very clayey
0.3		
0.4		
0.5		f, 130°/28° with residual clay coating
0.6		
0.7		grainy limestone, oolithic to pseudo-oolithic, with biodetritic material
0.8		coral fragments?
0.9		f, 240°/48° with residual clay coating
131 m		

131 m	sedimentology structure	description / comments
0.1		f, 60°
0.2		
0.3		131.2–131.5 m: brecciated zone, joint infilling?
0.4		
0.5		
0.6		pseudo-oolithic to oolithic limestone
0.7		f, flat
0.8		
0.9		f, flat
132 m		

132 m	sedimentology structure	description / comments
0.1		132.0–132.3 m clayey, brecciated zone joint infilling
0.2		
0.3		from 132.3 m: limestone, micritic, marble-like
0.4		
0.5		
0.6		with gastropods
0.7		
0.8		from 132.8 m: homogeneous micritic limestone
0.9		
133 m		

- Interpretation of facies/formation:

beige oolithic and micritic limestone

Reuchenette Formation

borehole BDS-5 drillcore mapping: jad page: 45

from 133 m to 136 m date of drillcore mapping: 27.06.2011 scale: 1 : 7.5

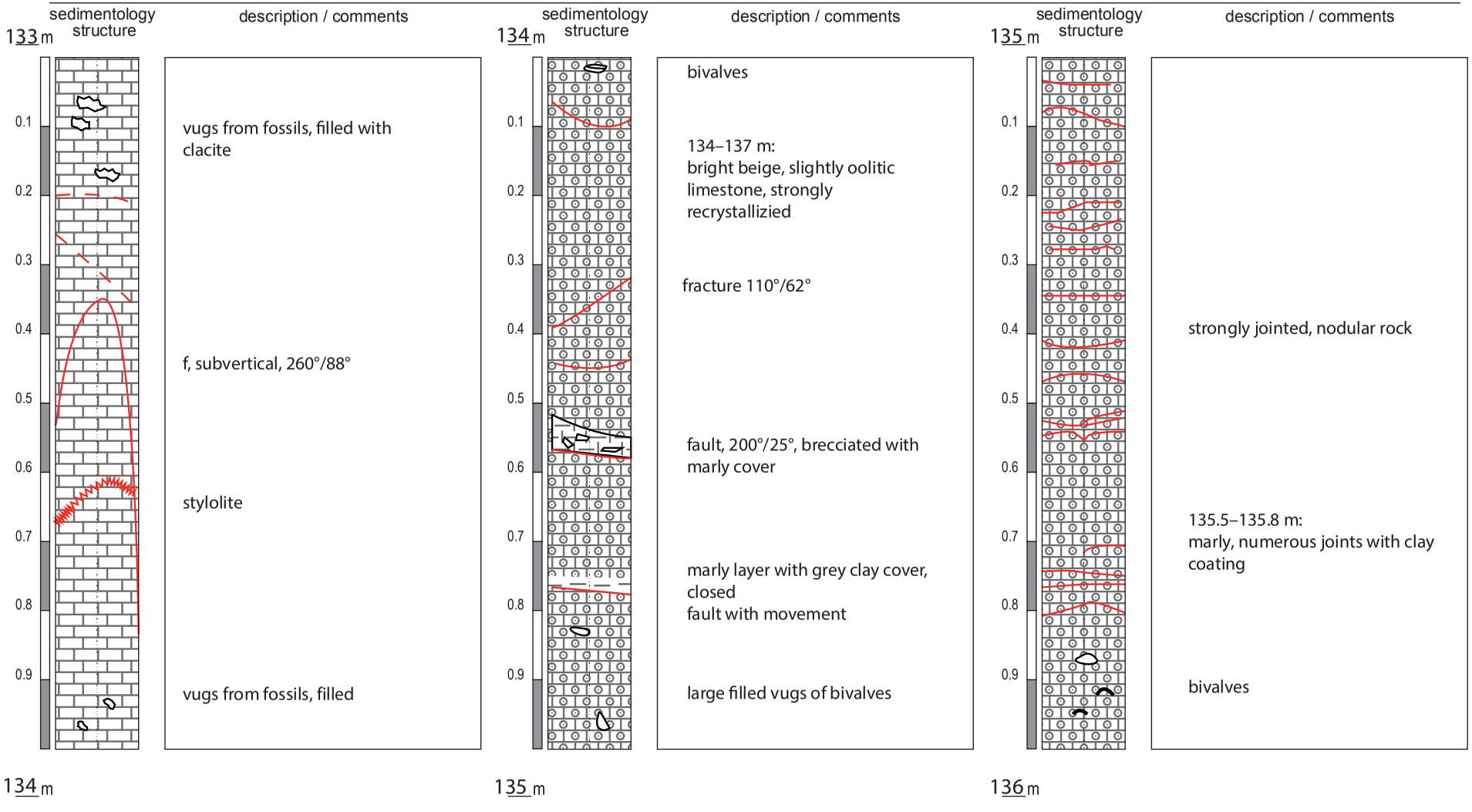

- Interpretation of facies/formation:

beige oolithic and micritic limestone

Reuchenette Formation

borehole BDS-5 drillcore mapping: jad page: 46

from 136 m to 139 m date of drillcore mapping: 27.06.2011 scale: 1 : 7.5

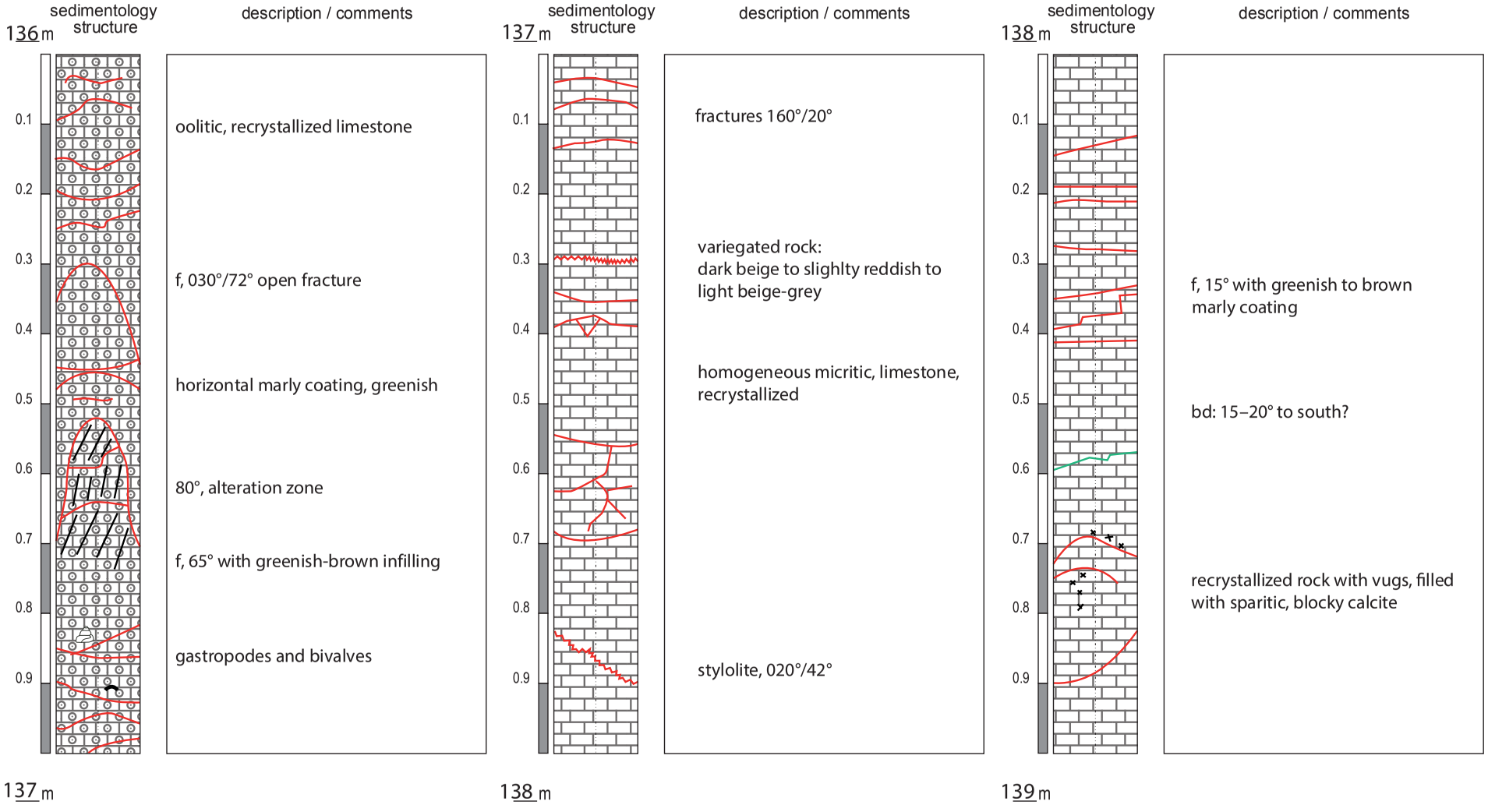

- Interpretation of facies/formation:

multi coloured micritic limestone

Reuchenette Formation

borehole BDS-5 drillcore mapping: jad page: 47

from 139 m to 142 m date of drillcore mapping: 27.06.2011 scale: 1 : 7.5

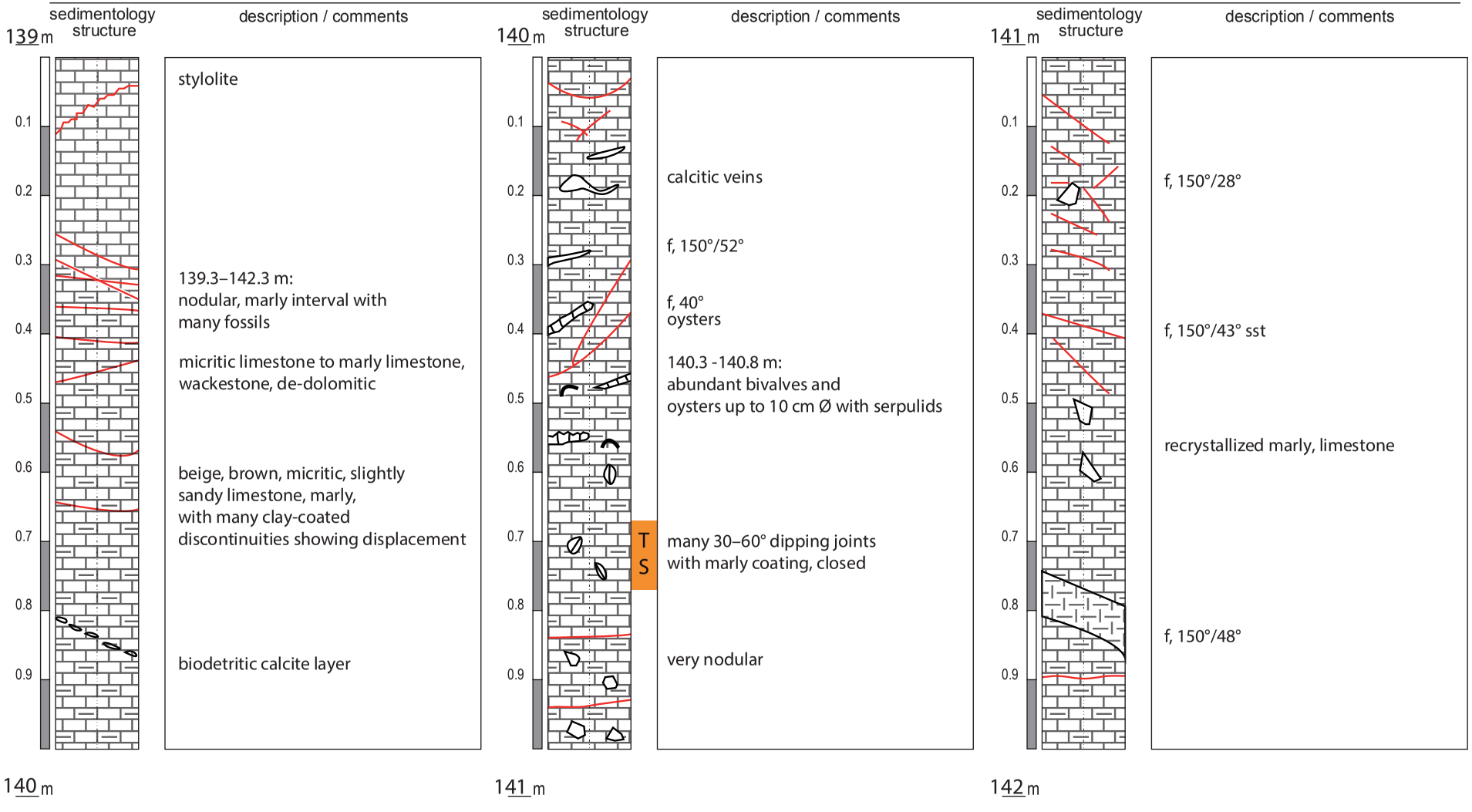

- Interpretation of facies/formation:

beige, marly limestone, micritic

Reuchenette Formation

borehole BDS-5 drillcore mapping: jad page: 48

from 142 m to 145 m date of drillcore mapping: 27.06.2011 scale: 1 : 7.5

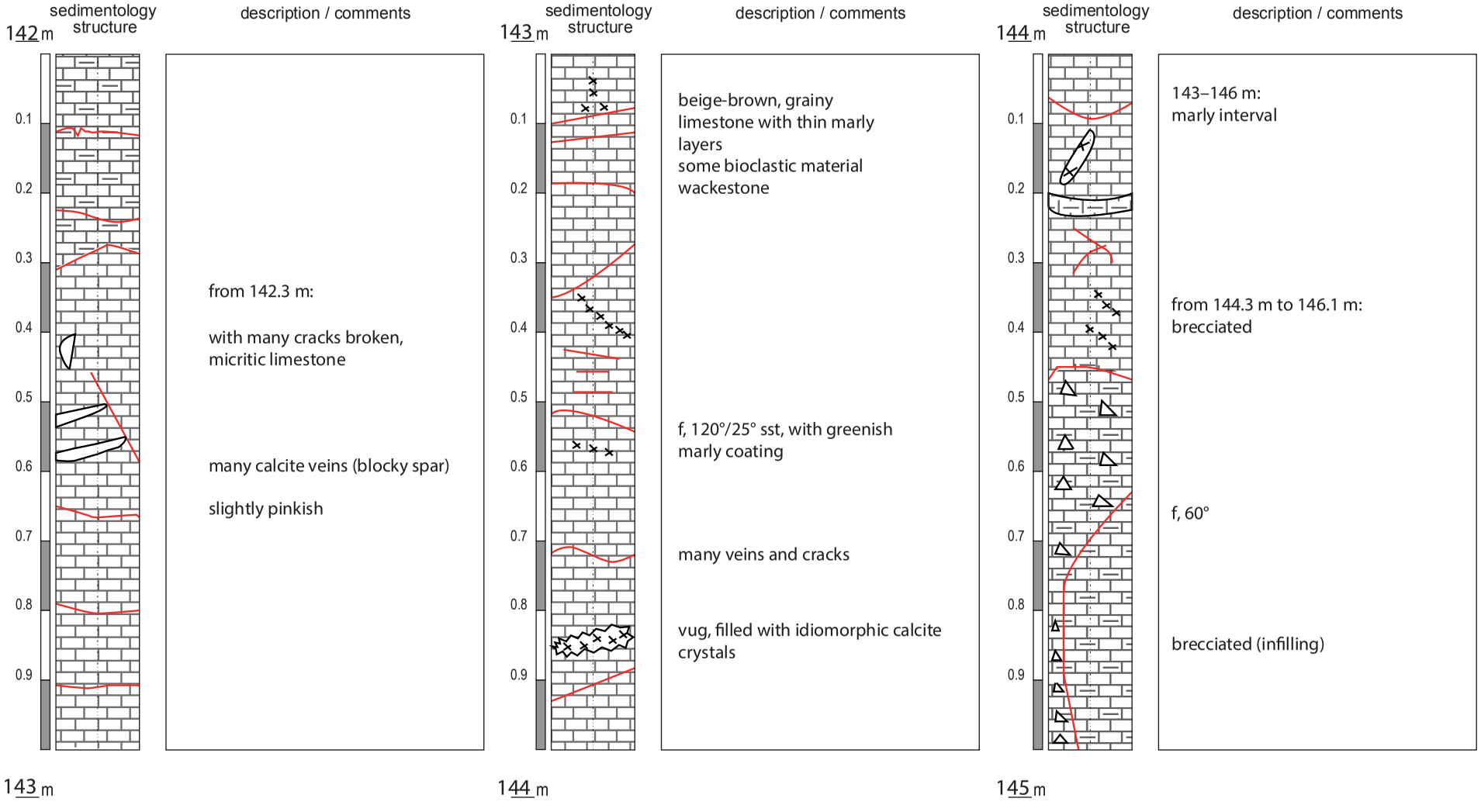

- Interpretation of facies/formation:

beige limestone, micritic

Reuchenette Formation

borehole BDS-5 drillcore mapping: jad page: 49

from 145 m to 148 m date of drillcore mapping: 28.06.2011 scale: 1 : 7.5

145 m	sedimentology structure	description / comments
0.1		
0.2		
0.3		
0.4		
0.5		
0.6		
0.7		
0.8		
0.9		
146 m		145–146 m: fault gouge fault breccia, strongly clayey with components up to 10 cm Ø, angular, matrix: sandy-clayey crumbly core normal fault or strike slip fault 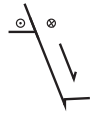

146 m	sedimentology structure	description / comments
0.1		120°/80° normal fault or strike slip fault
0.2		146–158 m: marble-like limestone with stylolites, reddish rims, micritic, porcelain-like slightly pinkish
0.3		micritic with bioclastic material in small layers, bivalves, echinoderms, oysters
0.4		
0.5		f, 22° with greenish clay coating
0.6		
0.7		artificiel discontinuites in cm-range with greenish clay coating no fossils visible
0.8		
0.9		
147 m		

147 m	sedimentology structure	description / comments
0.1		
0.2		
0.3		reddish, closed rims broken, with stylolites and thin greenish coating
0.4		
0.5		
0.6		
0.7		
0.8		
0.9		some shalls of bivalves recognizable
148 m		

- Interpretation of facies/formation:

–146.0 m:	Reuchenette Formation, Kimmeridgian
from 146.0 m on:	Courgenay Formation, Oxfordian

borehole BDS-5 drillcore mapping: jad page: 50

from 148 m to 151 m date of drillcore mapping: 28.06.2011 scale: 1 : 7.5

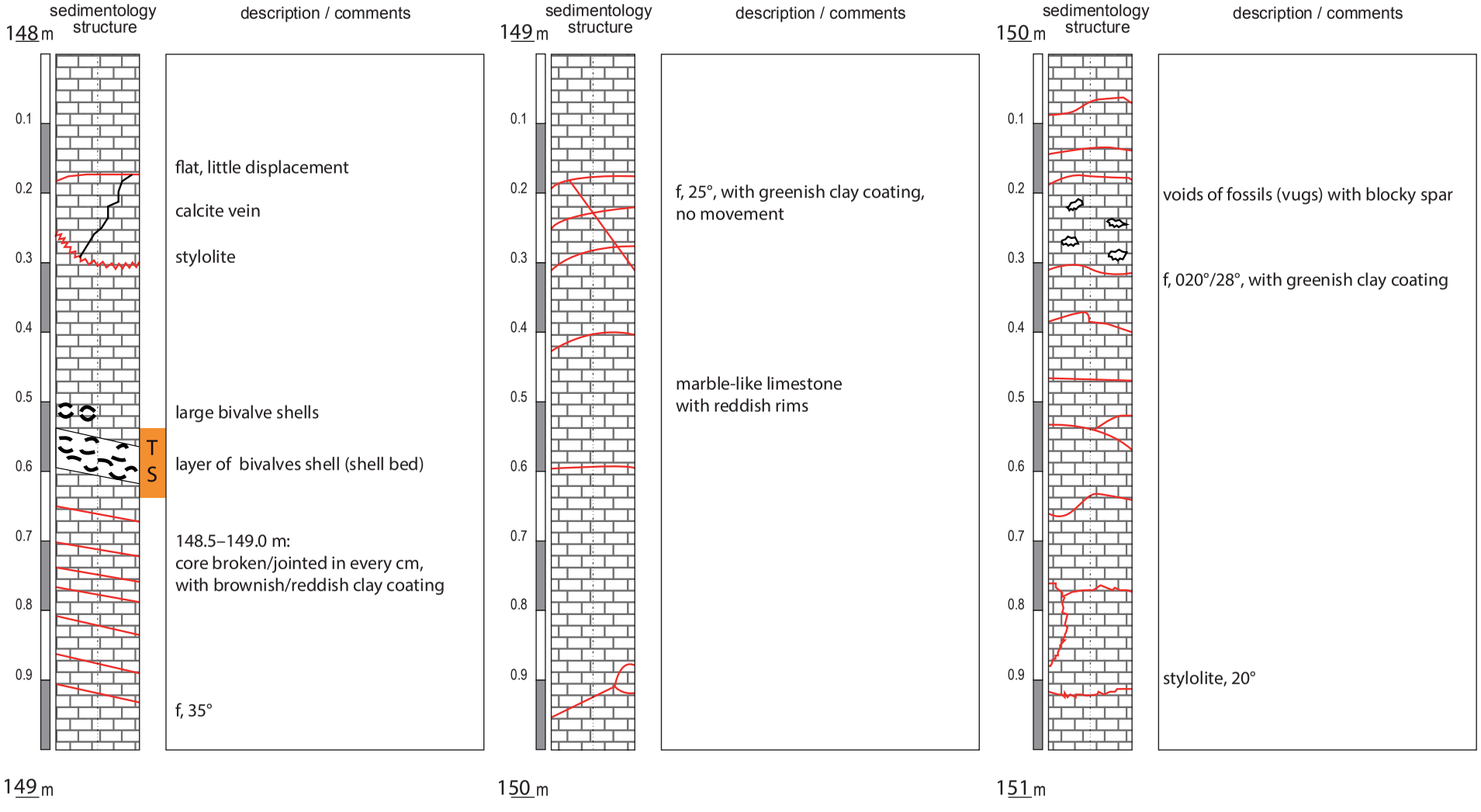

- Interpretation of facies/formation:

Courgenay Formation

borehole BDS-5 drillcore mapping: jad page: 51

from 151 m to 154 m date of drillcore mapping: 28.06.2011 scale: 1 : 7.5

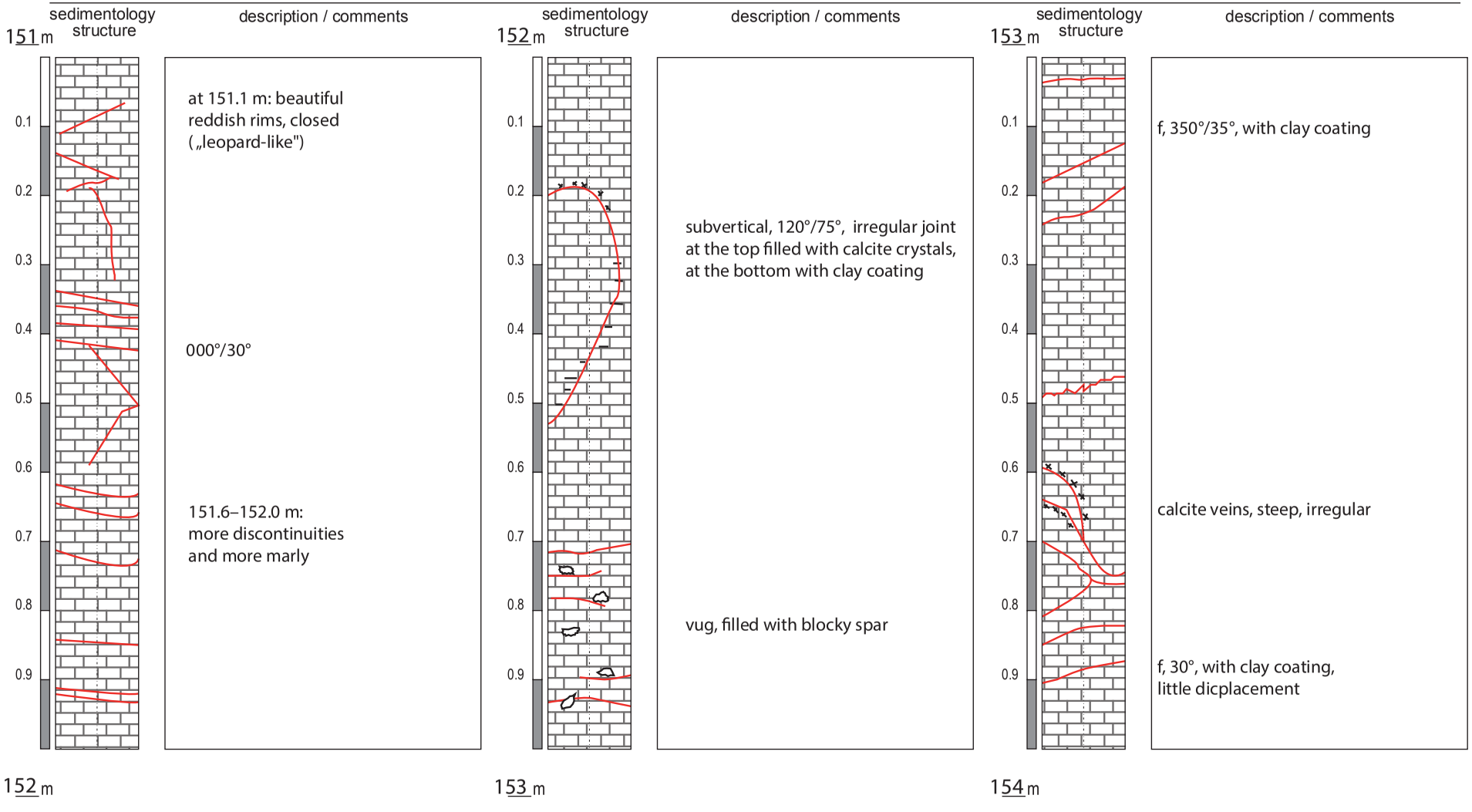

- Interpretation of facies/formation:

micritic limestone

Courgenay Formation

borehole BDS-5 drillcore mapping: jad page: 52

from 154 m to 157 m date of drillcore mapping: 28.06.2011 scale: 1 : 7.5

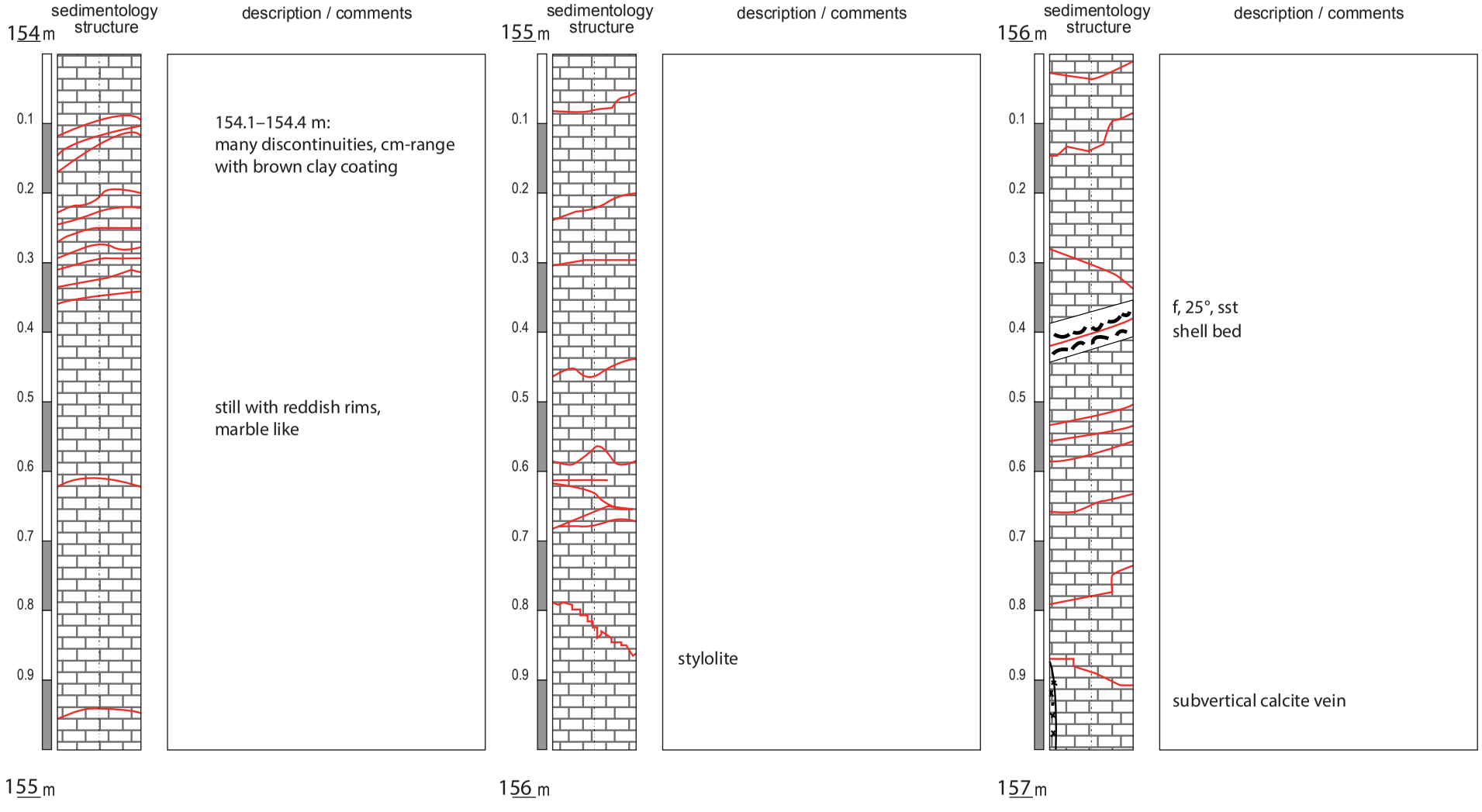

- Interpretation of facies/formation:

reddish-beige micritic limestone

Courgenay Formation

borehole BDS-5 drillcore mapping: jad page: 53

from 157 m to 160 m date of drillcore mapping: 28.06.2011 scale: 1 : 7.5

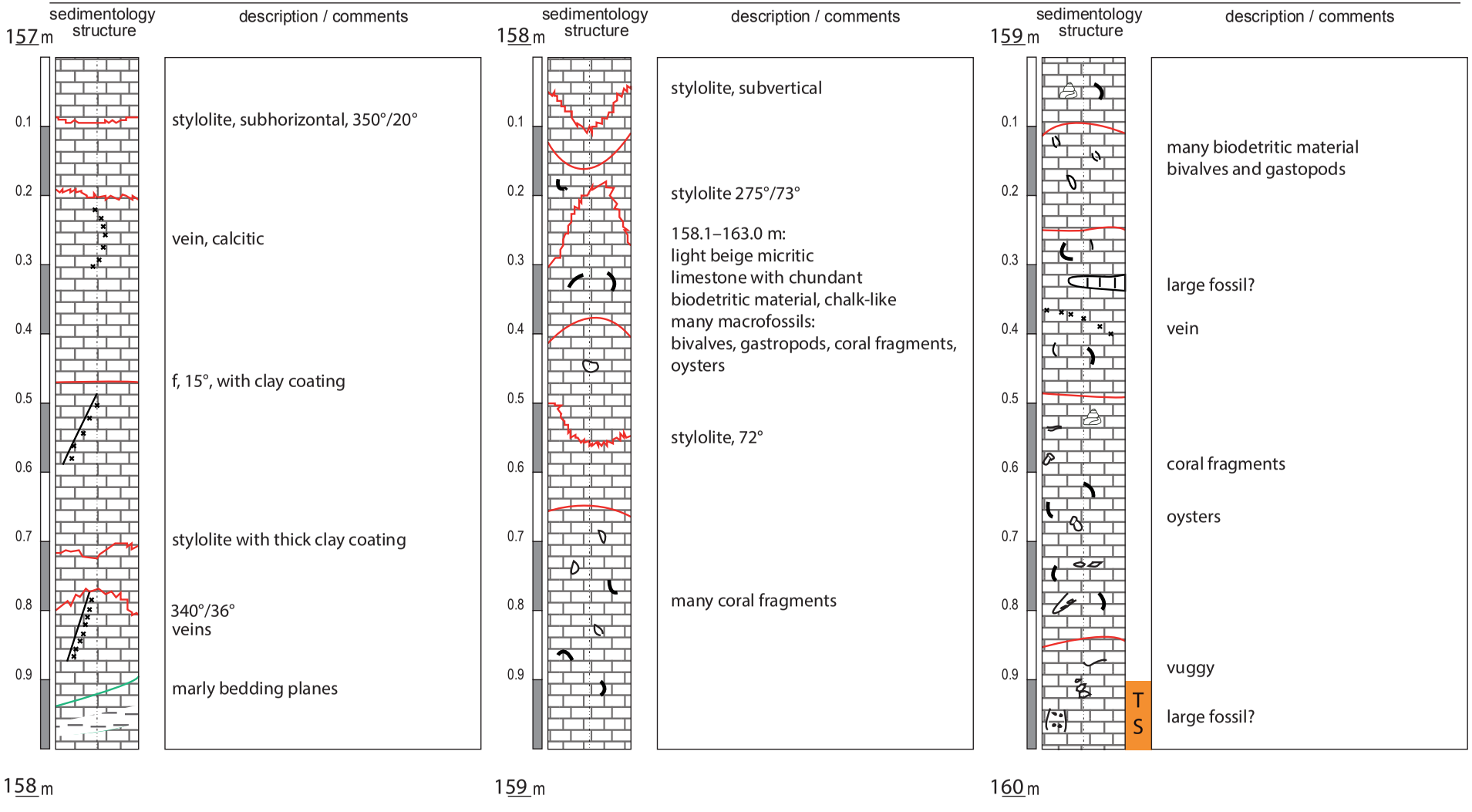

- Interpretation of facies/formation:

beige micritic limestone with a lot of bioclastic material

Courgenay Formation

borehole BDS-5 drillcore mapping: jad page: 54

from 160 m to 163 m date of drillcore mapping: 28.06.2011 scale: 1 : 7.5

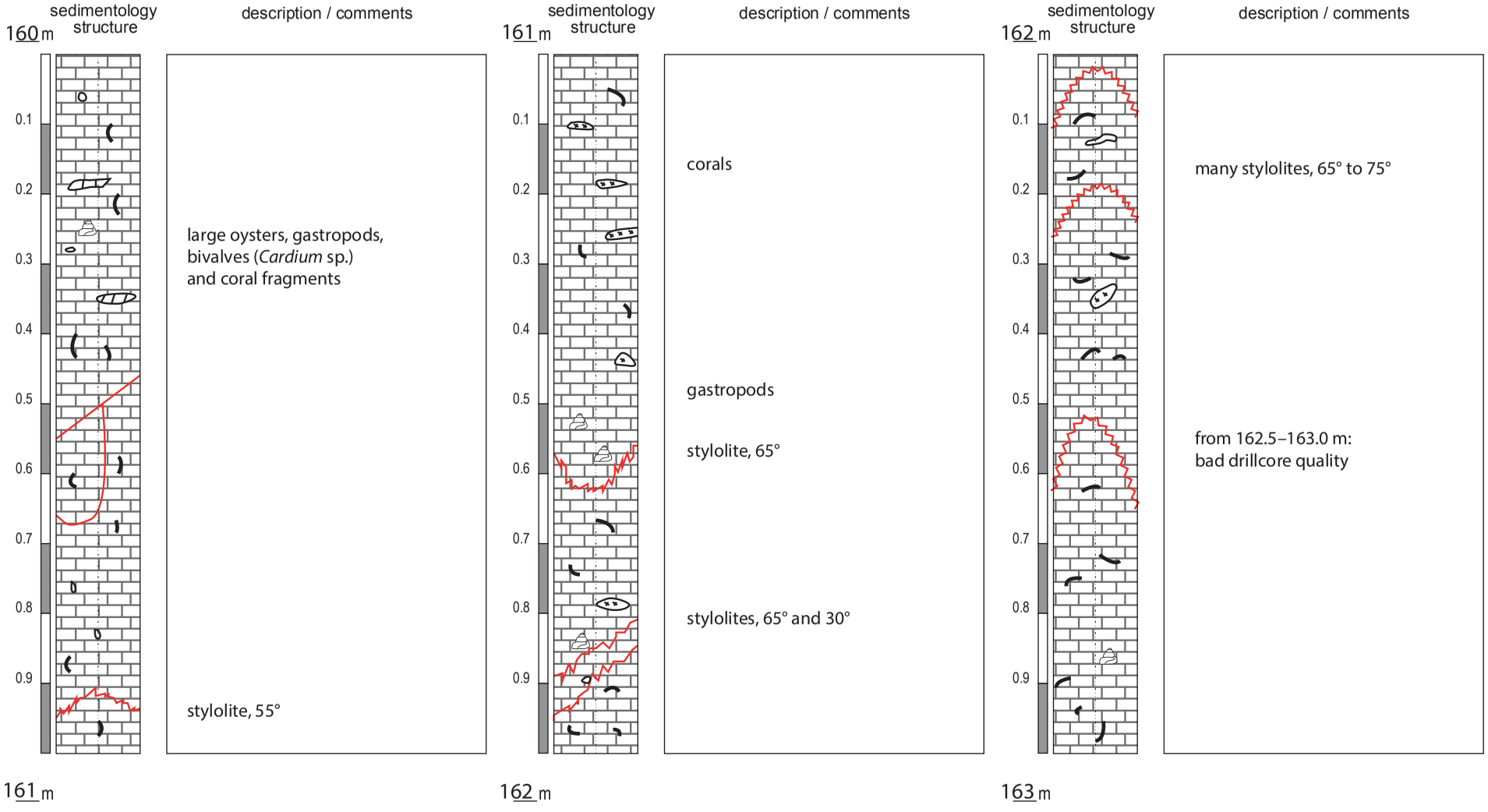

- Interpretation of facies/formation:

beige micritic limestone with lots of macroscopic fossils

Courgenay Formation

borehole BDS-5 drillcore mapping: jad page: 55

from 163 m to 166 m date of drillcore mapping: 28.06.2011 scale: 1 : 7.5

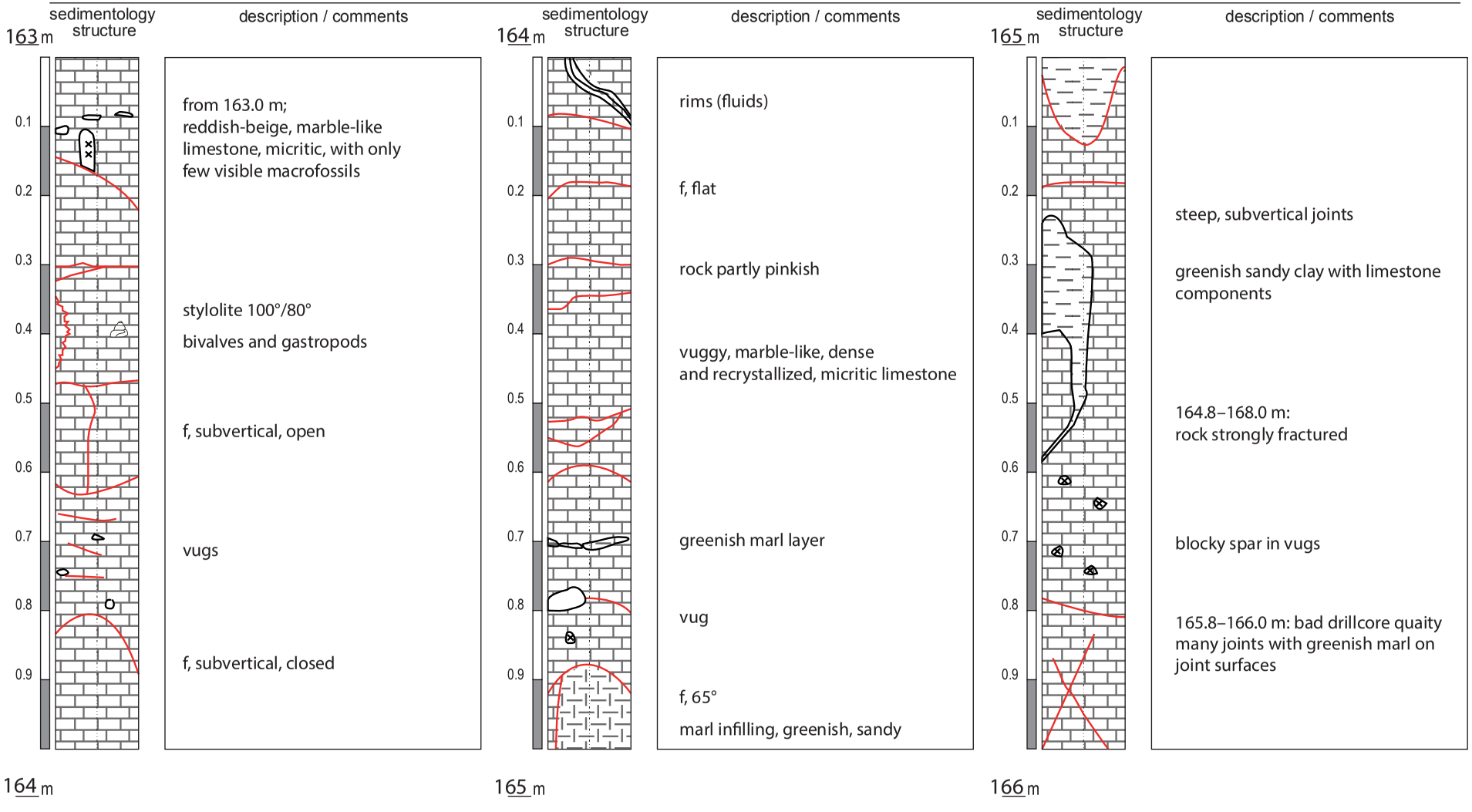

- Interpretation of facies/formation:

reddish-beige micritic limestone

Courgenay Formation

borehole BDS-5 drillcore mapping: jad page: 56

from 166 m to 169 m date of drillcore mapping: 28.06.2011 scale: 1 : 7.5

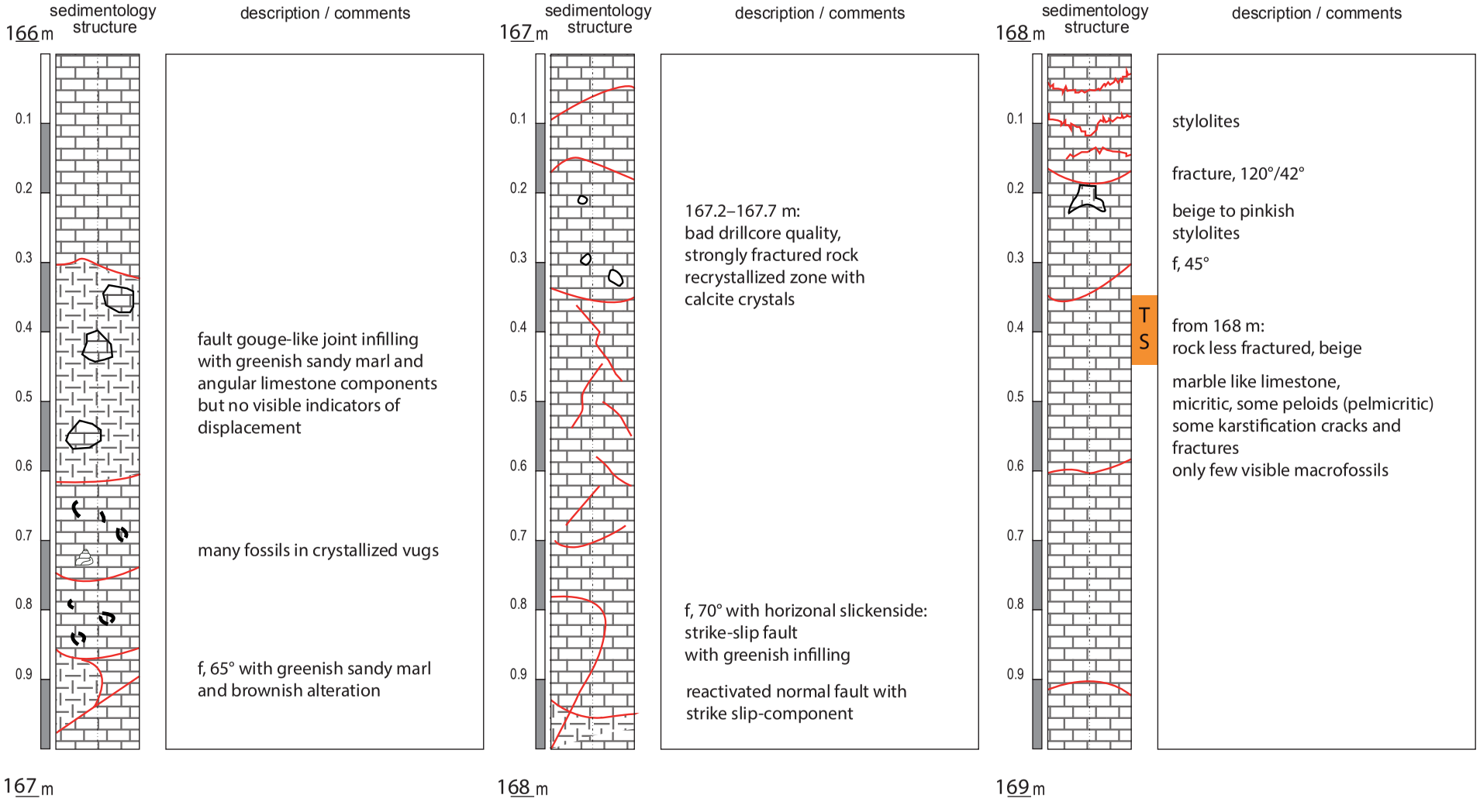

- Interpretation of facies/formation:

beige micritic limestone

Courgenay Formation

borehole BDS-5 drillcore mapping: jad page: 57

from 169 m to 172 m date of drillcore mapping: 28.06.2011 scale: 1 : 7.5

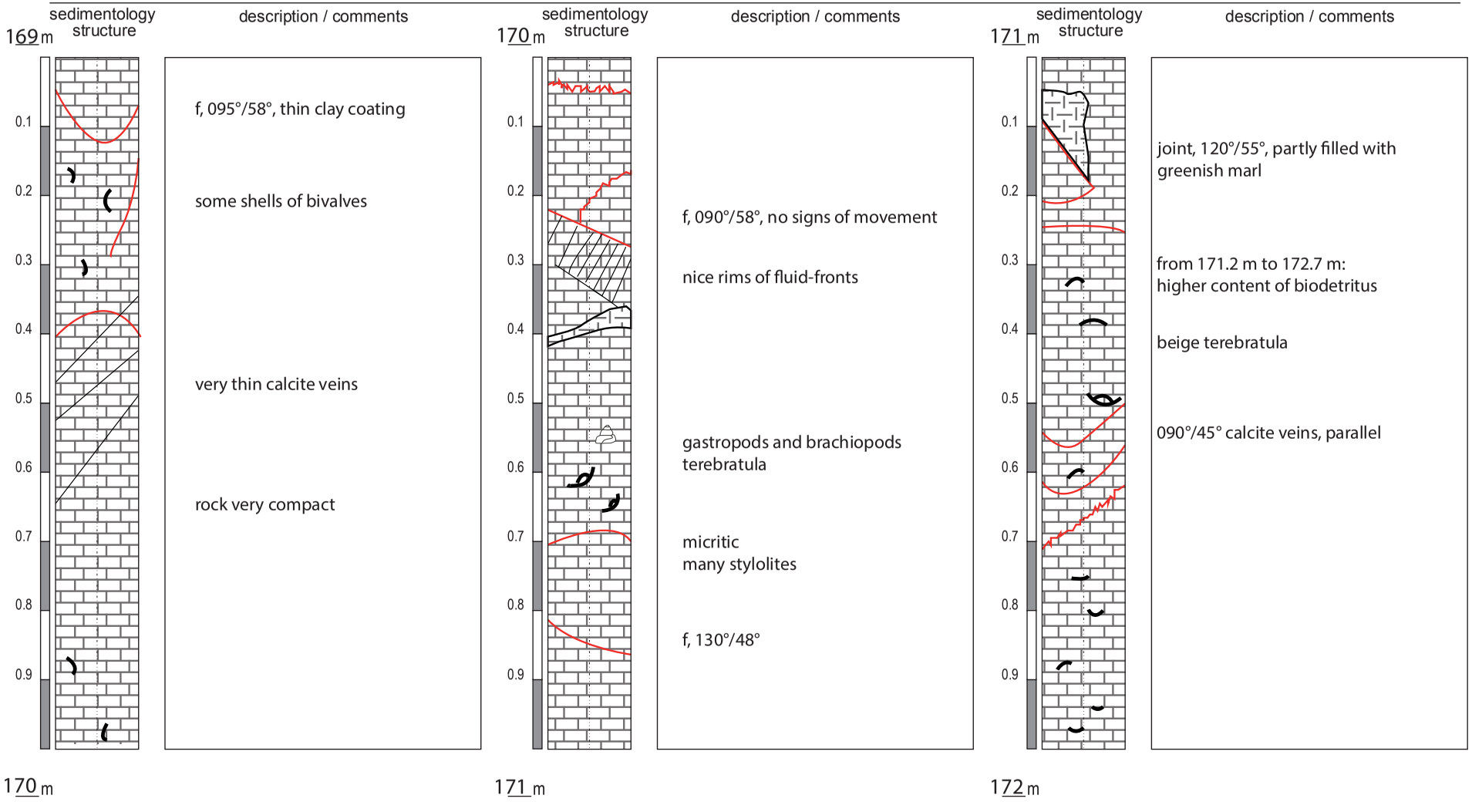

- Interpretation of facies/formation:

beige micritic limestone

Courgenay Formation

borehole BDS-5 drillcore mapping: jad page: 58

from 172 m to 175 m date of drillcore mapping: 28.06.2011 scale: 1 : 7.5

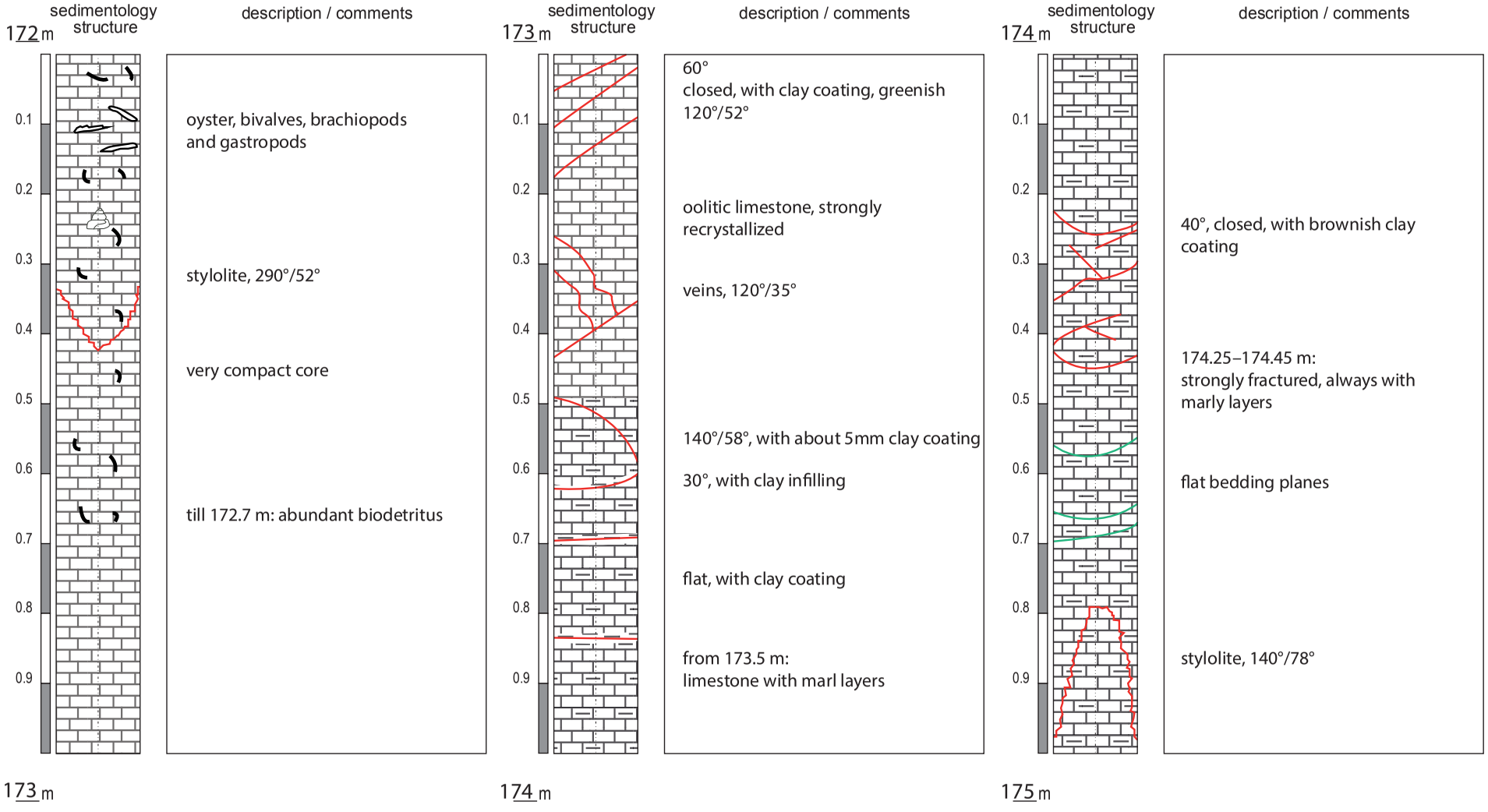

- Interpretation of facies/formation:

beige micritic limestone with some thin marly interlayers

Courgenay Formation

borehole BDS-5 drillcore mapping: jad page: 59

from 175 m to 178 m date of drillcore mapping: 29.06.2011 scale: 1 : 7.5

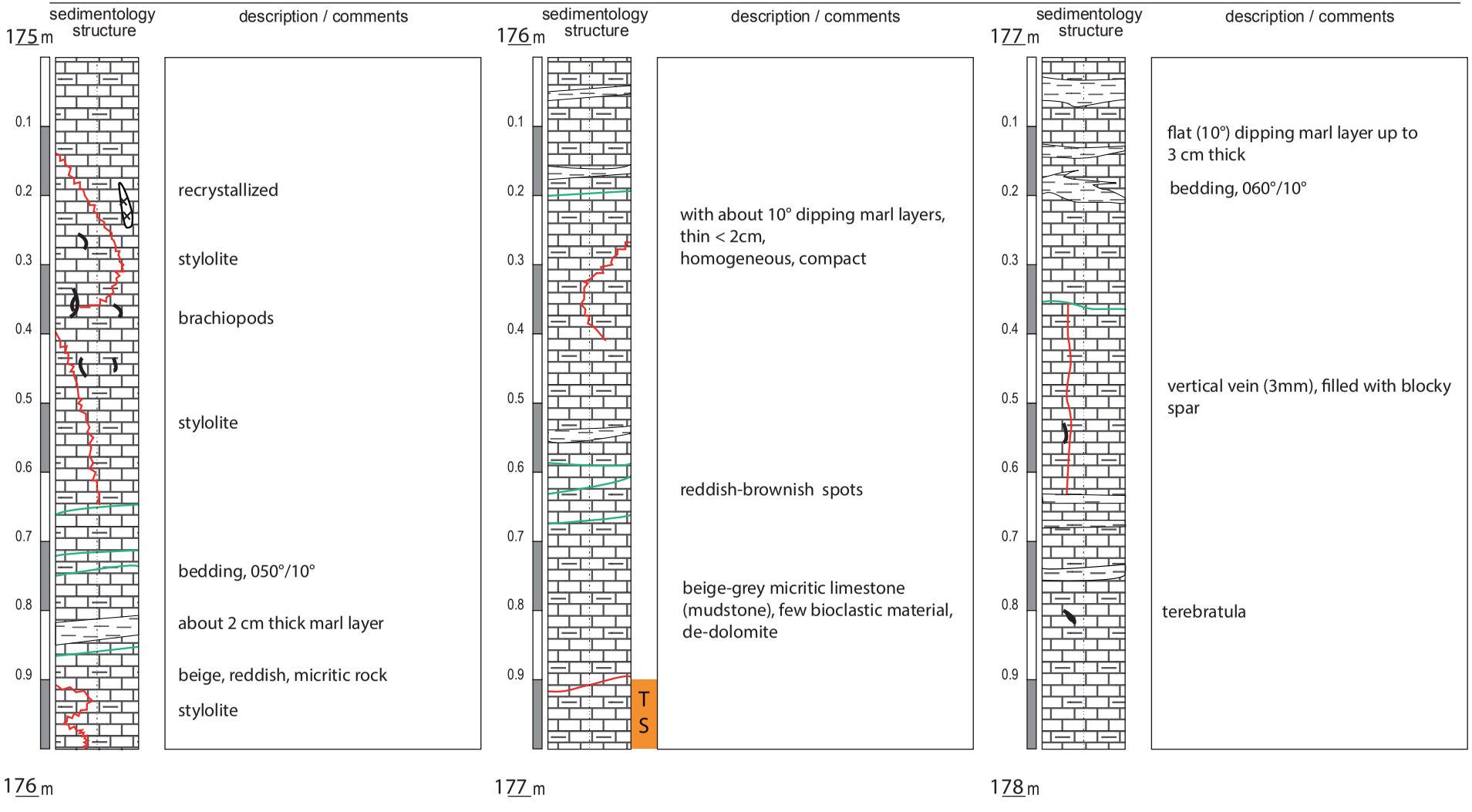

- Interpretation of facies/formation:

Courgenay Formation

borehole BDS-5 drillcore mapping: jad page: 60

from 178 m to 181 m date of drillcore mapping: 29.06.2011 scale: 1 : 7.5

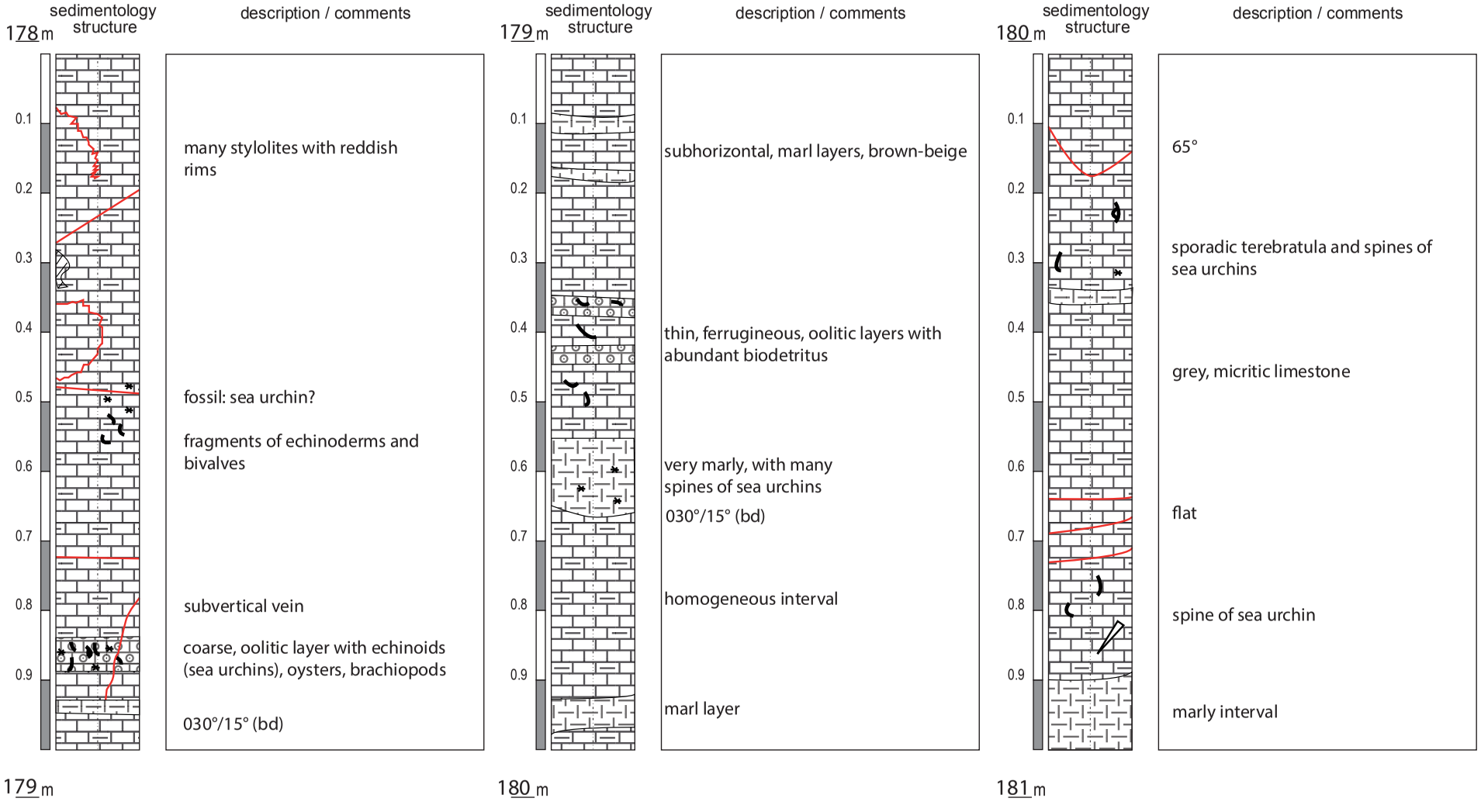

- Interpretation of facies/formation:

Courgenay Formation

borehole BDS-5 drillcore mapping: jad page: 61

from 181 m to 184 m date of drillcore mapping: 29.06.2011 scale: 1 : 7.5

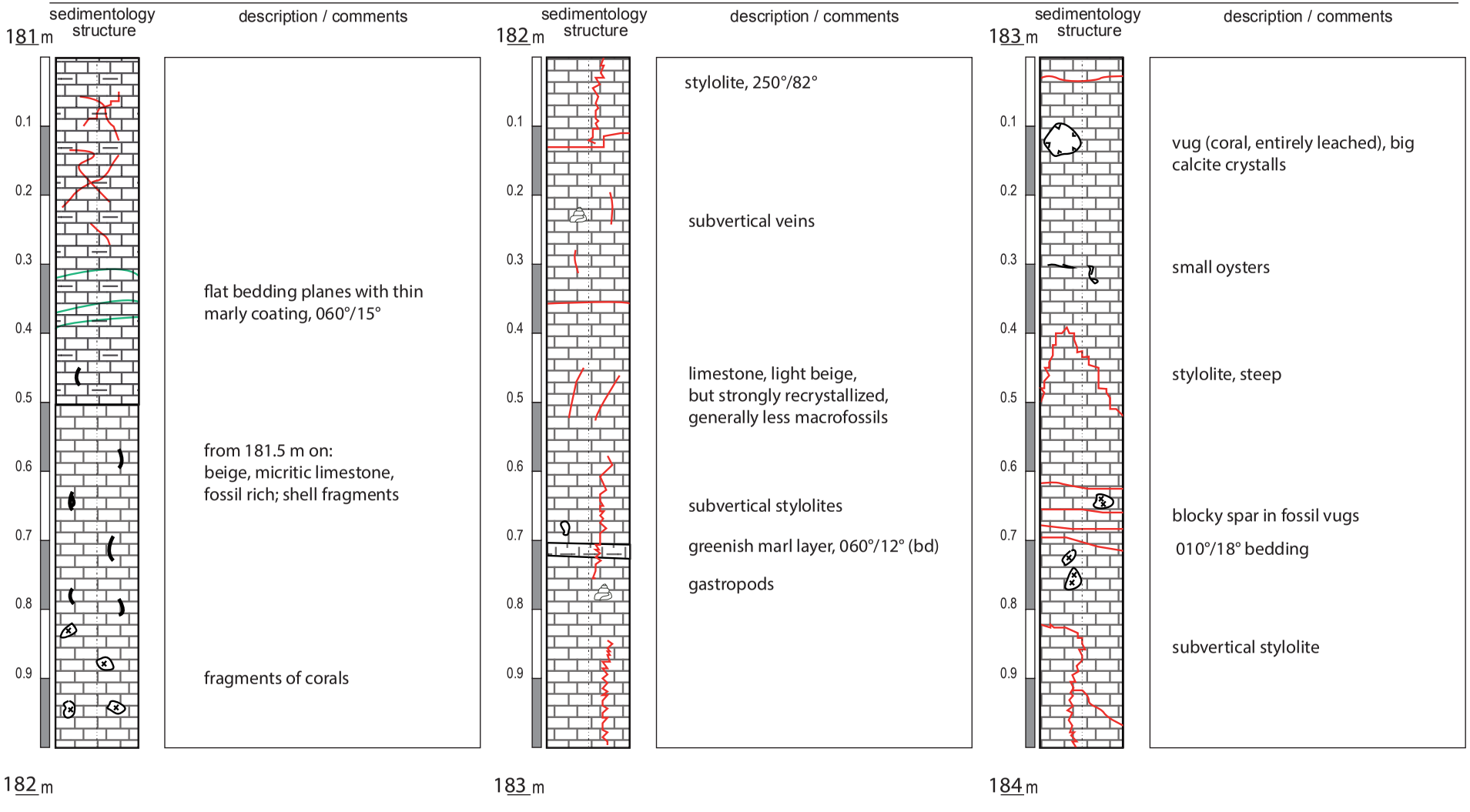

- Interpretation of facies/formation:

light beige limestone

Courgenay Formation

borehole BDS-5 drillcore mapping: jad page: 62

from 184 m to 187 m date of drillcore mapping: 29.06.2011 scale: 1 : 7.5

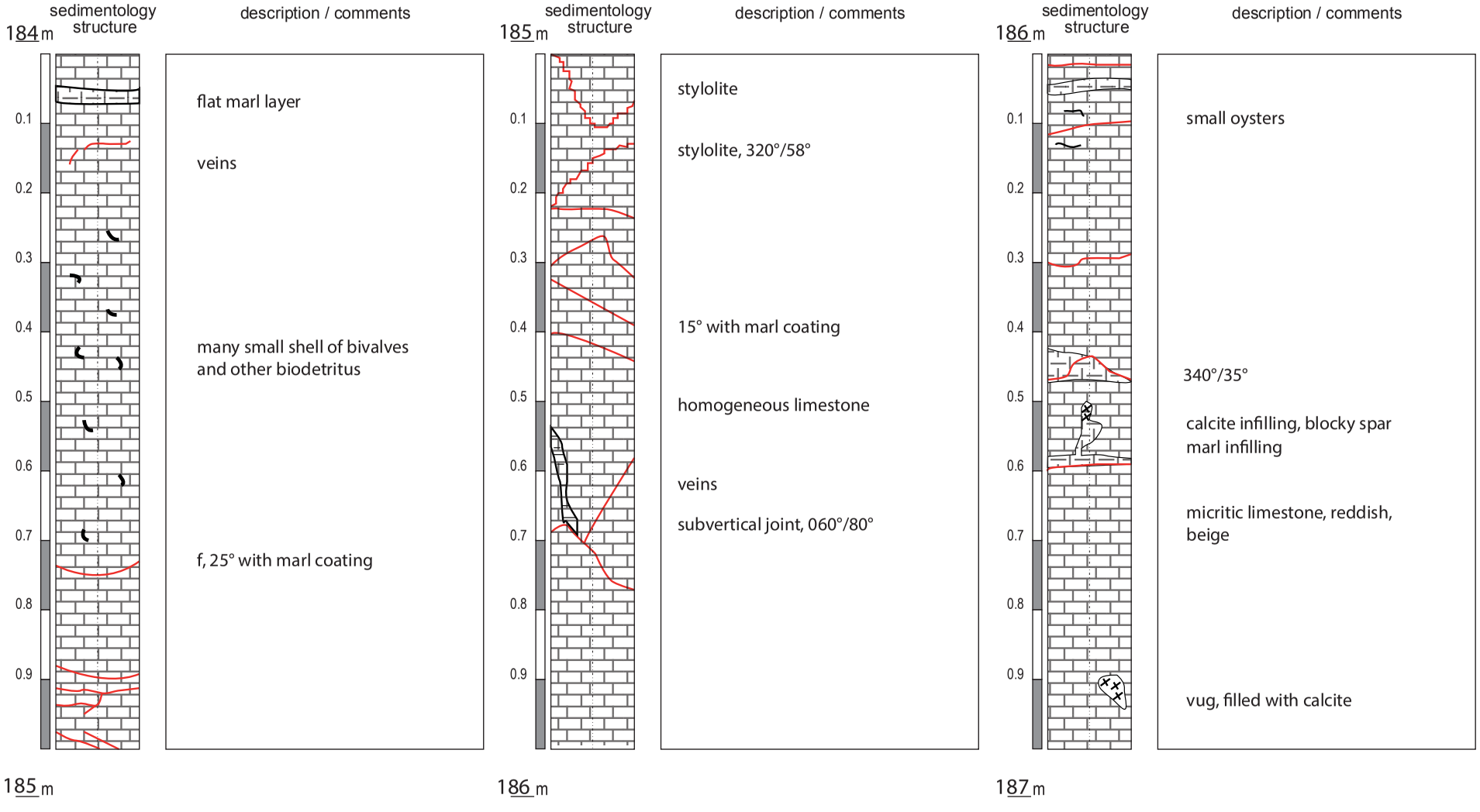

- Interpretation of facies/formation:

Courgenay Formation

borehole BDS-5 drillcore mapping: jad page: 63

from 187 m to 190 m date of drillcore mapping: 01.07.2011 scale: 1 : 7.5

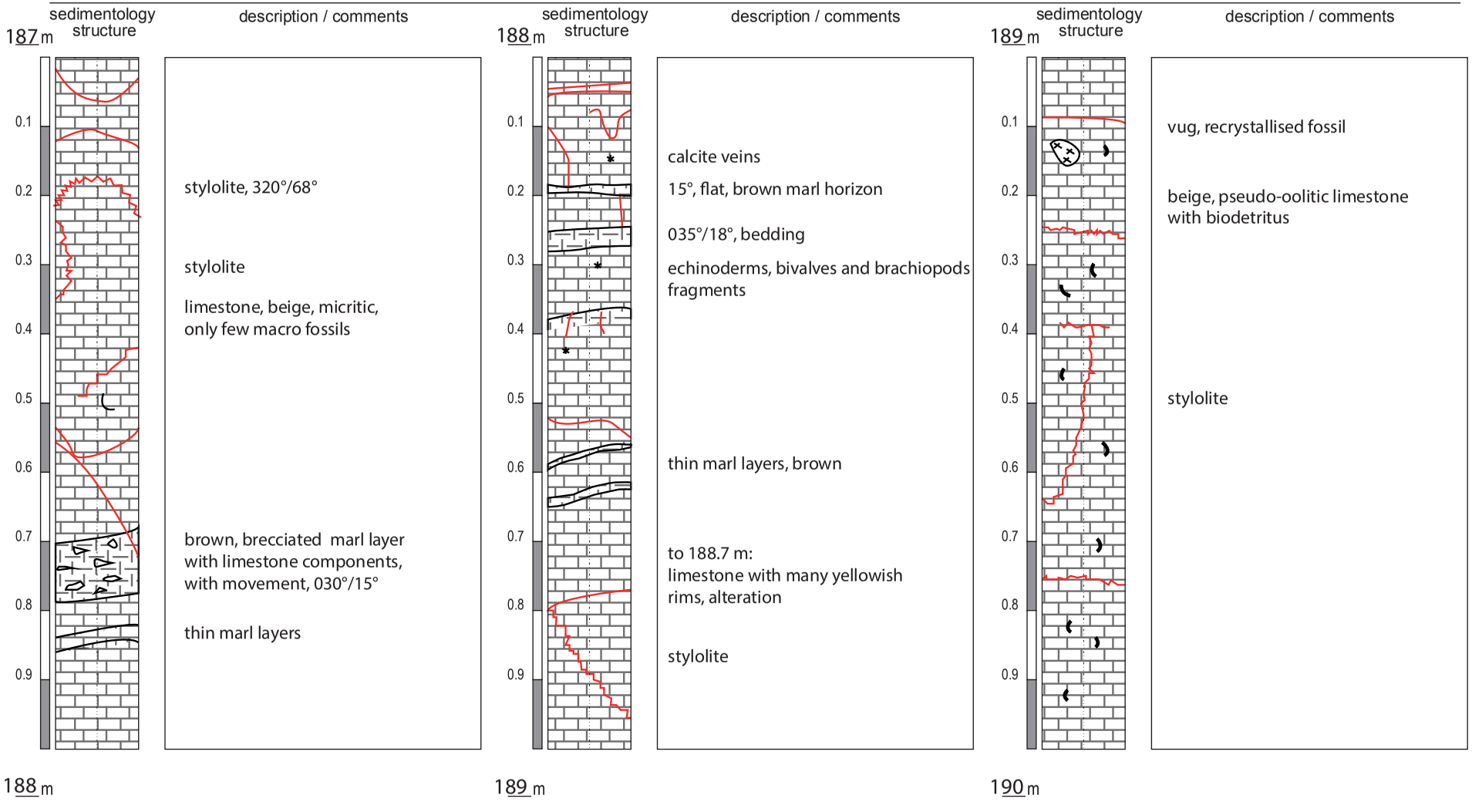

- Interpretation of facies/formation:

Courgenay Formation

borehole BDS-5 drillcore mapping: jad page: 64

from 190 m to 193 m date of drillcore mapping: 01.07.2011 scale: 1 : 7.5

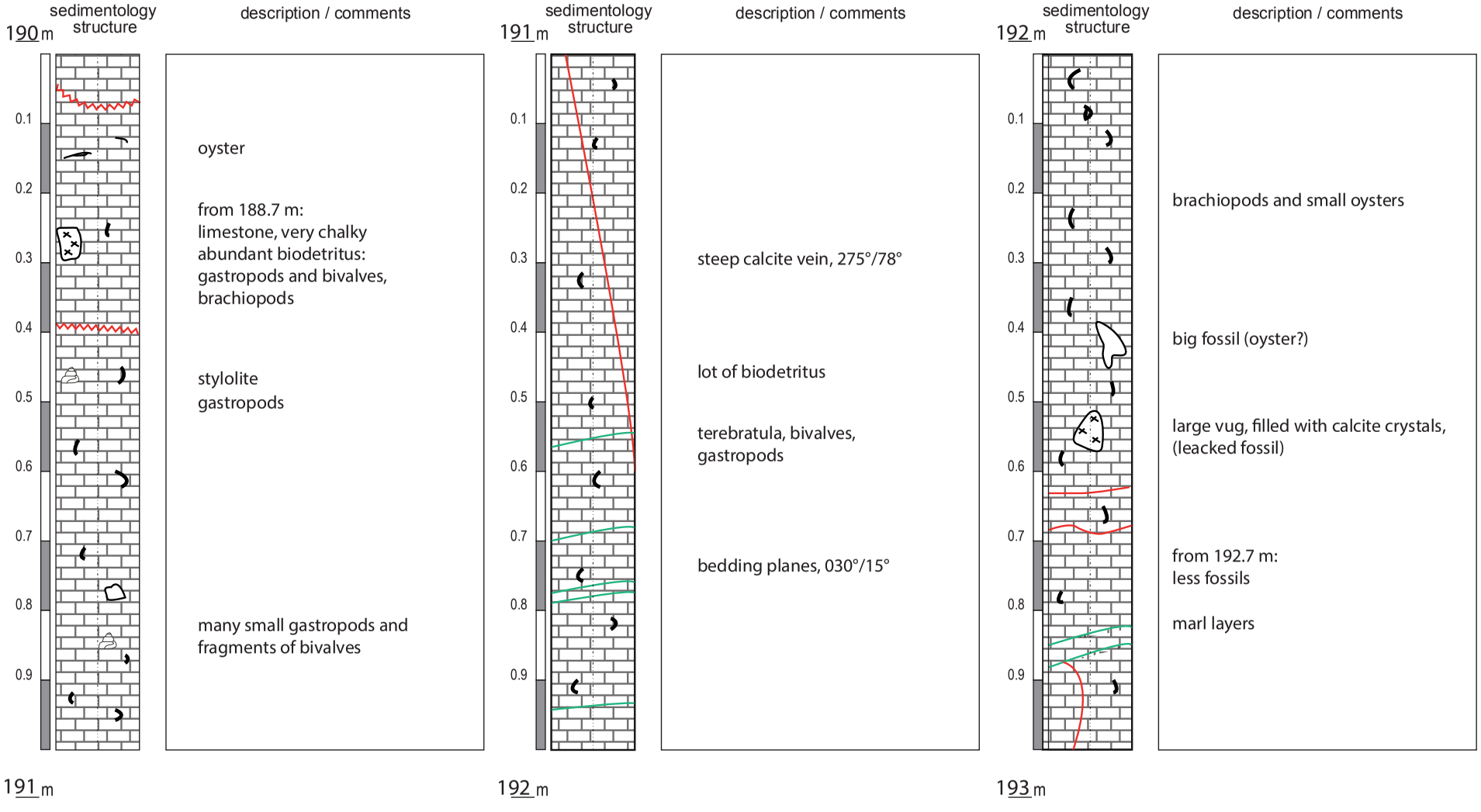

- Interpretation of facies/formation:

–192.85 m: Courgenay Formation, Oxfordian
from 192.85 m: Vellerat Formation, Oxfordian

borehole BDS-5 drillcore mapping: jad page: 65

from 193 m to 196 m date of drillcore mapping: 01.07.2011 scale: 1 : 7.5

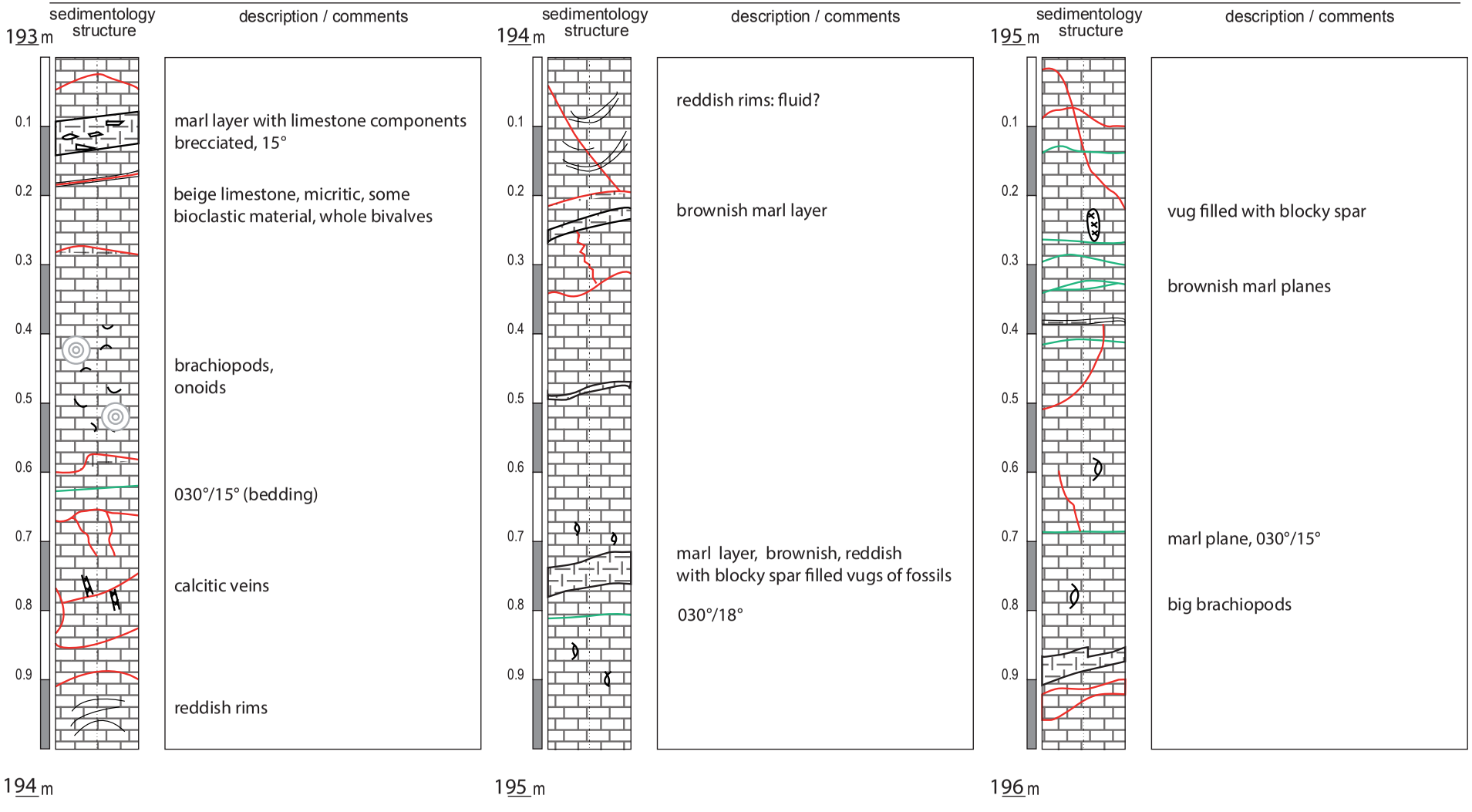

- Interpretation of facies/formation:

beige micritic limestone with some thin marly layers

Vellerat Formation

borehole BDS-5 drillcore mapping: jad page: 66

from 196 m to 199 m date of drillcore mapping: 01.07.2011 scale: 1 : 7.5

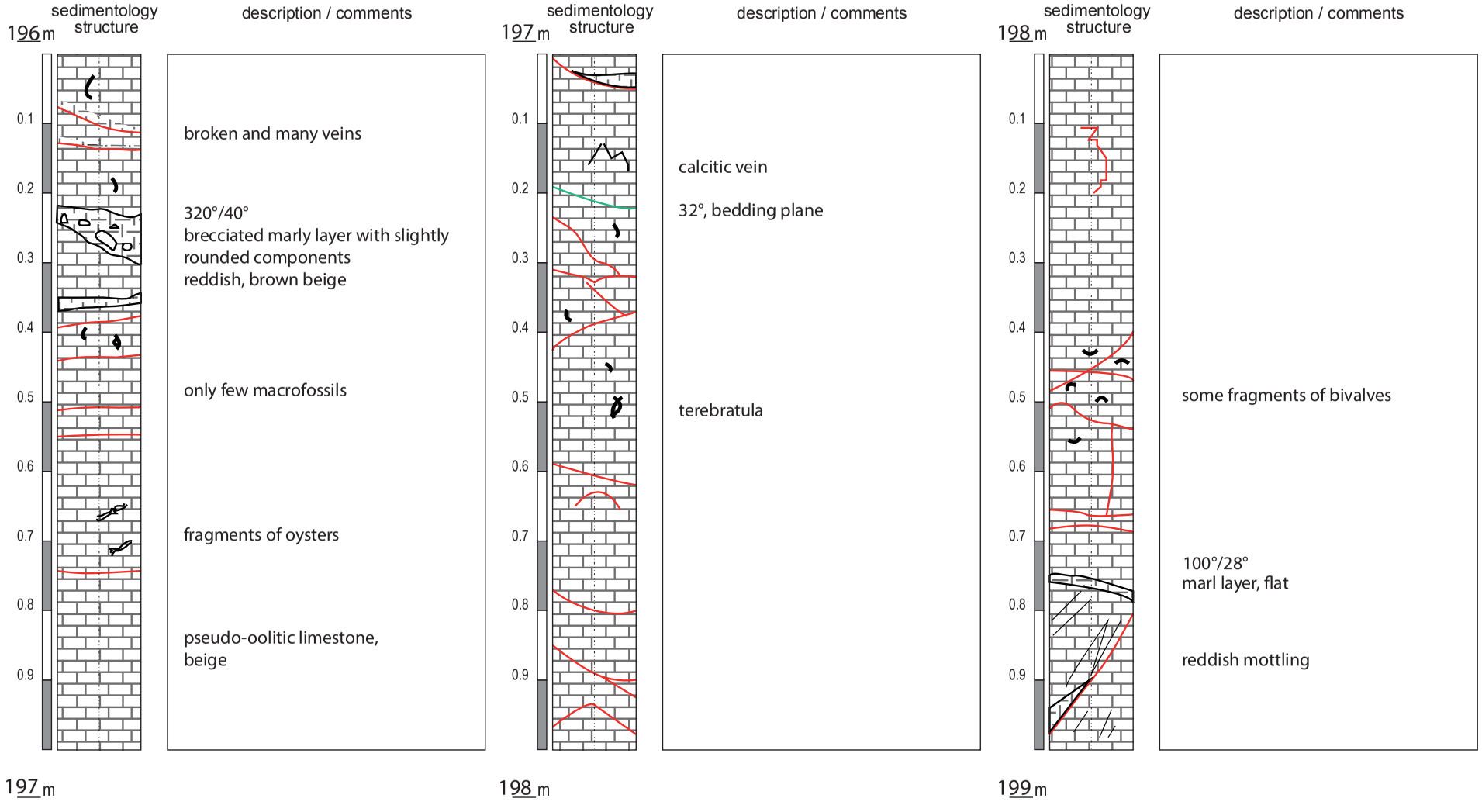

- Interpretation of facies/formation:

beige micritic limestone with some thin marly layers

Vellerat Formation

borehole BDS-5 drillcore mapping: jad page: 67

from 199 m to 202 m date of drillcore mapping: 01.07.2011 scale: 1 : 7.5

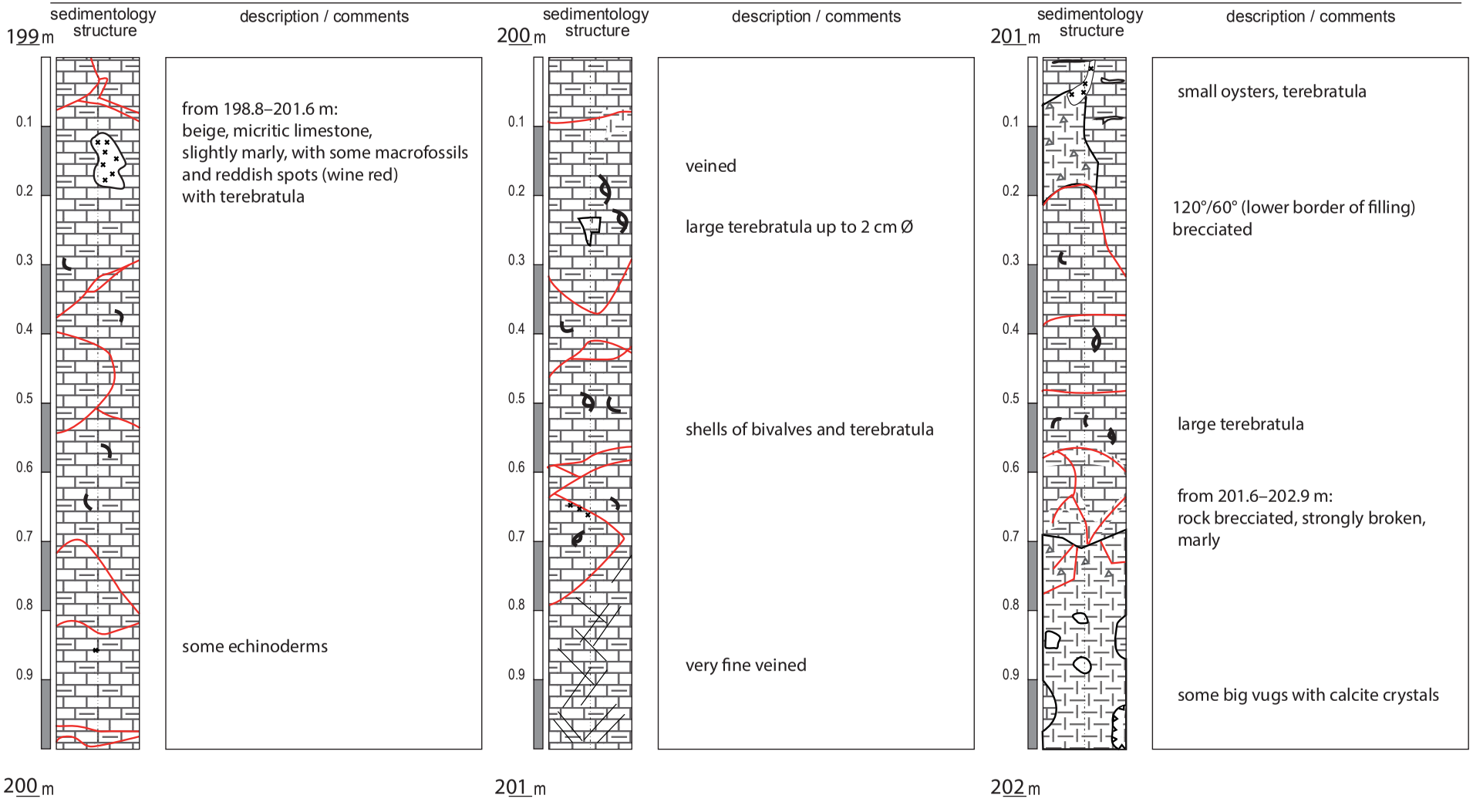

- Interpretation of facies/formation:

beige, slightly marly, micritic limestone

Vellerat Formation

borehole BDS-5 drillcore mapping: jad page: 68

from 202 m to 205 m date of drillcore mapping: 01.07.2011 scale: 1 : 7.5

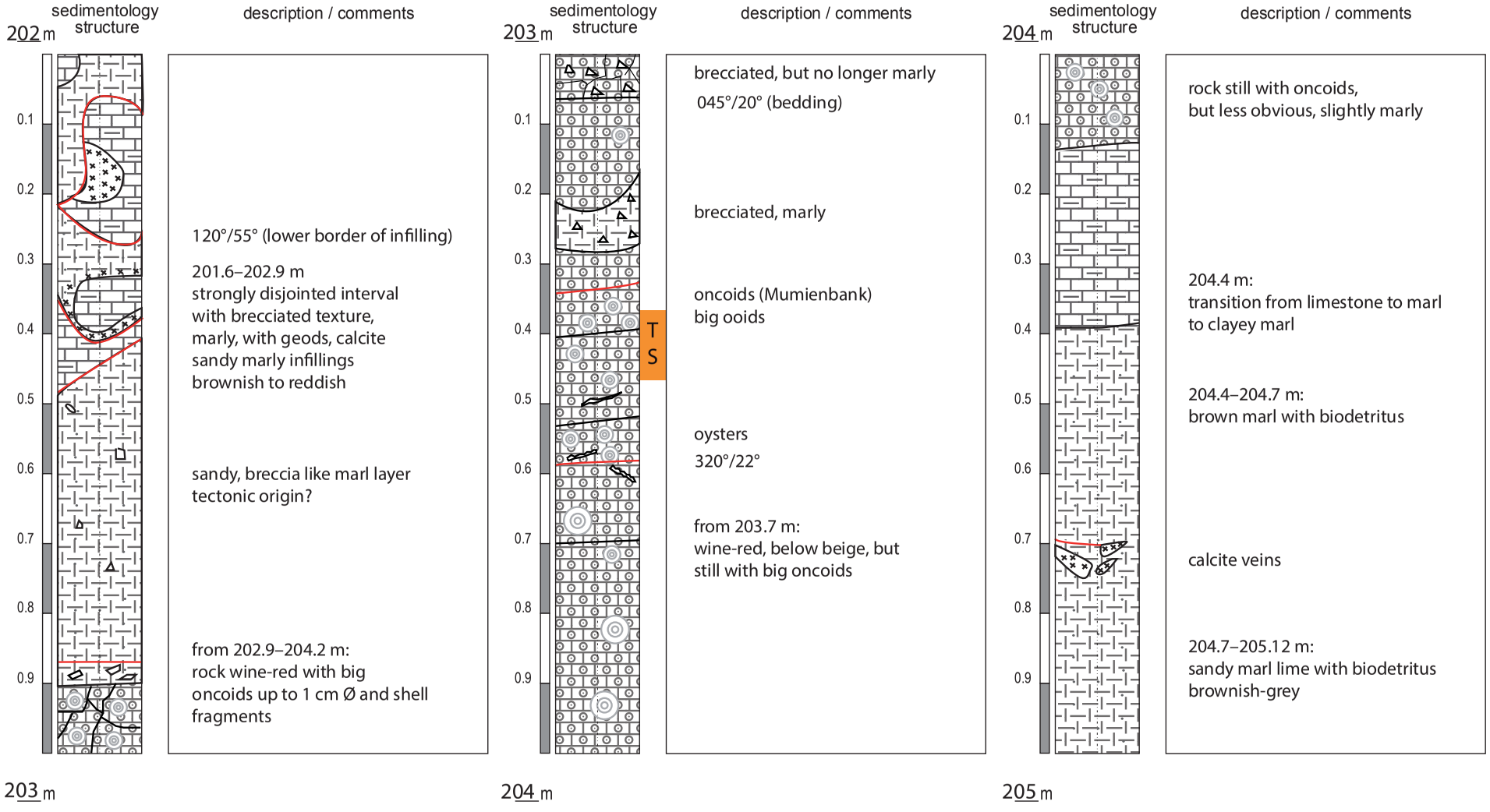

- Interpretation of facies/formation:

202.9–204.2 m: limestone beige with many oncoids (Hauptmumienbank Member)

Vellerat Formation

borehole BDS-5 drillcore mapping: jad page: 69

from 205 m to 208 m date of drillcore mapping: 01.07.2011 scale: 1 : 7.5

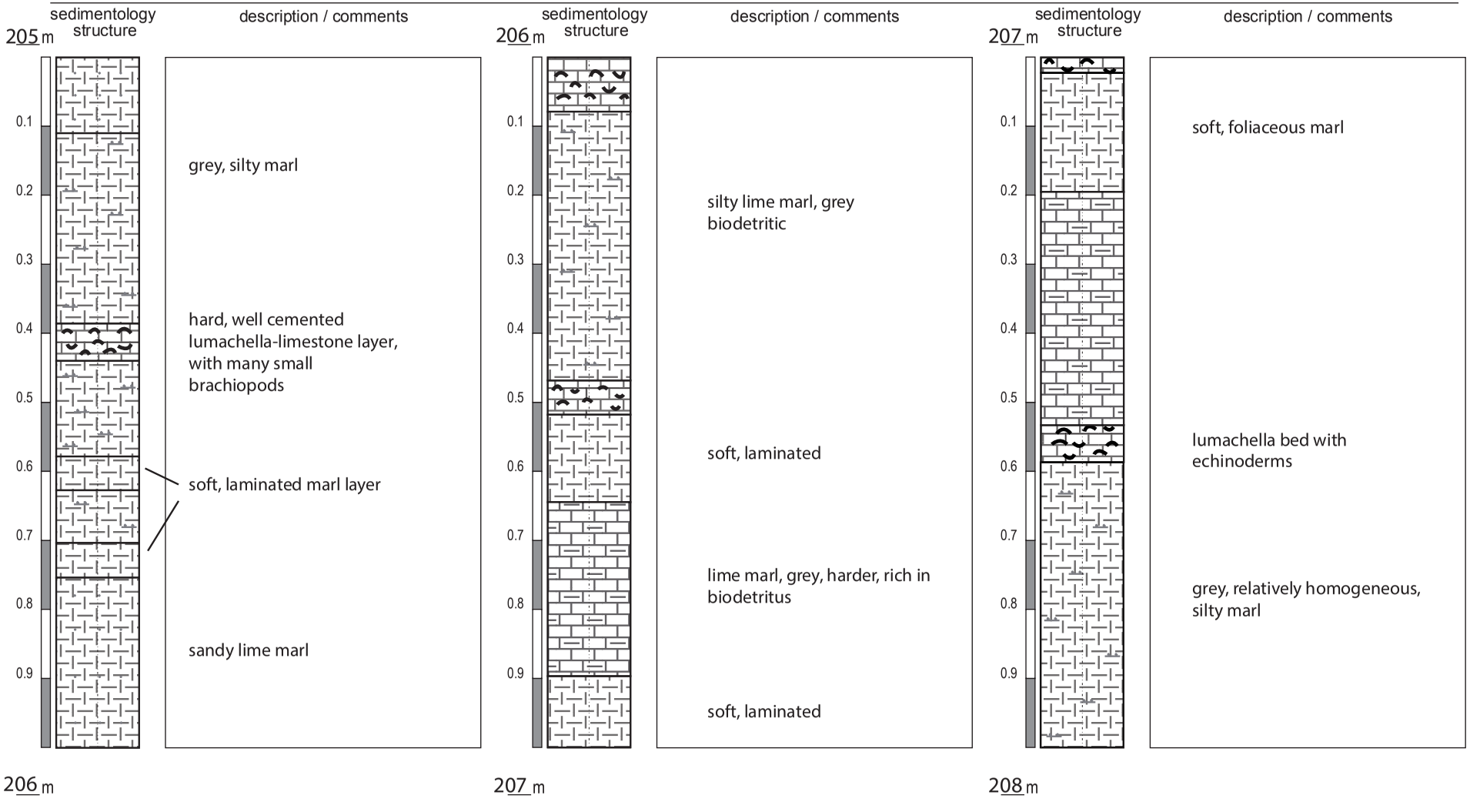

- Interpretation of facies/formation:

204.2–208.7 m: intercalation of grex marls and thin calcareous lumachella beds

Vellerat Formation

borehole BDS-5 drillcore mapping: jad page: 70

from 208 m to 211 m date of drillcore mapping: 04.07.2011 scale: 1 : 7.5

208 m

sedimentology structure

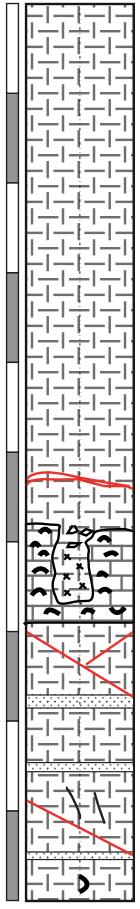

description / comments

grey lime marl, homogeneous

shear zone

bioturbated lumachella bed, crossed by big (sedimentary) dyke, upper part brecciated

f, sst 55°
sandy layers
veins

f, sst 45°
beige, grey lime marl

209 m

sedimentology structure

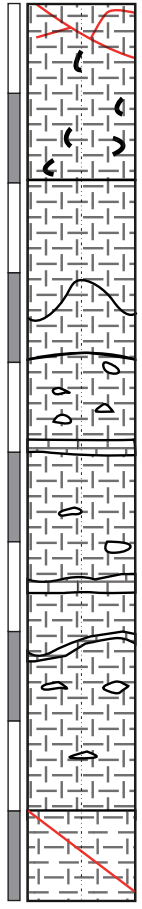

description / comments

35° steep calcite vein with breccia like parts

to 209.2 m:
beige, biodetritic clay marl

beige, grey, homogeneous lime marl

calcite vein

from 209.4 m:
beige, grey nodular marl

208.7–210.6 m: beige grey lime marl with sandy layers, nodular, with oysters and gastropods

f, sst, 55°

210 m

sedimentology structure

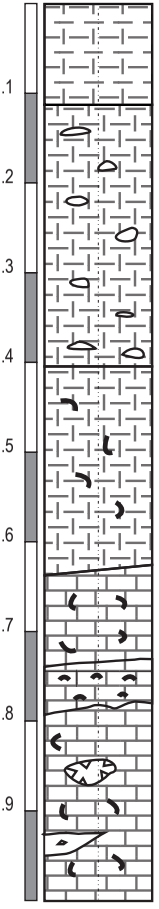

description / comments

grey clay marl, soft, with biodetritus

grey, limy, nodular marl with biodetritus (bioturbation)

from 210.4 m:
beige, brown lime marl

then partly limonitic, lime marl bioturbated

from 210.7–211.3 m:
limestone, limonitic

with small oysters

large vug (leacked fossil) with a lot of biodetritic material

209 m 210 m 211 m

- Interpretation of facies/formation:

beige grey lime marl

Vellerat Formation

borehole BDS-5 drillcore mapping: jad page: 71

from 211 m to 214 m date of drillcore mapping: 04.07.2011 scale: 1 : 7.5

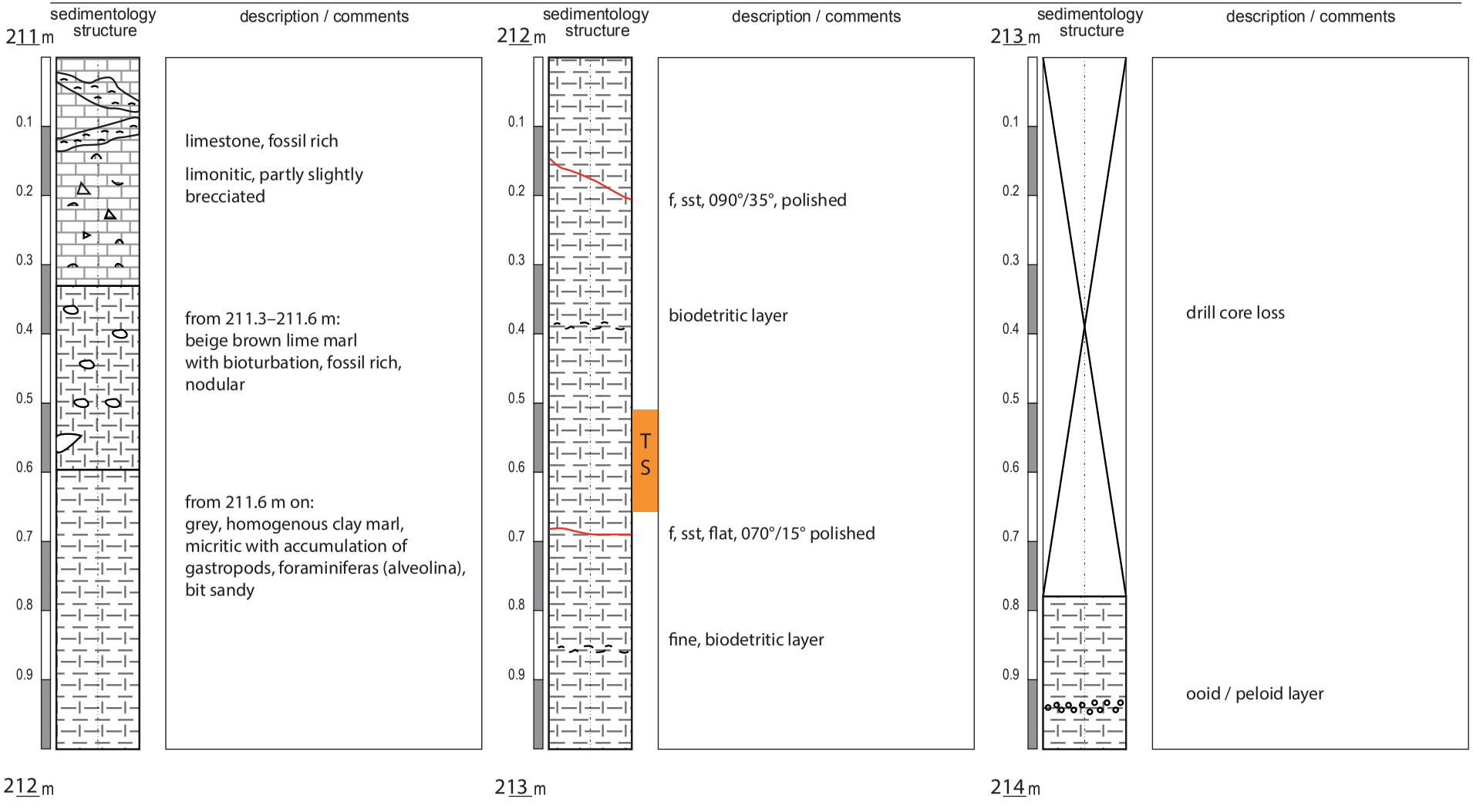

- Interpretation of facies/formation:

grey clay marl with gastropods

Vellerat Formation

borehole BDS-5 drillcore mapping: jad page: 72

from 214 m to 216 m date of drillcore mapping: 04.07.2011 scale: 1 : 7.5

214 m	sedimentology structure	description / comments
0.1	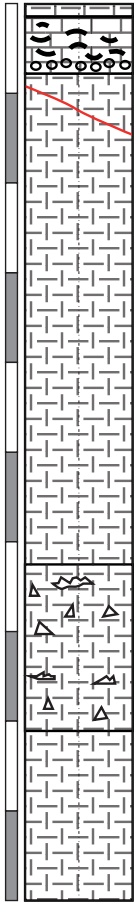	lumachella bed, strongly cemented and very hard, ooid layer at the base
0.2		f, sst
0.3		
0.4		beige brown lime marl, relatively homogeneous, brecciated from 214.65–214.8 m
0.5		
0.6		
0.7		with oysters and shells of bivalves
0.8		
0.9		
215 m		

215 m	sedimentology structure	description / comments
0.1	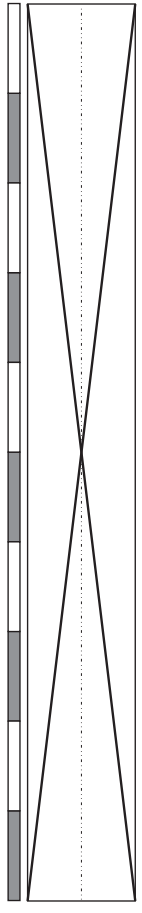	
0.2		drill core loss (almost 100%)
0.3		
0.4		till 216 m: beige, brown lime marl, relatively homogeneous
0.5		
0.6		
0.7		
0.8		
0.9		216.0 m: final depth of drill hole
216 m		

___ m	sedimentology structure	description / comments
0.1		
0.2		
0.3		
0.4		
0.5		
0.6		
0.7		
0.8		
0.9		
___ m		

- Interpretation of facies/formation:

grey clay marl, between 215 and 216 m brown lime marl

Vellerat Formation

Appendix D

Composite geophysical log with most important marker horizons

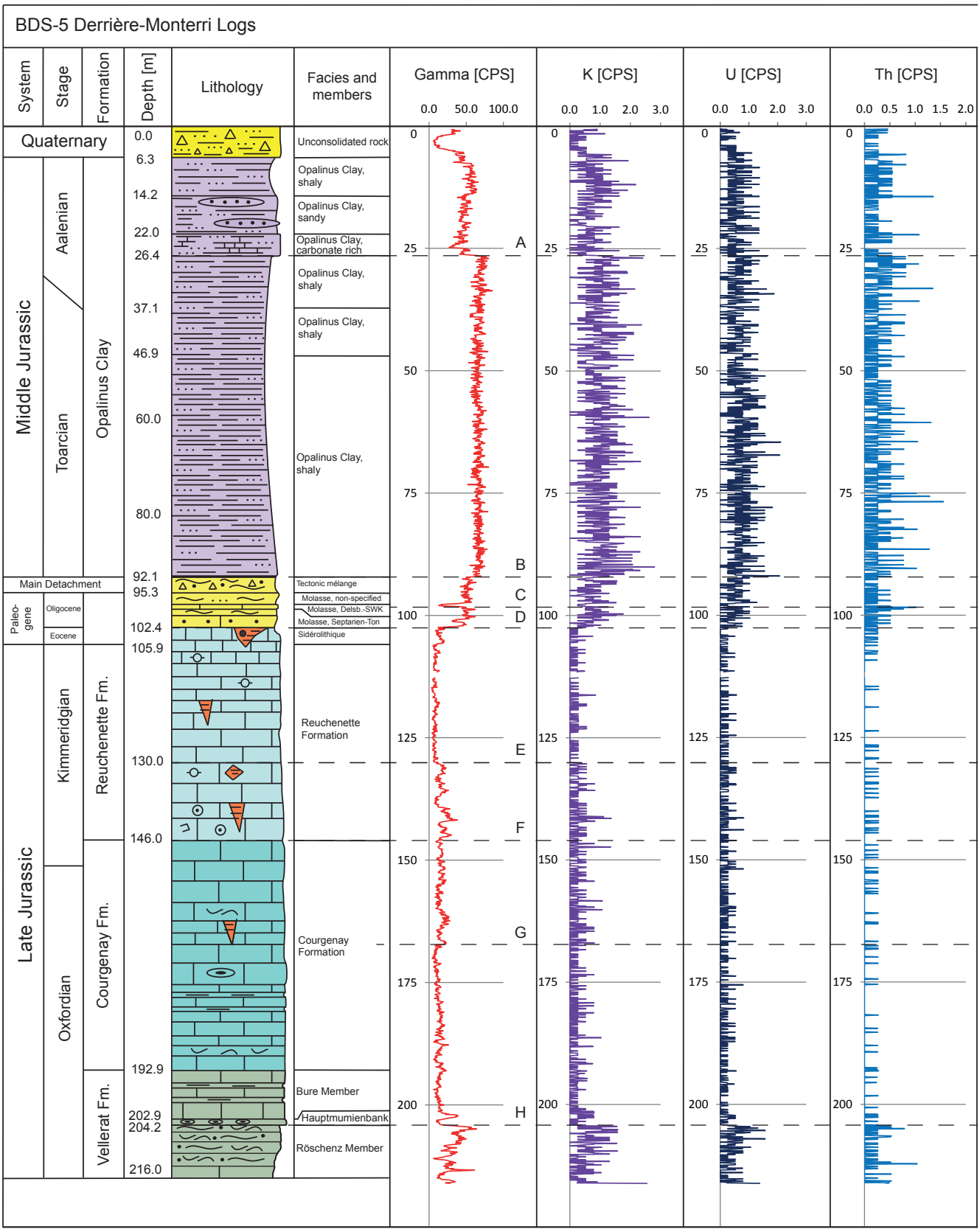

Fig. D-1: Composite log with stratigraphy from core mapping of borehole BDS-5, geophysical logs of the hanging wall and the footwall and most important marker horizons (labelled with letters A–H on the right of the Gamma log).

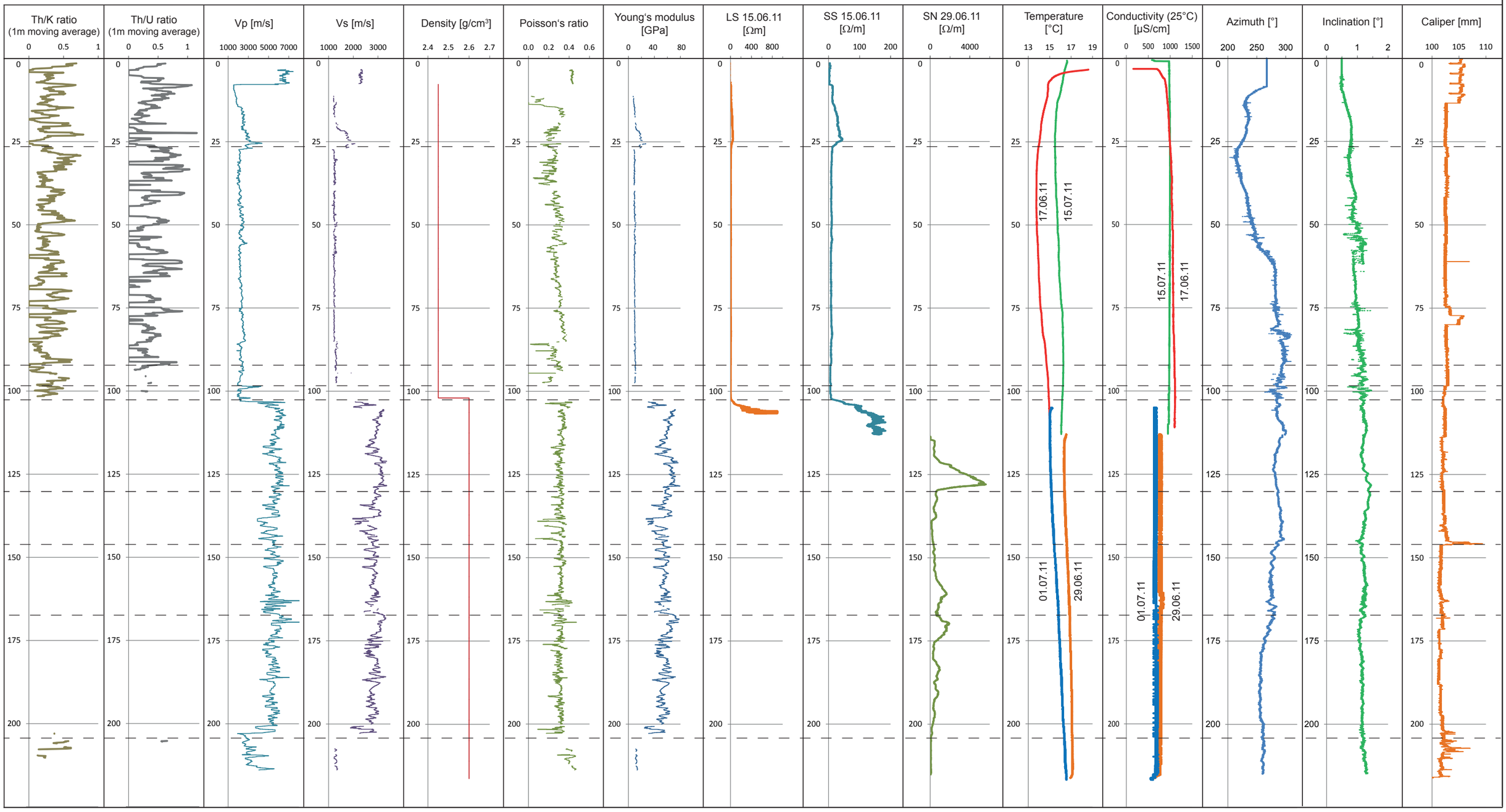
Th/K ratio (1m moving average)
0 0.5 1
Th/U ratio (1m moving average)
0 0.5 1
Vp [m/s]
1000 3000 5000 7000
Vs [m/s]
1000 2000 3000
Density [g/cm³]
2.4 2.5 2.6 2.7
Poisson's ratio
0.0 0.2 0.4 0.6
Young's modulus [GPa]
0 40 80
LS 15.06.11 [Ωm]
0 400 800
SS 15.06.11 [Ω/m]
0 100 200
SN 29.06.11 [Ω/m]
0 4000
Temperature [°C]
13 15 17 19
17.06.11
15.07.11
Conductivity (25°C) [µS/cm]
0 500 1000 1500
15.07.11
17.06.11
Azimuth [°]
200 250 300
Inclination [°]
0 1 2
Caliper [mm]
100 105 110
01.07.11
29.06.11
01.07.11
29.06.11
0 25 50 75 100 125 150 175 200

Appendix E

Pore water pressure evolution

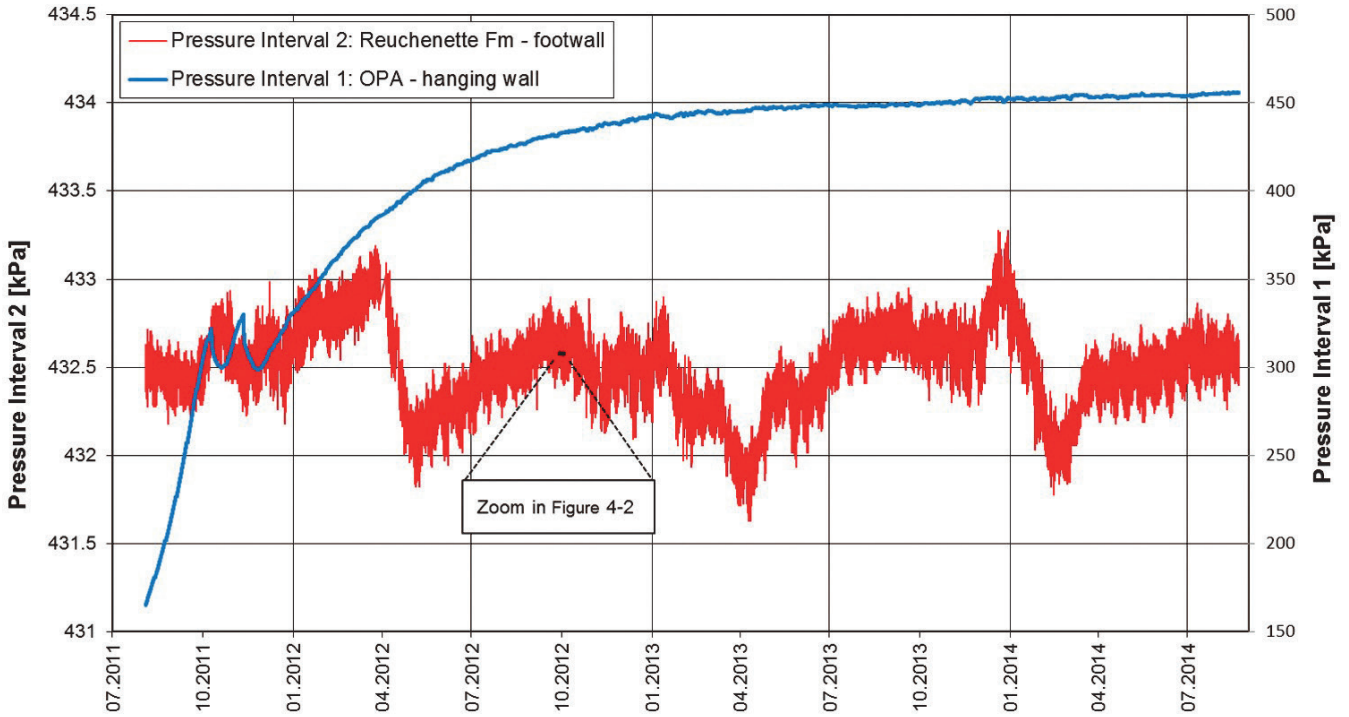

Fig. E-1: Pore water pressure evolution of the two intervals in borehole BDS-5 (P1 in blue at 67 m, right axis; P2 in red at 125 m, left axis). Whereas pressure interval 2 at 125 m in the footwall (Reuchenette Formation) shows seasonal variations since the beginning of recording, pressure interval 1 at a depth of 67 m in the hanging wall (Opalinus Clay) is still rising and not yet in equilibrium. The two distinct spikes at the beginning are interpreted as breakthrough curves due to the coupling of the perforated casing with the formation. The zoom in is shown in Figure 4-2 and highlights the diurnal and semidiurnal tidal effects.

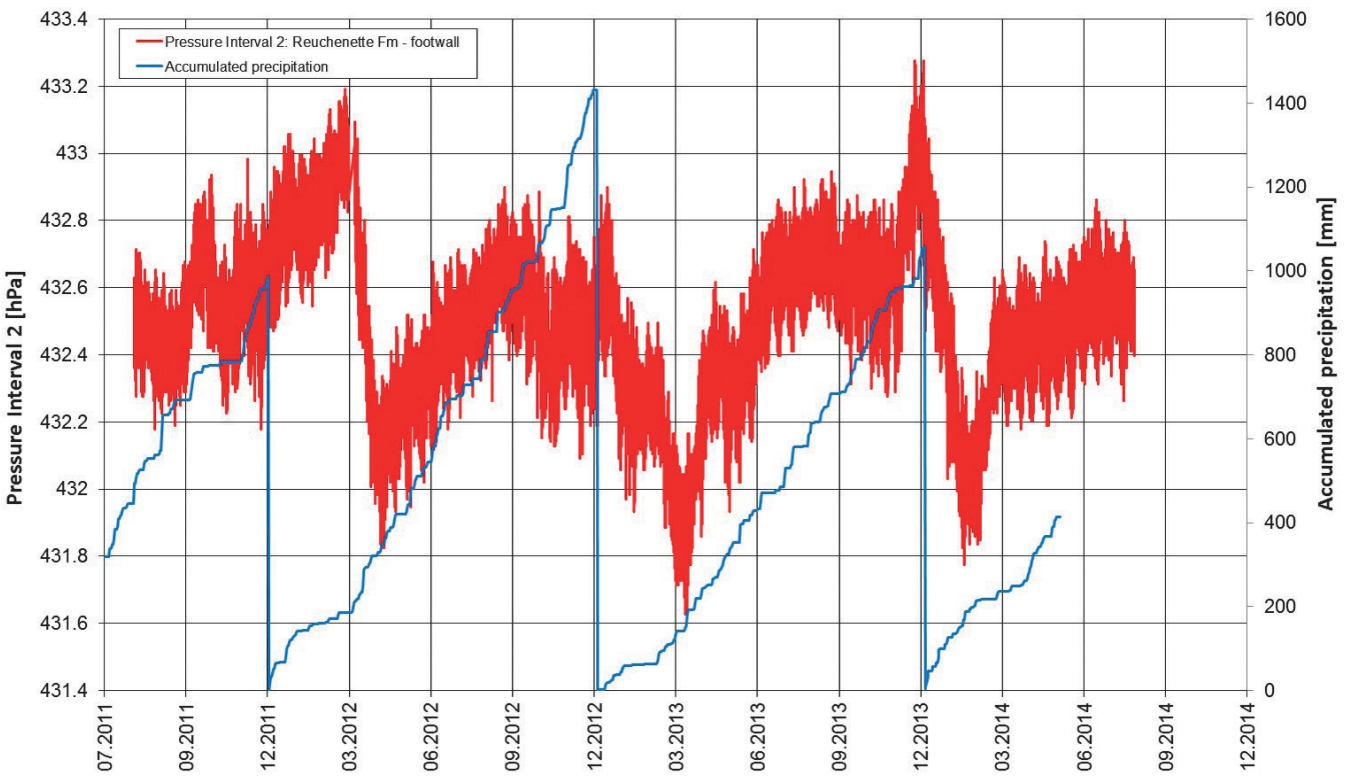

Fig. E-2: Pore water pressure evolution of pressure interval 2 at 125 m in the footwall, Reuchenette Formation (in red) and accumulated rainfall measured by Meteo Swiss at station Montenol (in blue). The variations of the pres-sure in this aquifer do not seem to be directly influenced by meteoric signals, such as rainfall or temperature. However, regarding the hydrogeological situation, a large time shift between precipitation and pressure response seems possible.

Appendix F

Raw and pre-processed pressure data in the time domain and for large-scale and daily frequency domains

a)

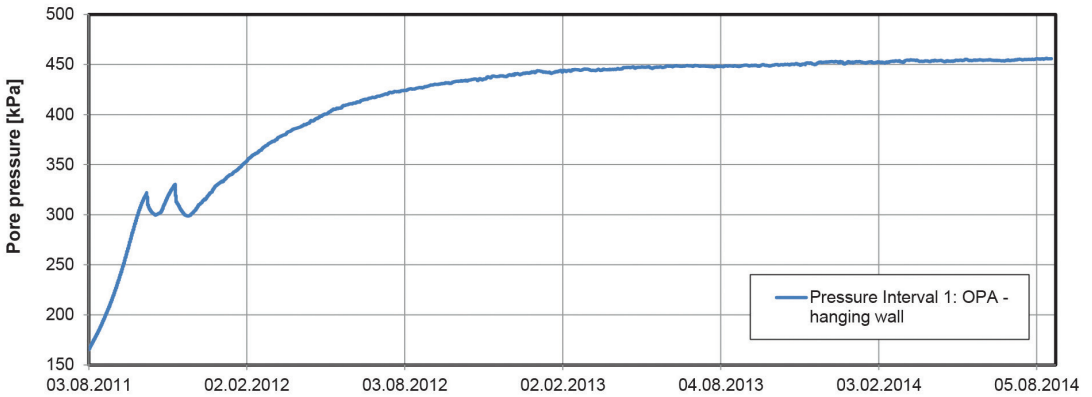

b)

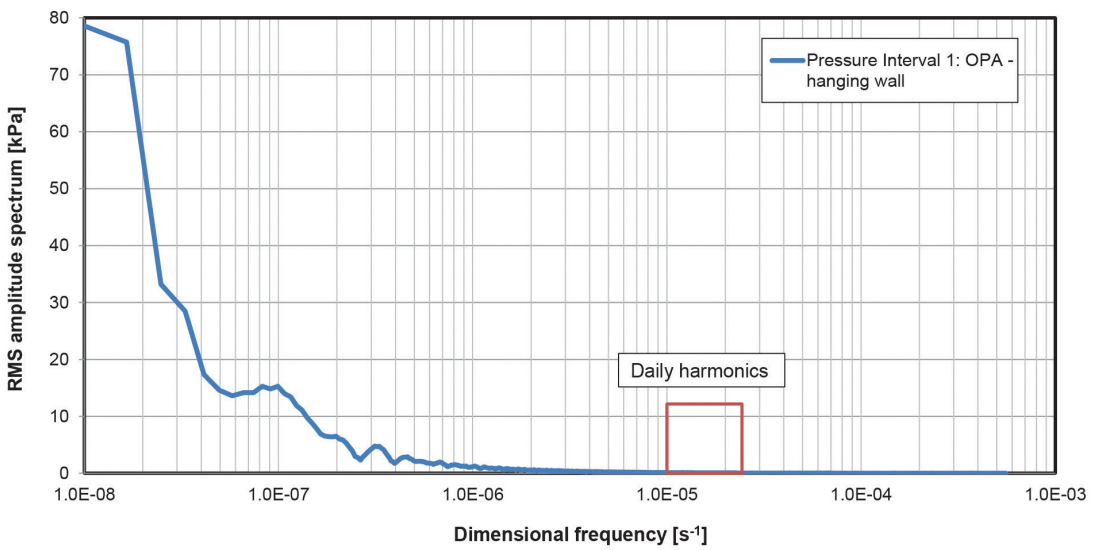

c)

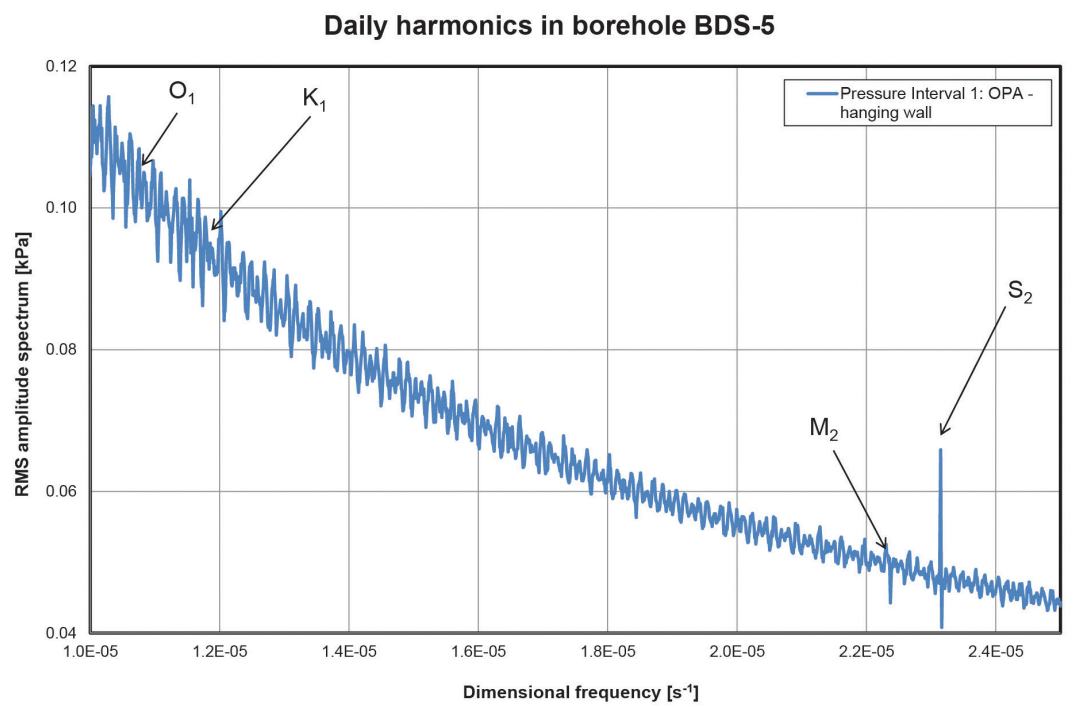

Fig. F-1: BDS5-P1 – raw pore pressure data in the time domain (a), and for large-scale (b) and daily (c) frequency domains. Note the occurrence of the S_2 harmonic. Principal lunar semi-diurnal (M_2), principal solar semi-diurnal (S_2), lunar diurnal (K_1), and lunar diurnal (O_1).

a)

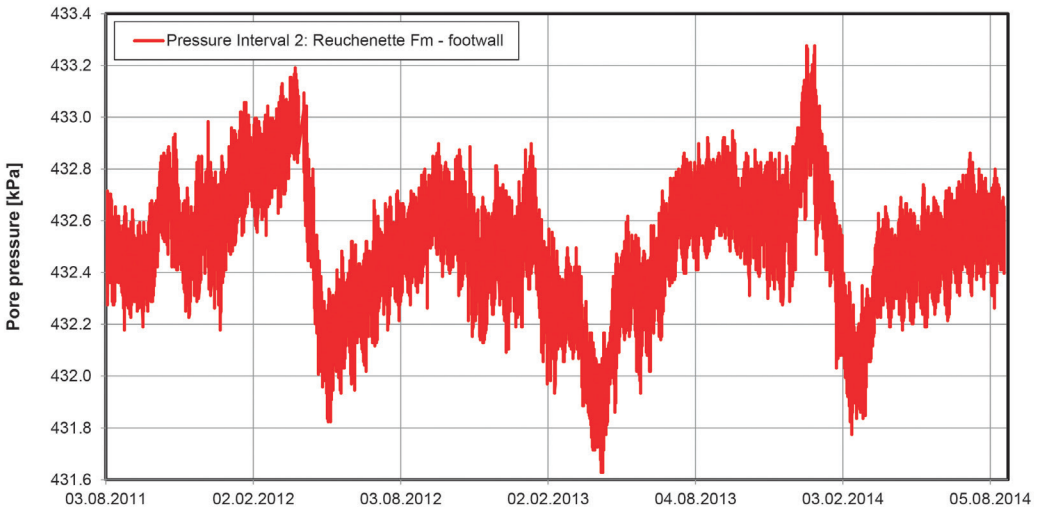

b)

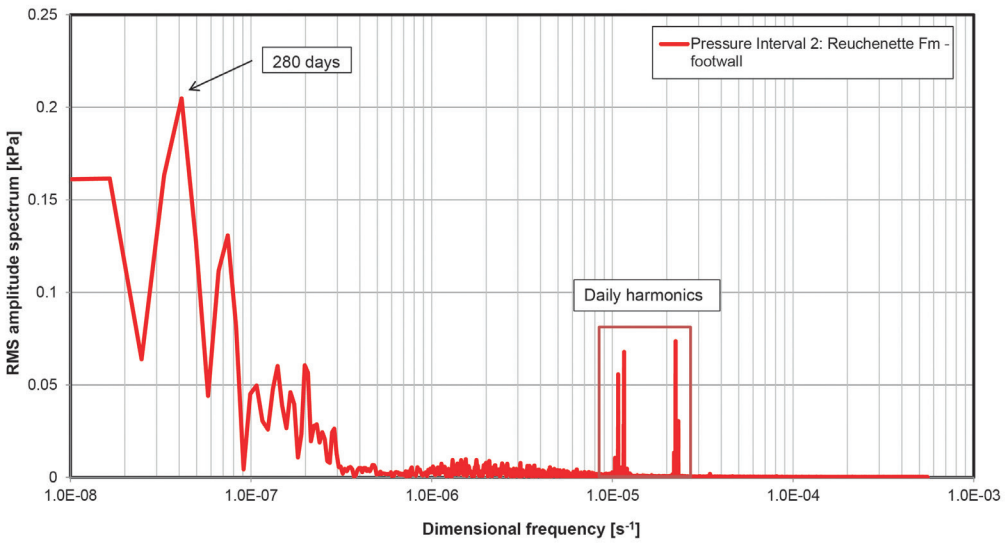

c)

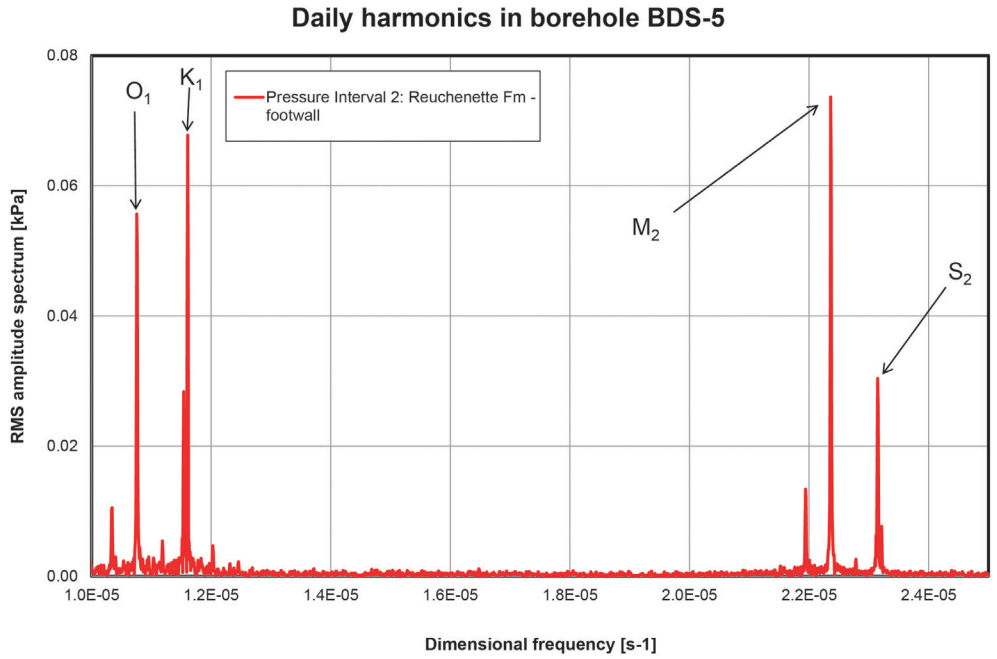

Fig. F-2: BDS5-P2 – raw pore pressure data in the time domain (a), and for large-scale (b) and daily (c) frequency domains. Note the occurrence of the diurnal O_1, K_1, M_2 and S_2 harmonics. Principal lunar semi-diurnal (M_2), principal solar semi-diurnal (S_2), lunar diurnal (K_1), and lunar diurnal (O_1).

Example of the calculation of the specific storage S_s from the amplitude of the gravitational M_2-signal (sensor BDS5-P2 at a depth of 125 m in the Reuchenette Formation)

The simplified Bredehoeft (1967) model takes into account that the magnitude of the hydraulic head fluctuation due to tidal effects is inversely proportional to the specific storage of the aquifer. This relationship can simply be expressed by equation [1] below:

$$\delta\epsilon_{Tidal} \approx S_s \delta H \qquad [1]$$

S_s specific storativity [m^{-1}]
$\delta\epsilon_{Tidal}$ Tidal amplitude for volumetric strain fluctuations related to the M_2 semi-diurnal earth tide [–]
δH amplitude of relative pressure fluctuations at the M_2-signal [m^{-1}]

- The amplitude for volumetric strain fluctuations related to the M_2 semi-diurnal earth tide is 2×10^{-8} m^3/m^3.
- The amplitude of the relative pressure fluctuations at the M_2-signal [kPa] must be converted into equivalent meter water column [mWS]. The conversion from Pa → mWS is done with factor 1×10^{-4} m.

Thus, solving equation [1] for S_s and converting the amplitude of the relative pressure fluctuations at the M_2-signal (value of M_2 in Figure F-2 [c] is 0.07362 kPa) into equivalent meter water column leads to:

$$S_s = \frac{2 \times 10^{-8}\ m^3/m^3}{(0.07362 \times 1000 \times 1 \times 10^{-4}\ m)} = 2.7 \times 10^{-6}\ m^{-1}$$

Appendix G

Compilation of stress measurements and calculation of an example (BDS-5 at 148 m)

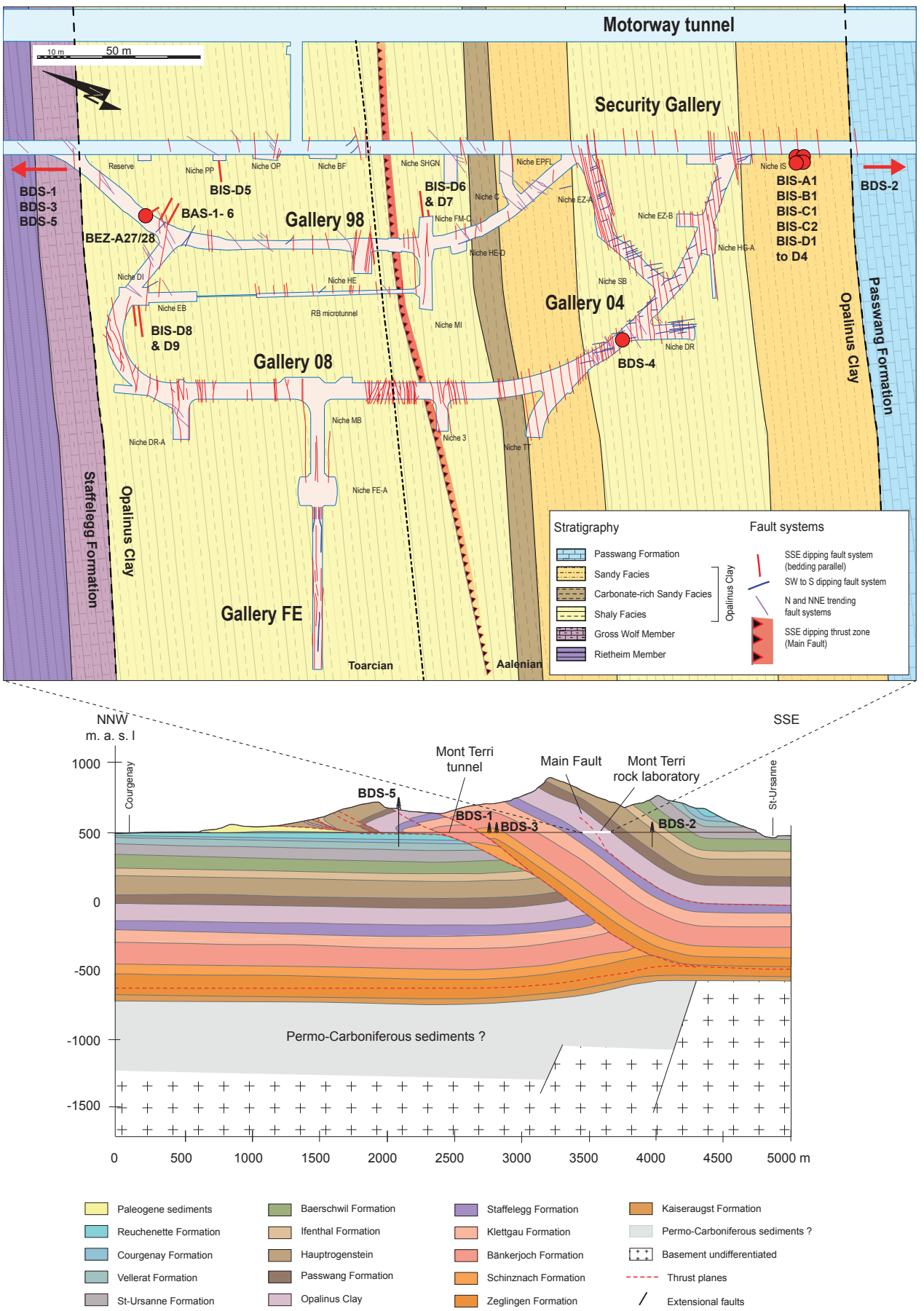

Fig. G-1: Location of stress experiments (boreholes) which have been carried out in and around the Mont Terri rock laboratory. The boreholes are localized on the map of the rock laboratory as well as on the cross-section through the Mont Terri anticline. For more details about the individual boreholes and corresponding in-situ tests, see Tables G-1 and G-2.

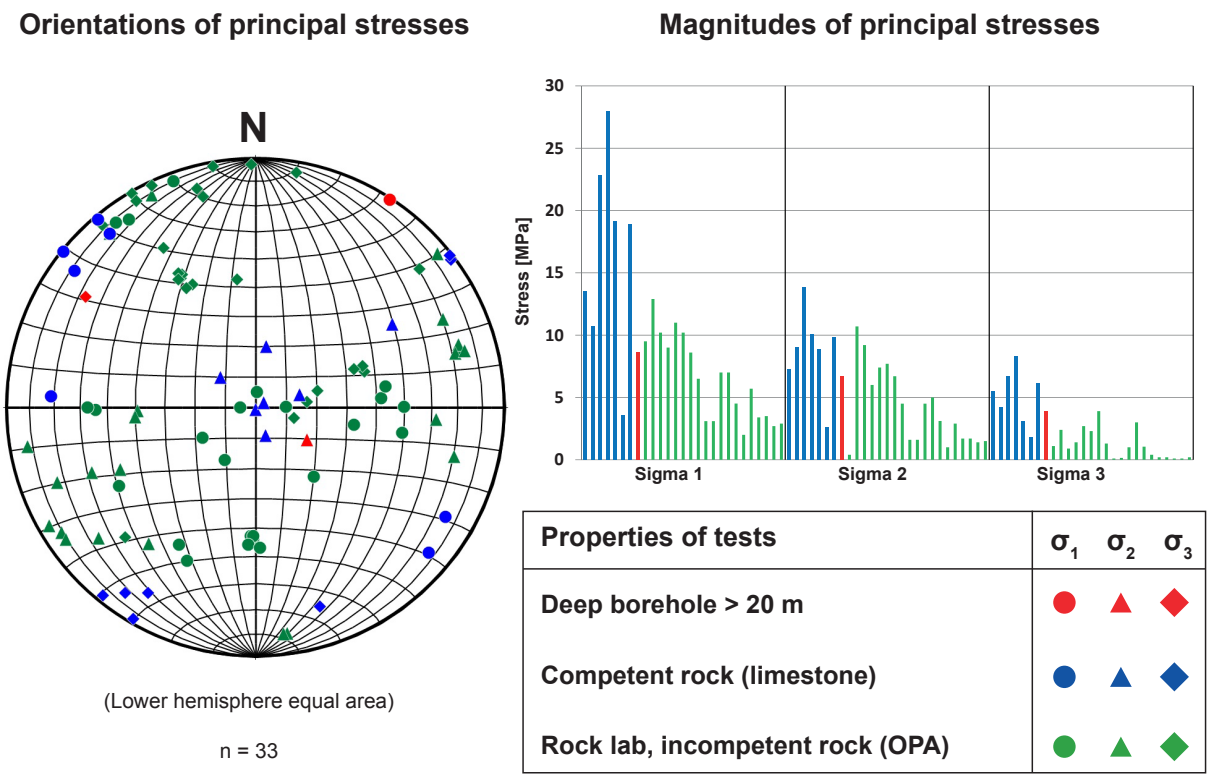

Fig. G-2: Results of all stress measurements carried out in the Mont Terri rock laboratory (n=33). Plotted are the principal stresses on a lower hemisphere equal area stereoplot (orientations, n=33) and on a histogram (magnitudes, n=27). The circles correspond to σ_1, triangles to σ_2 and squares to σ_3. Different colours were used for the distinction between in-situ data from a deep borehole >20 m (red), competent rock, dolomite (blue), and data from the rock laboratory, Opalinus Clay (green).

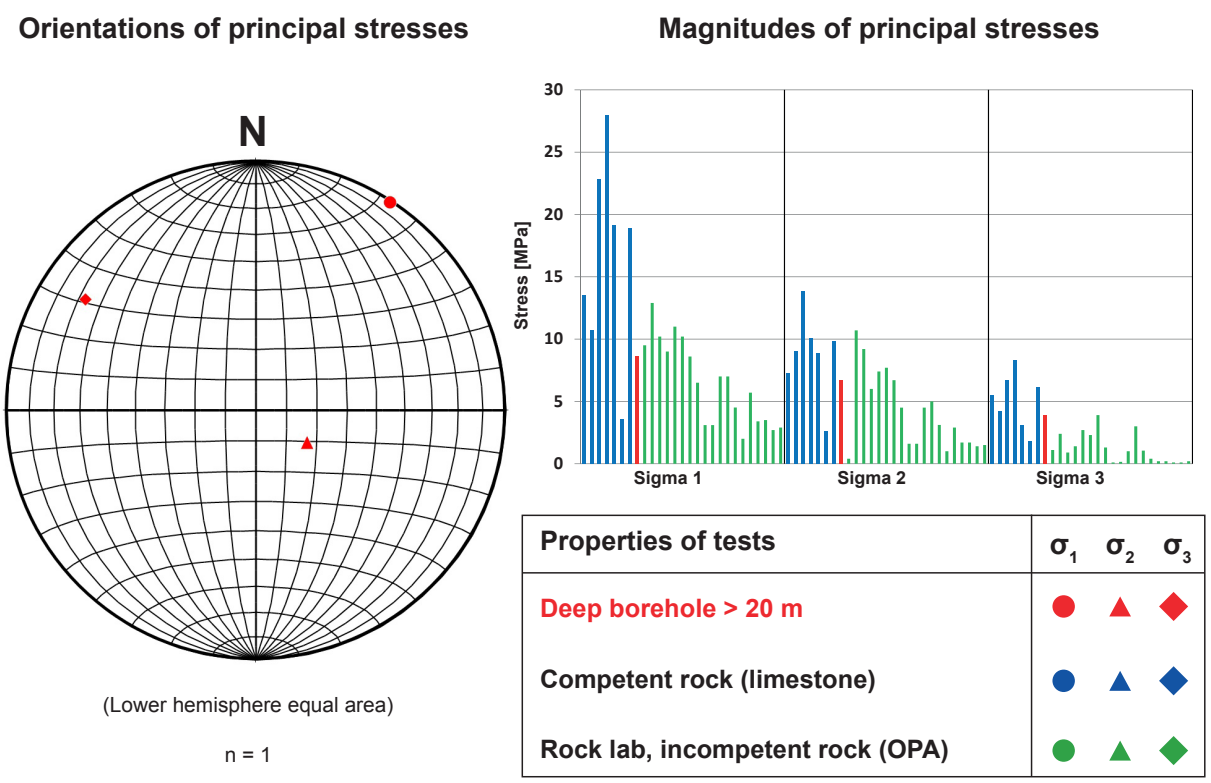

Fig. G-3: Results of stress measurements from a deep borehole (n=1). Plotted are the principal stresses on a lower hemisphere equal area stereoplot (orientations) and on a histogram (magnitudes). The circles correspond to σ_1, triangles to σ_2 and squares to σ_3. Note, that only one in-situ test is available for deep boreholes >20 m. σ_1 is oriented towards NNE with a magnitude of 8.6 MPa. σ_2 is oriented sub-vertically (6.7 MPa) and σ_3 points towards 300° with a magnitude of 3.9 MPa.

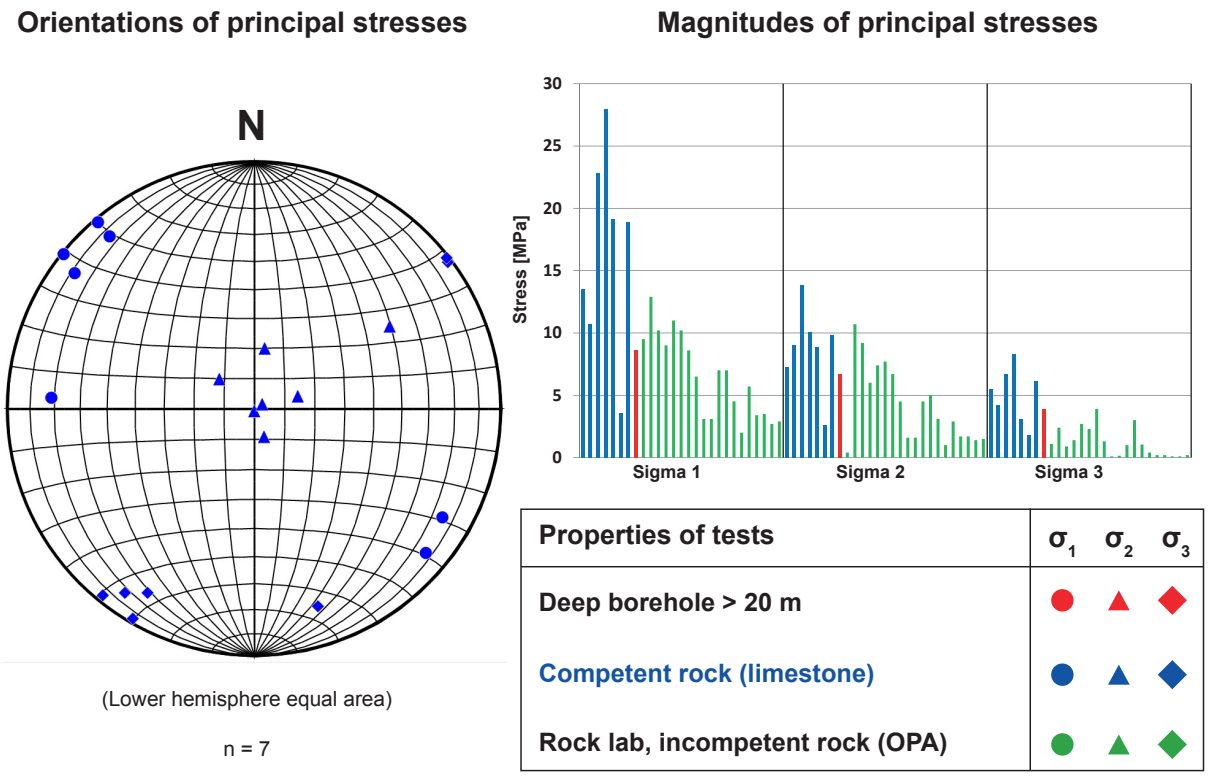

Fig. G-4: Results of stress measurements from competent rock (n=7). Plotted are the principal stresses on a lower hemisphere equal area stereoplot (orientations) and on a histogram (magnitudes). The circles correspond to σ_1, triangles to σ_2 and squares to σ_3. A clear NW–SE orientation for σ_1 is present. σ_2 is controlled by the overburden and sub-vertical. σ_3 shows a SW-NE direction. Magnitudes are generally higher for all principal stress axes compared to the other two classes.

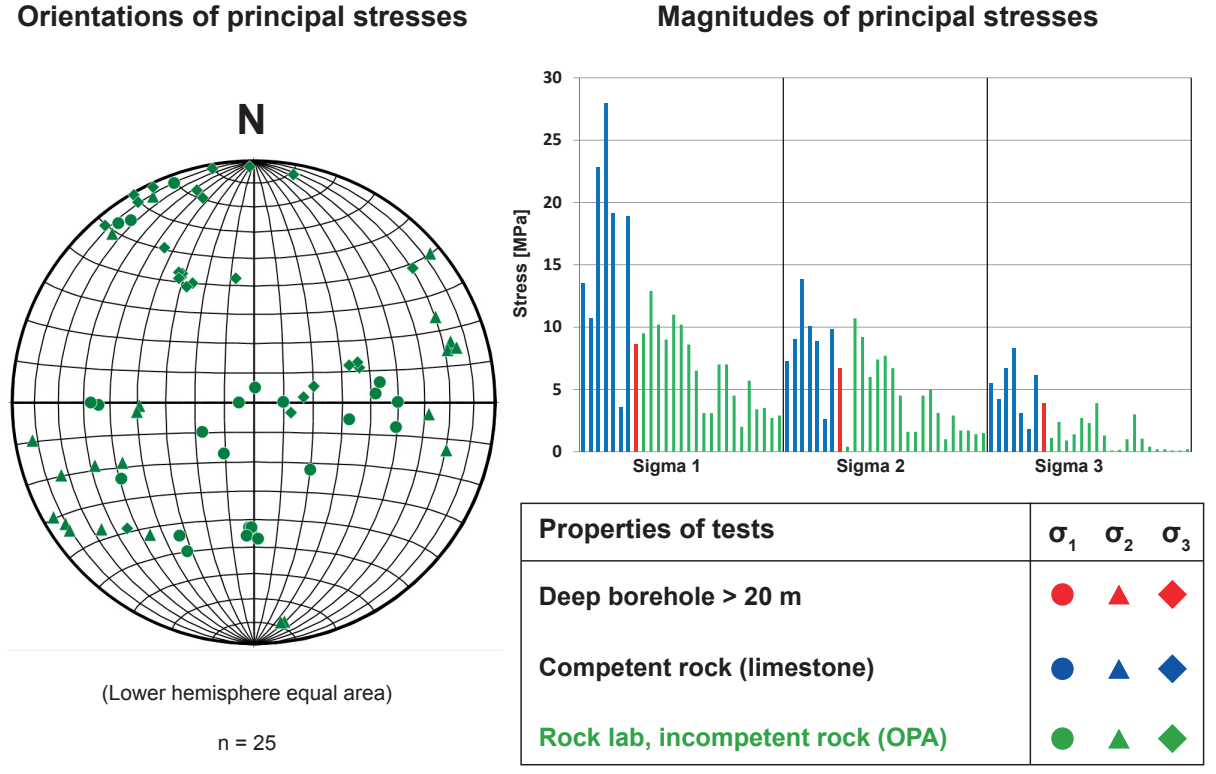

Fig. G-5: Results of stress measurements from incompetent rock (n=25). Plotted are the principal stresses on a lower hemisphere equal area stereoplot (orientations, n=25) and on a histogram (magnitudes, n=19). The circles correspond to σ_1, triangles to σ_2 and squares to σ_3. σ_1 is controlled by the overburden and sub-vertically oriented for most in-situ tests. σ_2 and σ_3 are generally located in the horizontal plane with σ_3 oriented in NNW–SSE direction.

Table G-1: *Listing of in-situ stress data from the Mont Terri rock laboratory and the bounding formations.*

σ	MPa	Azimut	Plunge	Lithology	Class	Borehole	Method	Name of report	Technical note	Authors	Location	Remarks
1	13.5	130	10	Lettenkohle	competent	BDS-1-1 (14.460 m) σ1	Overcoring	DS experiment: hydrofrac and overcoring results Presentation 2_DS.pdf		Presentation by Vietor et al. (2012)	Vent cavern	
2	7.3	10	70	Lettenkohle	competent	BDS-1-1 (14.460 m) σ2						
3	5.5	210	15	Lettenkohle	competent	BDS-1-1 (14.460 m) σ3						
1	10.7	320	2	Lettenkohle	competent	BDS-1-2 (15.650 m) σ1	Overcoring	DS experiment: hydrofrac and overcoring results Presentation 2_DS.pdf				
2	9	180	89	Lettenkohle	competent	BDS-1-2 (15.650 m) σ2						
3	4.2	53	2	Lettenkohle	competent	BDS-1-2 (15.650 m) σ3						
1	22.8	120	13	Lettenkohle	competent	BDS-1-3 (17.510 m) σ1	Overcoring	DS experiment: hydrofrac and overcoring results Presentation 2_DS.pdf				
2	13.8	310	75	Lettenkohle	competent	BDS-1-3 (17.510 m) σ2						
3	6.7	210	2	Lettenkohle	competent	BDS-1-3 (17.510 m) σ3						
1	28	307	10	Lettenkohle	competent	BDS-1-4 (21.500 m) σ1	Overcoring	DS experiment: hydrofrac and overcoring results Presentation 2_DS.pdf				
2	10.1	75	75	Lettenkohle	competent	BDS-1-4 (21.500 m) σ2						
3	8.3	215	10	Lettenkohle	competent	BDS-1-4 (21.500 m) σ3						
1	19.1	320	10	Lettenkohle	competent	BDS-1-5 (22.100 m) σ1	Overcoring	DS experiment: hydrofrac and overcoring results Presentation 2_DS.pdf				
2	8.9	160	80	Lettenkohle	competent	BDS-1-5 (22.100 m) σ2						
3	3.1	52	1	Lettenkohle	competent	BDS-1-5 (22.100 m) σ3						
1	3.6	90	80	Opalinus Clay	incompetent	BAS-1 to BAS-6	Overcoring	DS experiment: hydrofrac and overcoring results Presentation 2_DS.pdf		Presentation by Vietor et al. (2012)	Ga98 N	Data obtained from plot/graphic
1	3.6	240	70	Opalinus Clay	incompetent							
1	3.6	140	60	Opalinus Clay	incompetent							
1	3.6	100	57	Opalinus Clay	incompetent							
1	3.6	90	40	Opalinus Clay	incompetent							
1	3.6	86	48	Opalinus Clay	incompetent							
1	3.6	81	46	Opalinus Clay	incompetent							
2	2.6	65	18	Opalinus Clay	incompetent							
2	2.6	268	51	Opalinus Clay	incompetent							
2	2.6	260	8	Opalinus Clay	incompetent							
2	2.6	248	30	Opalinus Clay	incompetent							
2	2.6	245	40	Opalinus Clay	incompetent							
2	2.6	237	8	Opalinus Clay	incompetent							
2	2.6	218	31	Opalinus Clay	incompetent							
3	1.8	359	3	Opalinus Clay	incompetent							
3	1.8	350	2	Opalinus Clay	incompetent							
3	1.8	345	10	Opalinus Clay	incompetent							
3	1.8	346	14	Opalinus Clay	incompetent							
3	1.8	335	2	Opalinus Clay	incompetent							
3	1.8	330	27	Opalinus Clay	incompetent							
3	1.8	225	27	Opalinus Clay	incompetent							
1	6.5	210	70	Opalinus Clay	incompetent	BIS-A1 to BIS-A4	Undercoring	Excavation Disturbed Zone (EDZ) in Clay Shale: Mont Terri	TR 2001-01	Martin & Lanyon (2001)	IS-niche	
2	4.5	320	10	Opalinus Clay	incompetent							
3	1.3	50	15	Opalinus Clay	incompetent							
1		100	40	Opalinus Clay	incompetent	BED-B9 to BED-B11	Under-excavation	ED-B: stress Measurement Experiment	TN-98-09	Bigarré (1998)	Ga98	
2		265	50	Opalinus Clay	incompetent							
3		10	5	Opalinus Clay	incompetent							
1	3.1	181	45	Opalinus Clay	incompetent	Laboratory	Slotter	Excavation Disturbed Zone (EDZ) in Clay Shale: Mont Terri	TR 2001-01	Martin & Lanyon (2001)		
2	1.6	74	16	Opalinus Clay	incompetent							
3	0.1	330	1	Opalinus Clay	incompetent							

Only tests which yielded the principal stresses are listed. Locations of boreholes, niches and galleries are provided in Figure G-1 (part 1/2).

Table G-2: *Listing of in-situ stress data from the Mont Terri rock laboratory and the bounding formations.*

σ	MPa	Azimut	Plunge	Lithology	Class	Borehole	Method	Name of report	Technical note	Authors	Location	Remarks
1	7	270	85	Opalinus Clay	incompetent	BIS-A1 to BIS-A3	Undercoring	In-situ Stress measurements (IS-A): Results of the in-situ experiments: calculation of stresses	TN97-14	Bigarré & Lizeur (1997)		original data "subvertical" not a number
2	4.5	50	5	Opalinus Clay	incompetent							original data "subhorizontal" not a number
3	1	320	5	Opalinus Clay	incompetent							original data "subhorizontal" not a number
1	7	5	85	Opalinus Clay	incompetent	BIS-C1 and BIS-C2	Hydraulic fracturing	IS experiment: Hydrofracture Stress Tests in Boreholes BIS-C1 and BIS-C2	TN99-55	Evans et al. (1999)		original data "subvertical" not a number
2	5	240	5	Opalinus Clay	incompetent	Laboratory						original data "subhorizontal" not a number
3	3	330	5	Opalinus Clay	incompetent	Laboratory						original data "subhorizontal" not a number
1	4.51	273	19	Lettenkohle	competent	BDS-1	Overcoring	AS experiment: Results from in-situ tests. Short Report about the current state of AS experiment	TN2006-33	Shin (2006)	Vent cavern	
2	3.11	59	36	Lettenkohle	competent	BDS-1						
3	1.05	162	17	Lettenkohle	competent	BDS-1						
1	18.9	309	1	Lettenkohle	competent	BDS-1	Overcoring	DS (Determination of stress) Experiment: Overcoring stress measurement by CCBO Data report	TN2009-57	Shin (2009)	Vent cavern	
2	9.8	63	87	Lettenkohle	competent	BDS-1						
3	6.1	219	3	Lettenkohle	competent	BDS-1						
1	8.6	33	0	Opalinus Clay	deep	BDS-4	Hydraulic fracturing	DS (Determination of stress) Experiment: Hydraulic Fracturing Tests in BDS-2 and BDS-4 at the Mont Terri Underground Research Facility. FMT DS Experiment	TN2010-53	Echanescu (2010)	Ga 08, Sec. Gallery	Far field stress tensor. Data from BDS-4 break-outs. (Data from BDS-4 seems to fit BDS-2)
2	6.7	123	70	Opalinus Clay	deep	BDS-4						
3	3.9	303	20	Opalinus Clay	deep	BDS-4						
1	2	209	37	Opalinus Clay	incompetent	BIS-B1-B3 5.00 m	Borehole slotter	IS-B Experiment, Phase 2 In-Situ Stress Measurement with the INTERFELS Borehole Slotter Method along Boreholes BIS-B1, BIS-B2 and BIS-B3	TN97-15	König & Bock (1997)	IS Niche	
2	1	104	19	Opalinus Clay	incompetent	BIS-B1-B3 5.00 m						
3	0.4	352	47	Opalinus Clay	incompetent	BIS-B1-B3 5.00 m						
1	5.7	204	33	Opalinus Clay	incompetent	BIS-B1-3 8.40 m	Borehole slotter	IS-B Experiment, Phase 2 In-Situ Stress Measurement with the INTERFELS Borehole Slotter Method along Boreholes BIS-B1, BIS-B2 and BIS-B3	TN97-15	König & Bock (1997)	IS Niche	
2	2.9	94	28	Opalinus Clay	incompetent	BIS-B1-3 8.40 m						
3	0.2	333	44	Opalinus Clay	incompetent	BIS-B1-3 8.40 m						
1	3.4	182	47	Opalinus Clay	incompetent	BIS-B1-3 11.00 m	Borehole slotter	IS-B Experiment, Phase 2 In-Situ Stress Measurement with the INTERFELS Borehole Slotter Method along Boreholes BIS-B1, BIS-B2 and BIS-B3	TN97-15	König & Bock (1997)	IS Niche	
2	1.7	74	16	Opalinus Clay	incompetent	BIS-B1-3 11.00 m						
3	0.2	331	39	Opalinus Clay	incompetent	BIS-B1-3 11.00 m						
1	3.5	181	47	Opalinus Clay	incompetent	BIS-B1 12.60 m	Borehole slotter	IS-B Experiment, Phase 2 In-Situ Stress Measurement with the INTERFELS Borehole Slotter Method along Boreholes BIS-B1, BIS-B2 and BIS-B3	TN97-15	König & Bock (1997)	IS Niche	
2	1.7	73	16	Opalinus Clay	incompetent	BIS-B1 12.60 m						
3	0.1	330	38	Opalinus Clay	incompetent	BIS-B1 12.60 m						
1	2.7	183	44	Opalinus Clay	incompetent	BIS-B1-B3 17.20 m	Borehole slotter	IS-B Experiment, Phase 2 In-Situ Stress Measurement with the INTERFELS Borehole Slotter Method along Boreholes BIS-B1, BIS-B2 and BIS-B3	TN97-15	König & Bock (1997)	IS Niche	
2	1.4	75	18	Opalinus Clay	incompetent	BIS-B1-B3 17.20 m						
3	0.1	329	40	Opalinus Clay	incompetent	BIS-B1-B3 17.20 m						
1	2.9	178	43	Opalinus Clay	incompetent	BIS-B1-B3 19.20 m	Borehole slotter	IS-B Experiment, Phase 2 In-Situ Stress Measurement with the INTERFELS Borehole Slotter Method along Boreholes BIS-B1, BIS-B2 and BIS-B3	TN97-15	König & Bock (1997)	IS Niche	
2	1.5	75	14	Opalinus Clay	incompetent	BIS-B1-B3 19.20 m						
3	0.2	330	44	Opalinus Clay	incompetent	BIS-B1-B3 19.20 m						
1	9.5	240	37	Opalinus Clay	incompetent	BEZ-A27 & 28	Overcoring	EZ-A experiment: Stress measurements campaign by overcoring in the Mont Terri Laboratory using CSIRO cells	TN2004-86	F. Lahaye (2004)	EZ-A Niche	
2	0.4	334	6	Opalinus Clay	incompetent							
3	1.1	72	52	Opalinus Clay	incompetent							
1	12.9	269	36	Opalinus Clay	incompetent	BEZ-A27 & 28	Overcoring	EZ-A experiment: Stress measurements campaign by overcoring in the Mont Terri Laboratory using CSIRO cells	TN2004-86	F. Lahaye (2004)	EZ-A Niche	
2	10.7	172	9	Opalinus Clay	incompetent							
3	2.4	69	52	Opalinus Clay	incompetent							
1	10.2	270	33	Opalinus Clay	incompetent	BEZ-A27 & 28	Overcoring	EZ-A experiment: Stress measurements campaign by overcoring in the Mont Terri Laboratory using CSIRO cells	TN2004-86	F. Lahaye (2004)	EZ-A Niche	
2	9.2	173	9	Opalinus Clay	incompetent							
3	0.9	69	55	Opalinus Clay	incompetent							
1	9	326	10	Opalinus Clay	incompetent	BEZ-A27 & 28	Overcoring	EZ-A experiment: Stress measurements campaign by overcoring in the Mont Terri Laboratory using CSIRO cells	TN2004-86	F. Lahaye (2004)	EZ-A Niche	
2	6	235	8	Opalinus Clay	incompetent							
3	1.4	106	77	Opalinus Clay	incompetent							
1	11	340	4	Opalinus Clay	incompetent	BEZ-A27 & 28	Overcoring	EZ-A experiment: Stress measurements campaign by overcoring in the Mont Terri Laboratory using CSIRO cells	TN2004-86	F. Lahaye (2004)	EZ-A Niche	
2	7.4	249	16	Opalinus Clay	incompetent							
3	2.7	84	73	Opalinus Clay	incompetent							
1	10.2	323	8	Opalinus Clay	incompetent	BEZ-A27 & 28	Overcoring	EZ-A experiment: Stress measurements campaign by overcoring in the Mont Terri Laboratory using CSIRO cells	TN2004-86	F. Lahaye (2004)	EZ-A Niche	
2	7.7	230	19	Opalinus Clay	incompetent							
3	2.3	75	69	Opalinus Clay	incompetent							

Only tests which yielded the principal stresses are listed. Locations of boreholes, niches and galleries are provided in Figure G-1 (part 2/2).

Evaluation of principal stress components from hydraulic fracturing data (Test at 148 m depth in borehole BDS-5):

In case of a vertical borehole the Kirsch's solution is used in the Hubbert and Wills formula (1957) for the critical pressure P_c at the moment of fracture initiation:

$$P_c = 3S_h - S_H + T - P_p \quad \text{where} \quad (G.1)$$

S_h minimum horizontal stress [Pa]
S_H maximum horizontal stress [Pa]
S_v vertical stress [Pa]
P_c breakdown pressure or critical pressure [Pa]
P_w internal fluid pressure [Pa]
P_r re-opening pressure [Pa]
P_p pore pressure [Pa]
P_{si} shut-in pressure [Pa]
T tensile strength [Pa]

The main assumptions of this approach are:

- The overburden stress is a principal stress and a linear function of depth
- The rock is homogeneous, isotropic, and initially impermeable
- The minimum horizontal stress is equal to the shut-in pressure and the induced fracture is perpendicular to S_h
- The effective stress law for tensile failure is valid for Opalinus Clay and late Jurassic Limestone

With the assumptions above and by using equation G.1, the stress components can be calculated as follows:

$$S_h = P_{si} \quad [Pa] \quad (G.2)$$

$$S_H = 3P_{si} - P_r - P_p \quad [Pa] \quad (G.3)$$

$$S_v = \rho g h \quad [Pa] \quad (G.4)$$

$$P_r = P_c - T \quad [Pa] \quad (G.5)$$

The magnitudes of stress components can be calculated by the determination of shut-in pressure and re-opening pressure:

Shut-in pressure P_{si}

- Pressure to keep the fracture open after shut-in
- The pressure at which flow = 0 yields P_{si} max
- Transition from rapid linear pressure drop to the beginning of slow diffusion-dominated pressure drop

Re-opening pressure P_r

- Pressure to re-open the fracture after the frack
- Pressure at which the pressure built-up of the second hydraulic fracturing cycle deviates from the first cycle curve and thus from linearity

Additionally to the parameters above, which need to be evaluated, the interval pressure and the flow is controlled. The critical pressure P_c is only needed for the determination of the in-situ hydraulic tensile strength T. The calculated value can be cross-checked with data from Brazilian tests.

The orientation of stress components is determined by means of:

- Impression packer tests or optical borehole imager (OBI)/ acoustic borehole imager (ABI) logs before and after hydraulic fracturing
- Analysis of borehole breakouts from optical borehole imager logs (OBI), acoustic borehole imager logs (ABI) or caliper logs

On Figure G-6 below, the entire pressure/flow-sequence for a hydraulic fracturing-test at 148 m depth in the Courgenay Formation is shown. The analysis of the critical pressure P_c is given on Figure G-7, the analysis of the re-opening pressure P_r on Figures G-8 and G-9 and the determination of the shut-in pressure P_{si} on Figures G-10, G-11 and G-12.

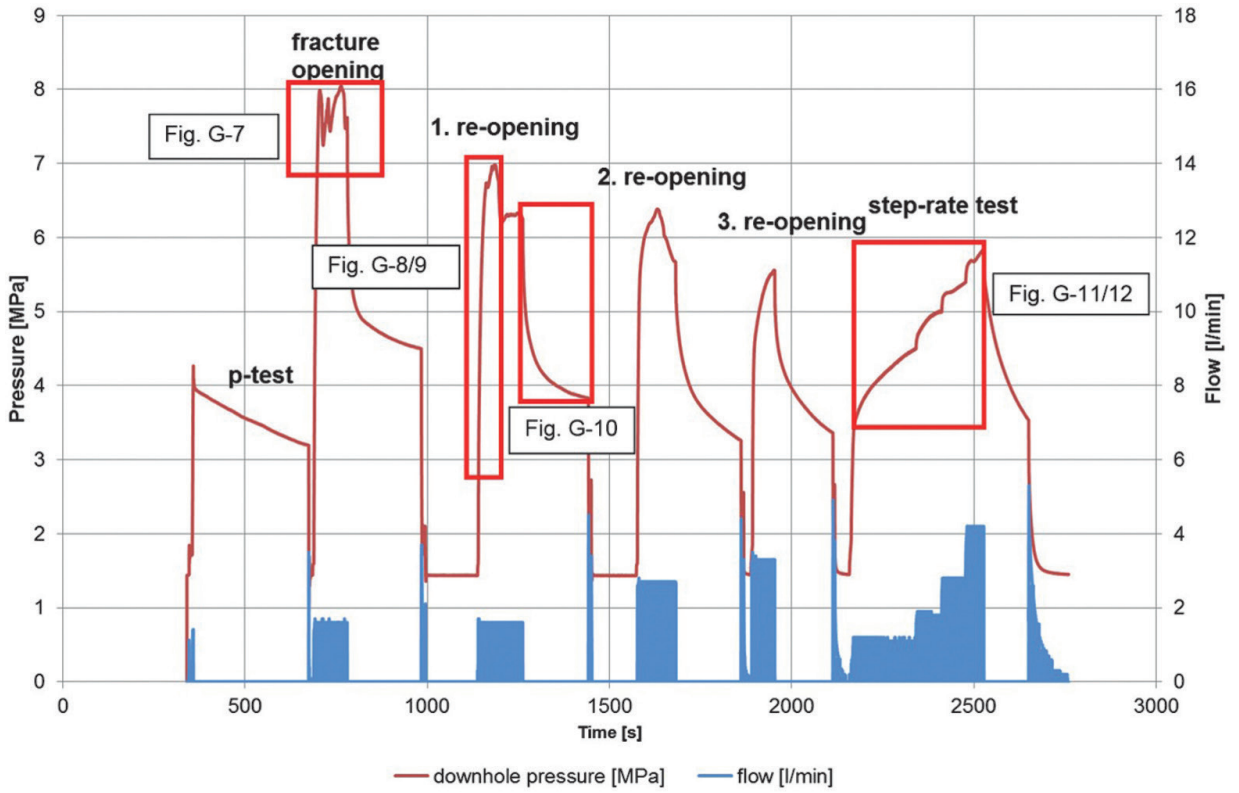

Fig. G-6: Plot of the entire test sequence pressure versus time for the hydraulic fracturing-test at 148 m depth (Courgenay Formation, Oxfordian). The highlighted zones show the parts which are analysed in the following figures.

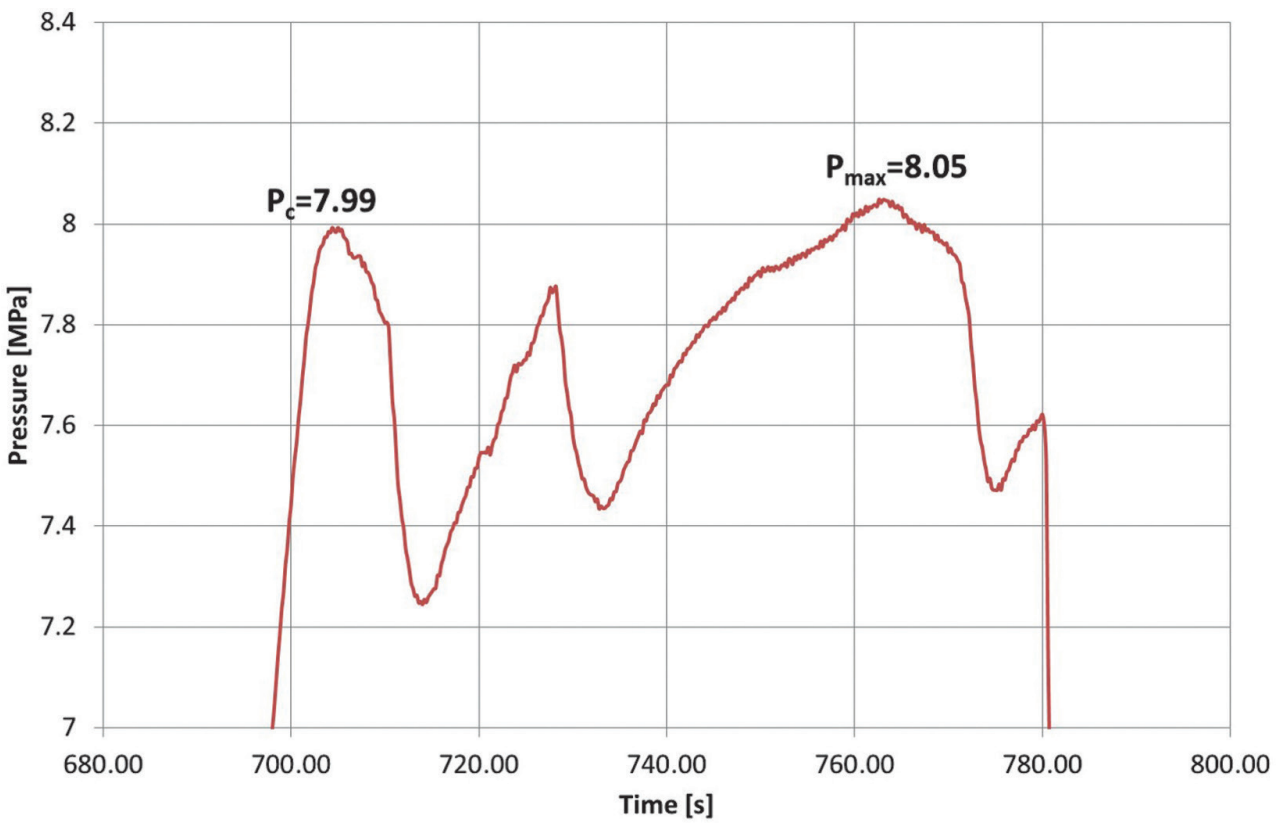

Fig. G-7: Zoom-in, which shows the critical pressure P_c at fracture initiation during first pressurization. There are several peaks on the pressure curve, since the crack propagation and crack formation leads to small pressure releases. Note that after reaching P_c = 7.99 MPa, the flow is kept constant.

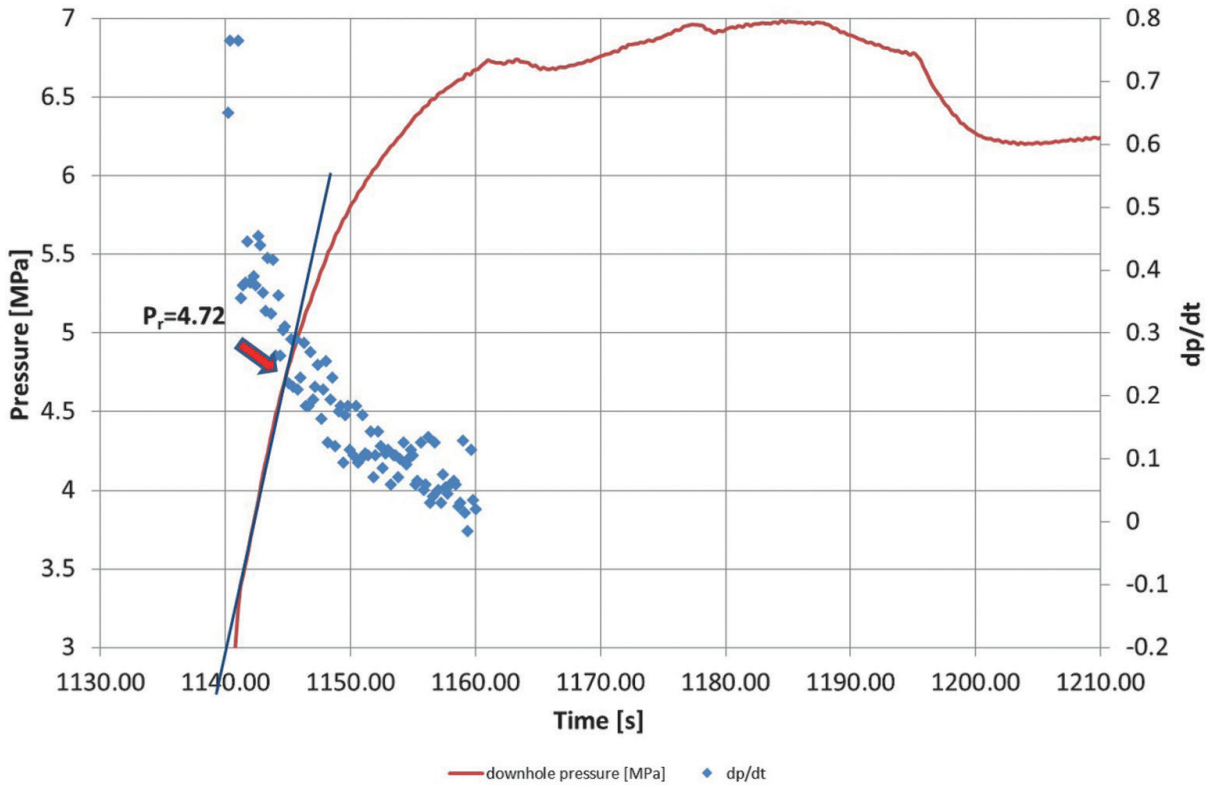

Fig. G-8: Determination of the re-opening pressure P_r on the first re-opening cycle. Note that the re-opening pressure is picked at the transition, where the pressure increase deviates from linear. The blue dots represent the derivative dp/dt of this part of the curve. At P_r there is a remarkable kink in the derivative.

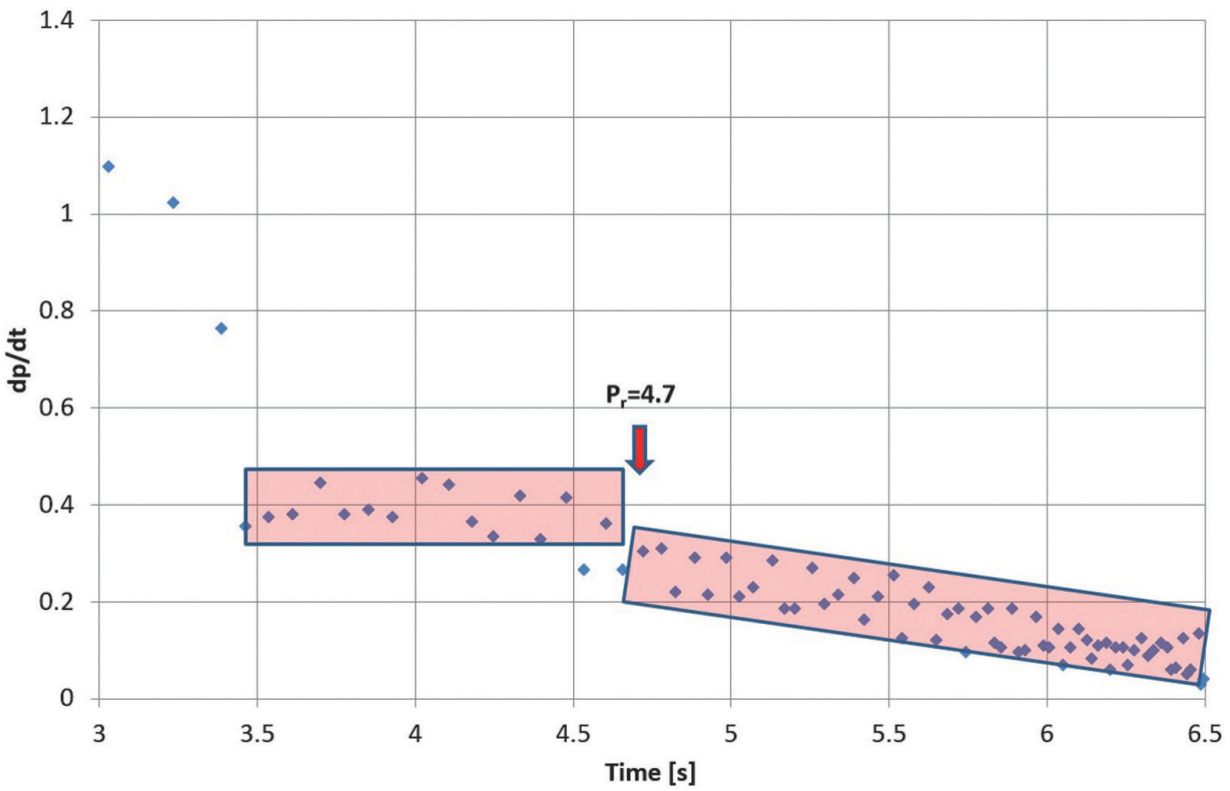

Fig. G-9: Another representation of the derivative in order to determine the re-opening pressure P_r. Note that the re-opening pressure is picked at the transition, where there is a kink in the derivative dp/dt, which is due to the re-opening of the fracture.

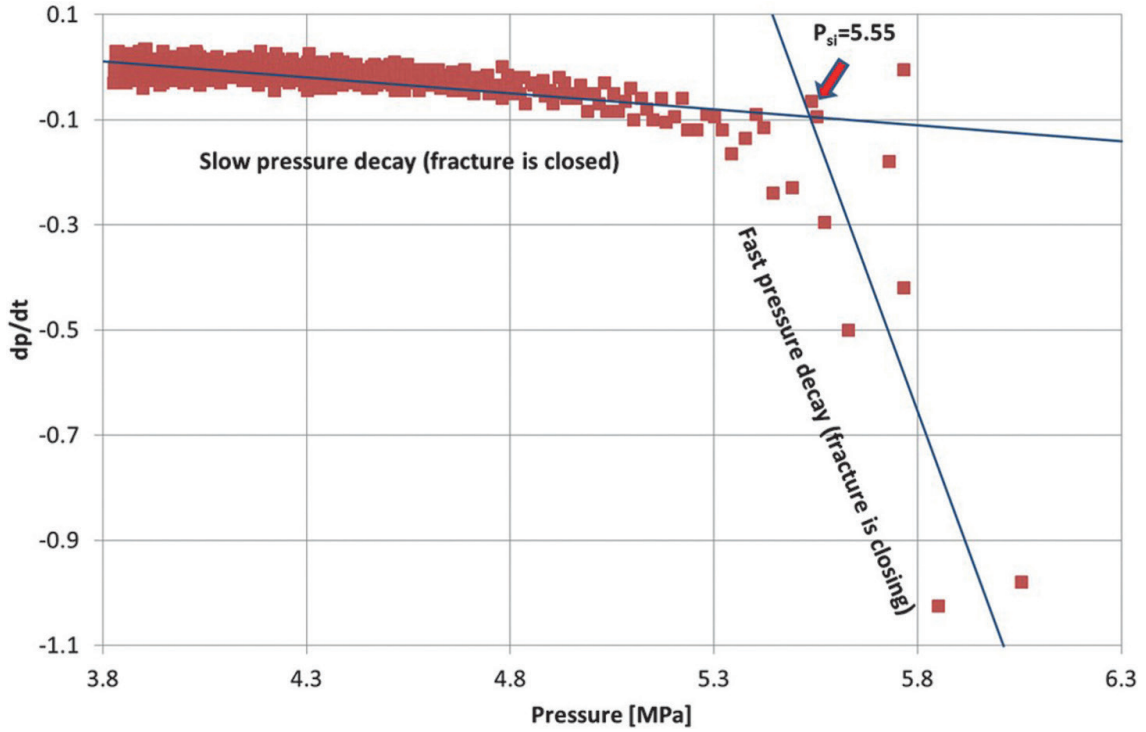

Fig. G-10: Representation of the derivative for the pressure curve (1. Re-opening cycle pressure decay after shut-in). Note that in this part of the curve flow is zero. The figure must be read from the right to the left. In an initial phase, there is a fast decay of pressure within the fracture, since the fracture is still open. In a second phase, the decay is much lower, since the fracture is closed. At the transition from fast to slow pressure decay, the shut-in pressure P_{si} can be picked. Finally, the average P_{si} from several re-opening cycles is taken for hydraulic fracturing analysis.

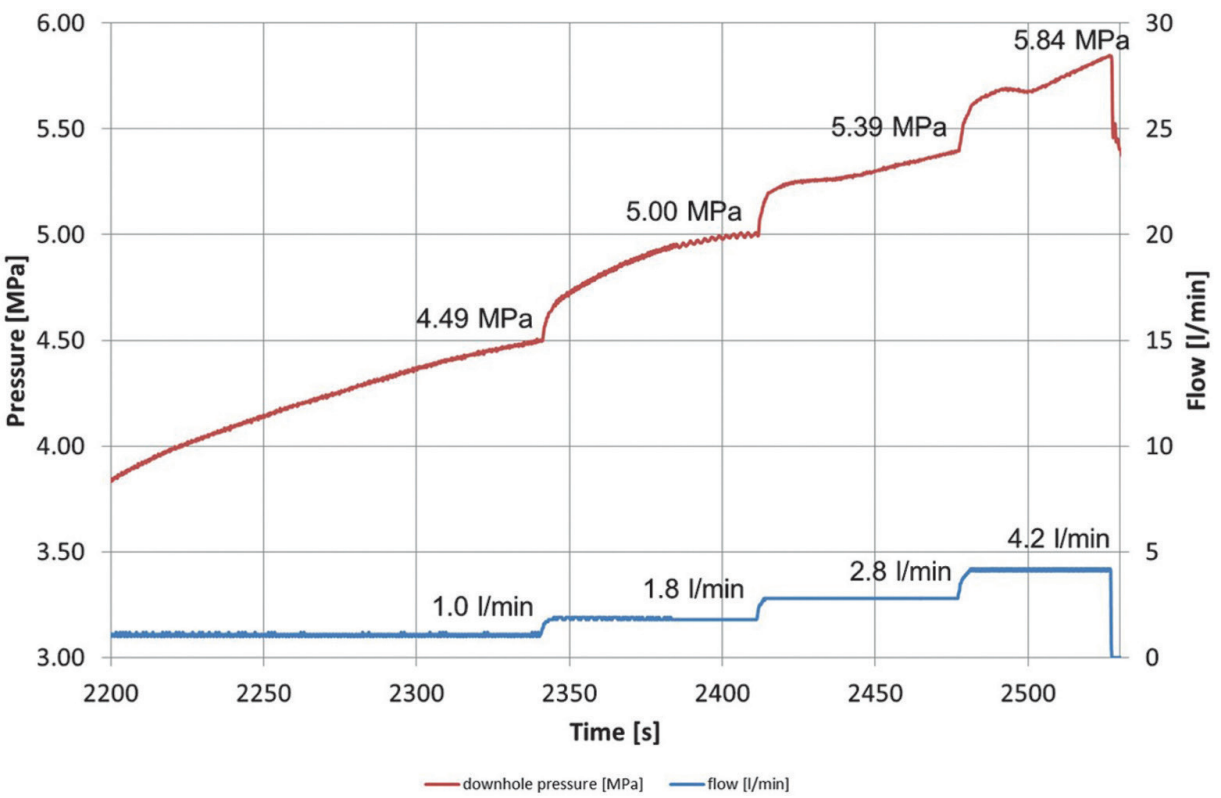

Fig. G-11: The step-rate-test consists of a step-wise increase of the injection flow rate and the corresponding pressures are monitored. The analysis of the flow/pressure pairs for every step is given in Figure G-12.

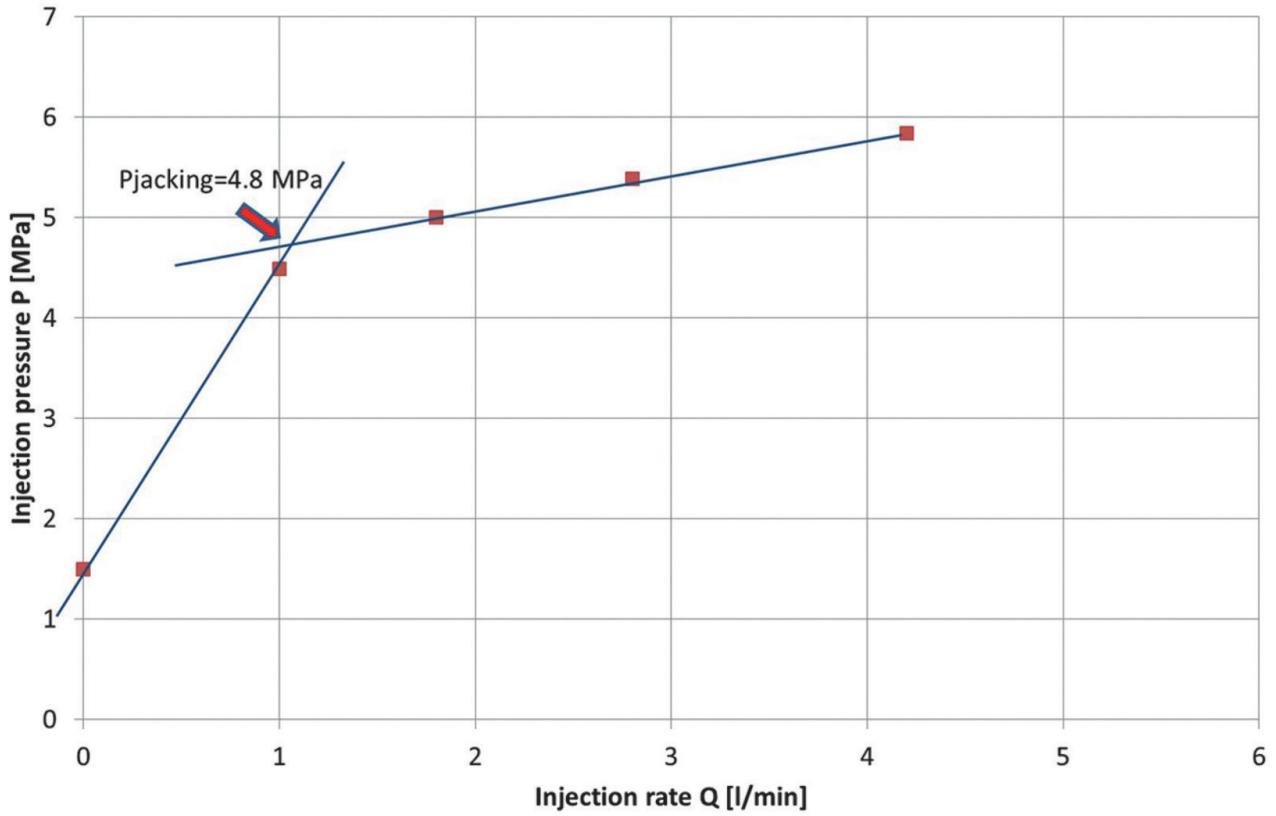

Fig. G-12: The quasi-steady state flow/pressure pairs from the step-rate-test are plotted on a flow rate Q versus injection pressure P plot. The intersection of the two linear interpolations yields the jacking pressure $P_{jacking}$, which is an additional estimation of the minimum principal stress. In most cases, the shut-in pressure P_{si} is equal to the jacking pressure.

Calculation of stress components (magnitudes) from the data obtained from the in-situ test at a depth of 148 m:

From the analysis of the pressure curve (Fig. G-6), critical or breakdown pressure P_c, re-opening pressure P_r and shut-in pressure P_{si} are determined.

- The critical pressure P_c was determined in Figure G-7 and is in the order of 8.0 MPa.
- The shut-in pressure P_{si} was determined from the derivative of the pressure curve versus pressure (Fig. G-10). From this graphic a P_{si} of 5.55 MPa was determined. As a cross-check, the $P_{jacking}$ should be more or less equal to the P_{si}. The plots in Figures G-11 and G-12 yielded a $P_{jacking}$ of 4.8 MPa, which is in good agreement with P_{si}. Finally, for calculation of the stress components, a mean P_{si} of all three re-opening cycles is taken, which yields a value of 5.1 MPa for P_{si}.
- The re-opening pressure P_r was determined graphically in Figures G-8 and G-9 and is in the order of 4.7 MPa.

In Figure G-13, all evaluated pressures (P_c, P_r and P_{si}) are represented on a depth plot. The values of the test at a depth of 148 m fit well into the trend of increasing pressures with depth.

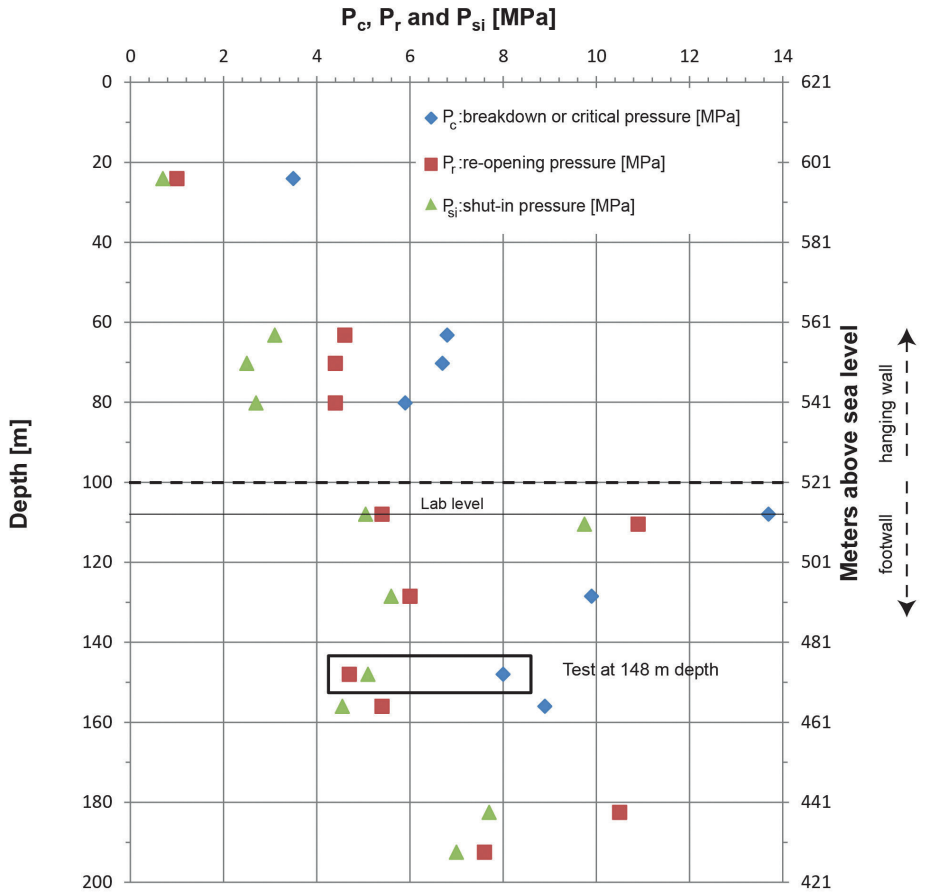

Fig. G-13: Depth plot of breakdown pressure P_c, re-opening pressure P_r and shut-in pressure P_{si} (modified after KLEE, 2012).

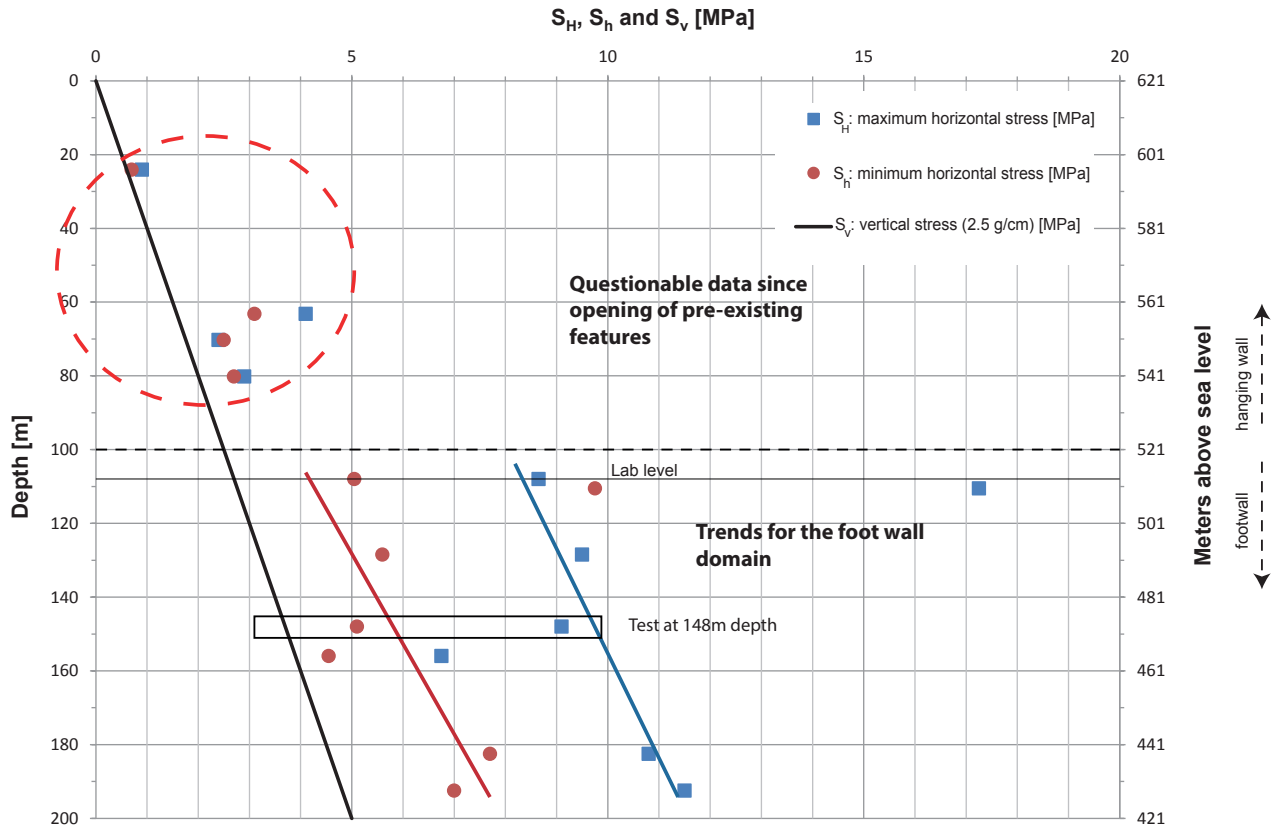

Fig. G-14: Depth plot of stress magnitudes S_H, S_h, S_v. The four tests in the hanging wall yielded questionable data due to missing induced axial features and are thus not included in the interpretation. For calculation of vertical stress a rock density of 2500 kg/m³ was assumed. The outliers at 110.5 m and 156 m were neglected for the calculation of the depth function (modified after KLEE 2012).

Hydraulic fracturing in the hanging wall (Opalinus Clay) did not induce any axial fractures. Only pre-existing features such as bedding planes and tectonic faults were re-activated or opended. Thus, the data from the hanging wall is not reliable and was not interpreted in the present study (Tab. G-4). Consequently, depth functions for S_H and S_h were only calculated for tests carried out in the footwall and furthermore without the two outliers at 110.5 m and 156 m.

The maximum horizontal stress S_H is calculated by using equation G.3. Together with the P_{si} and P_p, which is 1.48 MPa at 148 m depth, equation G.2 yields an S_H of 9.1 MPa. According to equation G.2, S_h is equal to P_{si} and thus 5.1 MPa for the mean value from all three re-openings. S_v finally is calculated by simply using equation G.4, which is the linear increase of vertical stress with depth caused by the overburden. By assuming an average density of 2500 kg/m³, at a depth of 148 m an S_v of 3.6 MPa is calculated.

With the re-opening pressure P_r and the critical pressure P_c, the in-situ hydraulic tensile strength can be calculated. P_r is 4.7 MPa and P_c from Figure G-7 is 8 MPa, yielding an in-situ hydraulic tensile strength T of 3.3 MPa for the limestone of the Courgenay Formation. This is in fairly good agreement with the results from the lab measurements, which yielded values of 2.3 ± 0.5 MPa (KLEE 2012).

Table G-3: *Listing of petrophysical data from lab testing conducted on samples from the Late Jurassic rocks in the footwall.*

Sample No	Depth	Density	V_p	V_s	E_{dyn}	υ_{dyn}	a_0	F_{max}	K_{1c}
	[m]	[g/cm³]	[km/s]	[km/s]	[GPa]	[–]	[mm]	[N]	[MNm$^{-3/2}$]
A	127.0–127.3	2.674	6.09	3.46	79.4	0.26	9.0	1013	0.65
B	136.0–136.3	2.662	5.47	3.17	65.9	0.25	9.2	967	0.64
C	143.5–143.7	2.629	5.27	3.19	64.9	0.21	—	—	—
D	156.6–157.0	2.667	5.58	3.22	68.6	0.25	9.3	1991	1.31
F	175.0–175.3	2.677	5.70	3.15	67.5	0.28	4.4	619	1.25
G	185.0–185.4	2.676	5.52	3.13	65.6	0.26	—	446	0.17
H	197.2–197.5	2.682	5.92	3.45	79.0	0.25	4.3	643	1.29

P-wave velocity (V_p), Shear-wave velocity (Vs) were used for the calculation of dynamic Young's Modulus (E_{dyn}) and Poisson's ratio (υ_{dyn}). Fracture toughness (K_{1c}) is determined from the 3-point bending test of Chevron-notched core pieces, with the Chevron notch depth (a_0) and the peak bending load (F_{max}).

Table G-4: *Listing of in-situ stress data from the tests critical pressure (P_c), re-opening pressure (P_r), tensile strength (T), shut-in pressure (P_{si}), jacking pressure ($P_{jacking}$) and pore pressure (P_p) and calculated values vertical stress (S_v), minimum horizontal stress (S_h) and maximum horizontal stress (S_H) with its direction (θ_{SH}).*

Test No	Depth	P_c	P_r	T	P_{si}	$P_{jacking}$	P_p	S_v	S_h	S_H	θ_{SH}
	[m]	[MPa]	[MPa]	[MPa]	[MPa]	[MPa]	[MPa]	[MPa]	[MPa]	[MPa]	[°]
6	24.1	3.5	1.0	2.5	0.7	0.7	0.2	0.6	0.7	0.9	85
5	63.2	6.8	4.6	2.2	3.1±0.3	3.3	0.6	1.5	3.1±0.3	4.1	104
4	70.3	6.7	4.4	2.3	2.5±0.2	2.6	0.7	1.7	2.5±0.2	2.4	185
3	80.2	5.9	4.4	1.5	2.7±0.1	2.7	0.8	2.0	2.7±0.1	2.9	58
2	**108.0**	**13.7**	**5.4**	**8.3**	**5.05±0.1**	**4.8**	**1.1**	**2.6**	**5.05±0.1**	**8.65**	**4**
1	110.5	–	10.9	–	9.75±0.1	–	1.1	2.7	9.75±0.1	17.25	39
11	**128.5**	**9.9**	**6.0**	**3.9**	**5.6**	**6.0**	**1.3**	**3.1**	**5.6±0.0**	**9.5**	**176**
10	**148.0**	**8.0**	**4.7**	**3.3**	**5.1±0.1**	**4.8**	**1.5**	**3.6**	**5.1±0.1**	**9.1**	**19**
9	156.0	8.9	5.4	3.5	4.55±0.1	4.6	1.5	3.8	4.55±0.1	6.75	38
8	**182.5**	**–**	**10.5**	**–**	**7.7**	**8.2**	**1.8**	**4.5**	**7.7±0.1**	**10.8**	**6**
7	**192.5**	**–**	**7.6**	**–**	**7.0±0.3**	**7.0**	**1.9**	**4.7**	**7.0±0.3**	**11.5**	**174**

Only **bold values** are interpreted in the present study and used for the calculation of the depth functions of S_H an S_h.